Universität Augsburg
Fakultät für Angewandte
Informatik

Modelling, Identification, and Online State Estimation for a Personalized Model-based Diabetes Monitoring

Dissertation

zur Erlangung des akademischen Grades

Doktor der Ingenieurwissenschaften (Dr.-Ing.)

eingereicht an der Fakultät für Angewandte Informatik

der Universität Augsburg

von

Dipl.-Ing. Christian Tolks

Augsburg, Mai 2021

Modelling, Identification, and Online State Estimation for a Personalized Model-based Diabetes Monitoring

Dipl.-Ing. Christian Tolks

Erstgutachter: Prof. Dr.-Ing. habil. Christoph Ament

Zweitgutachter: Prof. Dr. rer. nat. Jörg Hähner

Tag der mündlichen Prüfung: 29.07.2024

Abstract

In the present work, a model-based approach for personalized diagnostics in patients with diabetes mellitus is developed, which estimates blood glucose profiles based on a model of the glucose-insulin-glucagon metabolism.

Diabetes mellitus is a chronic metabolic disease. It results from the body's inability to produce and/or use insulin properly. Regardless of the specific type, patients who suffer from the disease require lifelong insulin therapy. Diabetes therapy aims to support the impaired physiological control loop of glucose-insulin homeostasis by artificial feedback control. As a sensor, the patient can measure glucose levels in the body. Insulin administration can be regarded as the actuator. The patient is responsible for the control regimen for which he or she receives appropriate education.

Just like in technical systems, metabolic processes can be described by mathematical models. It can therefore be assumed that a model-based approach will also have advantages in diagnosis and therapy. However, existing approaches take insufficient account of a patient's individual condition. Medicine is currently trying to address this by developing "personalized medicine."

A physiological model approach is chosen that allows the simulation of both healthy and pathophysiological metabolic systems. The unified model is identified using novel quasi-continuously measuring glucose sensors under everyday-life conditions. First, sensitivity analysis is applied to find those parameters that induce the most variability in the model output and thus, can be regarded as important. This is followed by analyses of the controllability and observability of states of the system. Hence, those variables are found which significantly contribute to the system behavior. Furthermore, the methods are adapted and extended to the specifics of the model class.

The essential parameter sets are, where technically feasible, adapted to the respective individual to achieve better predictions than it would be possible using generic model approaches. For this purpose, measurement data of different probands is recorded over several weeks, analyzed, and the parameters are subsequently identified solving an optimization problem. Finally, the blood glucose concentration is estimated in real-time on the basis of the personalized model, continuously collected glucose measurement data, and a nonlinear state observer. The developed algorithms are integrated into a web-based platform and a mobile application to support patients in their diagnosis and therapy.

Kurzfassung

In vorliegender Arbeit wird ein modellbasiertes Verfahren zur personalisierten Diagnostik bei Patienten mit Diabetes mellitus entwickelt, welches den Blutglukoseverlauf auf Basis eines Modells der Glukose-Insulin-Glukagon Verstoffwechselung schätzt.

Diabetes mellitus ist eine chronische Stoffwechselerkrankung. Sie resultiert aus der Unfähigkeit des Körpers Insulin zu produzieren und/oder zu nutzen. Unabhängig des konkreten Typs benötigen Betroffene eine lebenslange Insulintherapie. Die Diabetestherapie zielt darauf ab, den gestörten physiologischen Regelkreis der Glukose-Homöostase durch eine künstliche Regelung zu unterstützen. Als Sensor kann der Patient den Glukosespiegel im Körper messen. Als Aktor kann die Insulinvergabe angesehen werden. Die Regelung übernimmt der Patient nach erfolgter Schulung selber.

Ebenso wie technische Systeme sind Stoffwechselvorgänge durch mathematische Modelle beschreibbar. Daher ist anzunehmen, dass auch hier ein modellbasiertes Vorgehen Vorteile bei Diagnose und Therapie haben wird. Allerdings berücksichtigen bisherige Ansätze den individuellen Zustand eines Patienten nur unzureichend. Die Medizin versucht dies aktuell durch die Entwicklung einer „personalisierten Medizin“ anzugehen.

Es wird ein physiologischer Modellansatz gewählt, mit dem die Simulation von gesunden als auch von pathophysiologischen Stoffwechselsystemen ermöglicht wird. Das vereinheitlichte Modell wird mit Hilfe neuartiger quasi-kontinuierlich messenden Sensoren unter Alltagsbedingungen identifiziert. Dazu werden zunächst mittels Sensitivitätsanalyse diejenigen Parameter gefunden, die die größte Variabilität im Modellausgang erzeugen und damit als wichtig angesehen werden können. Analysen zur Steuerbarkeit und Beobachtbarkeit von Zuständen des Systems schließen sich an. Damit sind diejenigen Größen gefunden, die einen wesentlichen Beitrag für das Systemverhalten liefern. Weiterhin werden die Methoden an die Spezifika der Modellklasse angepasst und erweitert.

Die für das Modell wesentlichen Parametersätze werden, wo technisch realisierbar, an das jeweilige Individuum angepasst, um bessere Vorhersagen erzielen zu können, als dies mit generischen Modellansätzen möglich ist. Dazu werden Messdaten verschiedener Probanden über mehrere Wochen hinweg aufgenommen, analysiert und die Parameter anschließend durch Lösen eines Optimierungsproblems identifiziert. Abschließend wird die Blutglukosekonzentration in Echtzeit auf Basis des personalisierten Modells, kontinuierlich erfasster Glukosemessdaten und einem nichtlinearen Zustandsbeobachter geschätzt. Die entwickelten Algorithmen sind in einer Web-Applikation integriert und können Nutzer bei ihrer Selbstdiagnose und Therapie begleiten.

Contents

1 Introduction

1.1 Glucose-Insulin Homeostasis

Maintaining blood glucose concentration within a physiological range is crucial because glucose is a major source of energy for cellular respiration and therefore for the energy supply in the human body. Regulation of blood glucose is achieved by several feedback loops involving the antagonistic hormones insulin and glucagon, both produced by the pancreas. Each of these two hormones acts via an endocrine regulatory pathway, which is controlled by negative feedback. If the blood glucose level rises above a certain target value, released insulin ensures that glucose is absorbed from the blood by peripheral cells, so that its concentration decreases back to normal. Conversely, if the blood glucose level falls below the set point, glucagon promotes the release of glucose into the blood, so that its concentration increases. As insulin and glucagon have opposite effects, these hormones maintain strict control over blood glucose levels. Here, the pancreas is sensor, actuator, and controller in a single unit (Fig. 1.1).

Diabetes mellitus is a chronic metabolic disease that is caused by an insulin deficiency or by a reduced reaction to insulin in the target tissue. As a result, high glucose levels exceed the ability of the kidneys to reabsorb the sugar. Glucose remaining in the filtrate is excreted. Therefore, sugar in the urine is a typical characteristic of this disease. When glucose accumulates in the urine, more water is excreted, resulting in excessive volumes of urine. The word diabetes (Greek: *diabainein*, to pass through) alludes to this excessive urine production; mellitus (Greek: *meli*, honey) refers to the sugar contained in the urine. Regardless of the cause, patients require continuous insulin therapy. If not treated, the disorder can have serious consequences in long-term and short-term and affects the heart, blood vessels, eyes, and kidneys. There are two main types of diabetes mellitus. Both are characterized by

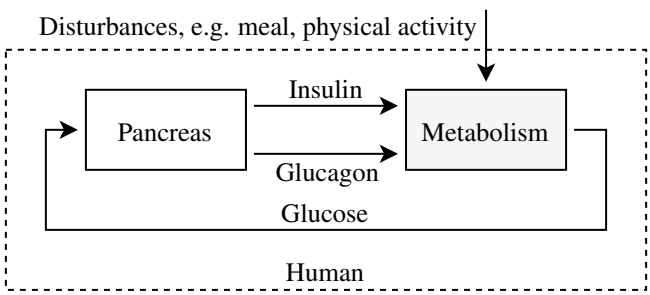

Figure 1.1: Physiological closed-loop system: The pancreas acts as a controller to maintain glucose metabolism in response to disturbances.

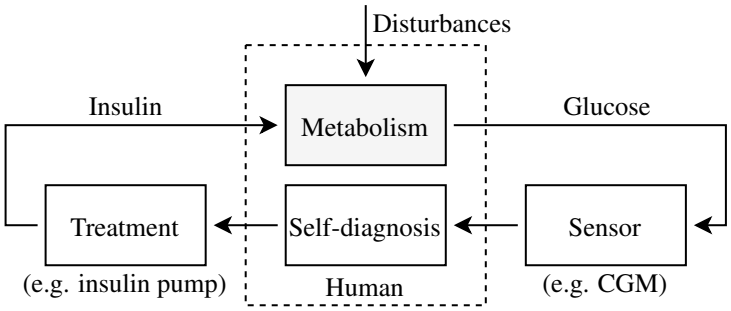

Figure 1.2: Treatment of diabetes: The patient has to measure glucose and acts as a controller for insulin treatment based on his or her self-diagnosis.

high blood glucose levels but have different causes. More than 90 % of all patients suffer from type 2. According to the International Diabetes Federation (2019), it is estimated that worldwide 463 million people have been diagnosed with diabetes in 2019. Diabetes therapy aims to replace or support the disturbed physiological control loop of glucose-insulin homeostasis by an artificial controller. As the sensor, the patient can determine the glucose concentration from a blood drop using a glucose meter. For a few years, continuous measuring devices have also been available that measure glucose in the subcutaneous tissue (continuous glucose monitoring, CGM). Injection of insulin can be seen as the actuator. The patient himself or herself performs the necessary self-diagnosis and therapy for which he or she receives appropriate training (Fig. 1.2).

1.2 Towards Personalized Medicine

In the design of control systems for technical systems, e. g., in the automotive sector, model-based design is nowadays a generally accepted and desired approach in engineering. A model of the dynamic system is the starting point for all further work such as simulation, analysis, controller design, diagnostics, etc. Even though glucose-insulin metabolism is not an engineering system but physiologic, it can also be described by mathematical equations. The benefits of a model-based approach to the analysis and treatment of glucose regulation are conceivable here. The idea is therefore to successfully transfer this methodology to the (patho-) physiological system of glucose-insulin metabolism in humans.

Existing approaches to modeling, system identification, or state estimation do not sufficiently take into account the individual condition of each patient, as there is great variability in the metabolic behavior from person to person. Even very good standard models can only correctly describe metabolic processes for averages over collectives. Medical research is currently trying to address this by the development of “personalized medicine.” Besides models of metabolic processes, this means developing efficient methods and algorithms for analysis, identification, and estimation, that take into account the specifics of physiological systems.

Due to the complexity of the underlying physiological mechanisms, fine-scale models cannot currently be used in everyday practice, since only a few variables can be measured directly, making parameter identification difficult. One possibility, however, is to focus on only major interactions. Nevertheless, this requires a profound knowledge of the system behavior including analysis of state controllability and observability, and parameter sensitivity.

Personalization is only possible on the basis of individual measurement data. In addition to established blood glucose measurements, the focus is on novel continuously measuring sensors. For the first time, it is technically feasible to capture the dynamics in the signal curves in everyday settings at reasonable costs. With the help of model knowledge and measurement data, parameter identification of a patient becomes possible.

With the help of customized models, therapy can be improved. On one hand, this can be achieved by adjusting insulin amounts and time points based on the patient's current metabolic state. On the other hand, the number of blood glucose measurements can be optimized when the current glucose status is known from model simulations. If disturbances such as meals or physical activities are also considered, the amount of insulin to be administered can be dosed even more precisely. Short-term prediction of future blood glucose levels can be particularly helpful in preventing potentially harmful conditions such as hyperglycemia or hypoglycemia. Applying an individual metabolic model is therefore useful in advising patients, which can result in relief in everyday use.

Conventional sensors measure the glucose concentration using a blood sample from the patient. With the help of this information, treatment decisions can be made. Functions for storing and processing data series or the development of the pathological condition over a longer period are not very common yet. However, the increasing availability of mobile devices with sufficient computing power or cloud-based services enables the application of personalized models and related algorithms as a universal, portable monitoring and diagnostic system.

1.3 Contribution and Structure of the Thesis

The present work focuses on a model-based method for personalized diagnostics in patients with diabetes mellitus, which estimates blood glucose concentrations on the basis of a model of glucose-insulin-glucagon metabolism.

This work incorporates available physiological models from literature for healthy and type 2 diabetics, as well as for type 1 diabetic patients into a single set of ordinary differential equations. The model is capable of expressing glucose-insulin-glucagon regulation after a mixed-meal, for which it includes parts for meal ingestion, insulin and glucagon administration, secretion and utilization of major hormones, and their distribution and diffusion within the body. Furthermore, available parameter sets from the literature are used as a basis for an algorithm to generate a population of virtual subjects. These subjects are characterized by their parameter vector which determines individual metabolic

conditions, thus, the model structure is independent of a concrete manifestation of the disease. The study of a whole population allows to investigate the behavior of individuals and groups and it allows to draw conclusions about inter-patient and inter-group variability.

The model is identified using novel quasi-continuous glucose sensors, i. e., parameters required for the model are adapted to the respective individual in order to be able to make better predictions than it would be possible with generic models. Alterations in the metabolic system, as they occur in diabetes, can be characterized individually by changing the parameters. Furthermore, continuous monitoring allows the use of state observers to estimate those states that are difficult or impossible to measure. For this purpose, an extended Kalman filter is designed that takes into account both the nonlinear system dynamics and the properties of process and measurement noise. The method is applied to the estimation of blood glucose concentration. As this quantity is typically measured only a few times a day, continuous monitoring could improve treatment decisions. Furthermore, a prediction of future glycemic trends would be also possible.

To identify the variables relevant for parameter identification and state estimation, two methods are applied and adapted to the model properties. On one hand, sensitivity analysis, a stochastic approach to identifying those variables that contribute most to the output variability, is used. And second, controllability and observability of states and parameters are analyzed based on their empirical Gramians. Adaptations to the model mainly cover the large number of variables and the nonlinearities in the system dynamics.

As a result, a self-monitoring platform is developed that permanently monitors the patient's current health status and provides diagnostic services. The platform uses a mobile app that connects to glucose sensors and handles data exchange. Presented methods and algorithms are incorporated into a web service for data storage and processing. Necessary computations are realized online and in real-time. Thus, patients will be enabled to take a more active part in their treatment process. Through permanent self-monitoring, potentially severe events of the disease could be mitigated or avoided altogether.

From the contributions shown above the thesis is structured as follows:

Chapter 2. An overview of the medical characteristics of a healthy glucose-insulin metabolism and its pathological alterations in the diabetic case is given. Furthermore, measurement principles and technology for glucose monitoring are introduced. To assess glucose metabolism several diagnostic tests are presented next, followed by common and novel diabetes treatment options.

Chapter 3. A review of the state-of-the-art is presented. The chapter is divided into a medical part addressing models of the glucose-insulin-glucagon metabolism including minimal and maximal approaches. This is followed by the technical part, which discusses techniques for analyzing states and parameters in nonlinear systems. Methods for parameter identification and online state estimation are followed by recent advancements in (mobile) diabetes monitoring and management.

Chapter 4. A unified model of glucose-insulin-glucagon metabolism is derived, capable of simulating healthy subjects, as well as type 2 and type 1 diabetics. In combination with the dynamical model a population of virtual subjects with individual metabolic profiles is generated, which allows simulation studies of different (patho-) physiologic glucose excursions. The modeling part is closed with an implementation of models of glucose sensors in order to incorporate measurement noise.

Chapter 5. Systems analysis first focuses on the investigation of sensitive parameters, that means, parameters whose alterations have a significant influence on the variation of glucose. For this purpose, methods of global sensitivity analysis are used and adapted to the characteristics of the model. In particular, this includes the functional model output and the large number of input variables. Furthermore, the concept of controllability and observability of states is introduced and extended to parameters and nonlinear systems. With the help of the calculated (empirical) Gramian matrices, those parameters and states are determined that can be theoretically derived from the observation of glucose time courses. Both techniques significantly reduce the number of states and parameters that must be considered in the subsequent steps.

Chapter 6. The recorded experimental database is first presented and evaluated. On the basis of the derived nominal model of glucose regulation and the model of virtual subjects, complemented by the investigation of properties of their states and parameters, the models are first adapted to individuals using continuous glucose measurement data. For this purpose, an optimization algorithm is deployed. Second, in the individualized model, non-measurable states such as the blood glucose concentration are estimated in real-time using a nonlinear hybrid observer design.

Chapter 7. The concept and implementation basics for a model-based diabetes monitoring (*MoDiM*) platform are shown, which integrates a model of glucose-insulin regulation, devices for continuous glucose measurement, and methods for continuous glucose estimation into a web service accessible by any (mobile) device.

Chapter 8. A summary and an outlook on future developments of patient-specific model building, identification, and estimation in the field of diabetes technology will conclude the present work.

2 Medical Background

Diabetes mellitus describes a group of disorders of the carbohydrate metabolism that are based on an absolute or relative lack of insulin which leads to chronic hyperglycemia. The term describes its main symptom, the excessive excretion of sugar along with the urine. It results from defects of insulin secretion, insulin action, or both together. Diabetes is a gradually progressing disease that can develop over several years. Often, symptoms are mild and can persist for a long time. But in the long-term diabetes is associated with changes in the nervous system and the blood vessel system which can lead to retinopathy, nephropathy, or neuropathy.

According to estimates from the International Diabetes Federation (2019), the prevalence of diabetes (i. e., the proportion of patients with diagnosis in relation to the total population) in Germany was 15.3 % in 2019[1]. In absolute numbers, this represents more than 9 million people diagnosed with diabetes. Approximately 5-10 % of patients are suffering from type 1 diabetes and approximately 90 % from type 2. From a global perspective, 9.3 % of the world's population suffer from diabetes which leads to a total health expenditure of $760.3 billion worldwide. If current trends continue, 700 million adults are going to have diabetes by 2045.

2.1 Normal Physiology

2.1.1 Mechanisms of the Glucose-Insulin-Glucagon Control

Energy ingested from food compensates for energy that is consumed by the metabolism through activity or that is stored in the organism. Surplus energy is stored in the form of glycogen, mainly in the liver and muscle cells.

Synthesis and breakdown of glycogen are not only important for maintaining the energy balance but also for preserving a defined glucose concentration in the blood. Since glucose is the main energy source for cell respiration and is used as a carbon source for many biosynthesis processes, maintaining a fixed glucose concentration in the blood is very important.

The regulation of blood glucose levels is the task of the two antagonistic hormones insulin and glucagon, both produced and secreted by the pancreas. Each of these hormones acts via an endocrine regulatory pathway that is controlled by negative feedback (Fig. 2.1). If the glucose level rises above

[1] Statistic includes only adults (20-79 years).

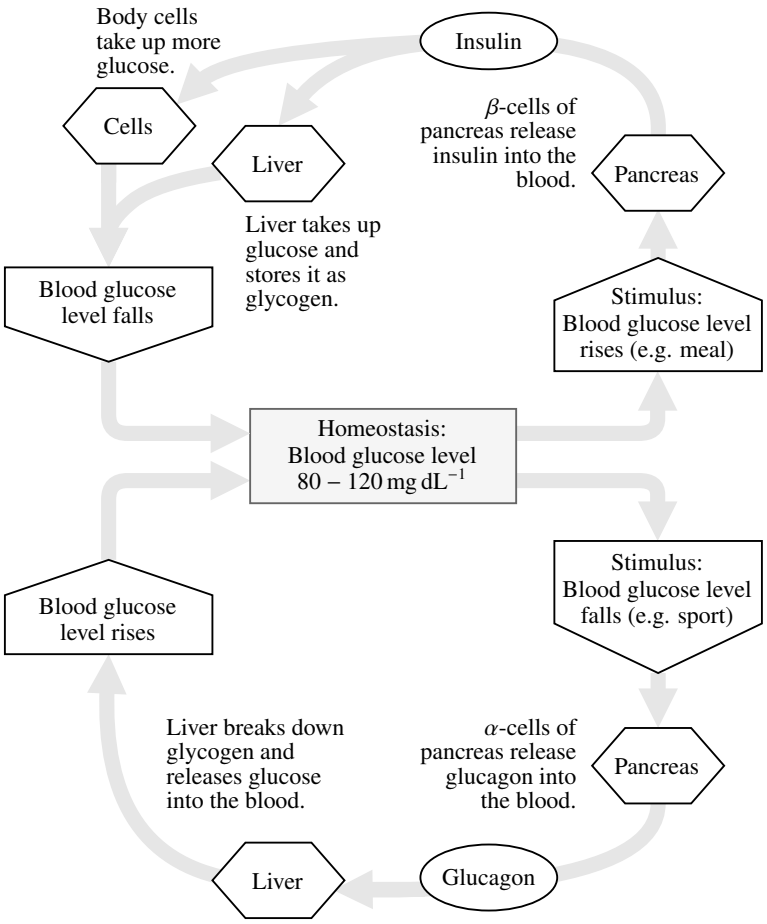

Figure 2.1: Homeostatic regulation (adapted from N. A. Campbell et al. (2016, p. 982)): The opposing effects of the two hormones insulin and glucagon contribute in keeping the blood glucose level close to the target range of 80 – 120 mg dL^{-1}.

a certain level, the release of insulin ensures that glucose is absorbed from the blood, so that its concentration decreases. On the other hand, if the glucose level falls below a certain level, glucagon promotes the release of glucose into the blood, so that its concentration increases again. Since insulin and glucagon have opposite effects, the combined action of both hormones exerts strict control over the blood sugar level.

In total, the hormone-producing cells make up only one to two percent of the pancreas mass. Its remaining cells produce and secrete digestive enzymes, among other substances. The pancreas thus fulfills functions for both the hormonal and digestive system (N. A. Campbell et al. 2016).

From a systems engineering point of view, glucose metabolism is a closed-loop control system, in which the blood glucose concentration is the set point that has to be stabilized within a certain range (Fig. 1.1). Endogenous and exogenous influences like food intake or physical activity can be regarded as disturbances to the control loop which must be compensated for. The pancreas serves as a natural controller that "senses" the current blood glucose level and releases the hormones insulin and glucagon which act as control variables to restore glucose homeostasis.

2.1.2 Characteristics of the Glucose-Insulin-Glucagon Metabolism

Glucose. Glucose is the main energy source for the human body. It is either ingested with food or produced endogenously in the liver from stored glycogen by a biochemical process (glycogenolysis). In the fasting state, endogenous glucose production (EGP) equals glucose consumption. Most of the glucose uptake is insulin-independent and occurs in the brain and erythrocytes to ensure a stable supply of energy. All other processes need insulin to activate mechanisms of glucose transport into the cells. The majority of insulin-dependent glucose disposal occurs in the liver and muscles and is either stored for future use or consumed directly. In humans without diabetes, glucose concentrations average between $80 - 120\,\mathrm{mg\,dL^{-1}}$. This is also called equilibrium, glucose-insulin homeostasis, or steady-state. A phase of glucose levels above $180\,\mathrm{mg\,dL^{-1}}$ induces hyperglycemia, whereas there is no clear threshold that defines hypoglycemia (Seaquist et al. 2013). In individuals without diabetes, symptoms of hypoglycemia typically develop at a glucose concentration below $55\,\mathrm{mg\,dL^{-1}}$ (Holt et al. 2010, p. 537). In healthy subjects, glucose-insulin-glucagon regulation quickly restores equilibrium.

Insulin. Insulin is a polypeptide hormone that is produced in the β-cells of the pancreas within the islets of Langerhans. From there, insulin is secreted into the circulatory system via the portal vein, where it lowers the blood glucose level by stimulating cells to absorb glucose from the blood. Thus, it plays a fundamental role in nutrient metabolism.

Insulin secretion is mainly determined by the circulating concentration of glucose and other nutrients. So, when food is absorbed from the gastrointestinal tract, the β-cells detect these changes and release insulin to enable glucose uptake in the tissues. In case of a decrease in nutrient concentrations in the blood, insulin secretion is switched off to prevent hypoglycemia.

The time course of insulin secretion in response to elevated glucose levels can be described by two phases: a rapidly rising and afterward rapidly falling first phase, followed by a comprehensive second phase that lasts as long as the high glucose level persists (Fig. 2.2), see Holt et al. (2010, pp. 92–93). Oral ingestion of 75 g of glucose will cause plasma insulin to rise from its basal level ($20-30\,\mathrm{pmol\,L^{-1}}$) to $250 - 300\,\mathrm{pmol\,L^{-1}}$ in 30 min (Fu et al. 2013; Polonsky, Given, and van Cauter 1988). From a control engineering point of view, the pancreas roughly behaves like a classical PID controller (Steil, Rebrin, and J. J. Mastrototaro 2006; Chee and Fernando 2007).

Glucagon. Glucagon is a peptide hormone whose main effect is to raise blood glucose levels by stimulating the production of energy-rich glucose from glycogen in the liver (glycogenolysis). This hormone is a counterpart of insulin in its effect on glucose, protein, and fatty acid metabolism. It is produced in the islets of Langerhans in the pancreas (α-cells). When blood glucose concentration drops (typically below $70\,\mathrm{mg\,dL^{-1}}$ (Schwartz et al. 1987)), but also after a protein-rich meal, glucagon is released by the pancreas into the circulatory system from where it is transported into the liver to stimulate glycogenolysis. This response is primarily intended to ensure energy supply to the brain.

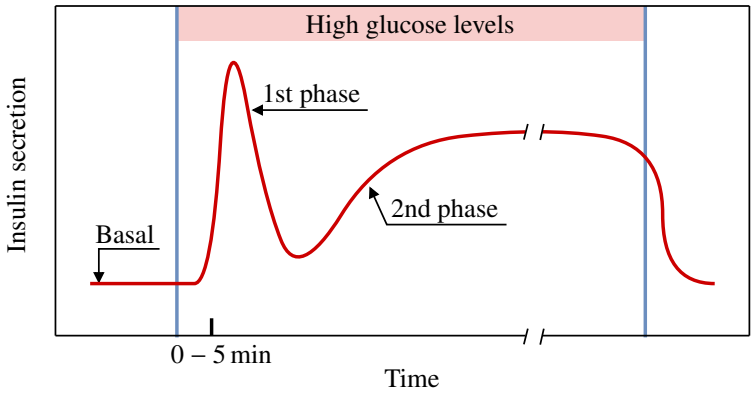

Figure 2.2: Pattern of insulin release in response to an increase in the glucose level (adapted from Holt et al. (2010, p. 93)): A highly dynamic first phase lasting a few minutes is followed by the second phase that persists for the duration of the high-glucose stimulus.

2.2 Diabetes mellitus

In 1999 the World Health Organization (1999) approved a new classification of diabetes mellitus under etiological aspects. The nomenclature distinguishes type 1 diabetes as immune-mediated diabetes, which is characterized by autoimmune destruction of the pancreatic β-cells. Absolute insulin deficiency usually leads to diabetic ketoacidosis in the absence of insulin therapy. Type 2 diabetes is the most common form of diabetes and is characterized by a variable combination of relative insulin deficiency and insulin resistance. A third and fourth group includes other types of diabetes and gestational diabetes, respectively.

2.2.1 Pathogenesis of Diabetes

Type 1 Diabetes mellitus. Type 1 diabetes mellitus (T1DM) is caused by chronic inflammation of the islets of Langerhans in the pancreas. As a consequence, the insulin-producing β-cells are destroyed, which leads to a loss of functionality in insulin secretion that is frequently accompanied by tissue-specific impaired insulin action (Yki-Järvinen and Koivisto 1986). The cause of this inflammation is only partially known. In addition to genetic factors (HLA complex and some other genes), environmental factors (especially nutrition and infections) appear to trigger autoimmunity. This process takes place over a long period before the clinical manifestation of type 1 diabetes, which is mainly observed in children, adolescents, or young adults (Schatz 2006, p. 49).

T1DM results from an almost complete loss of insulin secretion, which clinically manifests as hyperglycemia-related symptoms. The lack of endogenous insulin production leads to patients having to externally administer insulin to maintain their glucose metabolism.

Type 2 Diabetes mellitus. In type 2 diabetes mellitus (T2DM) genetic and acquired factors in combination affect β-cell function and insulin sensitivity. It is characterized both by a disturbance

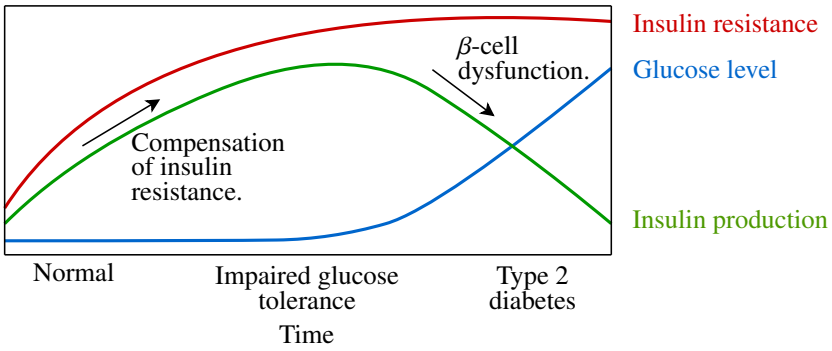

Figure 2.3: Progression of type 2 diabetes over time (adapted from Fonseca (2006)): Increasing insulin resistance is firstly compensated by a rise in pancreatic insulin production. With onward β-cell dysfunction, glucose level increase gradually.

of insulin secretion and by insulin resistance of the essential target tissues such as skeletal muscles, liver, and adipose tissue. With the aid of the glucose clamp technique, a method that allows the measurement of insulin sensitivity in the skeletal muscle, it has been shown that insulin resistance can exist decades before the clinical manifestation of type 2 diabetes. Other important pathogenic factors for the development of type 2 diabetes are insulin secretion defects and β-cell mass loss, which are also present long before the clinical manifestation of diabetes. This intermediate phase is already characterized by altered kinetics of insulin secretion (Fig. 2.3). In this phase, there is a slower but prolonged increase in insulin concentration after a glucose stimulus, resulting in hyperinsulinemia (Schatz 2006, p. 100).

When standard treatments such as weight loss or anti-diabetic medication fail, T2DM subjects depend on external insulin administration to compensate for postprandial glucose increases.

Other Types of Diabetes. Other types include endocrine causes such as an excess of hormones that are counter-regulatory to insulin or inhibit secretion or action; drug-induced hyperglycemia; or pancreatic diseases. Hyperglycemia can also occur during pregnancy (gestational diabetes) and affects about 15.8 % of women worldwide (International Diabetes Federation 2019).

2.2.2 Characteristics of the Diabetic Metabolism

Food ingestion does not increase insulin levels or decrease glucagon concentrations, therefore, glucose uptake by the muscles deteriorates and a high amount of glucose remains in the circulatory system (Gerich, Lorenzi, et al. 1975). People with T2DM have elevated fasting glucose levels and excessive glycemic excursions following carbohydrate intake (Polonsky, Given, Hirsch, et al. 1988). The first-phase insulin response is often absent and the second-phase is diminished. Insulin secretion is typically decreased and delayed (Dinneen et al. 1992). Abnormalities in glucose sensing, insulin processing, or intracellular signaling can alter insulin secretion. Insulin resistance leads to an impaired

suppression of endogenous glucose production in the liver, in the basal state as well as postprandial, and to a reduced glucose uptake in the peripheral tissues.

Glucagon counter-regulation in the case of low or high blood glucose levels is also diminished. In normal subjects, glucagon is secreted into the blood at glucose values below 70 mg dL^{-1}. In diabetics, the increase of glucagon secretion in response to low blood glucose levels may occur at significantly lower values (Schatz 2006, p. 87), which induces the risk of severe hypoglycemia. In addition, glucagon secretion cannot be properly inhibited at high postprandial glucose levels (Seino et al. 1978; Shah et al. 2000), which leads to failures in suppressing hepatic glucose production and therefore to a state of hyperglycemia. Missing glucagon suppression can be attributed to the lack of intra-islet insulin in T1DM. Administration of exogenous insulin rapidly lowers glucagon concentration in T1DM (Dagogo-Jack et al. 1994).

2.3 Glucose Monitoring: Principles and Technology

The overall goal of diabetes management is to achieve a near as possible normal physiology, without causing significant hypoglycemia. In patients whose natural glucose homeostasis is disturbed, monitoring the blood glucose levels is essential to determine therapeutic interventions.

The concentration of glucose in the blood and glycated hemoglobin (HbA_{1c}) are the most common measures of glycemia in practice. Blood glucose concentration provides current information reflecting the daily level of glycemic control, the variation in control, and the direct response to therapeutic intervention. Glycated hemoglobin provides information on the overall control of glucose levels over the last 6-8 weeks. That means, it is a kind of long-term average value, in which the intra-patient measurement variation is no longer relevant. Both, blood glucose and HbA_{1c}, help to identify poor glycemic control and facilitate the adjustment of therapeutic measures to achieve optimal glucose levels (Holt et al. 2010, p. 399). Besides that, continuous glucose sensors have gained increased attention due to their ability to measure glucose concentrations continuously in quasi-real-time, which provides new insights into the dynamics of glucose metabolism.

Measurement of glucose levels is usually carried out on either capillary or venous blood samples. The concentration is expressed in SI (Systeme International) units as millimoles/liter (mmol L^{-1}) or in milligrams/deciliter (mg dL^{-1}). A range of analytical techniques is used for the laboratory measurement of blood glucose levels. The enzymatic reference method for glucose is the hexokinase/G6PDH method. Chemical oxidation/reduction methods are less specific, but still valid and are frequently used because of their convenience and lower cost. Blood glucose self-monitoring (BGSM, also referred to as self-monitoring blood glucose, SMBG) is possible using capillary blood glucose meters and is a standard of care for patients with T1DM and necessary for insulin-treated patients with T2DM. BGSM should be carried out three or more times per day for patients using multiple insulin injections or an insulin pump (Holt et al. 2010, pp. 403–405).

In accordance with ISO 15197:2013[2] (International Organization for Standardization 2013), blood glucose meters must meet the following minimum criteria for acceptable system accuracy:

(a) 95 % of the measured glucose shall fall within a range of $\pm 15\,\mathrm{mg\,dL^{-1}}$ for glucose concentrations less than $100\,\mathrm{mg\,dL^{-1}}$ and within a range of ±15 % for concentrations greater or equal than $100\,\mathrm{mg\,dL^{-1}}$, compared to reference records,
(b) 99 % of individual glucose measurements must be within zones A and B of the Consensus Error Grid (CEG) for T1DM (Parkes et al. 2000).

The majority of commercially available devices conform to these international standards.

A variety of blood glucose measurement techniques exist and can be generally categorized into

(a) invasive,
(b) minimal-invasive, and
(c) non-invasive

techniques. It is also possible to distinguish between chemical/enzymatic or physical measurement principles. The first principle is based on a chemical reaction with glucose which varies depending on the enzymes used (Ferri et al. 2011), the method of sample collection, and the measurement location (inside the body or extra-corporeal). The second principle mostly relies on measuring optical, acoustic, or electromagnetic effects. In-depth reviews of techniques, sensors, and devices can be found in, Thomas et al. (e. g., 2006), Chee and Fernando (2007), and Villena Gonzales et al. (2019); their findings are summarized in the following paragraphs.

Invasive Measurement Techniques. In clinical settings, measurements of blood glucose are obtained by direct venous access and analysis of the whole blood[3] by laboratory instrumentation. The devices usually combine glucose oxidase technique with an amperometric detection to determine glucose concentrations. This procedure cannot be fulfilled by the patients themselves without proper instructions and raises the risk of infection and thrombosis. Thus, it is not suitable for long-term monitoring outside a hospital. However, as these systems provide the most accurate results, they can be used as a reference point to evaluate the performance of less exact sensors, e. g., BGSM.

Minimal-invasive Measurement Techniques. Blood glucose self-monitoring is the standard of care for in-home glucose monitoring for both T1DM and T2DM patients. Although the glucose concentration is determined from a blood sample and is therefore somewhat invasive, it is here classified as minimal-invasive. However, the quantity taken is small and can be carried out by most patients several times a day making it suitable for long-term glucose monitoring.

[2] In Germany, ISO 15197:2013 is replaced by DIN EN ISO 15197:2015.
[3] Whole blood refers to the entirety of blood cells suspended in blood plasma.

(a) Glucose meter, lancet, and test strips to measure the concentration of blood glucose taken from the finger pulp.

(b) Continuous glucose sensor, transmitter, receiver, and injection aid to measure subcutaneous glucose concentration.

Figure 2.4: Commercially available glucose measurement systems: Contour Next One (Ascensia Diabetes Care, Basel, Switzerland), (2.4a), Dexcom G5 Mobile (Dexcom, San Diego, CA, USA), (2.4b).

Typically, BGSM requires pricking the finger pulp with a lancet to acquire a drop of capillary blood (1 μL is often sufficient) that is then applied onto a test strip. Glucose reacts with a special enzyme directly on the strip, that produces a certain amount of current proportional to the glucose concentration in the sample. This current can be measured within the device (Fig. 2.4a). According to various studies (e. g., Freckmann, Schmid, et al. 2012; Freckmann, Baumstark, et al. 2014), most glucometers fulfill the minimum system accuracy requirements of ISO 15197:2013 (International Organization for Standardization 2013). Despite the simple handling and precise measurement results, long-term tissue damage in the fingers could occur (Holt et al. 2010, Ch. 38). In addition, measurements are typically taken a few discrete times a day only, therefore, no information can be obtained about the time course of glucose concentration between the measurement points.

In recent years, developments have increasingly focused not only on non-invasive measurements alone but rather on extending them to provide continuous glucose monitoring (CGM). Minimally invasive sensors adapt the proven chemical principles of invasive blood glucose measurement to continuous glucose monitoring. The concentration is not measured in the blood but in the interstitial fluid (ISF) of the subcutaneous fat tissue. Theoretically, such glucose electrodes could also be used to measure the concentration in blood. In practice, however, this is not possible due to the mechanical and electrical stability of the sensor and the probability of infections (Thomas et al. 2006).

CGM devices consist of three main parts: a sensor that is applied to the skin, a transmitter directly attached to the sensor to send the measurement data, and a receiver as a user interface (Fig. 2.4b). The sensor is a flexible needle, which is injected into the subcutaneous tissue to measure glucose levels in the ISF. There, the same chemical reaction takes place as with the invasive techniques. The transmitter is fixed onto the skin and connected to the sensor by a thin wire. It receives the recordings from the sensor while the receiver processes and displays the measured data. The accuracy of CGM systems is typically reported as the mean absolute relative difference (MARD) compared to reference measurements. Acceptable errors for regulatory approval lie between ±20 % over the complete glucose range, which is much larger than for blood glucose sensors (compare to ISO 15197:2015 on page 13), (Gifford 2013).

Table 2.1: Physical methods for minimal-invasive measurement of glucose.

Technique	Description	Evaluation
Capillary puncture (BGSM)	Drop of blood from the fingertip, chemical evaluation using glucose-oxidase on test strips	+ Blood glucose + Precise – Interdependence with other sugars – Single-use sensor
Needle-type sensor (CGM)	Flexible needle inserted into subcutaneous tissue, measurements using glucose-oxidase within interstitial fluid	+ Quasi-continuous – Time lag compared to blood glucose – Daily calibration – Short product life
Reverse iontophoresis	Electric field on skin, fluid probe transdermal via electrophoresis, evaluation using glucose-oxidase	+ Non-invasive – Skin irritation – Interfering substance
Microdialysis	Subcutaneously implanted sensor is supplied with glucose in a dialysate	+ No contaminant – Complex setup by clinician – Sensor size – Short product life

The main drawback in the use of CGM as a substitute for blood glucose measurement is the physiologic time lag in the equilibration of glucose concentrations between blood and surrounding tissues due to diffusion processes (Rebrin, Steil, et al. 1999). At equilibrium, the concentration of subcutaneous glucose correlates with that in plasma. But during transient behavior glucose in the subcutaneous site is delayed within a range of $3 - 12$ min (Keenan et al. 2009). In some cases, delays of 45 min have been reported (Rebrin, Steil, et al. 1999). A second issue is the higher measurement error, possible drift, and degeneration of the sensor signal over time due to inflammatory responses of the body to the inserted needle within the interstitial fluid. These effects lower the accuracy of the CGM system which must be, therefore, calibrated against blood glucose values at certain time points, preferably when the glucose level is relatively stable, and steady-state equilibrium is reached between glucose concentrations in blood and ISF (Holt et al. 2010, p. 443).

However, developments over the last years have made considerable improvements (see e. g., Kovatchev, Gonder-Frederick, et al. 2004; W. L. Clarke, Anderson, Farhy, et al. 2005; Kovatchev, Anderson, et al. 2008; Freckmann, Pleus, et al. 2013; Damiano et al. 2014; Freckmann, Link, et al. 2018; Boscari et al. 2018) regarding the accuracy of devices, closed-loop approaches using CGM (Hovorka 2006; Russell 2008), or algorithms for modeling, simulation, and sensor calibration (Breton and Kovatchev 2008; Facchinetti et al. 2010; Acciaroli et al. 2018). Also, several randomized studies have shown benefits in glycemic control (Deiss et al. 2006; Laffel 2016; Beck et al. 2017).

Besides discrete glucose readings in the finger pulp or continuous measurements with a needle-type in the subcutaneous tissue, several other minimal-invasive techniques exist. This includes, among others, techniques such as reverse iontophoresis or microdialysis (Table 2.1).

Table 2.2: Physical methods for non-invasive measurement of glucose.

Technique	Excitation of tissue using	Determination of glucose level from
Absorption spectroscopy	Irradiation of infrared light	Spectrum of reflected light
Refractometry	Irradiation of light	Light scattering
Photoacoustic light spectroscopy	Irradiation of light	Sound waves due to periodic expansion of the skin
Impedance	Electromagnetic field	Electrical resistance at different frequencies
Fluorescence	Irradiation of light	Wavelength shift of a fluorescent substance
Polarization	Irradiation of polarized light	Change of angle of polarization
Raman scattering	Irradiation of monochromatic light	Frequency shift

Non-invasive Measurement Techniques. For patients under daily glucose monitoring, a non-invasive technique would not only eliminate painful fingertip measurements but also reduce the risk of infection and tissue damage caused by skin puncture. Most non-invasive techniques use physical principles that evaluate the interaction of glucose with supplied energy (radiation, heat, electromagnetic fields, etc.) for measuring concentration and thus, no material samples need to be taken (Table 2.2). New measurement techniques have to be evaluated against the performance achieved with conventional blood glucose devices, which have become the standard for diabetes therapy. From a metrological point of view, new systems must meet the following requirements: chemical or physical quantities that vary with a change in glucose concentration should be only specific to glucose and not to changes in other substances; readings should change linearly even with small changes in glucose concentration; accuracy should be within the range of conventional sensors (Thomas et al. 2006).

So far, however, no product has been able to enter the market that can compete with the precision of blood-based monitoring techniques. Research projects such as the Google Lens or a sensor developed by the Fraunhofer IMT to determine blood glucose levels from tear fluid have been discontinued for several reasons (Verily Life Sciences LLC 2018-11-16; Fraunhofer IMS 2012-09-03).

2.4 Diagnostic Tests and Classification of Diabetes

The following paragraphs briefly describe some common test procedures that are applied for the diagnosis of diabetes or to assess metabolic sensitivity in the human body. These tests provide specific functions as inputs to a dynamical system, typically step or impulse-shaped, and are accompanied by measurements of glucose or insulin concentrations, which can be regarded as the outputs of the system. Since these procedures are clinically relevant, the input and output signals could also serve as a benchmark in computational experiments or they could be used in a model identification procedure. However, they are only feasible in a clinical environment and at a considerable expense but they cannot be used by the patient himself or herself, making them unsuitable in a daily routine.

Oral Glucose Tolerance Test. The OGTT is a highly standardized clinical test for diagnosing hyperglycemia. A 75 g glucose bolus is given orally to the patient in a fasting state[4] and the rise in blood glucose concentration is measured at several points of time afterward. Typically, the 2-hour value is used for the classification of diabetes[5] (see Table 2.3 for thresholds). In the normal-glycemic subject, glucose levels will fall back to their nominal value after a certain time. In diabetic patients, however, the glucose level remains at a high level for a considerably long period.

Intravenous Glucose Tolerance Test. The IVGTT is, like the OGTT, also used to evaluate the pancreatic insulin secretion rate. Typically, a glucose bolus of $0.3\,\mathrm{g\,kg^{-1}}$ body weight is administered intravenously (i.v.), which causes a peak in insulin concentration. The test indirectly estimates the β-cell destruction and predicts T1DM (Holt et al. 2010, p. 145). Assessment of the IVGTT leads to the development of the so-called *minimal model* from which insulin sensitivity was estimated (Bergman, Ider, et al. 1979). Its first computational implementation can be found in Pacini and Bergman (1986), where glucose and insulin concentrations were frequently sampled (frequently sampled intravenous glucose tolerance test, FSIGT).

Insulin Modified Frequently Sampled Intravenous Glucose Tolerance Test. An extension of the FSIGT is the IMFSIGT used to increase the dynamics of plasma glucose and insulin in states of insufficient or absent endogenous insulin secretion. Therefore, in addition to an i.v. glucose bolus, an exogenously induced insulin peak by i.v. injection of insulin is introduced 20 min after the glucose bolus. The test allows for investigating the natural pancreatic response to a glucose impulse while neglecting the gastrointestinal tract. And second, to analyze pancreatic counter-reaction to a sudden drop in glucose concentration which should reduce insulin secretion rates. The test is becoming the recommended protocol to estimate insulin sensitivity within a wide variety of situations.

Insulin Infusion Test. The IIT is undertaken to examine the counter-regulation mechanisms of insulin-induced hypoglycemia. In contrast to the intravenous insulin tolerance test (IVITT), where a high insulin bolus is injected one-time, the continuous infusion of physiologic doses of insulin leads to a sustained, physiologic elevation of insulin concentrations and enables the investigation of changes in glucose kinetics and secretion of counter-regulatory hormones.

Hyperglycemic Clamp Test. The hyperglycemic clamp test is used to determine the release of insulin from the β-cells in response to a glucose concentration in plasma that is fixed and maintained at a hyperglycemic plateau for several hours. Therefore, glucose is given intravenously and its rate is adapted to compensate for increasing insulin release (DeFronzo et al. 1979). Through that, the

[4] Fasting is defined as no caloric intake for at least 8 h (International Diabetes Federation 2019, p. 12).

[5] The 2-hour postprandial glucose test should be performed using a glucose load containing the equivalent of 75 g anhydrous glucose dissolved in water (International Diabetes Federation 2019, p. 12).

Table 2.3: Recommended criteria for the diagnosis of diabetes and intermediate hyperglycemia (International Diabetes Federation 2019, p. 12).

	Diabetes	**Impaired glucose tolerance**	**Impaired fasting glucose**
Fasting plasma glucose	$\geq 126\,\mathrm{mg\,dL^{-1}}$	$< 126\,\mathrm{mg\,dL^{-1}}$	110 to 125 $\mathrm{mg\,dL^{-1}}$
	or	and	and if measured
2-hour plasma glucose	$\geq 200\,\mathrm{mg\,dL^{-1}}$	140 to 200 $\mathrm{mg\,dL^{-1}}$	$< 140\,\mathrm{mg\,dL^{-1}}$
	or		
HbA_{1c}	$\geq 6.5\,\%$		
	or		
Random glucose value	$> 200\,\mathrm{mg\,dL^{-1}}$		

biphasic insulin release becomes apparent. The first-phase is characterized by an acute increase in insulin release, followed by a slowly increasing second phase of a more sustainable insulin release (Holt et al. 2010, p. 163).

Euglycemic Hyperinsulinemic Glucose Clamp Test. This clamp test is the highest standard for determining insulin sensitivity. In this procedure an i.v. insulin bolus is administered and glucose is then infused to maintain euglycemia (Schatz 2006). From the glucose infusion rate, the insulin sensitivity is then calculated. The amount of given i.v. glucose corresponds to the amount of metabolized glucose by the body. The higher the intake of glucose while keeping the insulin infusion rate constant, the higher the sensitivity of the cells (DeFronzo et al. 1979).

Diagnosis. Diabetes is diagnosed by identifying chronic hyperglycemia. As described in Section 2.2.1, a lack of insulin, or the inability of cells to properly respond to it, leads to a high level of blood glucose (hyperglycemia), which is a clinical indicator of diabetes. Besides the main classification into type 1 and type 2 diabetes (Section 2.2), some risk factors such as impaired glucose tolerance (IGT)[6] or impaired fasting glucose (IFG)[7] were introduced since they are markers for an increased risk of developing diabetes. These factors became known as "intermediate hyperglycemia." Typically, the glucose concentration is determined when the patient is fasting or two hours after an OGTT (World Health Organization 2006). The threshold levels diagnosing diabetes and its risk factors are shown in Table 2.3.

2.5 Treatment of Diabetes

All forms of diabetes have in common that blood glucose levels cannot be lowered like in metabolically healthy people. Either because the pancreas is no longer able to produce insulin or because the body

[6] Postprandial glucose level is higher than normal but below the diagnostic cutoff.
[7] Fasting plasma glucose is above normal but below diagnostic criteria.

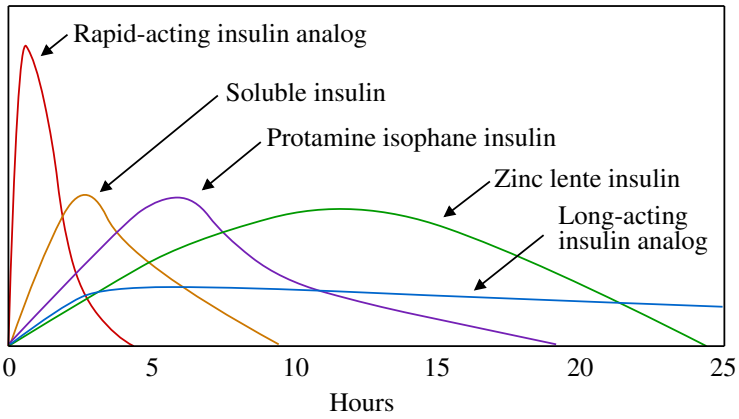

Figure 2.5: Time-action profiles of different insulin formulations (adapted from Holt et al. (2010, p. 430)).

cells have become insensitive to it. Insulin therapy attempts to compensate for this deficiency with artificially supplied insulin. While this is currently the only treatment option for T1DM, the therapy for people with type 2 diabetes is typically indicated when the blood glucose concentration does not reach the desired level despite a change in lifestyle and medication (e. g., oral anti-diabetics).

Insulin therapy aims to mimic physiological insulin secretion as far as possible by using both slow-acting insulin (basal) supplements to provide background control between meals, and rapid-acting insulin (bolus) which is given at mealtimes to compensate for postprandial glucose rises. This can be seen in the time-action profiles for different insulin formulations in Fig. 2.5. Exogenous insulin can be given through different routes:

- subcutaneous (s.c.)
- intravenous (i.v.)
- intraperitoneal (i.p.)
- intramuscular (i.m.)
- non-invasive routes, e. g., oral or nasal.

The preferred administration of insulin by patients is via subcutaneous injection, from where it diffuses into the circulatory system. This route is different from the way insulin is normally secreted by the pancreas and causes a time lag between injection and the effect of insulin on metabolic processes. The mechanisms of the absorption process are still not known exactly and are influenced by many variables. Besides the known differences in timing between different insulin preparations (rapid-acting, long-acting, etc.), the size of the dosage, the injected volume, and the insulin concentration are determinants of absorption speed (Binder et al. 1984; Chee and Fernando 2007, pp. 45–46). Fast and rapid-acting insulin analogs typically exhibit an onset of action in less than 30 min after s.c. injection (Schatz 2006, p. 174). Insulin amounts are typically expressed in “I.U.” (International Unit, in short, “U”), where 1 U contains 34.7 μg of insulin (Dt. Apotheker-Verl. 2014, insulin, human).

(a) Pen with exchangeable cartridge for manual insulin injection[a].

[a] https://de.wikipedia.org/wiki/Pen_(Spritze)

(b) Pump for automatic insulin delivery[a].

[a] https://de.wikipedia.org/wiki/Insulinpumpe

Figure 2.6: Commercially available pen NovoPen3 (Novo Nordisk, Bagsværd, Denmark) and pump Paradigm 511 (Medtronic Minimed, Northridge, CA, USA) for exogenous administration of insulin.

T1DM-Treatment. The following insulin treatment regimens are common, depending on the progress of the disorder and personal needs:

- Conventional insulin therapy (CT) is a treatment form easier to apply. Mostly, a combination of fast-acting and slow-acting insulin is injected a limited number of times a day by a pen (Fig. 2.6a). The amount and time of meals are fixed to the patient's needs. Due to the inflexible handling, nowadays it is only rarely used and if so only for specific groups. An advantage of this method, however, is, that a close-meshed blood glucose self-monitoring system is not necessary.
- Intensified conventional therapy (ICT, also called "basal-bolus-principle") is the standard therapy for type 1 diabetes. The goal of this approach is to keep the metabolic regulation close to normal. In order to carry out an intensified conventional insulin therapy, the patient must reliably manage blood glucose levels and insulin application, also using a pen. BGSM is an essential component of the ICT since only with knowledge of the current glucose value an insulin dose adjustment can be made. The patient's basal insulin requirement during fasting is achieved by injection of a long-acting insulin analog 1 or 2 times a day. At mealtimes, patients inject a suitable amount of a short-acting insulin analog. This so-called bolus insulin is calculated on the basis of the current blood glucose level, target range, and planned carbohydrate intake.
- Insulin pump therapy (CSII, continuous subcutaneous insulin infusion) is based on a continuous infusion of rapid-acting insulin into the subcutaneous tissue via a pump (Fig. 2.6b). Basal insulin requirements are programmed according to an individual injection profile. Insulin given at mealtime is manually applied as a bolus (like in the ICT). This therapy form is the most flexible since patients can adjust their basal rate and bolus according to their needs. It is technically complex and requires good self-assessment training and frequent blood glucose records. One extension to overcome the latter is continuous glucose measuring (CGM), where glucose concentration in the interstitial fluid is measured with a comparably high sampling rate. A connection between continuous glucose monitoring and continuous insulin delivery could be a step toward developing an artificial pancreas (Cobelli, Dalla Man, et al. 2009).

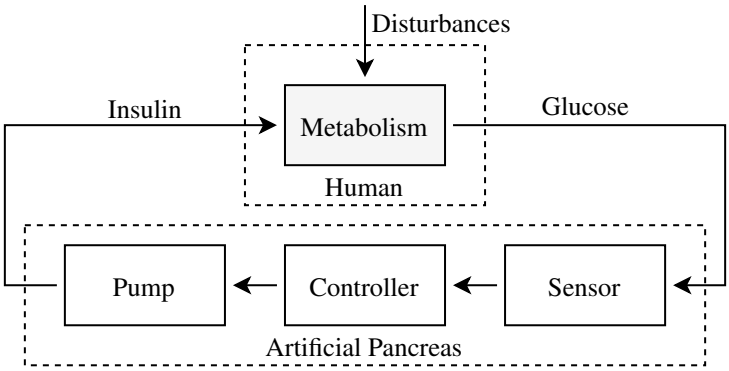

Figure 2.7: Scheme of a closed-loop approach: An artificial pancreas combines glucose sensor, insulin pump, and an algorithm to control the patient's metabolism.

T2DM-Treatment. In T2DM patients, the insulin treatment is, in principle, the same, even though the pancreas may be able to produce some insulin. Additional delivery of exogenous insulin can be used to control blood glucose levels. Several insulin regimens are available for patients who may already be treated with non-insulin-based therapies. These include once-daily injections of long-acting insulin, once-daily injections of long-acting insulin together with an injection of short-acting insulin with the main meal, twice-daily injections of insulin mixtures, or multiple-dose injections.

Closed-loop Control. The aforementioned glucose monitoring and insulin regimen can be seen as the open-loop in a control scheme (lower part in Fig. 2.7), in which the patient acts as the controller and makes decisions about when to measure glucose levels and how to interpret and react to that information. A closed-loop system integrates a continuous glucose monitor and an insulin pump, together with an algorithm that is capable of automatically adjusting insulin delivery in a physiological way as a replacement for the pancreas ("artificial pancreas", AP), see e. g. Hovorka, Chassin, Wilinska, et al. (2004), Bequette (2005), and Hovorka (2006).

Continuous glucose sensors measure glucose levels in the subcutaneous tissue. In the last years, considerable improvements have been made (Christiansen, Bailey, et al. 2013; Freckmann, Link, et al. 2018), but the main disadvantage remains sensor degeneration over time, so they have to be calibrated at certain time points (Acciaroli et al. 2018). Another drawback is the inherent physiological time lag between the concentration in blood and the subcutaneous space (Rebrin, Steil, et al. 1999).

Insulin pumps consist of an insulin reservoir and a catheter to continuously administer small amounts of insulin into the subcutaneous tissue. They have been shown to reduce the risk of hypoglycemia and intensify glycemic control (Pickup et al. 2002; Holt et al. 2010, pp. 440–442).

Control algorithms would remove the patient from the decision loop. The inputs to the controller are mainly current and target glucose levels. The output is the required amount of insulin. First algorithms were designed to turn off insulin delivery to prevent hypoglycemia (Marchetti et al. 2008; Buckingham et al. 2009). Modern approaches often use mathematical models (Oviedo et al. 2017) for controller

design or to estimate the "metabolic state" of the patient (e. g., Parker et al. 1999; Hajizadeh et al. 2017) and apply model predictive control (MPC) to determine insulin amounts (Lynch et al. 2002; Hovorka, Canonico, et al. 2004; Chee and Fernando 2007; K. Lunze et al. 2013; Messori et al. 2018). Control approaches may benefit from personalized blood glucose prediction strategies as investigated in this work (Chapter 6). Additionally, bi-hormonal closed-loop systems deliver both insulin and glucagon for glucose control (El-Khatib, Jiang, and Damiano 2009; El-Khatib, Russell, et al. 2010).

Clinical trials are limited in number, have to follow strict ethical guidelines, and must ensure permanent monitoring of patients (Chee, Fernando, and van Heerden 2003; W. L. Clarke, Anderson, Breton, et al. 2009; Elleri et al. 2011; Russell et al. 2016). To overcome these restrictions, the performance of a closed-loop system is often evaluated in virtual clinical studies, so-called *in-silico* trials (L. Magni et al. 2007; Kovatchev, Raimondo, et al. 2008; Messori et al. 2018). Animal studies are an alternative, e. g., in diabetic swine (El-Khatib, Jiang, and Damiano 2007; K. Lunze 2014). For many diabetics, however, technological developments are not accessible. Slow commercialization, overpricing, or lack of interoperability are only a few factors that have led to the emergence of do-it-yourself AP solutions with openly shared algorithms (Asarani et al. 2020; Kesavadev et al. 2020).

2.6 Glucose Monitoring as an Integral Part of Diabetes Self-Management

Besides proper patient training, the prognosis of diabetes relies to a large extent on the attitudes and behavior of the patient's self-care. Modern treatment concepts are committed to self-management and empowerment approaches. The aim is to enable patients to cope with the disease-specific requirements and integrate them into their daily lifestyle. The major interest is adequate glucose control which may result in the reduction of hypoglycemia and other complications associated with diabetes. Insulin treatment decisions are mainly made on the basis of the patient's current blood glucose levels and self-assessment. Technological advances in continuous glucose monitoring and continuous subcutaneous insulin infusion may contribute to safer and improved therapy management (Georga et al. 2014).

While it was common practice to note down blood glucose values by hand, together with meals and insulin administrations, to derive recommendations for treatment in consultation with a physician, now, electronic and mobile solutions are the standard today – especially for younger and technologically interested patients. Various concepts and (mobile) applications (*mHealth*) exist to track glucose measurements, medication, and diet. Especially with the introduction of continuous glucose meters, it has become possible to effectively record glucose time courses, which enables immediate treatment decisions. Nevertheless, collecting and processing measurements is only one part of the process. Another critical part involves delivering the collected data to specialists or caregivers in charge (Lanzola et al. 2016). Finally, it is crucial to support the patient in the decision-making process. This can be achieved by e. g., a warning system for out-of-range glucose levels or advice on calculating the proper amount of insulin depending on diet and physical activity.

3 State-of-the-Art

3.1 Modeling Glucose Regulation

Over the past four decades, numerous models describing glucose regulation in humans have been developed. They can be roughly classified into physiological models (or knowledge-based) and empirical models (also called data-driven).

Physiological approaches try to model and identify the underlying biomedical processes that are involved in glucose metabolism. They require detailed *a priori* knowledge about physiology, acquired in clinical trials. They are mainly used for simulation studies, e. g., to predict blood glucose or the concentration of other substances in a kind of "virtual experiment." Typically, these models are structured into further sub-models, which in turn describe certain aspects of physiology. This can be, e. g., the digestion of ingested carbohydrates, the distribution of subcutaneously administered insulin, or parts related to physical activity. The major limitation of this approach is the large number of physiological parameters that have to be determined by measurements and identification procedures.

Data-driven models rely only on the input-output data without considering any physiological knowledge. These approaches have attracted increasing attention since the introduction of subcutaneous glucose sensors has made continuous measurement data available for the first time. Information contained in CGM measurements, insulin treatment data, or food content are typical inputs to data-driven models, supported by machine learning techniques like time series models, fuzzy logic, Gaussian mixture models, support vector machines, or artificial neuronal nets. The output is often the blood glucose concentration. Models of this type are usually simply structured and can be therefore identified in a short time with only a few parameters describing the major behavior. However, these approaches cannot provide any insights into physiology or relate specific outcomes to tissues or organs.

A combination of knowledge-based and data-driven approaches are hybrid models that rely on physiological descriptions of parts of the whole system as well as on learning input-output relationships to predict blood glucose values. Typically, models of meal and insulin absorption are physiologically motivated as they enrich the overall prediction accuracy of the data approach (Oviedo et al. 2017).

In the following, only physiological models are further examined. Comprehensive overviews on recent developments for data-driven modeling approaches can be found in, e. g., Cobelli, Dalla Man, et al. (2009), Balakrishnan, Rangaiah, et al. (2011), Marmarelis (2014), and Oviedo et al. (2017).

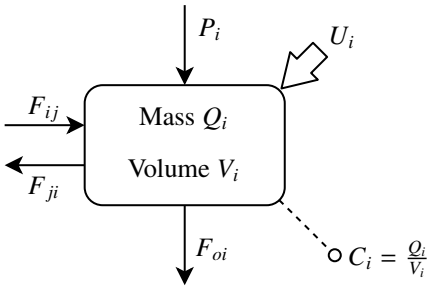

Figure 3.1: A general compartment, i, its input and output fluxes, and measurement of concentration.

Physiological models are typically described by a set of interconnected compartments. A compartment is a quantity of material assumed to be well-mixed, i. e., no concentration gradient, and kinetically homogeneous. Interconnections between compartments represent material fluxes from one location in the body to another or a chemical transformation (Carson et al. 2014). This technique is widely used in pharmacokinetics to describe the overall processes a drug undergoes in the body. A general representation is shown in Fig. 3.1, where Q_i denotes the mass and V_i the volume of the i-th compartment in an n-compartment model.

Arrows represent fluxes into and out of the compartment, where P_i is the endogenous production and U_i an exogenous input, F_{ij} and F_{ji} denote fluxes from or to other compartments, respectively, and F_{oi} is the flux to the environment and thus, out of the system. In general, the mass balance equation for each compartment can be written as

$$\dot{Q}_i = \sum_{\substack{j=1 \\ i \neq j}}^{n} F_{ij}(t) - \sum_{\substack{j=1 \\ i \neq j}}^{n} F_{ji}(t) - F_{oi}(t) + P_i(t) + U_i(t), \quad i = 1 \ldots n. \tag{3.1}$$

For linear relationships in $F_{ij}(t)$ equation (3.1) can be rewritten to

$$\dot{Q}_i = \sum_{\substack{j=1 \\ i \neq j}}^{n} k_{ij} Q_j(t) - \sum_{\substack{j=1 \\ i \neq j}}^{n} k_{ji} Q_i(t) - k_{oi} Q_i(t) + P_i(t) + U_i(t), \quad i = 1 \ldots n, \tag{3.2}$$

where k_{ij} and k_{ji} are constant transfer coefficients expressing a chain of first-order lag elements. The coefficients can also be functions of any Q, which allows control of the fluxes by other compartments, e. g., by Michaelis-Menten kinetics.

If a compartment is accessible to measurements, the concentration C_i is expressed by

$$C_i = \frac{Q_i}{V_i}. \tag{3.3}$$

Physiological modeling tries to find the most parsimonious model approach that is able to describe experimental findings. Therefore, data from clinical trials using standardized tests are fulfilled as described in Section 2.4. From that, concentrations of desired substances are measured. The next

step is to identify successively models and verify whether they can describe the measurement series well enough, beginning with the most parsimonious approach, e. g., one compartment, linear, and time-invariant. If the model is not suitable, a different or more complex modeling approach must be chosen, involving more physiological knowledge. Each of the system models is then tested for parameter identifiability and is subsequently numerically identified from experimental data. This concept has been applied in many different studies, e. g., starting with glucose and insulin regulation after intravenous glucose injection (Bolie 1961; Bergman, Phillips, et al. 1981; Toffolo and Cobelli 2003), oral glucose tolerance tests (Ackerman et al. 1964; Cretti et al. 2001; Natalucci et al. 2003), meal intake (Worthington 1997; Dalla Man, Caumo, et al. 2002), the kinetics of insulin (Sherwin et al. 1974; Toffolo, Bergman, et al. 1980) or glucagon (Lv et al. 2013; Emami et al. 2017), or subcutaneous administration of insulin (Nucci et al. 2000; Wong et al. 2008).

The so-called *minimal* models represent the key physiological components of a system making suitable assumptions and simplifications about the behavior on a larger scale. A low model order with only a few parameters to estimate from experimental data allows the quantification of specific metabolic relationships. In contrast, *maximal* models are built attempting to represent a comprehensive description of the metabolic regulation in detail leading to high-order, nonlinear models with often larger numbers of parameters. These models are, in general, not identifiable from a single experimental trial, but useful for simulations, also called *in silico* trials. Large-scale models can serve as a substitute for clinical studies, as it is often not possible, convenient, or appropriate to perform experiments *in vivo*. A good illustration of the application of the models is, for example, the assessment of new insulin treatment methods or the design and testing of closed-loop control algorithms (e. g., J. T. Sorensen 1985; Andreassen et al. 1994; Hovorka, Canonico, et al. 2004).

The structure and parameters of minimal models are typically determined by measurement data obtained in clinical trials following a predefined experimental design. Thus, these models, and also the conclusions drawn by them, are only valid for this particular kind of investigation. For example, a minimal model derived from an IVGTT can have another topology and altered parameter values than a model derived from an OGTT or meal input because the gastrointestinal tract and meal compositions must be considered. Maximal models, on the other hand, usually represent only averages of the population. Statements for a single individual are difficult.

Besides that, several studies can be found in the literature, that aim at predicting blood glucose from which some are extensions of the classic minimal model and some propose other modeling approaches (Table 3.1). Widely used models are the (extended) Bergman's minimal model (Bergman, Phillips, et al. 1981) and the model from Hovorka, Chassin, Wilinska, et al. (2004), which is common in model predictive control (MPC). Furthermore, the UVA/Padova working group offers a meal simulation model as a toolbox (Dalla Man, Raimondo, et al. 2007; Dalla Man, Micheletto, et al. 2014), so it is easy to implement for simulation studies and controller design. J. T. Sorensen (1985) developed a full-body model that comprises glucose, insulin, and glucagon regulation. A comprehensive collection of prediction strategies for type 1 diabetics is given in, e. g., Balakrishnan, Rangaiah, et al. (2011).

Table 3.1: Selection of physiological-based modeling approaches to predict glucose metabolism.

Reference	Model type
Bergman, Ider, et al. (1979)	Classic minimal model
J. T. Sorensen (1985)	Full body physiological model for T1DM
Fisher (1991)	Minimal model for T1DM
Lehmann et al. (1992)	Glucose and insulin regulation in T1DM for education
Caumo and Cobelli (1993)	New minimal model using IVGTT data
Balakrishnan, Samavedham, et al. (2014)	Personalized hybrid model for T1DM
Wilinska et al. (2010)	Simulation environment of closed-loop insulin delivery systems for T1DM
Hovorka, Canonico, et al. (2004)	Nonlinear model for T1DM used in MPC design
Eberle et al. (2012b)	Extended Bergman model
Dalla Man, Rizza, et al. (2007)	Meal simulation model for TNDM and T2DM
Dalla Man, Micheletto, et al. (2014)	UVA/Padova T1DM Simulator
Zavitsanou (2014)	Framework for blood glucose control and optimization

The following paragraphs briefly describe some advancements in model building related to glucose-insulin-glucagon metabolism.

Insulin Secretion and Kinetics. Insulin is the only glucose-lowering hormone. It stimulates glucose uptake in the peripheral tissues and inhibits glucose production in the liver. From clinical trials, insulin secretion in the pancreas is assumed to be biphasic, with a short first phase lasting about 5 min and a following prolonged second phase. In Toffolo, Bergman, et al. (1980), several models have been identified to quantitatively estimate β-cell sensitivity to glucose in healthy organisms. There, the superior model describes insulin secretion by a linear function of time and by the difference in glucose levels relative to a threshold value. This approach has also been used in Bergman's minimal model (Bergman, Phillips, et al. 1981).

Insulin is secreted into the portal vein and enters the liver, where approx. 50 % of the total amount is extracted. Thus, modeling insulin secretion must consider this effect. The problem can be assessed by measuring C-peptide concentrations from which insulin levels can be estimated (Eaton et al. 1980). Modeling pancreatic secretion must take into account C-peptide kinetics and the biphasic pattern (Ferrannini and Cobelli 1987b; Toffolo, Grandi, et al. 1995) as depicted in Fig. 3.2. There, the insulin secretion rate (ISR) is modeled by a combination of a fast insulin release from a pool F, which depends on the rate of increase of glucose, and a delayed second phase, which depends on the difference between current glucose levels and a threshold. The model was originally identified using an IVGTT and modified to match insulin kinetics after an OGTT or meal (Breda et al. 2001) since oral glucose absorption is slower due to digestion processes. The insulin secretion model was further refined using an up-and-down glucose infusion test (Toffolo, Breda, et al. 2001).

Insulin kinetics have been described by a multi-compartment approach, taking into account insulin concentrations in the liver, plasma, and extra-cellular space. From that, estimates of the hepatic extraction are possible (Sherwin et al. 1974; Ferrannini and Cobelli 1987b; Piccinini et al. 2016).

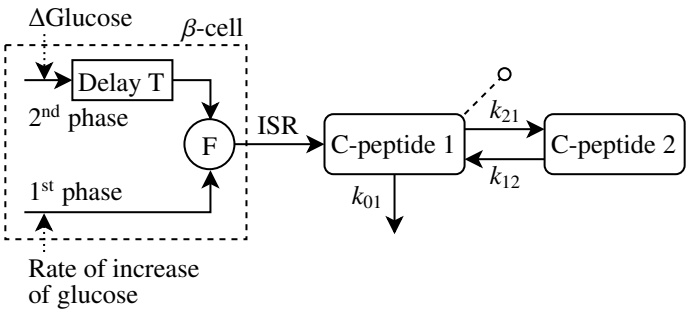

Figure 3.2: IVGTT C-peptide insulin secretion minimal model (adapted from Toffolo, Grandi, et al. (1995)).

Glucose Kinetics. In diabetic subjects, the ability to properly react to an elevated glucose concentration is impaired due to reduced insulin sensitivity. To quantify this influence, extensive experiments had to be carried out to observe interactions of glucose and insulin under varying situations using clamp techniques or tracers (Sherwin et al. 1974; Insel et al. 1975). These tests are invasive and not applicable to patients in a clinical routine. Thus, one aim in developing minimal models was to estimate insulin sensitivity from only a few samples of glucose and insulin after a system perturbation. Therefore, applying a mathematical model would be less invasive than other methods.

In one of the first works on the balance of glucose and insulin during glucose injection, a linearized model was used to numerically determine the coefficients of glucose regulation in normal subjects from experimental data (Bolie 1961). The linear relationship between glucose and insulin is given by

$$\dot{G}(t) = -p_1 G(t) - p_2 I(t) + u_{\mathrm{G}}^{\mathrm{iv}}(t), \tag{3.4}$$

$$\dot{I}(t) = -p_3 I(t) + p_4 G(t), \tag{3.5}$$

where $G(t)$ and $I(t)$ denote deviations of glucose and insulin concentrations from their basal values, $u_{\mathrm{G}}^{\mathrm{iv}}(t)$ is the intravenous glucose injection, and parameters $p_1, \ldots, p_4$ define rate constants that were determined experimentally. It can be seen that glucose disappearance is proportional to both $G(t)$ and $I(t)$ and that insulin secretion is stimulated by glucose and inhibited by insulin levels. The model covers the main assumptions about glucose-insulin regulation. It was uniquely identifiable but too simplistic to adequately represent the nonlinear interactions of hepatic glucose production and uptake by glucose and insulin. Nevertheless, the model has been widely used in conjunction with intravenous injections (Segre et al. 1973) and with oral glucose tests (Ackerman et al. 1964) in different metabolic situations.

Bergman, Ider, et al. (1979) first described a nonlinear mathematical model able to estimate the time course of glucose and insulin sensitivity from a single glucose injection using system decomposition (Bergman and Cobelli 1980). Model-based system decomposition enables to modeling different subsystems independently from each other by using measurements of glucose and insulin as input and output to a subsystem, and vice versa for another subsystem, thus reducing difficulties in modeling.

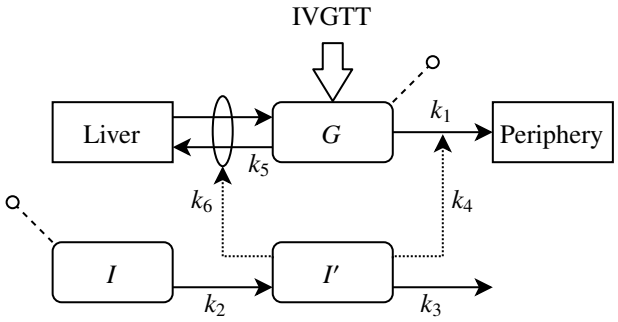

Figure 3.3: IVGTT minimal model consisting of accessible compartments of glucose and insulin, G respectively I, and a remote insulin pool I' (adapted from Bergman, Ider, et al. (1979)). Solid and dashed lines denote fluxes and control signals, respectively.

The model consists of three compartments, one each for glucose and insulin in plasma and one for remote insulin, i. e., for the first time considering that insulin action on glucose does not occur in plasma but in a compartment remote from it. That was experimentally proven to be the interstitial fluid (Bergman 1989). From the mass balance (Fig. 3.3), the following equations can be derived:

$$\dot{G}(t) = -(k_1 + k_5)G(t) - (k_4 + k_6)I'(t)G(t) + B_0 + u_{\mathrm{G}}^{\mathrm{iv}}(t) \qquad G(0) = G^{\mathrm{b}}, \tag{3.6}$$

$$\dot{I}'(t) = -k_3 I'(t) + k_2(I(t) - I^{\mathrm{b}}) \qquad I'(0) = 0, \tag{3.7}$$

where $G(t)$ and $I(t)$ denote the concentrations of glucose and insulin in plasma, respectively, G^{b} and I^{b} are their basal values, and $I'(t)$ is the insulin concentration (deviation from basal) remote from plasma. Parameters $k_1, \ldots, k_6$ are constants and B_0 is the net hepatic glucose balance at zero glucose. The rate of change of glucose depends on the net hepatic glucose balance (Bergman and Bucolo 1974) and the glucose uptake by peripheral tissues, both directly dependent on the concentration of insulin in $I'(t)$, that enters the remote compartment from plasma. This model was only identifiable after a reparametrization with $X(t) = (k_4 + k_6)I'(t)$, $p_1 = k_1 + k_5$, $p_2 = k_3$, $p_3 = k_2(k_4 + k_6)$ leading to the form given by Eqs. (3.8) and (3.9).

Taking into account a minimal model of insulin kinetics leads to the common representation:

$$\dot{G}(t) = -\left(p_1 + X\right)G(t) + p_1 G^{\mathrm{b}} + u_{\mathrm{G}}^{\mathrm{iv}}(t) \qquad G(0) = G^{\mathrm{b}}, \tag{3.8}$$

$$\dot{X}(t) = -p_2 X(t) + p_3(I(t) - I^{\mathrm{b}}) \qquad X(0) = 0, \tag{3.9}$$

$$\dot{I}(t) = -n(I(t) - I^{\mathrm{b}}) + \max\left[0, \gamma(G(t) - h)t\right], \quad t \geq t_0 \qquad I(0) = I^{\mathrm{b}}, \tag{3.10}$$

(Bergman, Phillips, et al. 1981), where $G(t)$, $I(t)$, G^{b}, and I^{b} are as defined above. State $X(t)$ is the insulin action on glucose. The increase of insulin is proportional to the degree of glucose exceeding the threshold h, and n is the time constant for insulin disappearance.

Fisher (1991) modified Bergman's model to also handle diabetic subjects by replacing the natural pancreatic secretion rate with an intravenous insulin infusion.

All approaches are based on the intravenous injection of glucose or insulin, i. e., the substances are immediately apparent in the blood. Other physiological modeling approaches depend on the oral administration of glucose and must therefore take into account its delayed appearance in the blood. Oral minimal models couple the minimal model from (3.8)-(3.10) with a description of the rate of appearance of glucose R_G (Caumo, Bergman, et al. 2000). R_G can be determined by either a piecewise linear function or by measuring labeled glucose (allowing to distinguish between exogenous and endogenous glucose (R. Basu et al. 2003)) and estimate R_G from that (Dalla Man, Caumo, et al. 2002; Dalla Man 2005b). Validation of the oral minimal model (OMM) was fulfilled using a tracer protocol (R. Basu et al. 2003) or clamp-technique (DeFronzo et al. 1979; Dalla Man 2005a). From these insights, a system model of oral glucose absorption could be derived (Dalla Man, Camilleri, et al. 2006; Dalla Man, Rizza, et al. 2006). Furthermore, labeled glucose absorption models allow the assessment of time courses of endogenous glucose production (EGP) in the liver[1] (Dalla Man, Toffolo, et al. 2008), which is essential in maintaining blood glucose concentration in the absence of meals.

Glucagon Secretion and Kinetics. Glucagon, also secreted from the pancreas, is the counter-regulating hormone to insulin and has a major role in maintaining glucose concentration during fasting by stimulating hepatic glucose production. After an increased focus on glucagon-related clinical trials (Gerich, Lorenzi, et al. 1975; Cherrington et al. 1976; Unger and Orci 1976), the first models of glucagon secretion in healthy and diabetic subjects have been proposed, differing in the input signals (oral glucose administration or insulin infusion). Model simulations suggested that glucagon is important under conditions when blood glucose levels are lower than $50\,\mathrm{mg\,dL^{-1}}$ and that it is responsible for a rapid recovery from hypoglycemia (Celeste et al. 1978). J. T. Sorensen (1985) presented a full-body model also incorporating glucagon kinetics and verification with data from the literature. Many clinical studies have investigated glucagon in various scenarios like in a fasting state, under hypoglycemia, or during glucose intake (Saccà et al. 1979; Meier, Kjems, et al. 2006; Aronoff et al. 2004; Gylfe et al. 2014). Dobbins et al. (1995) proposed a one-compartment linear model to describe glucagon kinetics in plasma and Farhy et al. (2010) developed a pulsatile model of glucagon secretion that is consistent with most *in vivo* experimental data for the insulin-deficient pancreas. Another point to consider is the glucagon action on hepatic glucose production. Several mathematical models for type 1 diabetics have been compared that try to predict this effect from experimental data using multiple subcutaneous glucagon boluses (Emami et al. 2017). A model of glucagon secretion proposed in Dalla Man, Micheletto, et al. (2014) is also stated in Visentin et al. (2018) and Breton, Kovatchev, et al. (2015) using different notations, but no further reference is given. Their model is based on a similar approach to that of insulin secretion. It describes glucagon appearance in plasma by one component proportional to the rate of decrease of glucose concentration in blood and by one component considering the difference of glucose levels to a threshold value. Regardless, glucagon regulation and its interaction with other hormones is still not well understood and only a few mathematical models exist.

[1] Both terms, hepatic and endogenous glucose production are used interchangeably.

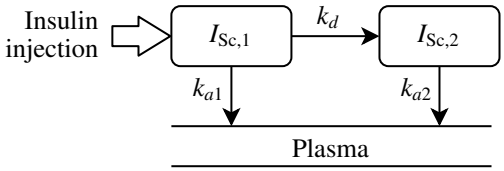

Figure 3.4: Example of a two-compartment model of insulin diffusion within the subcutaneous space.

Subcutaneous Space. Insulin treatment is essential for diabetics to maintain their glucose regulation and thus, to avoid both, long-term hyperglycemia and the risk of hypoglycemia. Since insulin is mainly administered through the subcutaneous space, understanding how insulin is absorbed and enters the circulatory system can significantly improve the treatment regimen. The absorption and distribution processes are subject to many influential factors like different preparations and dose sizes, blood flow, or the injection site and depth (Binder 1969; Lepore et al. 2000). The first works stated that insulin diffusion and absorption can not be described by only a first-order system and that absorption curves highly depend on the volume and concentration of the given insulin (Mosekilde et al. 1989). Over time, different models have been proposed, from one-compartment models to distributed-parameter specifications and empirical descriptions (Kobayashi et al. 1983; Kraegen et al. 1984; Nucci et al. 2000; Wong et al. 2008). An example of a two-compartment model describing insulin injection and the dissolution of nonmonomeric ($I_{Sc,1}$) and monomeric ($I_{Sc,2}$) components into the blood plasma is shown in Fig. 3.4, where parameters k_{a1}, k_{a2}, and k_d are rate constants.

In recent years, subcutaneous glucagon administration has gained increased attention, due to its feasible application in a bihormonal closed-loop trial (El-Khatib, Jiang, and Damiano 2007; El-Khatib, Jiang, and Damiano 2009). Pharmacodynamics of subcutaneously infused glucagon has been investigated by, e. g., El-Khatib, Jiang, Gerrity, et al. (2007) and Blauw et al. (2016). Furthermore, different model structures describing glucagon absorption have been compared (Lv et al. 2013), most similar to those applied for insulin administration.

With the development of CGM devices, it became possible to observe the time course of glucose with a comparatively high temporal resolution. However, since these measurements are no longer made in the plasma but in the surrounding subcutaneous interstitial fluid (ISF), detailed knowledge of the distribution of glucose, from plasma into the periphery, is necessary to interpret the measured data correctly (Kovatchev, W. L. Clarke, et al. 2005). Clinical trials show improved glycemic control using CGM (Deiss et al. 2006; Girardin et al. 2009; Beck et al. 2017). First depicted by Rebrin, Steil, et al. (1999) and Rebrin and Steil (2000), CGM takes place in the ISF between the capillary blood system and glucose-consuming tissues like muscles and fat. Thus, ISF glucose concentration equilibrates with a time lag due to diffusion processes from one tissue to another. This model approach has been under discussion but is widely accepted (Kovatchev, King, et al. 2006; Keenan et al. 2009; Cobelli, Schiavon, et al. 2016). Due to the physiological time lag, continuous measurements are more difficult to interpret, especially at large glucose gradients. Hence, new statistical tools and analytical methods must be developed (W. L. Clarke and Kovatchev 2009).

3.2 Sensitivity Analysis

Sensitivity analysis (SA) can be used to systematically investigate a model response to a perturbation of its input factors, which can be related to the model's inputs and also its parameters.

While technical systems can be disassembled to a certain extent to investigate components in detail, this is not easily possible in biology or systems medicine. Measuring *in vivo* is associated with high effort and parameter values are estimated from experimental data by model fitting. In addition to measurement errors, a high number of unknown influential variables also leads to considerable uncertainty regarding system understanding. For a successful application of models, however, detailed knowledge about model parameters and their influence on the model output is crucial (Saltelli, Tarantola, and Campolongo 2000). SA provides a possible method to quantify the influence of input factors on the model behavior. It is widely used in technical applications, but its popularity is also growing in biology, systems medicine, and environmental sciences.

Depending on the specific objective and application area, the methods vary considerably. One can distinguish between different types of sensitivity analysis. For example, local and global SA, quantitative vs. qualitative examination, or how samples of input factors are generated. Local methods take into account the deflection of one factor at a time around a nominal value set. In contrast, global methods allow the variation of all input factors at a time over the full input space using a suitable sampling scheme. A methodological overview is given by Saltelli, K. Chan, et al. (2000).

For models with complex input-output behavior, sensitivity indices cannot be calculated analytically. Thus, they are approximated by samples of input factors and the related model outcome. The sampling strategy determines how concrete values of the input factors are determined from the input space. It also specifies whether only one parameter or all parameters are varied simultaneously at a time. With the latter, statements about interacting factors are also possible. However, this typically leads to more model evaluations that must be carried out and therefore to a higher computational effort.

All methods have in common that the model output must be summarized to a single scalar quantity. This can be the maximum value of a concentration or the error between simulation and experimental data. Often, however, it is necessary to explicitly take into account progressions over time. How to extend existing techniques is explained in more detail in Section 5.1.3.

There are only limited studies about sensitivity analysis in the field of diabetes or glucose-insulin metabolism on system level (Radomski et al. 2019; Pistikopoulos et al. 2018). One of the early works by Geevan et al. (1990) used a derivative-based SA for a nonlinear model that incorporated beta-cell kinetics and a gastrointestinal absorption term into a glucose-insulin feedback system. More studies are available for models of signaling pathways (Sumner 2010). An interesting relation between steady-state sensitivity analysis and cross Gramians (Section 3.3.1) in systems biology as a concept of state observability has been drawn by Streif et al. (2006). More general reviews on SA and recent advances can be found in Saltelli, Ratto, et al. (2005), Borgonovo et al. (2016), and Iooss et al. (2015).

In the following paragraphs, a short review of broad classes of sensitivity analysis techniques is given following the classification scheme in Pianosi et al. (2016).

Derivative Methods. Derivative methods are local SA techniques that assess the influence of input factors around the nominal point of the model, typically by the partial derivatives of the output to the respective input factors. If an analytical solution is not feasible, e. g., the function is not differentiable at certain points, a numerical solution must be found. The partial derivatives can be approximated by the finite differences

$$S_i(\bar{\boldsymbol{X}}) \approx \frac{f\left(\bar{X}_1, \ldots, \bar{X}_i + \Delta_i, \ldots, \bar{X}_K\right) - f\left(\bar{X}_1, \ldots, \bar{X}_i, \ldots, \bar{X}_K\right)}{\Delta_i}, \tag{3.11}$$

where K is the number of input factors. The model is evaluated at its nominal point $\bar{\boldsymbol{X}}$ and at some perturbed value of each parameter $\bar{X}_i + \Delta_i$, where Δ_i is a suitable variation of the i-th input factor.

For K input factors, this method requires at least $K + 1$ model evaluations and is therefore computationally cheap. It is well suited for models that require a lot of computing time or if many input factors have to be investigated. However, the method has some limitations. First, it only provides information about local sensitivities, but in biological systems, parameters often vary over a large range (Marino et al. 2008), which cannot be captured by linear approximation. Second, only one parameter at a time is considered, while all other parameters are fixed at their nominal values. Hence, it is not possible to investigate interactions between parameters as it is often needed (van Riel 2006). These drawbacks can be addressed through generalized techniques or global sensitivity analysis.

Multiple-starts Methods. The derivative technique described above can be globally extended if each sensitivity is computed starting from multiple points within the input space. A global sensitivity measure can then be obtained by aggregating these individual sensitivities. One of the most common techniques is the so-called Elementary Effects Test (EET) first described by Morris (1991) and improved by Campolongo, Cariboni, et al. (2007). The finite differences in (3.11) are also called elementary effects (EEs). They are computed at r arbitrary chosen grid points for each factor and averaged according to $\mu_i^\star$:

$$\begin{aligned} \mu_i^\star &= \frac{1}{r} \sum_{j=1}^{r} \left| EE_i^{(j)} \right| \\ &= \frac{1}{r} \sum_{j=1}^{r} \left| \frac{f\left(\bar{X}_1^{(j)}, \ldots, \bar{X}_i^{(j)} + \Delta_i^{(j)}, \ldots, \bar{X}_K^{(j)}\right) - f\left(\bar{X}_1^{(j)}, \ldots, \bar{X}_i^{(j)}, \ldots, \bar{X}_K^{(j)}\right)}{\Delta_i^{(j)}} \right|. \end{aligned} \tag{3.12}$$

Thus, it is a measure of the influence of the i-th input factor on the output, where larger values indicate a higher contribution. In addition to the mean value, the standard deviation of the EEs can also be taken into account. It provides information on the degree of interaction of the i-th factor with others.

Different types of sampling strategies have been proposed to select the points $\boldsymbol{X}^{(j)}$, $j = 1, \ldots, r$. Morris (1991) originally created r trajectories of $K + 1$ points, randomly chosen over a uniform grid. This setup allows rather high perturbation of the input factors with only a limited set of evaluations but can produce misleading effects if the model f is highly nonlinear and the perturbation Δ_i is not well chosen. The sampling strategy can be improved using Latin Hypercube Sampling (LHS) method first introduced by McKay et al. (1979). In contrast to simple random sampling, LHS guarantees that the entire range of each factor is representative of the real variability. Campolongo, Saltelli, and Cariboni (2011) proposed a radial-based design, where the finite differences Δ_i all start from the same randomly chosen point in the input space.

All techniques have in common the same number of model evaluations, $r(K + 1)$, which is far lower than for global approaches. Therefore, EET can be used as a screening method to investigate models with many input factors. This means that inputs declared as non-influential are unlikely to be identified as influential by another method. It is also suitable to prune the number of factors before applying a global sensitivity analysis method (Saltelli 2008).

Correlation or Sampling-based Analysis Methods. Sampling-based SA relies on the statistical analysis of the input-output mappings of a model generated by Monte Carlo (MC) simulations. These simulations are based on a large number of model evaluations using random or pseudo-random input samples. The deviations in the model outputs depend on the uncertainty in the input factors, and sensitivity analysis refers to the determination of the contributions of individual uncertain inputs to the uncertainty in the results. According to Saltelli, K. Chan, et al. (2000) or Helton et al. (2006) sampling-based approaches involve several main steps:

1. Define the input variability space that characterizes the uncertainties in the input factors. This includes the range of values as well as their distribution.
2. Generate a set of n samples according to the problem structure and the number of input factors using a proper sampling strategy.
3. Evaluate the model for each input sample. This returns a set of scalar model outputs $y_j = f(\boldsymbol{X}), j = 1, \ldots, n$. It also includes checking for proper model behavior to filter out samples that may lead to unacceptable outputs.
4. Post-processing includes visualization of the results, quantification of the sensitivity indices, and evaluation of robustness and convergence.

In contrast to local SA where only one factor at a time is perturbed (OAT-sampling), sampling-based SA can use, in principle, any random or pseudo-random sampling strategy. This usually follows a factorial design scheme widely called AAT-sampling (All-[factors]-At-a-Time). One main issue is the large number of model evaluations that must be fulfilled to ensure that the whole input space is sampled appropriately. Therefore, the most common method is the LHS which was shown to be more efficient than random sampling (Saltelli 2008).

Typically, the model output is a scalar. Then, the overall uncertainty can be described by its mean and variance. This can be accomplished by plotting the probability density function (PDF) or the cumulative distribution function (CDF) of the output (Iman et al. 1988; Saltelli and Marivoet 1990). If the model output is not a scalar, one can try to define a set of scalar features, like some aggregate statistic or the model performance compared to measurements, and investigate the sensitivities from these derived outputs. If the output is a function of time, sensitivities can be calculated at particular time points of interest, which results in time-varying sensitivity indices (Zheng et al. 2006; Marino et al. 2008). They can be integrated over time to find the most influential input factors.

Variance-based Methods. Variance-based sensitivity analysis (VBSA) is a class of global sensitivity analysis (GSA) techniques where input factors are treated as stochastic variables, and thus, the model output is stochastic. The variance in the output is determined by variations of the uncertain input factors, and sensitivity indices are a quantification of the amount of influence.

Depending on the aims of the SA, different tests are possible, e. g., factor prioritization or factor fixing. Factor prioritization is applied to find factors that account for most of the output variance. In other words, a factor, when fixed to its true value, leads to the highest reduction of variance in the output. On the other hand, factor fixing is used to find factors that have no significant contribution to the output variance. Besides that, many more settings are conceivable, like variance cutting or factor mapping (Saltelli 2008).

VBSA techniques have several benefits: they are model-free, so no assumption about the input-output relationship must be made; in contrast to local SA, each input factor can be varied over its full range of variation; also interactions between factors can be taken into account (Saltelli 2008).

Beginning in the 1970s, Cukier et al. (1973) developed a method to determine the sensitivity of coupled reaction systems to uncertainties in rate constants. There, the Fourier coefficients were used as a measure of sensitivity. This method is known as FAST (Fourier Amplitude Sensitivity Test) and was later extended for higher-order sensitivities (eFAST), (Saltelli, Tarantola, and K. P.-S. Chan 1999).

Sobol' (1993) proposed a decomposition of the output function into terms of increasing dimensionality. The total variance of the output can be decomposed in the same manner. From that, 2^K terms can be derived, from which the linear ones are called first-order indices. This expansion is also referred to as high-dimensional model representation (HDMR), (Saltelli 2008, p. 212) and is also linked to ANOVA (analysis of variance) decomposition (Saltelli, Annoni, et al. 2010). First-order indices, also called main effects, represent the direct contribution to the output from individual input factors. The total-order indices are a measure for the first-order and all higher-order contributions to the output which can be directly derived from Sobol's method, although firstly described in Homma et al. (1996) and Saltelli (2002). Model decomposition has been adopted and expanded many times (Hora et al. 1986; Saltelli, T. H. Andres, et al. 1993; Homma et al. 1996; Saltelli, Annoni, et al. 2010).

Extension to Non-scalar Model Outputs. As mentioned earlier, the transient or dynamic behavior of a system is a frequent topic of interest. That means, the output of such systems is a function of time, and therefore typical SA techniques cannot be applied, since they rely on a scalar measure as output. One possibility to overcome this problem is to calculate sensitivities along the output trajectories, as shown by Ingalls et al. (2003) for stoichiometric networks. This can be seen as an extension of metabolic control analysis (MCA), primarily used for steady-state analysis only. Another way is to derive a scalar feature from the dynamic output that is able to describe the key elements. But constructing a proper set is highly problem-specific (K. Campbell et al. 2006), and, without previous knowledge about the underlying problem, many features are feasible.

An alternative methodology for global SA is a functional principal component analysis (FPCA) of the output data and a subsequent application of standard SA techniques. FPCA is a statistical method for investigating the dominant modes of variation of functional data. K. Campbell et al. (2006) proposed that any standard sensitivity analysis technique can be fulfilled when the model output is transformed into an appropriate functional coordinate system, i. e., into a set of basis functions. Consequently, sensitivity analysis can be performed on the coefficients of this basis.

This concept has also been shown by Yamanishi et al. (2005) for some numeric examples. In the field of biology, Sumner et al. (2012) applied FPCA and GSA to a model of the insulin signaling pathway identifying key parameters of the system. A general introduction to functional data analysis is given by Ramsay et al. (2009). A review of statistical methods for functional data analysis can be found in Müller (2008), who was also involved in an extension to sparse longitudinal data (Yao et al. 2005).

3.3 Identification and Estimation

Identification and estimation mean determining a particular uncertain variable of a mathematical model on the basis of measurement data obtained from a system and specific cost functions. Variables can be either time-dependent states or constant parameters, which may be treated as time-independent states (for details see Section 5.2). Within this work, the term identification is a deterministic process to determine uncertain or unknown parameters by solving an optimization problem. These variables are free, which means, they provide some kind of degree of freedom within the model, while all remaining variables are kept constant. The optimization problem can be solved by adapting the free parameters in such a way, that, e. g., the error between experimental and simulated outputs will be minimized. This typically happens offline, which means, after an experiment and with full knowledge about all relevant signals. Second, the term estimation will be used for the stochastic approach to determine the time-dependent states and time-independent parameters of a model, typically online, i. e., in real-time by an analog or digital filter. Some key properties are listed in Table 3.2.

To assess whether it is theoretically possible to determine unknown states or parameters from input-output measurements of a system, controllability and observability respectively identifiability analysis may be applied.

Table 3.2: Key properties of identification and estimation procedures.

Identification	Estimation
Constant variables, such as parameters	Time-dependent variables, such as states
Offline, i. e., after an experiment with full knowledge about all signals	Online, i. e., during run-time
Minimization of an optimization problem	Digital filter regarding model and sensor variances
Direct (linear case) or iterative solution (nonlinear case)	Recursive least-squares algorithm that improves the solution with every new time step
Deterministic approach	Stochastic approach

3.3.1 Empirical Controllability, Observability, and Identifiability Analysis

Controllability and observability are basic concepts for analyzing the input-output behavior of linear, dynamical systems (Fig. 3.5). Controllability can be seen as a measure of how well a particular state $\boldsymbol{x}(t)$ can be driven from an arbitrary initial state into an arbitrary final state by an appropriate choice of the input $\boldsymbol{u}(t)$. Further, observability defines to which extent the trajectory of a particular state can be determined by the observation of the outputs $\boldsymbol{y}(t)$. Controllability and observability for linear systems can be assessed by the common criteria of Kalman, Hautus, or Gilbert (J. Lunze 2014, Ch. 3) and are mainly associated with the structure of the system. If e. g., a state is neither directly nor indirectly connected to an input of the system, the state will not be controllable. The same holds for the connection of a state with an output. This concept is known as structural controllability respectively observability. Structural identifiability aims in determine whether it is *a priori* possible to estimate a parameter from a given input-output experiment (Cobelli and Romanin-Jacur 1976) and can be tested, e. g., by using differential algebra (Ljung et al. 1994). Identifiability is further related to the observability of parameters when they are considered as constant states (Geffen et al. 2008). This is an accepted concept in biological (Streif et al. 2006) or chemical (Sun et al. 2006) processes.

Controllability and observability are also associated with their respective controllability and observability Gramian matrices. They play a role in the solution of the controllability respective observability problem. For linear systems, they can be computed from a Lyapunov equation, thus, by solving linear matrix equations. Empirical Gramians extend the concept of Gramian-based controllability and observability to nonlinear systems. They are computed from process data, i. e., by calculating trajectory simulations or experimental data following a special design of experiment. It was first motivated by Moore (1981) but systematically developed by Lall et al. (1999). The main idea of this approach is to compute local Gramians for variations of any desired variables, such as the inputs or initial states around an operating point, and to average over these local Gramians (Himpe 2018).

Besides that, the cross Gramian encodes the information given by the controllability and observability Gramian in one single matrix which is computationally more efficient. It is only suitable for stable and symmetric systems (Himpe and Ohlberger 2014) but can be approximated for non-symmetric systems (Himpe and Ohlberger 2016).

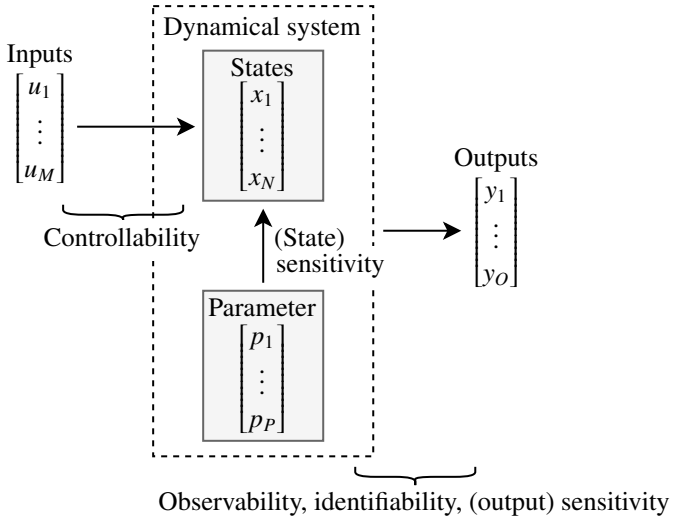

Figure 3.5: Concept of controllability, observability, identifiability, and sensitivity of a dynamical system.

One further concept to mention is the sensitivity of parameters regarding the states of a linear system (here called state sensitivity) which allows a controllability-based parameter analysis (Sun et al. 2006). For systems in state-space notation with additive parameters of the form

$$\dot{\boldsymbol{x}}(t) = \boldsymbol{A}\boldsymbol{x}(t) + \boldsymbol{B}\boldsymbol{u}(t) + \boldsymbol{F}\boldsymbol{p} = \boldsymbol{A}\boldsymbol{x}(t) + \begin{pmatrix}\boldsymbol{B} & \boldsymbol{F}\end{pmatrix}\begin{pmatrix}\boldsymbol{u}(t) \\ \boldsymbol{p}\end{pmatrix}, \tag{3.13}$$

the parameters $\boldsymbol{p}$ are treated as additional inputs, where $\boldsymbol{F}$ is a matrix of suitable dimension. The contributions of inputs and parameters are superimposed and can be represented by a series of state-space equations. For each subsystem the controllability Gramian can be computed and from that the so-called sensitivity Gramian (Himpe and Ohlberger 2013). This is in contrast to the techniques of (output) sensitivity analysis presented in Section 3.2, where the influence of the parameters on the outputs of the system is under investigation.

The concept of (empirical) Gramians is also widely used in the field of balancing where the system is state-transformed in such a way that the energy transfer from the inputs into the states equals the energy transfer from the states into the outputs. If a system is in a balanced form, its Hankel singular values provide a measure of the importance of a state regarding the input-output behavior (Hahn et al. 2002). From that, a model order reduction (MOR) can be fulfilled by, e. g., balanced truncation (Antoulas and D. C. Sorensen 2001) of those states with small singular values, as they contribute little to the input-output behavior (Baur et al. 2014; Himpe 2020a). The applicability to a nonlinear model of glucose-insulin regulation has been shown in Tolks and Ament (2017b). Hence, empirical Gramians are a universal, problem-independent concept not only suitable for controllability, observability, and identifiability analysis but also ideal for a subsequent model order reduction, which may help to design reduced-order controllers for glucose control in an artificial pancreas or reduced-order state estimators (Misgeld et al. 2017).

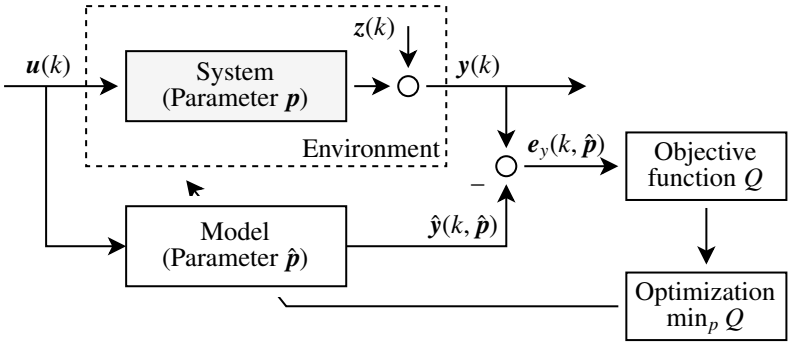

Figure 3.6: Adaptation of a model by varying the parameter vector $\hat{\boldsymbol{p}}$ in order to minimize Q, the objective function derived from the output error $\boldsymbol{e}_y(k, \hat{\boldsymbol{p}})$ between measured system outputs $\boldsymbol{y}(k)$ and simulated model outputs $\hat{\boldsymbol{y}}(k, \hat{\boldsymbol{p}})$.

3.3.2 Parameter Identification

Simulated and measured outputs are compared in terms of a cost function Q. It is here defined as the sum of the squared error between system output $\boldsymbol{y}(k)$ and model output $\hat{\boldsymbol{y}}(k)$ given by

$$Q(\boldsymbol{p}) = \sum_{k=1}^{n} \left(\boldsymbol{y}(k) - \hat{\boldsymbol{y}}\left(k, \hat{\boldsymbol{p}}\right)\right)^2 , \tag{3.14}$$

where n is the number of discrete-time measurement points k. The objective function Q is then minimized by an optimization algorithm that adapts the model parameters. The whole procedure is shown in Fig. 3.6, where $\boldsymbol{u}(k)$ is the input to the system, $\boldsymbol{z}(k)$ are unknown disturbances, and $\boldsymbol{e}_y(k, \hat{\boldsymbol{p}})$ is the output error between experiment and model.

For linear relationships between parameters $\boldsymbol{p}$ and outputs $\boldsymbol{y}(k)$, a direct solution can be given. If this is not the case iterative search methods must be applied. Besides gradient-based approaches such as line search, the NelderMead method is a commonly applied numerical method used to find the minimum or maximum of a nonlinear objective function for which derivatives may not be known (Nelder et al. 1965). For both methods, the solution may not converge to the true minimum but to only a local minimum, which often depends on the initial values from where the optimization was started.

Often, nonlinear least-squares problems must be solved, which arise in nonlinear curve fitting, which means, the process of adapting a mathematical function that best fits a series of data points, as it is the case when, e. g., several blood glucose and insulin values were obtained from a patient. In these cases, the Levenberg-Marquardt algorithm or Trust-Region approaches are satisfactory, depending on the presence or absence of bound constraints (Isermann et al. 2011, Ch. 19).

Building physiologic models always includes a determination of the underlying parameters. Numerous mathematical models of glucose metabolism exist, beginning with the first minimal models which describe glucose-insulin regulation after an IVGTT (Insel et al. 1975; Cobelli, Toffolo, et al. 1984; Pacini and Bergman 1986; Pacini, Tonolo, et al. 1998), models of glucose absorption (Dalla Man, Camilleri, et al. 2006), insulin absorption (Hovorka, Canonico, et al. 2004), models of critical-ill

T1DM patients (Hovorka, Canonico, et al. 2004), mixed-meal simulation models (Dalla Man, Rizza, et al. 2006), or models derived from animal trials (Eberle et al. 2020). In most cases, they are identified by least-squares fitting or maximum likelihood estimation based on measurement data obtained under rigorous experimental design in clinical settings. Several aspects should be mentioned:

- equal physiological conditions in all participants, typically during fasting,
- highly standardized inputs, such as an IVGTT, OGTT, or a well-defined mixed meal,
- laboratory equipment with minimal errors, compared to BGSM or CGM sensors,
- frequent measurements, up to 30 samples within a four-hour interval (P. Magni et al. 2006),
- access to physiological signals not available by patients in daily life, such as the insulin concentration in plasma or the glucose absorption rate after meal ingestion (R. Basu et al. 2003).

Parameter identification from measurements other than plasma glucose and insulin, or from outside a clinical setting is seldom. Particularly, the concentration of glucose within the interstitial fluid, measured by a CGM device, is of interest here, since it provides frequent measurements of glucose and thus, enables permanent monitoring in daily life (compare to Fig. 6.3). Boiroux et al. (2016) used simulated CGM data obtained from a virtual patient to compare different identification strategies, including least-squares and maximum likelihood in combination with Kalman filters. They reached an RMSE of approx. $10\,\mathrm{mg\,dL^{-1}}$ for all considered methods. Facchinetti et al. (2007) first identified parameters of a first-order model from frequent blood glucose and CGM samples in order to describe glucose diffusion from blood into the interstitium. Second, they reconstructed blood glucose values from CGM in retrospect using a time-based deconvolution method. They also provided a recalibration step to take into account CGM sensor degradation over time.

3.3.3 State Estimation

The aim of state estimation is the computation of possibly non-measurable inner states $\tilde{\boldsymbol{x}}(k)$ of a system on the basis of a (nonlinear) discrete-time model and measurements of inputs $\boldsymbol{u}(k)$ and outputs $\boldsymbol{y}(k)$ of that system (Fig. 3.7). In the case of linear systems, the most common state observers are the Luenberger observer (Luenberger 1964), typically derived by pole-placement, and the Kalman filter (KF), considering stochastic process and measurement noise (Kalman 1960). After each measurement, minimization of the quadratic error is performed in the sense of optimality. However, this procedure is unsuitable for practical use at run-time since all quantities have to be recalculated after each step and the dimensions of the required matrices are constantly increasing. With the KF, a recursive state estimation algorithm has been developed, that provides an optimal state estimation at run-time. The limitation to linear systems was subsequently overcome with the extended Kalman filter (EKF), which extends the algorithm by linearizing the model at the current operating point. From 1960 until the mid-1990s, these methods found their way into many applications in different variants. The restriction to linear systems or linearization led to the development of the so-called unscented transformation and the unscented Kalman filter (UKF) on which it is based (Julier et al. 1997).

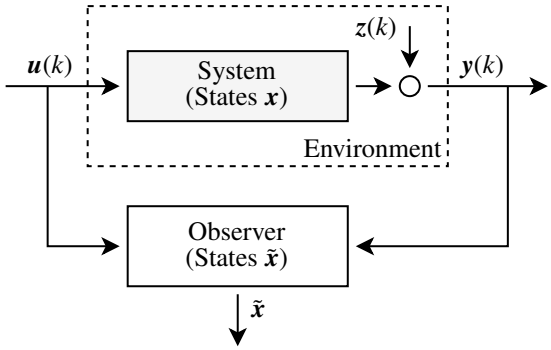

Figure 3.7: Observer for estimating states $\tilde{\boldsymbol{x}}$ from input and output measurements of a system with disturbances.

In the field of diabetes technology, digital filters were first introduced when a quasi-continuous measurement of glucose within the interstitial fluid became possible with the availability of CGM devices. Bequette (2004) was the first who applied a Kalman filter on simulated noisy CGM data and a simple linear first-order diffusion model in order to estimate blood glucose levels. The first EKF was applied by Knobbe et al. (2005) to estimate blood glucose from patient CGM data obtained in a clinical trial, using a nonlinear model with five states. A dual-rate Kalman filter, taking into account simulated and experimental data from frequent CGM measurements and infrequent blood glucose samples, was developed by Kuure-Kinsey et al. (2006). The filter was derived from a simple two-state linear model, also able to estimate the sensor degradation over time. Palerm et al. (2007) applied a KF on clinical hypoglycemic clamp data to predict hypoglycemia for prediction horizons between 10 and 30 min. As an alternative to model-based estimation or prediction methods, time-series techniques, such as polynomial or autoregressive (AR) models, can be used to predict glucose concentration ahead of time (Sparacino et al. 2007; Leal et al. 2010). An overview of real-time algorithms for sensor calibration, filtering, and alarms can be found in Bequette (2010). Besides blood glucose estimation, Kalman filtering was also applied to estimate the concentration of insulin from glucose data obtained from an IVGTT using a UKF (Eberle et al. 2011) or from CGM data using an EKF (Hajizadeh et al. 2017). Moreover, Kalman filtering allows the estimation of both, dynamical states (Eberle et al. 2012b) and constant but unknown diagnostic parameters of the glucose-insulin regulation, such as the insulin sensitivity (Eberle et al. 2012a; Misgeld et al. 2017).

3.3.4 Model Evaluation

Several performance measures exist to quantify the error between signals or even a whole model. The following paragraphs briefly describe some common metrics in the field of diabetes science and technology.

Mean Absolute Relative Deviation. The mean absolute relative deviation (MARD; or MARE, mean absolute relative error) is a common performance metric to assess the overall quality of glucose measurements compared to a reference. It is dimensionless, although it is typically given in percent.

However, this rather corresponds to the mean absolute percentage error (MAPE). Both are given by

$$\text{MARD} = \frac{1}{n}\sum_{k=1}^{n}\left|\frac{y(k)-\hat{y}(k)}{y(k)}\right|, \tag{3.15}$$

$$\text{MAPD} = 100\% \cdot \text{MARD}, \tag{3.16}$$

where $y(k)$ and $\hat{y}(k)$ are the reference and comparison values, respectively, for discrete samples $k = 1, \ldots, n$.

Root Mean Squared Error. The root mean squared error (RMSE) is widely used to assess the error between an experimental output $y(k)$ and a model output $\hat{y}(k)$. It is calculated by

$$\text{RMSE} = \sqrt{\frac{1}{n}\sum_{k=1}^{n}(y(k)-\hat{y}(k))^2}, \tag{3.17}$$

where $k = 1, \ldots, n$ are the samples. By squaring the difference, large errors are weighted more heavily than smaller ones. Moreover, the RMSE is expressed in the same units as the obtained signals. To compare errors of different quantities, the RMSE can be normalized.

***t*-test.** The two-sample t-test is a significance test to check whether the mean values of two populations are equal or different from each other. Let $\bar{x}$ and $\bar{y}$ be the means of two independent data samples from populations X respective Y. The test statistic is

$$t = \frac{\bar{x}-\bar{y}}{\sqrt{\frac{s_x^2}{n_x}+\frac{s_y^2}{n_y}}}, \tag{3.18}$$

where s_x and s_y are the sample standard deviations and n_x and n_y are the sample sizes. For the significance level α, the null hypothesis $H_0 : \bar{x} = \bar{y}$ is rejected in favor of the alternative, if

$$|t| > t\left(1-\frac{\alpha}{2}, n_x + n_y - 2\right).$$

The equation only holds for equal standard deviations in both populations. In the case of inequality, the solution can be approximated by using the Welch-test (Papula 2016, Ch. 4.5.3).

***F*-test.** An F-test is a group of statistical tests in which the test statistics follow an F-distribution under the null hypothesis. In the context of analysis of variance, an F-test is a test that can be used to determine with a certain degree of confidence whether two samples from different, normally distributed populations differ significantly in their variance. Among other things, it is thus used for general testing of differences between two statistical populations.

Let σ_x^2 and σ_y^2 be the variances of two independent and normally distributed populations X respective Y. Then, the test statistic under the null hypothesis $H_0 : \sigma_x^2 = \sigma_y^2$

$$F = \frac{s_x^2}{s_y^2} \tag{3.19}$$

has F-distribution with s_x and s_y being the sample standard deviations and $n_x - 1$ and $n_y - 1$ the degrees of freedom, where n_x and n_y are the number of samples in X and Y, respectively. The null hypothesis is rejected if F is too large or too small based on the statistical significance level α, which is typically set to 5 % (Papula 2016, Ch. 4.5.4).

Error Grid Analysis. The error grid analysis (EGA) is used to evaluate the clinical significance of inaccuracies of glucose measurements compared to a reference values. Therefore, pairs of sensor measurements are plotted against each other, where a pair is here defined as two records within a ±5 min interval. The plot is further separated into zones A-E of varying degrees of accuracy, denoting different clinical impacts when treatment decisions were made from these records (Fig. 3.8). Values on the diagonal are error-free. Values in zones A (within a ±20 % range around the diagonal) and B are clinically acceptable, whereas values in zone C would result in an overcorrection of acceptable values. Zones D and E are potentially dangerous and thus, are clinically significant errors (W. L. Clarke, Cox, et al. 1987). The original EGA was extended for use with continuous glucose sensors (CG-EGA) to take into account the inherent time delay between glucose concentration in blood and interstitial fluid by introducing a dependency on the rate of change of glucose (W. L. Clarke 2005). Moreover, EGA is also used to compare glucose estimates derived by simulations with experimental data. (K. Lunze 2014). Nevertheless, other analysis tools exist, such as the consensus error grid (Parkes et al. 2000).

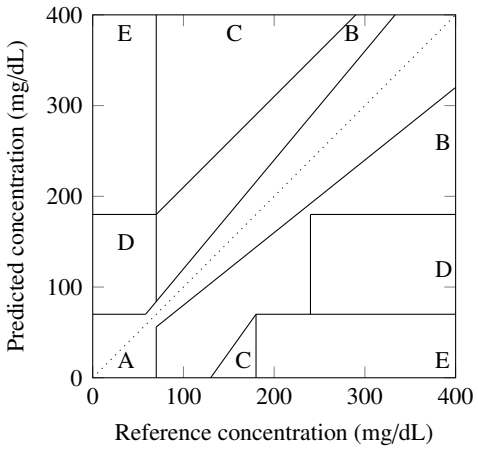

Figure 3.8: Empty EGA (error grid analysis) plot for the evaluation of glucose sensor performance.

3.4 Wearable Systems for Mobile Diabetes Monitoring

Standard diabetes treatment involves frequent measurements of blood glucose levels and insulin administration, typically via the subcutaneous route in order to maintain tight glycemic control. Treatment decisions are made by the patient himself or herself, for which he or she has been specially instructed. Collected data can be evaluated afterward by a physician to optimize insulin therapy.

To record glucose concentration, patients need a glucose meter that measures the amount of glucose in the blood, usually given on a small test strip (Section 2.3). Beginning in the 1950s, the first blood glucose dry-reagent test strips were developed, which used glucose oxidase reaction. A semiquantitative blood glucose value could be derived by visual inspection against a color code. The first blood glucose meters were introduced in the 1970s for in-hospital use. The key principle was to measure reflected light from the surface of the test strips. From that, quantitative glucose values could be determined. Over the years, these devices have become smaller, more accurate, and easier to handle. Furthermore, the amount of blood needed for measurement decreased from 50-100 μL in 1964 to only 0.3-1 μL nowadays. Advancements in electronics and software led to more functionalities like autocalibration, electronic journals, alarms, and capabilities to connect to other devices to synchronize the collected data (S. F. Clarke et al. 2012).

Subcutaneous glucose sensors have a comparable high temporal resolution, typically between 1-5 min, and provide real-time information of the current glucose value and trend. That enables patients to have a more precise and reactive self-assessment. Several randomized control studies showed short- and long-term improvements in glycemic excursions, a reduced HbA_{1c} value, and a reduction of severe events in T1DM as well as in T2DM (S. Garg et al. 2006; Vigersky et al. 2012).

Shichiri, Yamasaki, et al. (1982) were the first to introduce an artificial endocrine pancreas with a needle-type glucose sensor in 1982. With an added telemetry unit, they created the first essential components for a wearable CGM system (Shichiri, Asakawa, et al. 1986). Beginning at the end 1990s, the first commercial devices were available on the market. Today, all approved systems are comparable in the underlying technology, the need for calibration, and lifetime (Gifford 2013). An overview of currently available CGM systems, technological trends, and challenges can be found in Cappon et al. (2017). One milestone would be to reduce the error to a comparable value as glucose meters, thus, CGM could be used as a substitute for blood glucose measurements (Kovatchev, Patek, et al. 2015).

Recent advancements in medical devices and (mobile) computing power enabled extensive monitoring of vital signals, not only in the field of diabetes but also in physical activity, blood pressure, electrocardiogram (ECG), or electroencephalography (EEG). Devices that act on or close to the body can be summarized as a body area network (BAN), nowadays typically connected wirelessly via Bluetooth or near-field communication (NFC) to a smartphone used to collect and process the data. It further serves as a user interface and acts as a network hub that connects to a cloud service or data repository (Fig. 3.9). These remote services are typically delivered by healthcare professionals who provide

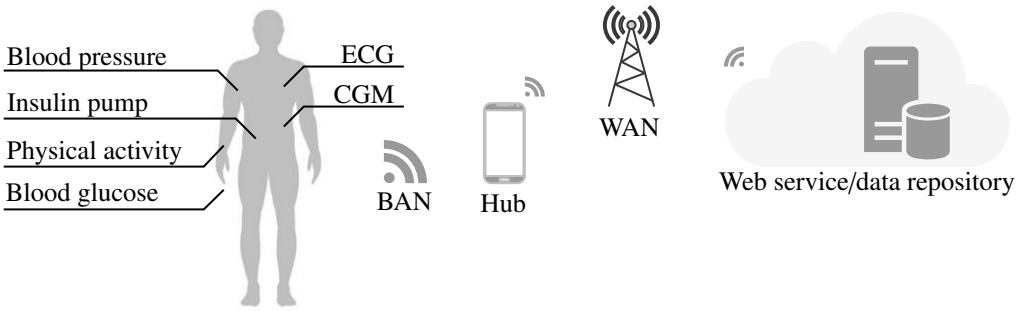

Figure 3.9: Concept of mobile health devices acting in or on the body. They build a body area network (BAN), typically connected to a smartphone via Bluetooth or other proprietary protocols. The smartphone acts as a central communication hub and user interface. It is connected to a web platform or data repository via a wide area network (WAN) that may provide additional healthcare services.

additional functionalities like data analysis, personalized decision-support information, care planning, education, or emergency healthcare (Georga et al. 2014; Islam et al. 2015; Lanzola et al. 2016).

According to Lanzola et al. (2016), three main phases of remote monitoring can be identified. The early phase from the 1990s to 2000 was characterized by asynchronous communication between a patient's personal stationary computer and the medical unit. Users usually had to note their health records manually and were supported with alarms, treatment plans, and data interpretation. Second, a switch to a service-oriented architecture from 2000 until 2010 (Hernando et al. 2008). This phase was characterized by a client-server approach, granting (mobile) access to centralized services over unified interfaces like websites or SMS (Short Message Service). The third phase is still ongoing and is defined by data processing of multiple sensors attached to the body or even implanted, e. g., under the patient's skin. These devices span a small range BAN and are controlled only locally due to limitations in size, power consumption, or radio emission (Yuce 2010). A BAN is typically managed by a dedicated body gateway or a hub like a smartphone, which also enables remote monitoring via web services (Fig. 3.9).

That open platforms for remote monitoring are highly appreciated by patients can be demonstrated by the Nightscout Project, originally developed by some parents of diabetic children, to bring CGM into the cloud. They developed a platform for real-time access to their CGM devices, which is accessible by smartphones or the web (The Nightscout Foundation 2018). Currently, the application can connect to the CGM sensors G4 Platinum and G5 Mobile (Dexcom, San Diego, CA, USA) and the Freestyle Libre (Abbott Diabetes Care, Alameda, CA, USA), and to insulin pumps 640g, 530g, and Veo (Medtronic Minimed, Northridge, CA, USA). Moreover, the Contour Next series (Ascensia Diabetes Care, Basel, Switzerland) of blood glucose sensors are supported. As this application is open-source and supports a variety of medical devices it serves as the basis for the model-based diabetes monitoring (*MoDiM*) concept introduced in Chapter 7.

Various remote managing platforms and care models in diabetes management have been developed over recent years (Georga et al. 2014). One of the most advanced and approved ones is the Diabetes

Assistant (DiAs) artificial pancreas research system (Keith-Hynes et al. 2014). It was developed within the European Union-funded *AP@home* project that aimed at bringing the artificial pancreas from clinical trials to in-home utilization without supervision by a physician for several months (Heinemann et al. 2016). A broader review on glucose monitoring in *mHealth* scenarios can be found in Lanzola et al. (2016).

Besides smartphone apps that connect to manufacturer-specific hardware devices like glucose meters or insulin pumps, there exists a broad variety of *mHealth* apps for diabetic patients. Most of them serve as an electronic health journal, followed by nutritional information and insulin bolus calculators. Compared to approx. 425 million diabetics worldwide, the percentage of users of diabetes-specific *mHealth* applications is still low at approx. 11 % (Eberle et al. 2019).

4 Derivation of the Mathematical Models

4.1 Dynamical Model of the Glucose-Insulin-Glucagon Metabolism

In Section 3.1 some key parts in the mathematical description of glucose, insulin, and glucagon regulation have been described. On the basis of these physiological relationships, several models have been developed, taking into account single or multiple components of glucose metabolism. Most works aim at simulating T1DM subjects (Table 3.1), mainly because of their permanent insulin dependency for which continuous monitoring, glucose prediction strategies, and insulin delivery systems are eminent for daily life. Despite this, most models are obtained from experiments in well-defined clinical trials. Thus, their validity is limited in other clinical settings. For instance, models for predicting blood glucose and insulin concentrations after a meal are usually not able to give precise results for, e. g., an insulin infusion test since different physiological parts in the body were under investigation. Moreover, it is also difficult to carry out multiple tests with subsequent identification of several model parts, as superimposed effects and feedback within the system cannot be distinguished from each other. These problems make it difficult to compare dynamical states and related parameters derived from different models and environmental settings with each other. Hence, a proper model has to be selected depending on the desired test criteria.

Modeling Aims. Taking into account the limitations given above and since the focus of this work is on the study of daily-life scenarios, which includes meal intakes in combination with subcutaneous insulin delivery a meal simulation model would meet the requirements.

From a physiological point of view, a model is desirable that is capable of simulating a person's metabolism, regardless of a specific disease condition. Thus, the ability to have valid outcomes for non-diabetics as well as for type 1 and type 2 diabetics. A unified set of equations has the advantage of defining glucose metabolism at a glance, where it is assumed that healthy people and different manifestations of diabetes are represented by varying parameter sets within the same model. That means a single individual should be characterized by a subject-specific set of parameters that determine the clinical state in a long-term manner. In contrast, the dynamic states of a person determine the current metabolic status.

Having a unified model structure and parameters, a subsequent system analysis as described in Chapter 5 can be fulfilled, which includes investigations on controllability and observability, and sensitivity analysis.

Overall Model Structure. The mathematical model described in the following sections is based on the compartment modeling technique. It mainly describes the kinetics of glucose, insulin, and glucagon in the blood circulation system, endogenous secretion and consumption processes, and components for external administration as depicted in Fig. 4.1. It aims to investigate the glucose regulation system during meals and normal life.

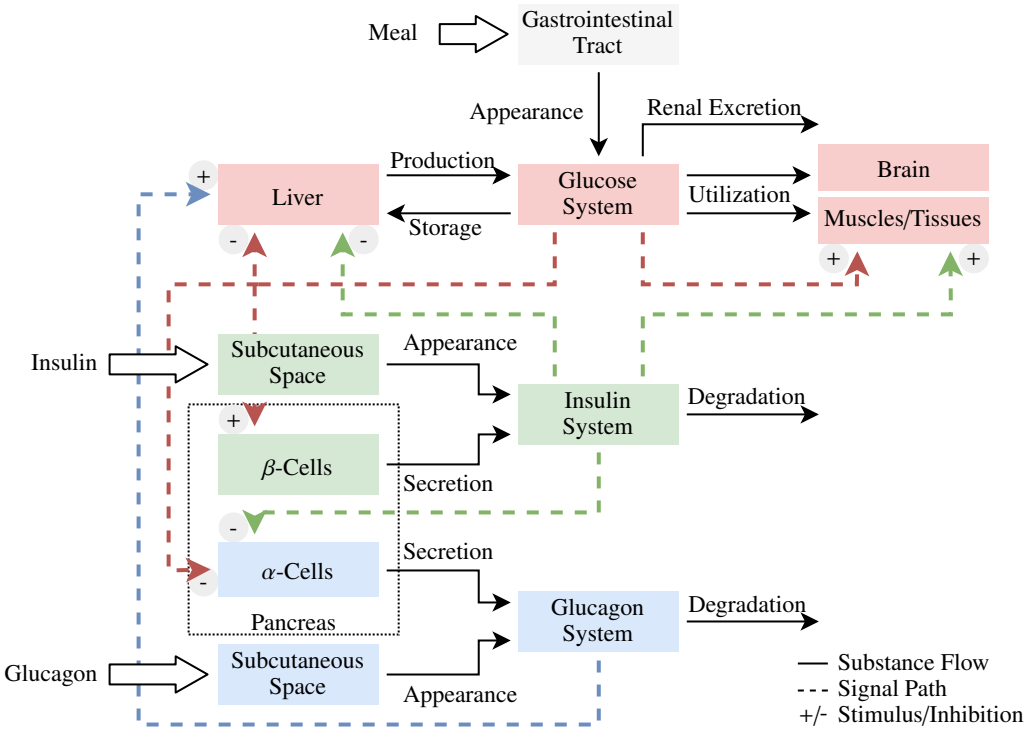

Figure 4.1: Main structure of the model (adapted from Dalla Man, Raimondo, et al. (2007) and Dalla Man, Micheletto, et al. (2014)). The model consists of three compartments: glucose (red), insulin (green), and glucagon (blue), and the gastrointestinal tract (gray). Each system has elements for substance secretion or external delivery (left panel), kinetics (middle panel), and consumption (right panel).

The dynamics of glucose, insulin, and glucagon are decomposed as follows:

- The glucose subsystem (upper panel marked in red) consists of the liver where glucose is produced from internal storage, the blood circulatory system, and the brain, muscles, and tissues where glucose is utilized.
- The insulin subsystem (middle panel marked in green) consists of the pancreatic β-cells from where insulin is secreted into the circulatory system and the subcutaneous space from where externally injected insulin appears in plasma.
- The glucagon subsystem (lower panel marked in blue) consists of the pancreatic α-cells from where glucagon is released into the blood and also a subcutaneous space from where externally administered glucagon appears in plasma.
- In addition, the gastrointestinal tract (top block marked in gray) describes the appearance of glucose in the blood after food ingestion.

When the system is in steady-state (homeostasis), all substance concentrations are at their basal levels. The liver produces as much glucose as the body utilizes to supply all organs with energy. Moreover, insulin and glucagon secretion rates are as high as their degradation. After meal ingestion glucose appears in plasma. In a healthy human insulin secretion is increased and glucagon release is inhibited. A rise in glucose and insulin concentration lowers hepatic glucose production and stimulates glucose uptake by the muscles and tissues, which in turn, lowers blood glucose concentration back to steady-state. In T2DM stimulation of glucose utilization is deteriorated, whereas in T1DM patients pancreatic insulin secretion is impaired or even absent and insulin has to be injected through the subcutaneous space.

Although the model is designed for simulating meal ingestion and thus, oral glucose administration is the major input to the system, the following inputs are considered as well:

- $u_{\mathrm{G}}^{\mathrm{oral}}(t)$: Oral glucose administration ($\mathrm{mg\,min^{-1}}$),
- $u_{\mathrm{G}}^{\mathrm{iv}}(t)$: Intravenous glucose infusion ($\mathrm{mg\,kg^{-1}\,min^{-1}}$),
- $u_{\mathrm{I}}^{\mathrm{sc}}(t)$: Subcutaneous insulin infusion ($\mathrm{mU\,min^{-1}}$),
- $u_{\mathrm{I}}^{\mathrm{iv}}(t)$: Intravenous insulin infusion ($\mathrm{mU\,kg^{-1}\,min^{-1}}$),
- $u_{\mathrm{H}}^{\mathrm{sc}}(t)$: Subcutaneous glucagon infusion ($\mathrm{ng\,kg^{-1}\,min^{-1}}$),

where oral glucose input acts as a disturbance from homeostasis and insulin s.c. is the major input for diabetes treatment. Furthermore, the following system outputs are assumed to be measurable:

- $G(t)$: Glucose concentration in plasma ($\mathrm{mg\,dL^{-1}}$),
- $G_{\mathrm{I}}(t)$: Glucose concentration in subcutaneous space ($\mathrm{mg\,dL^{-1}}$),
- $I(t)$: Insulin concentration in plasma ($\mathrm{mU\,L^{-1}}$),
- $H(t)$: Glucagon concentration in plasma ($\mathrm{ng\,L^{-1}}$),

where the glucose concentration in plasma is the most common measure for diabetics to control their current health status. For T1DM with intensified insulin therapy, continuous glucose measurement from the s.c. space is widely used. Measuring insulin and glucagon is only applicable in a clinical environment and not in daily routine.

For each of the single components in Fig. 4.1, the differential equations, their related parameters, and their origin, are discussed in detail in the following sections, starting with the glucose-related parts in Sections 4.1.1 to 4.1.6. Kinetics of insulin, its secretion, and appearance follow in Sections 4.1.7 to 4.1.9. Sections 4.1.10 to 4.1.12 are structured in the same way for the glucagon-related parts. A summary of all equations can be found in Section A. All states and parameters, their variable names, and units are listed in Table A.1 respectively Table A.2 for each group of subjects.

4.1.1 Glucose Kinetics

The model shown here has its origin in Bergman's minimal model as given in (3.8) that describes glucose kinetics after an IVGTT. This model was not able to distinguish between endogenous glucose

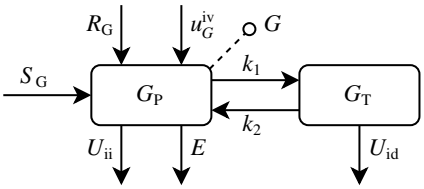

Figure 4.2: Two-compartment model of glucose kinetics (adapted from Dalla Man, Rizza, et al. (2007)). Glucose concentration $G(t)$ is accessible by measurements of plasma glucose mass $G_P(t)$ which is in exchange with slowly-equilibrating tissue $G_T(t)$.

production and glucose utilization from only the measurement of insulin and glucose. Administration of labeled glucose could overcome this limitation and led to a new single-compartment model for glucose kinetics (Cobelli, Pacini, et al. 1986). However, this model produced a non-physiologic pattern of estimated hepatic glucose production which made it necessary to propose an extended model approach (Caumo and Cobelli 1993). The new minimal model describes glucose kinetics using two compartments. The first one is the accessible pool of glucose in plasma and rapidly-equilibrating tissues, $G_P(t)$, the second one accounts for slowly-equilibrating tissues, $G_T(t)$, as shown in Fig. 4.2. The exchange rates between both compartments are given by parameters k_1 and k_2. $S_G(t)$ is the endogenous glucose production by the liver (Section 4.1.3), $R_G(t)$ is the rate of appearance of glucose in plasma during ingestion of a meal (Section 4.1.2). In addition, glucose can be administered intravenously given by $u_G^{iv}(t)$. It instantaneously appears in plasma, bypassing the gastrointestinal tract. Glucose uptake from plasma, $U_{ii}(t)$, is assumed to be insulin-independent and constant and takes into account glucose uptake by the brain, nervous system, and red blood cells (Best et al. 1981). Insulin-dependent utilization, $U_{id}(t)$, takes place in the slowly exchanging pool and is controlled by insulin from a remote compartment (Section 4.1.4). $E(t)$ denotes the renal excretion above which glucose is excreted by the kidneys (Section 4.1.6). Glucose concentration $G(t)$ is derived from plasma glucose mass $G_P(t)$ within the distribution volume V_G. These relationships lead to the two linear systems of first order given by

$$\dot{G}_P(t) = S_G(t) + R_G(t) - U_{ii}(t) - E(t) - k_1 G_P(t) + k_2 G_T(t) + u_G^{iv}(t) \qquad G_P(0) = G_P^b, \tag{4.1}$$

$$\dot{G}_T(t) = -U_{id}(t) + k_1 G_P(t) - k_2 G_T(t) \qquad G_T(0) = G_T^b, \tag{4.2}$$

$$G(t) = \frac{G_P(t)}{V_G}, \tag{4.3}$$

where the basal glucose masses at steady-state are given by G_P^b respectively G_T^b. When setting all derivatives to zero, G_T^b can be calculated by

$$G_T^b = \frac{U_{ii} - S_G^b + k_1 G_P^b}{k_2}, \tag{4.4}$$

with G_P^b being a free variable. All states, signals, and parameters are summarized in Table 4.1.

Table 4.1: Variables of glucose kinetics.

Variables	Description	Unit
States		
$G_P(t)$	Glucose mass in plasma	$\mathrm{mg\,kg^{-1}}$
$G_T(t)$	Glucose mass in slowly equilibrating tissues	$\mathrm{mg\,kg^{-1}}$
Signals		
$G(t)$	Glucose concentration in plasma	$\mathrm{mg\,dL^{-1}}$
$S_G(t)$	Hepatic glucose production	$\mathrm{mg\,kg^{-1}\,min^{-1}}$
$R_G(t)$	Rate of appearance of glucose in plasma	$\mathrm{mg\,kg^{-1}\,min^{-1}}$
$U_{ii}(t)$	Insulin-independent glucose utilization	$\mathrm{mg\,kg^{-1}\,min^{-1}}$
$U_{id}(t)$	Insulin-dependent glucose utilization	$\mathrm{mg\,kg^{-1}\,min^{-1}}$
$E(t)$	Glucose renal excretion	$\mathrm{mg\,kg^{-1}\,min^{-1}}$
$u_G^{iv}(t)$	External i.v. glucose administration	$\mathrm{mg\,kg^{-1}\,min^{-1}}$
Parameter		
G_P^b	Basal plasma glucose mass	$\mathrm{mg\,kg^{-1}}$
G_T^b	Basal tissue glucose mass	$\mathrm{mg\,kg^{-1}}$
G^b	Basal plasma glucose concentration	$\mathrm{mg\,dL^{-1}}$
V_G	Glucose distribution volume	$\mathrm{dL\,kg^{-1}}$
k_1	Exchange rate constant	$\mathrm{min^{-1}}$
k_2	Exchange rate constant	$\mathrm{min^{-1}}$

4.1.2 Gastrointestinal Tract

One major issue in the proper description of glucose and insulin kinetics is the lack of knowledge of the appearance of glucose in the systemic circulation after oral ingestion, which is in contrast to IVGTT-like protocols, where glucose is immediately available in plasma after injection. Thus, processes of gastrointestinal absorption have been investigated. First models applied a piecewise linear description (Dalla Man, Caumo, et al. 2002) or a one (Lehmann et al. 1992) or two-compartment chain (Hovorka, Canonico, et al. 2004) to describe glucose intestinal absorption. With the availability of tracer data (R. Basu et al. 2003), the rate of appearance of glucose in plasma could be determined and from that, a system model of oral glucose absorption was developed. The model of third-order describes glucose in the stomach and gut and has a highly nonlinear gastric emptying function (Dalla Man, Camilleri, et al. 2006).

A much simpler but sufficient model proposed by Hovorka, Chassin, Ellmerer, et al. (2008) is linear and has two compartments (Fig. 4.3). The relationship is given by

$$\dot{Q}_{\mathrm{Gas},1}(t) = -k_{G1} Q_{\mathrm{Gas},1}(t) + u_G^{\mathrm{oral}}(t) \qquad Q_{\mathrm{Gas},1}(0) = 0, \tag{4.5}$$

$$\dot{Q}_{\mathrm{Gas},2}(t) = -k_{G2} Q_{\mathrm{Gas},2}(t) + k_{G1} Q_{\mathrm{Gas},1}(t) \qquad Q_{\mathrm{Gas},2}(0) = 0, \tag{4.6}$$

where $Q_{\mathrm{Gas},i}(t), i = 1, 2$ represent the amount of glucose in stomach and small intestine, respectively. Parameters $k_{Gi}, i = 1, 2$ are rate constants and $u_G^{\mathrm{oral}}(t) = D \cdot \delta(t)$ is the oral glucose ingestion rate, where D is the total amount of glucose and $\delta(t)$ the unit impulse.

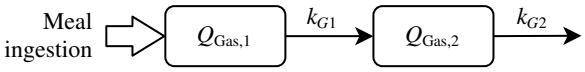

Figure 4.3: Two-compartment model of the gastrointestinal tract representing glucose amount in stomach, $Q_{\text{Gas},1}$, and intestine, $Q_{\text{Gas},2}$, respectively. A linear second order system is assumed.

The model was originally developed and fitted to experimental data from critically ill patients with enteral glucose delivery. Nevertheless, the model can be fitted to match the available data of a mixed meal study from Dalla Man, Camilleri, et al. (2006) which is described at the end of Section 4.2.

Furthermore, the rate of appearance of glucose in plasma, $R_{\text{G}}(t)$, is expressed by

$$R_{\text{G}}(t) = \frac{f_{\text{G}} \cdot k_{G2} Q_{\text{Gas},2}(t)}{BW}, \tag{4.7}$$

where BW is the body weight and f_{G} is the fraction of ingested glucose and the amount that reaches the systemic circulation (Dalla Man, Camilleri, et al. 2006). Variables are listed in Table 4.2.

Table 4.2: Variables of the gastrointestinal tract.

Variables	Description	Unit
States		
$Q_{\text{Gas},1}(t)$	Glucose mass in stomach (solid phase)	mg
$Q_{\text{Gas},2}(t)$	Glucose mass in intestine (liquid phase)	mg
Signals		
$R_{\text{G}}(t)$	Glucose rate of appearance in plasma	$\text{mg}\,\text{kg}^{-1}\,\text{min}^{-1}$
$u_{\text{G}}^{\text{oral}}(t)$	Oral glucose administration	$\text{mg}\,\text{min}^{-1}$
Parameter		
k_{G1}	Exchange rate constant	min^{-1}
k_{G2}	Absorption rate constant	min^{-1}
f_{G}	Oral bioavailability of glucose in plasma	–
BW	Body weight	kg
D	Amount of ingested glucose	mg

4.1.3 Hepatic Glucose Production

The liver is responsible for the production (mainly by glycogenolysis and gluconeogenesis) and storage (by glycogenesis) of glucose to maintain its concentration within the physiological range. From clinical studies (e. g., Seino et al. (1978), Gerich, Davis, et al. (1979), Saccà et al. (1979), Aronoff et al. (2004), Holt et al. (2010), Hinshaw et al. (2015), and Adeva-Andany et al. (2019)) it is known that endogenous production is modulated by concentrations of glucose, insulin, and glucagon.

During fasting, hepatic glucose production, S_{G}^{b}, equals glucose disappearance, which is the total glucose uptake U^{b} and renal excretion E^{b}:

$$S_{\text{G}}^{\text{b}} = U^{\text{b}} + E^{\text{b}}, \tag{4.8}$$

where $U(t) = U_{\mathrm{ii}}(t) + U_{\mathrm{id}}(t)$ as further described in Section 4.1.4. Glucagon facilitates endogenous production and thus, promotes glucose appearance in plasma, especially at low glucose levels (Section 4.1.10). Whereas insulin is the key hormone regulating glucose uptake $U_{\mathrm{id}}(t)$ in the postprandial state and thus, lowers glucose levels. To quantify the effect of glucose and the two counter-regulating hormones on hepatic production during a meal, a tracer protocol is needed (R. Basu et al. 2003). From the measurements given there several models of endogenous glucose production have been proposed (Dalla Man, Toffolo, et al. 2006). From that, a mixed meal model was developed by Dalla Man, Rizza, et al. (2006) and Dalla Man, Rizza, et al. (2007) and a model of glucagon action was incorporated by Micheletto et al. (2010). Other models have been compared by Emami et al. (2017).

Hepatic glucose production $S_{\mathrm{G}}(t)$ depends on glucose in plasma $G_{\mathrm{P}}(t)$, the amount of insulin in the portal vein $I_{\mathrm{Po}}(t)$, a delayed insulin signal $X_{\mathrm{I}}(t)$, and a delayed glucagon signal $X_{\mathrm{H}}(t)$, all with respect to their basal values. The functional description is given by

$$S_{\mathrm{G}}(t) = k_{p1} - k_{p2}G_{\mathrm{P}}(t) - k_{p3}X_{\mathrm{I}}(t) - k_{p4}I_{\mathrm{Po}}(t) + k_{p5}X_{\mathrm{H}}(t) \qquad S_{\mathrm{G}}(0) = S_{\mathrm{G}}^{\mathrm{b}}, \tag{4.9}$$

where k_{p1} is the extrapolated glucose production at zero glucose, insulin, and glucagon. $S_{\mathrm{G}}^{\mathrm{b}}$ is the basal glucose production and k_{p2} to k_{p5} are constants as shown in Table 4.3. Note that in T1DM, $I_{\mathrm{Po}}(t)$ is zero (see Section 4.1.8 for details). Insulin action on glucose production is realized by a chain of two compartments

$$\dot{I}_1(t) = -k_{\mathrm{I}} \cdot (I_1(t) - I(t)) \qquad I_1(0) = I^{\mathrm{b}}, \tag{4.10}$$

$$\dot{X}_{\mathrm{I}}(t) = -k_{\mathrm{I}} \cdot (X_{\mathrm{I}}(t) - I_1(t)) \qquad X_{\mathrm{I}}(0) = I^{\mathrm{b}}, \tag{4.11}$$

with $I(t)$ being the concentration of insulin in plasma, I^{b} its basal level, and k_{I} the delay between a change in insulin concentration from basal level and its action on $S_{\mathrm{G}}(t)$ (Section 4.1.7). $S_{\mathrm{G}}^{\mathrm{b}}$ is a free variable as measured in Dalla Man, Toffolo, et al. (2006). From basal steady-state, one gets

$$k_{p1} = S_{\mathrm{G}}^{\mathrm{b}} + k_{p2}G_{\mathrm{P}}^{\mathrm{b}} + k_{p3}I^{\mathrm{b}} + k_{p4}I_{\mathrm{Po}}^{\mathrm{b}} - k_{p5}X_{\mathrm{H}}^{\mathrm{b}}. \tag{4.12}$$

The delayed glucagon signal $X_{\mathrm{H}}(t)$ on glucose production is given by

$$\dot{X}_{\mathrm{H}}(t) = -k_{\mathrm{H}} \cdot X_{\mathrm{H}}(t) + k_{\mathrm{H}} \cdot \max\left(H(t) - H^{\mathrm{b}}, 0\right) \qquad X_{\mathrm{H}}(0) = X_{\mathrm{H}}^{\mathrm{b}} = 0, \tag{4.13}$$

where k_{H} is the delay between changes in glucagon concentration $H(t)$, related to its basal level H^{b} (Section 4.1.10) and action on hepatic glucose production. Moreover, hepatic glucose production is also constrained to be non-negative.

Table 4.3: Variables of hepatic glucose production.

Variables	Description	Unit
States		
$I_{\mathrm{Po}}(t)$	Insulin mass in portal vein	$\mathrm{pmol\,kg^{-1}}$
$X_{\mathrm{I}}(t)$	Insulin action	$\mathrm{pmol\,L^{-1}}$
$I_{1}(t)$	Delayed insulin signal	$\mathrm{pmol\,L^{-1}}$
$X_{\mathrm{H}}(t)$	Glucagon action	$\mathrm{ng\,L^{-1}}$
Signals		
$I(t)$	Insulin concentration in plasma	$\mathrm{pmol\,L^{-1}}$
$S_{\mathrm{G}}(t)$	Hepatic glucose production rate	$\mathrm{mg\,kg^{-1}\,min^{-1}}$
Parameter		
$S_{\mathrm{G}}^{\mathrm{b}}$	Basal hepatic glucose production	$\mathrm{mg\,kg^{-1}\,min^{-1}}$
k_{p1}	Extrapolated glucose production	$\mathrm{mg\,kg^{-1}\,min^{-1}}$
k_{p2}	Liver glucose effectiveness	$\mathrm{min^{-1}}$
k_{p3}	Amplitude modulation of insulin action on liver	$\mathrm{mg\,kg^{-1}\,min^{-1}}$ per $\mathrm{pmol\,L^{-1}}$
k_{p4}	Amplitude modulation of portal insulin action on liver	$\mathrm{mg\,kg^{-1}\,min^{-1}}$ per $\mathrm{pmol\,kg^{-1}}$
k_{p5}	Amplitude modulation of glucagon action on liver	$\mathrm{mg\,kg^{-1}\,min^{-1}}$ per $\mathrm{ng\,L^{-1}}$
k_{I}	Delay between insulin concentration and action	$\mathrm{min^{-1}}$
k_{H}	Delay between glucagon concentration and action	$\mathrm{min^{-1}}$

4.1.4 Glucose Utilization

Glucose utilization is the main effect of reducing plasma glucose concentration. After fasting, approx. 80 % of glucose disposal is insulin-independent and takes place in the brain, splanchnic tissues, and erythrocytes (Ferrannini and Groop 1989). Insulin-dependent glucose uptake mainly occurs in muscle (R. Andres et al. 1956). Furthermore, according to findings by Rizza et al. (1981) and Prager et al. (1986) it is assumed that glucose utilization can be modeled by an insulin-independent component, $U_{\mathrm{ii}}(t)$, that occurs in plasma and an insulin-dependent component, $U_{\mathrm{id}}(t)$, that occurs in the remote glucose compartment (Dalla Man, Rizza, et al. 2007). Insulin-independent utilization maintains glucose balance during fasting and is assumed to be constant with

$$U_{\mathrm{ii}}(t) = F_{\mathrm{ii}}, \tag{4.14}$$

according to experimental data in Best et al. (1981).

Glucose uptake $U_{\mathrm{id}}(t)$ in the postprandial state is mediated by insulin in normal subjects (Ferrannini, Bjorkman, et al. 1985) and is deteriorated in diabetics (Ferrannini, Simonson, et al. 1988). Clinical studies found a nonlinear dependence on glucose in the tissue, $G_{\mathrm{T}}(t)$, (Yki-Järvinen, Young, et al. 1987; Nielsen et al. 1998). It was mathematically expressed by Michaelis-Menten kinetics (Dalla Man, Rizza, et al. 2007) as given by

$$U_{\mathrm{id}}(t) = \frac{V_m(X(t)) \cdot G_{\mathrm{T}}(t)}{K_m(X(t)) + G_{\mathrm{T}}(t)}, \tag{4.15}$$

with the linear functions

$$V_m(X(t)) = V_{m0} + V_{mx} \cdot X(t), \tag{4.16}$$

$$K_m(X(t)) = K_{m0} + K_{mx} \cdot X(t), \tag{4.17}$$

and

$$\dot{X}(t) = -k_X X(t) + k_X \left(I(t) - I^{\mathrm{b}}\right) \qquad X(0) = 0, \tag{4.18}$$

where $X(t)$ is insulin in the interstitial fluid and k_X is the delay between deviations in insulin concentration from basal value I^{b} and action. Note that when the model was fitted to available data, K_{mx} was identified to zero and thus, K_m does not depend on $X(t)$ anymore which yields to

$$U_{\mathrm{id}}(t) = \frac{(V_{m0} + V_{mx} \cdot X(t))\, G_{\mathrm{T}}(t)}{K_{m0} + G_{\mathrm{T}}(t)}. \tag{4.19}$$

Given Eqs. (4.14) and (4.19), the total glucose uptake is

$$U(t) = U_{\mathrm{ii}}(t) + U_{\mathrm{id}}(t). \tag{4.20}$$

When in basal state, insulin action $X(t) = 0$ and glucose utilization U^{b} equals hepatic glucose production $S_{\mathrm{G}}^{\mathrm{b}}$. From (4.14) and (4.19)-(4.20) follows

$$U^{\mathrm{b}} = S_{\mathrm{G}}^{\mathrm{b}} = F_{\mathrm{ii}} + \frac{V_{m0} \cdot G_{\mathrm{T}}^{\mathrm{b}}}{K_{m0} + G_{\mathrm{T}}^{\mathrm{b}}}, \tag{4.21}$$

from which parameter V_{m0} is determined by

$$V_{m0} = \frac{\left(S_{\mathrm{G}}^{\mathrm{b}} - F_{\mathrm{ii}}\right) \cdot \left(K_{m0} + G_{\mathrm{T}}^{\mathrm{b}}\right)}{G_{\mathrm{T}}^{\mathrm{b}}}. \tag{4.22}$$

All signals and parameters are listed in Table 4.4.

The process of insulin-stimulated glucose uptake by the tissue plays a major role in the self-regulation of glucose concentration in plasma and alterations in the parameters have a significant influence on hyperglycemia after a glucose load, especially for diabetic subjects (Section 4.3).

4.1.5 Subcutaneous Glucose Kinetics

The shift from blood glucose data to minimal invasive techniques such as CGM includes sensing the glucose concentration from within the subcutaneous interstitial fluid (ISF). Thus, the dynamics of glucose diffusion from plasma to ISF have to be investigated.

Table 4.4: Variables of glucose utilization.

Variables	Description	Unit
States		
$X(t)$	Insulin in the interstitial fluid	$\mathrm{pmol\,L^{-1}}$
Signals		
$U_{\mathrm{ii}}(t)$	Insulin-independent glucose utilization	$\mathrm{mg\,kg^{-1}\,min^{-1}}$
$U_{\mathrm{id}}(t)$	Insulin-dependent glucose utilization	$\mathrm{mg\,kg^{-1}\,min^{-1}}$
Parameter		
U^{b}	Basal glucose utilization	$\mathrm{mg\,kg^{-1}\,min^{-1}}$
F_{ii}	Constant glucose uptake by brain and erythrocytes	$\mathrm{mg\,kg^{-1}\,min^{-1}}$
V_{mx}	Michaelis-Menten parameter	$\mathrm{mg\,kg^{-1}\,min^{-1}}$ per $\mathrm{pmol\,L^{-1}}$
V_{m0}	Michaelis-Menten parameter	$\mathrm{mg\,kg^{-1}\,min^{-1}}$
K_{mx}	Michaelis-Menten parameter	$\mathrm{mg\,kg^{-1}}$ per $\mathrm{pmol\,L^{-1}}$
K_{m0}	Michaelis-Menten parameter	$\mathrm{mg\,kg^{-1}}$
k_X	Delay between insulin concentration and action	$\mathrm{min^{-1}}$

Glucose in the ISF is subject to diffusion processes from blood plasma through the capillary wall. First experiments in diabetic rats showed that glucose in the ISF lags behind plasma glucose when its concentration in plasma increases, and leads plasma glucose when glucose decreases (Thomé-Duret et al. 1996). However, several studies contradicted this observation and proposed that ISF glucose always lags the plasma concentration (Rebrin, Steil, et al. 1999; Wentholt et al. 2007). The dynamical model proposed by Rebrin, Steil, et al. (1999) is now a widely accepted explanation for the diffusion of glucose among plasma, ISF, and muscles and fat tissues. As depicted in Fig. 4.4, glucose diffusion between plasma, $G_{\mathrm{P}}(t)$, and ISF, $G_{\mathrm{Isf}}(t)$, can be described by the rate constants k_{12} and k_{21}, clearance from plasma and ISF is given by parameters k_{01} and k_{02}, respectively:

$$\dot{G}_{\mathrm{Isf}}(t) = -(k_{02} + k_{12})G_{\mathrm{Isf}}(t) + k_{21}\frac{V_1}{V_2}G_{\mathrm{P}}(t), \tag{4.23}$$

where V_1 and V_2 are the volumes of plasma and ISF, respectively. The sensor measure $G_{\mathrm{Sc}}(t)$ is formulated to be proportional to the ISF glucose concentration with $G_{\mathrm{Sc}}(t) = \alpha G_{\mathrm{Isf}}(t)$ which yields to

$$\dot{G}_{\mathrm{Sc}}(t) = -p_2 G_{\mathrm{Sc}}(t) + p_3 G_{\mathrm{P}}(t), \tag{4.24}$$

where $p_3 = \alpha k_{21}\frac{V_1}{V_2}$ and $p_2 = k_{02} + k_{12}$ are identifiable from plasma glucose data and ISF sensor samples. From that, ISF delay time is $\tau = \frac{1}{p_2}$ and was estimated to be within 5 min to 12 min (Rebrin and Steil 2000). Rewriting (4.24) in terms of τ yields to

$$\dot{G}_{\mathrm{Sc}}(t) = -\frac{1}{\tau}G_{\mathrm{Sc}}(t) + \frac{g}{\tau}G_{\mathrm{P}}(t) \quad \text{with } k_g = \frac{1}{\tau} \qquad G_{\mathrm{Sc}}(0) = G_{\mathrm{P}}^{\mathrm{b}}, \tag{4.25}$$

where $g = p_3\tau$, which can be regarded as a steady-state gain. That means, in steady-state, g is the ratio $\frac{G_{\mathrm{Sc}}}{G_{\mathrm{P}}}$ of the glucose concentrations in ISF and plasma and should be, from physiology, equal to 1 (Steil, Rebrin, J. Mastrototaro, et al. 2003), which was also estimated from measurement data (Facchinetti

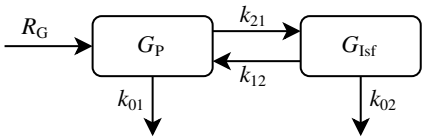

Figure 4.4: Model of subcutaneous glucose concentration (adapted from Rebrin and Steil (2000)). Diffusion of glucose between plasma and surrounding interstitial fluid is assumed to be linear first-order.

et al. 2007). Setting $g = 1$, the variable is not considered further. Moreover, k_g is a rate constant. Given the relation in (4.3), the s.c. glucose concentration $G_I(t)$ is given as

$$G_I(t) = \frac{G_{Sc}(t)}{V_G}, \tag{4.26}$$

where V_G is the plasma distribution volume listed in Table 4.1. Signal $G_I(t)$ serves as one measurable output of the system. Other technical characteristics of subcutaneous glucose measuring devices like sensor induced time lags or noise are discussed in Section 4.5.2. All variables are reported in Table 4.5.

Table 4.5: Variables of subcutaneous glucose kinetics.

Variables	Description	Unit
States		
$G_{Sc}(t)$	Subcutaneous glucose mass	$\mathrm{mg\,kg^{-1}}$
Signals		
$G_I(t)$	Subcutaneous glucose concentration	$\mathrm{mg\,dL^{-1}}$
Parameter		
k_g	Subcutaneous glucose rate	$\mathrm{min^{-1}}$

4.1.6 Renal Excretion

Renal excretion $E(t)$ occurs if glucose in plasma $G_P(t)$ exceeds a certain threshold at which the capacity of the kidneys to absorb glucose is reached. This limit is around $180\,\mathrm{mg\,dL^{-1}}$, but varies individually. The renal threshold hypotheses (RTH) model given by De Gaetano, Panunzi, Eliopoulos, et al. (2014) assumes linear behavior in urinary glucose loss with filtration rate k_{e1} and renal threshold k_{e2}:

$$E(t) = \begin{cases} k_{e1} \cdot [G_P(t) - k_{e2}] & \text{if } G_P(t) > k_{e2}, \\ 0 & \text{if } G_P(t) \leq k_{e2}\,. \end{cases} \tag{4.27}$$

The model variables are given in Table 4.6. In the non-diabetic subject, renal excretion is seldom. In diabetic patients, this can occur and is detectable by a urine test.

Table 4.6: Variables of glucose excretion.

Variables	Description	Unit
Signals		
$E(t)$	Glucose renal excretion	$\mathrm{mg\,kg^{-1}\,min^{-1}}$
Parameter		
k_{e1}	Renal filtration rate	$\mathrm{min^{-1}}$
k_{e2}	Renal threshold	$\mathrm{mg\,kg^{-1}}$

4.1.7 Insulin Kinetics

Insulin kinetics can be described by a two-compartment model as shown in Fig. 4.5, taking into account insulin mass in plasma and liver (Ferrannini and Cobelli 1987a). The dynamics are given by

$$\dot{I}_\mathrm{P}(t) = -\left(m_2 + m_4\right) I_\mathrm{P}(t) + m_1 I_\mathrm{L}(t) + R_\mathrm{I}(t) + u_\mathrm{I}^\mathrm{iv}(t) \qquad I_\mathrm{P}(0) = I_\mathrm{P}^\mathrm{b}, \tag{4.28}$$

$$\dot{I}_\mathrm{L}(t) = -\left(m_1 + m_3(t)\right) I_\mathrm{L}(t) + m_2 I_\mathrm{P}(t) + S_\mathrm{I}(t) \qquad I_\mathrm{L}(0) = I_\mathrm{L}^\mathrm{b}, \tag{4.29}$$

$$I(t) = \frac{I_\mathrm{P}(t)}{V_\mathrm{I}} \qquad I(0) = I^\mathrm{b}, \tag{4.30}$$

where $I_\mathrm{P}(t)$ and $I_\mathrm{L}(t)$ are the insulin masses in plasma and liver, respectively. Parameter V_I is the distribution volume of insulin, m_1 and m_2 are rate constants describing insulin exchange between the compartments, and $m_3(t)$ and m_4 describe insulin degradation. Note that $m_3(t)$ is time-dependent. $S_\mathrm{I}(t)$ is the insulin secretion rate as explained in Section 4.1.8, $R_\mathrm{I}(t)$ is the rate of appearance of subcutaneously injected insulin into plasma (Section 4.1.9), and $u_\mathrm{I}^\mathrm{iv}(t)$ is the intravenous insulin infusion rate. In T2DM patients, $S_\mathrm{I}(t)$ is elevated, while it is assumed to be not existent in T1DM. To compensate for this, $R_\mathrm{I}(t)$ is the source of insulin supply, although it is not needed in healthy people.

By setting the derivative $\dot{I}_\mathrm{L}(t)$ in (4.29) to zero, the basal insulin concentration in the liver, I_L^b, can be derived. In normal and T2DM patients, it is given by

$$I_\mathrm{L}^\mathrm{b} = \frac{m_2 I_\mathrm{P}^\mathrm{b} + S_\mathrm{I}^\mathrm{b}}{m_1 + m_3^\mathrm{b}}, \tag{4.31}$$

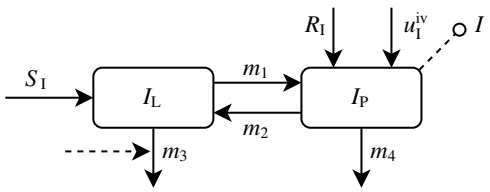

Figure 4.5: Two-compartment model of insulin kinetics (adapted from Dalla Man, Rizza, et al. (2007)). Insulin concentration $I(t)$ is accessible from measurements of plasma insulin mass $I_\mathrm{P}(t)$ which is in exchange with the liver $I_\mathrm{L}(t)$. In healthy and T2DM people, $S_\mathrm{I}(t)$ is the natural insulin secretion rate, in T1DM its absence must be compensated by external insulin supply $R_\mathrm{I}(t)$. Insulin clearance takes place in both the liver and plasma compartment.

whereas in T1DM patients, it is

$$I_{\mathrm{L}}^{\mathrm{b}} = \frac{m_2 I_{\mathrm{P}}^{\mathrm{b}}}{m_1 + m_3^{\mathrm{b}}}, \tag{4.32}$$

with m_3^{b} as defined in (4.36). Degradation takes place in the periphery and is assumed to be linear with constant m_4. From measurements of C-peptides, it is known that the liver extracts a significant amount of insulin that was secreted by the pancreas through the portal vein. Hepatic extraction $HE(t)$ can then be defined as the insulin flux that leaves the liver irreversible, $m_3(t)$, divided by the total insulin flux leaving the liver as given by

$$HE(t) = \frac{m_3(t)}{m_1 + m_3(t)}, \text{ from which } m_3(t) = \frac{HE(t) \cdot m_1}{1 - HE(t)}, \tag{4.33}$$

the hepatic clearance, can be determined. From measurements of the post-hepatic plasma insulin concentration, hepatic extraction was found to be linearly correlated with insulin secretion $S_{\mathrm{I}}(t)$ as

$$HE(t) = -m_5 S_{\mathrm{I}}(t) + m_6 \qquad HE(0) = HE^{\mathrm{b}}, \tag{4.34}$$

with m_5 respectively m_6 denoting slope and offset (Meier, Veldhuis, et al. 2005). In basal state,

$$m_6 = m_5 S_{\mathrm{I}}^{\mathrm{b}} + HE^{\mathrm{b}}, \tag{4.35}$$

$$m_3^{\mathrm{b}} = \frac{HE^{\mathrm{b}} \cdot m_1}{1 - HE^{\mathrm{b}}}, \tag{4.36}$$

$$S_{\mathrm{I}}^{\mathrm{b}} = m_3^{\mathrm{b}} \cdot I_{\mathrm{L}}^{\mathrm{b}} + m_4 \cdot I_{\mathrm{P}}^{\mathrm{b}} = D_{\mathrm{I}}^{\mathrm{b}}, \tag{4.37}$$

can be determined, where $S_{\mathrm{I}}^{\mathrm{b}}$ and $D_{\mathrm{I}}^{\mathrm{b}}$ denote basal insulin secretion and degradation, respectively. From Eqs. (4.33) and (4.34) follows that hepatic extraction falls with rising insulin secretion and thus, more insulin passes the liver and enters the systemic circulation, where it stimulates glucose uptake.

In humans, the liver is responsible for 40 % to 80 % insulin clearance, CL, in steady-state (Meier, Veldhuis, et al. 2005). When fixing $CL = 60\,\%$ (Dalla Man, Rizza, et al. 2007), i. e.,

$$\frac{m_3^{\mathrm{b}} \cdot I_{\mathrm{L}}^{\mathrm{b}}}{m_3^{\mathrm{b}} \cdot I_{\mathrm{L}}^{\mathrm{b}} + m_4 \cdot I_{\mathrm{P}}^{\mathrm{b}}} = 0.6, \tag{4.38}$$

parameters m_4 and m_2 yield to

$$m_4 = \frac{2}{5} \cdot \frac{S_{\mathrm{I}}^{\mathrm{b}}}{I_{\mathrm{P}}^{\mathrm{b}}} \cdot \left(1 - HE^{\mathrm{b}}\right), \tag{4.39}$$

$$m_2 = \left(\frac{S_{\mathrm{I}}^{\mathrm{b}}}{I_{\mathrm{P}}^{\mathrm{b}}} - \frac{m_4}{1 - HE^{\mathrm{b}}}\right) \cdot \frac{1 - HE^{\mathrm{b}}}{HE^{\mathrm{b}}}. \tag{4.40}$$

In T1DM subjects, insulin secretion is absent and thus, HE and m_3 are constants given by

$$m_6 = HE^{\mathrm{b}}, \tag{4.41}$$

$$m_3 = \frac{HE^{\mathrm{b}} \cdot m_1}{1 - HE^{\mathrm{b}}}. \tag{4.42}$$

Furthermore, to maintain steady-state, a basal insulin infusion rate $IIR^{\mathrm{b}} = u_{\mathrm{I}}^{\mathrm{sc}}(t) = \text{const}$ must be administered through the s.c. site, which is given by

$$IIR^{\mathrm{b}} = I_{\mathrm{P}}^{\mathrm{b}} \cdot \left(m_2 + m_4 - \frac{m_1 \cdot m_2}{m_1 + m_3} \right). \tag{4.43}$$

That leads to a closed-loop approach with $I_{\mathrm{P}}^{\mathrm{b}}$ being the set point from which the optimal infusion rate can be determined to maintain steady-state. On the other hand, rearranging (4.43) for $I_{\mathrm{P}}^{\mathrm{b}}$ can be seen as open-loop control, where basal insulin depends on the insulin infusion rate. All states, signals, and parameters are reported in Table 4.7.

Table 4.7: Variables of insulin kinetics.

Variables	Description	Unit
States		
$I_{\mathrm{P}}(t)$	Insulin mass in plasma	$\mathrm{pmol\,kg^{-1}}$
$I_{\mathrm{L}}(t)$	Insulin mass in liver	$\mathrm{pmol\,kg^{-1}}$
Signals		
$I(t)$	Insulin concentration in plasma	$\mathrm{pmol\,L^{-1}}$
$S_{\mathrm{I}}(t)$	Insulin secretion rate	$\mathrm{pmol\,kg^{-1}\,min^{-1}}$
$R_{\mathrm{I}}(t)$	Insulin rate of appearance in plasma	$\mathrm{pmol\,kg^{-1}\,min^{-1}}$
$u_{\mathrm{I}}^{\mathrm{iv}}(t)$	External i.v. insulin infusion rate	$\mathrm{pmol\,kg^{-1}\,min^{-1}}$
$m_3(t)$	Hepatic insulin clearance	$\mathrm{min^{-1}}$
$HE(t)$	Hepatic insulin extraction	–
Parameter		
$I_{\mathrm{P}}^{\mathrm{b}}$	Basal plasma insulin mass	$\mathrm{pmol\,kg^{-1}}$
$I_{\mathrm{L}}^{\mathrm{b}}$	Basal liver insulin mass	$\mathrm{pmol\,kg^{-1}}$
I^{b}	Basal plasma insulin concentration	$\mathrm{pmol\,L^{-1}}$
V_{I}	Insulin distribution volume	$\mathrm{L\,kg^{-1}}$
m_1	Insulin exchange rate	$\mathrm{min^{-1}}$
m_2	Insulin exchange rate	$\mathrm{min^{-1}}$
m_4	Insulin clearance from into periphery	$\mathrm{min^{-1}}$
m_5	Hepatic extraction slope	$\mathrm{min\,kg\,pmol^{-1}}$
m_6	Hepatic extraction offset	–

4.1.8 Insulin Secretion

To control the proper amount of insulin in plasma, pancreatic β-cells have mechanisms to detect changes in various hormones and nutrients within the circulatory system, with glucose in plasma being the main determinant. Insulin is secreted into the portal vein, and from there it is extracted

to a large extent by the liver (Section 4.1.7). Thus, only the post-hepatic insulin concentration is directly measurable. To overcome this problem insulin secretion rate is usually reconstructed from C-peptide data, which is a side product of insulin production and does not undergo liver extraction. Pre-hepatic insulin secretion was first investigated and modeled by Eaton et al. (1980) and assumes a two-compartment linear model for C-peptide kinetics as

$$\dot{CP}_1(t) = -(k_{01} + k_{21})CP_1(t) + k_{12}CP_2 + SR(t), \tag{4.44}$$

$$\dot{CP}_2(t) = k_{21}CP_1(t) - k_{12}CP_2(t), \tag{4.45}$$

where CP_1 and CP_2 are the C-peptide concentrations in plasma and periphery above basal level, respectively, and $SR(t)$ is the above basal secretion rate entering the accessible pool CP_1. Parameter k_{12} and k_{21} are transfer rates and k_{01} is the irreversible loss.

A functional description between glucose concentration and insulin secretion is based on the insulin packet storage theory proposed by Grodsky (1972) and assumes secretion as the sum of two compartments, mimicking static and dynamic insulin release as

$$SR(t) = S_I^s(t) + S_I^d(t). \tag{4.46}$$

Static insulin control $S_I^s(t)$ is assumed to be equal to the provision of new insulin to the β-cells $Y(t) = S_I^s(t)$ which is related to the glucose level above basal by

$$\dot{Y}(t) = \begin{cases} -\alpha\left[Y(t) - \beta\left(G(t) - G^b\right)\right] & \text{if } G(t) \geq G^b \\ -\alpha Y(t) & \text{if } G(t) < G^b \end{cases} \qquad Y(0) = 0, \tag{4.47}$$

where $\frac{1}{\alpha}$ is the time constant with which $Y(t)$ tends to the steady-state value linearly related to static glucose control parameter β.

Dynamic insulin control $S_I^d(t)$ accounts for promptly releasable insulin in the β-cells after an increase in glucose concentration, which is typically related to the first insulin response. The flux is proportional to the derivative of the glucose signal $G(t)$ with

$$S_I^d(t) = \begin{cases} \kappa \dfrac{dG(t)}{dt} & \text{if } \dfrac{dG(t)}{dt} > 0 \text{ and } G(t) > G^b, \\ 0 & \text{otherwise,} \end{cases} \tag{4.48}$$

where κ can be seen as a derivative control of increasing glucose concentration on insulin secretion. If the glucose concentration is falling or below the basal level G^b, dynamic insulin secretion is assumed to be zero (Toffolo, Breda, et al. 2001). Setting the derivatives in (4.44)-(4.45) to zero yields to the basal insulin secretion rate S_I^b as

$$S_I^b(t) = k_{01}CP_1^b, \tag{4.49}$$

where CP_1^b is the basal C-peptide concentration in the accessible compartment. The model of C-peptide kinetics and insulin secretion have been extended into a model describing the insulin flux $S_{Po}(t)$ into the portal vein:

$$S_{Po}(t) = S_I^b(t) + S_I^s(t) + S_I^d(t) = \begin{cases} S_I^b + Y(t) + \kappa\dot{G}(t) & \text{if } \dot{G}(t) > 0 \text{ and } G(t) > G^b, \\ S_I^b + Y(t) & \text{if } \dot{G}(t) \leq 0, \end{cases} \tag{4.50}$$

with

$$\dot{Y}(t) = \begin{cases} -\alpha \cdot \left[Y(t) - \beta\left(G(t) - G^b\right)\right] & \text{if } \beta\left(G(t) - G^b\right) \geq -S_I^b \\ -\alpha \cdot Y(t) - \alpha S_I^b & \text{if } \beta\left(G(t) - G^b\right) < -S_I^b \end{cases} \qquad Y(0) = Y^b = 0, \tag{4.51}$$

where $S_{Po}(t)$ contains the terms for basal, static, and dynamic insulin control. Pancreatic insulin secretion $S_I(t)$ is then described by

$$S_I(t) = \gamma \cdot I_{Po}(t), \tag{4.52}$$

$$\dot{I}_{Po}(t) = -\gamma I_{Po}(t) + S_{Po}(t) \qquad I_{Po}(0) = I_{Po}^b, \tag{4.53}$$

where $I_{Po}(t)$ is the insulin concentration within the portal vein, I_{Po}^b its basal value, and γ the transfer rate between the portal vein and liver (Dalla Man, Rizza, et al. 2007). In steady-state, glucose concentration equals its basal value and thus, $Y^b = 0$, from which $S_{Po}(t) = S_I^b$. Setting the derivative $\dot{I}_{Po}(t)$ to zero, it follows that $S_I(t) = S_I^b$. All states, signals, and parameters are reported in Table 4.8.

Equations (4.50)-(4.53) describe pancreatic insulin secretion in the healthy, beginning in the β-cells, secretion into the portal vein, and extraction of insulin by the liver before entering the circulatory system (Section 4.1.7). The secretory process is determined by the deviation of glucose above basal level (static control) and second, by the rate of increase of glucose (dynamic control). In T2DM or people with impaired glucose tolerance the equations still hold, but it can be assumed that parameter values are altered, especially dynamic gain κ and static gain β as it is further shown in Section 4.3. In T1DM, a complete lack of insulin secretion is assumed and thus, all parameters are set constant to zero as there is no action on glucose changes anymore.

4.1.9 Subcutaneous Insulin Kinetics

In healthy subjects, insulin is secreted by the pancreas. In T2DM this mechanism is disturbed, whereas in T1DM patients it is completely absent. Thus, exogenous insulin treatment is needed to control glucose metabolism manually. Depending on the diabetes type and treatment regime, rapid-acting and short-acting insulin analogs have to be injected subcutaneously to compensate for basal or postprandial lack of insulin. For patients who have to inject insulin, it is therefore important to be able to estimate the onset and duration of insulin action to avoid under-supply or over-supply. Insulin kinetics in the s.c. space depends, among other factors, on its type, amount, and injected volume (Binder 1969).

Table 4.8: Variables of insulin secretion.

Variables	Description	Unit
States		
$I_{\mathrm{Po}}(t)$	Insulin concentration in portal vein	$\mathrm{pmol\,kg^{-1}}$
$Y(t)$	Provision of new insulin to the β-cells	$\mathrm{pmol\,kg^{-1}\,min^{-1}}$
Signals		
$S_{\mathrm{Po}}(t)$	Insulin flux within the portal vein	$\mathrm{pmol\,kg^{-1}\,min^{-1}}$
$S_{\mathrm{I}}(t)$	Pancreatic insulin secretion rate	$\mathrm{pmol\,kg^{-1}\,min^{-1}}$
Parameter		
$S_{\mathrm{I}}^{\mathrm{b}}$	Basal insulin secretion rate	$\mathrm{pmol\,kg^{-1}\,min^{-1}}$
$I_{\mathrm{Po}}^{\mathrm{b}}$	Basal insulin concentration in portal vein	$\mathrm{pmol\,kg^{-1}}$
α	Transfer rate between glucose signal and action	$\mathrm{min^{-1}}$
β	β-cell responsivity to glucose changes	$\mathrm{pmol\,kg^{-1}\,min^{-1}\,per\,mg\,dL^{-1}}$
γ	Transfer rate between portal vein and liver	$\mathrm{min^{-1}}$
κ	β-cell responsivity to glucose rate of increase	$\mathrm{pmol\,kg^{-1}\,per\,mg\,dL^{-1}}$

From a modeling point of view, s.c. insulin injection is not instantaneously available in blood plasma as it would be if secreted by the pancreas, but it is delayed and typically described by a combination of first-order systems approximating the dissolution of insulin from a nonmonomeric to a monomeric state (Gradel et al. 2018). Several clinical trials (Lepore et al. 2000) have been fulfilled and from that, models have been developed (Mosekilde et al. 1989; Steil, Rebrin, Darwin, et al. 2006; Wong et al. 2008). Reviews are also available (Nucci et al. 2000). Here, a modified version of a two-compartment model proposed by Kraegen et al. (1984) is considered, which was also implemented by Dalla Man, Raimondo, et al. (2007).

The model structure consists of two compartments as depicted in Fig. 4.6. It is described by two first-order differential equations:

$$\dot{I}_{\mathrm{Sc},1}(t) = -(k_{i1} + k_{i2})I_{\mathrm{Sc},1}(t) + u_{\mathrm{I}}^{\mathrm{sc}}(t) \qquad I_{\mathrm{Sc},1}(0) = I_{\mathrm{Sc},1}^{\mathrm{b}}, \tag{4.54}$$

$$\dot{I}_{\mathrm{Sc},2}(t) = k_{i1}I_{\mathrm{Sc},1}(t) - k_{i3}I_{\mathrm{Sc},2}(t) \qquad I_{\mathrm{Sc},2}(0) = I_{\mathrm{Sc},2}^{\mathrm{b}}, \tag{4.55}$$

where $I_{\mathrm{Sc},i}(t), i = 1, 2$ are the mass concentrations of insulin in nonmonomeric (slowly dissolving) and monomeric (rapidly dissolving) state, respectively, k_{i1} is the rate of insulin dissociation between them, and $u_{\mathrm{I}}^{\mathrm{sc}}(t)$ is the insulin infusion rate. Parameters k_{i2} and k_{i3} are rates with which the insulin components are absorbed into the plasma $I_{\mathrm{P}}(t)$. From that, the rate of appearance of insulin in plasma yields to

$$R_{\mathrm{I}}(t) = k_{i2} \cdot I_{\mathrm{Sc},1}(t) + k_{i3} \cdot I_{\mathrm{Sc},2}(t). \tag{4.56}$$

Insulin clearance from plasma is modulated as described in Section 4.1.7 and all variables are reported in Table 4.9. In TNDM and T2DM subjects, basal insulin in the subcutaneous tissue is $I_{\mathrm{Sc},1}^{\mathrm{b}} = I_{\mathrm{Sc},2}^{\mathrm{b}} = 0$ since no insulin is injected. For T1DM, insulin must be continuously administered to maintain steady-

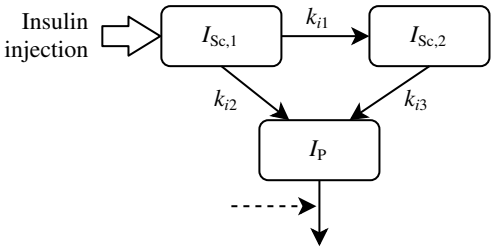

Figure 4.6: Exogenous insulin administration follows a two-compartment structure until it reaches plasma (solid lines), from where its clearance is modulated by different signals (dotted line).

state as already pointed out in Section 4.1.7. Thus, setting the derivatives in Eqs. (4.54) and (4.55) to zero and defining $u_I^{sc}(t) = IIR^b$, the basal insulin in the subcutaneous compartments yields to

$$I_{Sc,1}^b = \frac{IIR^b}{k_{i1} + k_{i2}}, \tag{4.57}$$

$$I_{Sc,2}^b = I_{Sc,1}^b \cdot \frac{k_{i1}}{k_{i3}}. \tag{4.58}$$

It is worth noting that parameters $k_{i1,\ldots,i3}$ reflect both the physiological characteristics of the subject under investigation as well as the pharmacokinetics of the administered substance. That means, identified parameters are only valid for a specific type of insulin (e. g. rapid-acting).

Table 4.9: Variables of subcutaneous insulin kinetics.

Variables	Description	Unit
States		
$I_{Sc,1}(t)$	Slowly dissolving insulin mass	pmol kg^{-1}
$I_{Sc,2}(t)$	Rapidly dissolving insulin mass	pmol kg^{-1}
Signals		
$R_I(t)$	Insulin rate of appearance in plasma	pmol kg^{-1} min^{-1}
$u_I^{sc}(t)$	External s.c. insulin infusion rate	pmol kg^{-1} min^{-1}
Parameter		
$I_{Sc,1}^b$	Basal insulin mass within injection site	pmol kg^{-1}
$I_{Sc,2}^b$	Basal insulin mass within intermediate pool	pmol kg^{-1}
k_{i1}	Insulin dissolution rate	min^{-1}
k_{i2}	Insulin absorption rate	min^{-1}
k_{i3}	Insulin absorption rate	min^{-1}

4.1.10 Glucagon Kinetics

The physiology and pathophysiology of glucagon in healthy and diabetic subjects have been widely studied in clinical trials (Unger 1971; Gerich, Lorenzi, et al. 1975; Unger and Orci 1976; Seino et al. 1978; Shah et al. 2000; Brehm et al. 2006). A linear one-compartment model of glucagon kinetics in plasma derived from measurements in the conscious dog was first built by Dobbins et al. (1995) and is

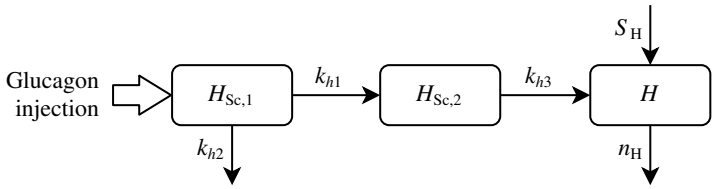

Figure 4.7: Model of glucagon kinetics and exogenous administration. Injected glucagon follows a two-compartment structure until it reaches plasma, a one-compartment model.

shown in the right part of Fig. 4.7. The model equation is given by

$$\dot{H}(t) = -n_{\mathrm{H}} H(t) + S_{\mathrm{H}}(t) + R_{\mathrm{H}}(t) \qquad H(0) = H^{\mathrm{b}}, \tag{4.59}$$

where $H(t)$ is the glucagon concentration in plasma, H^{b} the basal value, and parameter n_{H} is the clearance rate. $S_{\mathrm{H}}(t)$ is the glucagon secretion rate (Section 4.1.11) and $R_{\mathrm{H}}(t)$ is the rate of appearance of glucagon in plasma after a subcutaneous infusion (Section 4.1.12). States and parameter descriptions can be found in Table 4.10.

Table 4.10: Variables of glucagon kinetics.

Variables	Description	Unit
States		
$H(t)$	Glucagon concentration in plasma	$\mathrm{ng\,L^{-1}}$
Signals		
$S_{\mathrm{H}}(t)$	Glucagon secretion rate	$\mathrm{ng\,L^{-1}\,min^{-1}}$
$R_{\mathrm{H}}(t)$	Glucagon rate of appearance in plasma	$\mathrm{ng\,L^{-1}\,min^{-1}}$
Parameter		
H^{b}	Basal glucagon concentration in plasma	$\mathrm{ng\,L^{-1}}$
n_{H}	Glucagon clearance rate	$\mathrm{min^{-1}}$

4.1.11 Glucagon Secretion

There is a lack of widely accepted model approaches regarding the secretion and action of glucagon. According to Micheletto et al. (2010), secretion $S_{\mathrm{H}}(t)$ can be described as the sum of two compartments. Similarly to insulin secretion, one has a static glucose control, $S^{\mathrm{s}}_{\mathrm{H}}(t)$, with respect to glucose deviation from basal and a dynamic glucagon control, $S^{\mathrm{d}}_{\mathrm{H}}(t)$, proportional to the glucose rate of decline.

In T1DM patients, state $S^{\mathrm{s}}_{\mathrm{H}}(t)$ can be expressed by

$$\dot{S}^{\mathrm{s}}_{\mathrm{H}}(t) = \begin{cases} -k_\rho \left[S^{\mathrm{s}}_{\mathrm{H}}(t) - S^{\mathrm{b}}_{\mathrm{H}} \right] & \text{if } G(t) \geq G^{\mathrm{b}}\,, \\ -k_\rho \left[S^{\mathrm{s}}_{\mathrm{H}}(t) - \max\left(\frac{k_\sigma \cdot \left(G^{\mathrm{b}} - G(t) \right)}{I(t)+1} + S^{\mathrm{b}}_{\mathrm{H}}, 0 \right) \right] & \text{if } G(t) < G^{\mathrm{b}}, \end{cases} \tag{4.60}$$

where k_σ is the reaction of α-cells to a deviation of glucose concentration from its basal level, $\frac{1}{k_\rho}$ is the delay between glucose change and action on glucagon secretion, and $S_{\mathrm{H}}^{\mathrm{b}}$ the basal secretion rate (Visentin et al. 2018). From (4.60) it can be seen that no static secretion is assumed when glucose is above basal, it will only return to its basal secretion rate. That means, after a typical scenario like meal ingestion, glucagon secretion will not fall and thus, hepatic glucose production is not suppressed after a meal (compare to Eqs. (4.9) and (4.13)). When glucose falls below basal level, glucagon secretion is stimulated but modulated by insulin.

Unfortunately, secretion models for normal subjects are rare. Therefore (4.60) is adapted as

$$\dot{S}_{\mathrm{H}}^{\mathrm{s}}(t) = -k_\rho \left[S_{\mathrm{H}}^{\mathrm{s}}(t) - \max\left(\frac{k_\sigma \cdot \left(G^{\mathrm{b}} - G(t)\right)}{I(t)+1} + S_{\mathrm{H}}^{\mathrm{b}}, 0 \right) \right], \tag{4.61}$$

which allows a decline in glucagon concentration when glucose rises above basal as can be seen in clinical trials (e. g., Aronoff et al. 2004; Knop et al. 2007).

Dynamic secretion is

$$S_{\mathrm{H}}^{\mathrm{d}}(t) = k_\delta \cdot \max\left(-\frac{\mathrm{d}G(t)}{\mathrm{d}t}, 0 \right), \tag{4.62}$$

where k_δ is the α-cell responsivity to falling glucose levels (Micheletto et al. 2010). That means, it is assumed no dynamic glucagon release when glucose levels are rising. Furthermore, no distinction is made whether glucose or glucagon are above or below their basal concentration.

The complete functional description is given by

$$S_{\mathrm{H}}(t) = S_{\mathrm{H}}^{\mathrm{s}}(t) + S_{\mathrm{H}}^{\mathrm{d}}(t). \tag{4.63}$$

In steady-state, glucose concentration equals its basal value and $\dot{G}(t) = 0$. From that, $S_{\mathrm{H}}^{\mathrm{d}}(t)$ is zero and $S_{\mathrm{H}}^{\mathrm{s}}(t) = S_{\mathrm{H}}^{\mathrm{b}}$. Inserting into (4.59) yields to

$$S_{\mathrm{H}}^{\mathrm{b}} = n_{\mathrm{H}} \cdot H^{\mathrm{b}}, \tag{4.64}$$

where H^{b} is the freely settable basal glucagon concentration. Glucagon action on hepatic glucose production has already been stated in Section 4.1.3. All variables are summarized in Table 4.11.

4.1.12 Subcutaneous Glucagon Kinetics

Administration of s.c. glucagon has gained increased attention after its feasibility was shown in a closed-loop control trial on diabetic swine (El-Khatib, Jiang, and Damiano 2009). To further evaluate the kinetics of glucagon in the s.c. site, new mathematical models had to be developed since a one-compartment approach could not explain experimental data (Lv et al. 2013). More complex

Table 4.11: Variables of glucagon secretion.

Variables	Description	Unit
States		
$S_{\mathrm{H}}^{\mathrm{s}}(t)$	Static glucagon secretion rate	$\mathrm{ng\,L^{-1}\,min^{-1}}$
Signals		
$S_{\mathrm{H}}^{\mathrm{d}}(t)$	Dynamic glucagon secretion rate	$\mathrm{ng\,L^{-1}\,min^{-1}}$
Parameter		
$S_{\mathrm{H}}^{\mathrm{b}}$	Basal glucagon secretion rate	$\mathrm{ng\,L^{-1}\,min^{-1}}$
k_δ	α-cell responsivity to glucose rate of decline	$\mathrm{ng\,L^{-1}}$ per $\mathrm{mg\,dL^{-1}}$
k_ρ	Transfer rate between static glucagon secretion and glucose	$\mathrm{min^{-1}}$
k_σ	α-cell responsivity to glucose changes	$\mathrm{ng\,L^{-1}\,min^{-1}}$ ($\mathrm{pmol\,L^{-1}}$ per $\mathrm{mg\,dL^{-1}}$)

models include clearance at the injection site or saturation of the transport with respect to the amount of injected glucagon. According to Lv et al. (2013), who compared several models of increasing complexity to clinical data from type 1 diabetics, the linear two-compartment structure shown in the left part of Fig. 4.7 is proposed. It adequately fits experimental data. It can be expressed by

$$\dot{H}_{\mathrm{Sc},1}(t) = -\left(k_{h1} + k_{h2}\right) H_{\mathrm{Sc},1}(t) + u_{\mathrm{H}}^{\mathrm{sc}}(t) \qquad H_{\mathrm{Sc},1}(0) = H_{\mathrm{Sc},1}^{\mathrm{b}}, \tag{4.65}$$

$$\dot{H}_{\mathrm{Sc},2}(t) = k_{h1} H_{\mathrm{Sc},1}(t) - k_{h3} H_{\mathrm{Sc},2}(t) \qquad H_{\mathrm{Sc},2}(0) = H_{\mathrm{Sc},2}^{\mathrm{b}}, \tag{4.66}$$

where $H_{\mathrm{Sc},i}(t), i = 1, 2$ are the glucagon masses in the s.c. space. $H_{\mathrm{Sc},1}(t)$ represents the injection site to which exogenous glucagon infusion $u_{\mathrm{H}}^{\mathrm{sc}}(t)$ is administered. It also incorporates local clearance with constant k_{h2}. Compartment $H_{\mathrm{Sc},2}(t)$ represents an intermediate pool before plasma. Parameters k_{h1} to k_{h3} are rate constants as reported in Table 4.12.

The rate at which glucagon enters plasma is given as

$$R_{\mathrm{H}}(t) = \frac{1}{V_{\mathrm{H}}} k_{h3} \cdot H_{\mathrm{Sc},2}(t), \tag{4.67}$$

where $R_{\mathrm{H}}(t)$ denotes the rate of appearance and V_{H} the glucagon distribution volume. Basal levels of glucagon in the subcutaneous space, $H_{\mathrm{Sc},1}^{\mathrm{b}}$ and $H_{\mathrm{Sc},2}^{\mathrm{b}}$ are generally set to zero in all subject types.

Summary. In the preceding sections, the general equations of glucose-insulin-glucagon regulation and model differences between non-diabetics, type 1, and type 2 diabetics have been acquired successively. Table A.1 on page 191 summarizes all states and the main signals of the model.

4.2 Model of Virtual Subjects

After the general model equations have been derived in Sections 4.1.1 to 4.1.12, models of subjects are now to be generated in order to properly simulate and analyze their behavior. It is assumed that

Table 4.12: Variables of subcutaneous glucagon kinetics.

Variables	Description	Unit
States		
$H_{\mathrm{Sc},1}(t)$	Glucagon mass in injection site	$\mathrm{ng\,kg^{-1}}$
$H_{\mathrm{Sc},2}(t)$	Glucagon mass in intermediate pool	$\mathrm{ng\,kg^{-1}}$
Signals		
$R_{\mathrm{H}}(t)$	Glucagon rate of appearance in plasma	$\mathrm{ng\,L^{-1}\,min^{-1}}$
$u_{\mathrm{H}}^{\mathrm{sc}}(t)$	External s.c. glucagon infusion rate	$\mathrm{mg\,kg^{-1}\,min^{-1}}$
Parameter		
$H_{\mathrm{Sc},1}^{\mathrm{b}}$	Basal glucagon mass in injection site	$\mathrm{ng\,kg^{-1}}$
$H_{\mathrm{Sc},2}^{\mathrm{b}}$	Basal glucagon mass in intermediate pool	$\mathrm{ng\,kg^{-1}}$
V_{H}	Glucagon distribution volume	$\mathrm{L\,kg^{-1}}$
k_{h1}	Glucagon absorption rate	$\mathrm{min^{-1}}$
k_{h2}	Glucagon absorption rate	$\mathrm{min^{-1}}$
k_{h3}	Glucagon absorption rate	$\mathrm{min^{-1}}$

the metabolic characteristics of a person in a long-term manner can be expressed by a mathematical description of a vector of basal states and parameters. This means, that for a single person, parameters are assumed to be time-independent and fixed. The parameter vector will differ within a (patho)-physiological range, reflecting different metabolic constitutions in each subject. A wide range of parameter values is therefore desired also to include atypical but quite common metabolic conditions. Since diabetes, especially type 2, is a gradually progressing disease, this should also become apparent in the parameter variations and thus, developments from person to person are seamless. Nevertheless, when comparing groups with each other, mean values and variance of the parameters will differ. To summarize, the inter-subject variability should be large enough to include a wide variety of metabolic states, but the inter-group variability should allow a distinction between different diabetes types.

From the patient databases given below three standard subjects have been adopted who reflect the average behavior of three groups: non-diabetics, type 2, and type 1 diabetics. The modeling process aims to create a set of virtual subjects in each group that satisfy given statistical properties. This includes the distribution of each parameter, which is typically log-normal as most variables in biology and medicine. Further, the covariance between different variables, as it cannot be assumed that parameters are independent of each other. The modeling involves the following steps:

1. From available virtual subject databases, analyze statistics for all reported parameters.
2. Find reasonable assumptions when little or no information is available.
3. Fulfill a multivariate sampling process to generate TNDM, T2DM, and T1DM virtual subjects, taking into account the obtained statistical relationships.
   a) Chose the same covariance and distribution for parameters available in all groups.
   b) Apply the covariance matrix on the mean value given for TNDM and T2DM.
   c) Generate a set of multivariate random variables.
4. Proof the validity of the new subjects.

4.2.1 Virtual Patient Databases

Here, two sources from available literature are used as a basis for generating virtual subjects. In both publications, the same experimental protocol presented in R. Basu et al. (2003) and A. Basu, Dalla Man, Mariatoffolo, et al. (2004) was used to determine the model parameters.

Database for TNDM and T2DM. The publication by Dalla Man, Rizza, et al. (2007) presents experimental data from 204 healthy subjects (age: 56 ± 2 years, body weight: 78 ± 1 kg) and 14 type 2 diabetics (age: 57 ± 3 years, body weight: 91 ± 5 kg) who received a triple tracer and a mixed-meal containing 1.00 ± 0.02 g per kg body weight of glucose (10 kcal kg^{-1}, 45 % carbohydrate, 15 % protein, 40 % fat). The database includes measurement data for various glucose and insulin fluxes from which parameters were estimated. From that, a virtual population could be derived by their joint parameter distribution (Kovatchev, Breton, et al. 2009). The functions are not published, but the mean values for both types, $\boldsymbol{\mu}_{\text{TNDM}}$ and $\boldsymbol{\mu}_{\text{T2DM}}$, are reported in Cobelli and Carson (2008, p. 284).

Database for T1DM. The type 1 diabetes mellitus simulator (T1DMS), developed by Dalla Man, Micheletto, et al. (2014) and The Epsilon Group (2013) is equipped with 30 virtual patients, here denoted as T1DMS subjects. They have been generated from the joint parameter distribution of the non-diabetic adult population referred above. The inter-subject variability was assumed to be the same, which means, that T1DMS and TNDM subjects share the same covariance matrix. Furthermore, some changes were made to the average parameter vector to reflect clinically relevant alterations of the glucose metabolism in T1DM. Mean vector and covariance matrix are denoted by $\boldsymbol{\mu}_{\text{T1DMS}}$ and $\boldsymbol{\Sigma}_{\text{T1DMS}}$, respectively.

As mentioned in the preceding sections, the model consists of free variables, dependent variables, and constants. Free factors can be set to arbitrary values, whereas dependent variables can be derived from steady-state considerations or other constraints. Constants are static values independent of the subject type and are mostly derived from population data. Table A.2 lists all parameters, their units, and statistical information, further described in the following section.

4.2.2 Analysis of the Virtual Patient Databases

The T1DMS comes with predefined virtual subjects, from which 38 variables are freely settable, 23 are dependent on certain restrictions, and 10 are constant (Tables A.2 and A.3 on pages 192 and 193). Since there is no insulin secretion in T1DM patients, related parameters have been set to zero. Furthermore, the simulator comes with another model of the gastrointestinal tract which has been replaced by the model in Section 4.1.2. As no information is available for k_{G1} and k_{G2} they are not included in the analysis here but will be identified later (page 76). Hence, from a total of 68 variables, 29 parameters have to be chosen for further analysis illustrated in Fig. 4.8. Investigating

the linear relationship of the parameter matrix $\boldsymbol{P}$ results in a rank($\boldsymbol{P}$) = 29 and thus, all variables are linearly independent of each other.

The correlation coefficient of two random variables X and Y is their covariance, Cov $\{X, Y\}$, divided by the product of their standard deviations, which is

$$\begin{aligned}\rho &= \frac{\mathrm{Cov}\,\{X,Y\}}{\sigma_X \cdot \sigma_Y},\\ &= \frac{\mathrm{E}\,\{(X-\mathrm{E}\,\{X\})\,(Y-\mathrm{E}\,\{Y\})\}}{\sqrt{\mathrm{E}\left\{(X-\mathrm{E}\,\{X\})^2\right\}}\cdot\sqrt{\mathrm{E}\left\{(Y-\mathrm{E}\,\{Y\})^2\right\}}},\end{aligned} \tag{4.68}$$

where E $\{\cdot\}$ is the expectation value, Cov $\{\cdot\}$ is the covariance, and σ_X, σ_Y are the standard deviations of X and Y, respectively. The correlation coefficient is normalized between ± 1, where positive values indicate a positive correlation, negative values show a negative correlation, and zero means no correlation between X and Y. When ρ is applied to a limited sample of observations, the expectation value is substituted by the mean of the sample as

$$\rho = \frac{\sum_{i=1}^{n}(x_i-\bar{x})(y_i-\bar{y})}{\sqrt{\sum_{i=1}^{n}(x_i-\bar{x})^2}\cdot\sqrt{\sum_{i=1}^{n}(y_i-\bar{y})^2}}, \tag{4.69}$$

where n is the number of observations, x_i and y_i denote the i-th observation, and $\bar{x}$, $\bar{y}$ are the mean values of X and Y, respectively. Applying (4.69) on each pairwise parameter combination in P for the 30 delivered T1DMS virtual subjects (i. e. $n = 30$ observations) results in the correlation matrix in Fig. 4.8. Each tile indicates the linear relationship of a parameter with all others. Positive correlations are colored in tones of red, elements with a negative relationship in blue, whereas correlations towards zero are drawn paler. The white color indicates no linear correlation. The main diagonal shows the variance of each parameter, which is always one. From P, the matrix $P_r \subset P$ of reduced size is derived, containing 14 parameters with the highest absolute correlation. These are glucagon secretion parameters k_δ, k_σ, which are also correlated to the duration of diabetes that explains their relationship, and k_{i2}, k_{i3} with coefficients higher 0.9. Furthermore, glucagon clearance n_H and transfer rate k_ρ are highly negatively correlated. With rising basal glucose production S_G^b the ability of insulin action to suppress glucose production k_{p3} rises, too. It is also positively related to k_I, the rate constant between a change in insulin concentration and its action on hepatic glucose production. A similar behavior arises between k_H and k_{p5}, the transfer rate between glucagon changes in plasma and action on glucose production and gain of action. Last, m_1, m_5, and V_I are related to insulin kinetics. All other parameters having a correlation lower than 0.5 are not shown here. For further information, a combined scatter and histogram plot of the aforementioned parameters is shown in Fig. A.1 on page 193 as red dots. A scatter graph displays values for each pair of variables in one axis and provides suggestions on various kinds of correlation between the variables. In addition, on the main diagonal, a histogram over each parameter is drawn to visualize a possible distribution of that parameter.

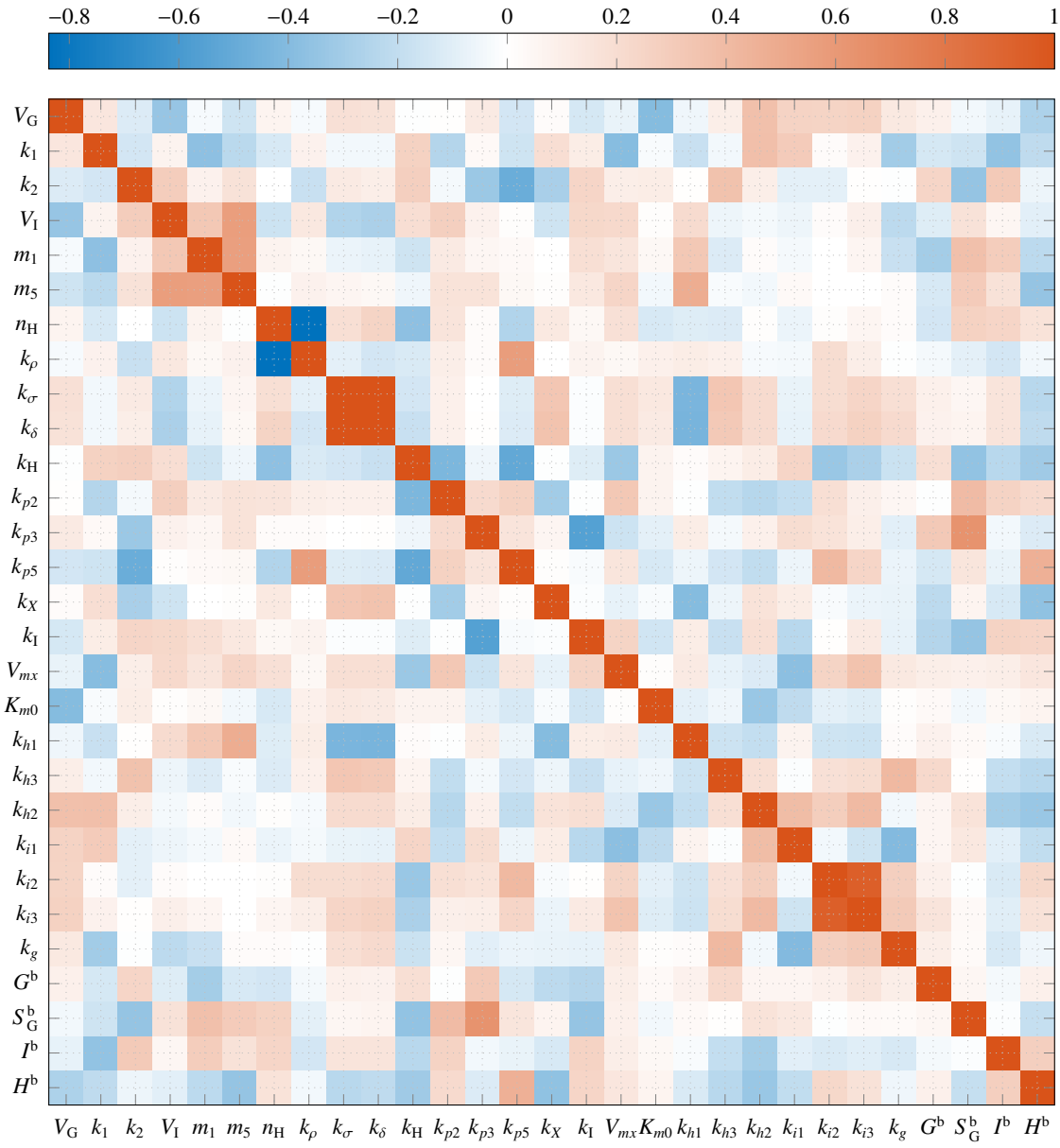

Figure 4.8: Correlation matrix of the T1DMS parameters: The values are normalized between ±1, where positive values indicate a positive correlation (colored in red), negative values denote a negative correlation (colored in blue), and 0 denotes no linear relationship (colored in white). The correlation of parameters with themselves is always one as seen on the main diagonal.

After determining the correlation between the parameters of the T1DMS, their distribution has to be analyzed. Here, the histogram is used as an estimate for the underlying probability density function as depicted in Fig. 4.9 for all variables. The bars represent the normalized occurrence of each continuous variable. A visual inspection shows that most parameters seem to follow a log-normal or normal distribution, except for k_σ and k_δ where this cannot be assumed from the given samples.

A continuous random variable X that is normally distributed with $X \sim \mathcal{N}(\mu_X, \sigma_X)$, where μ_X is the mean and σ_X the standard deviation, has the probability density function (PDF):

$$f_X(x) = \frac{1}{\sqrt{2\pi}\sigma_X} \exp\left(-\frac{1}{2}\left(\frac{x-\mu_X}{\sigma_X}\right)^2\right), \quad \sigma_X > 0. \tag{4.70}$$

From that, the log-normal distribution can be defined as a distribution whose logarithm has a normal distribution. Thus, a random variable $Y \sim \mathcal{LN}(\mu_Y, \sigma_Y)$ with log-normal distribution is $Y = e^{\mu_Y + \sigma_Y X}$ and its PDF is defined by

$$f_Y(y) = \frac{1}{\sqrt{2\pi}\sigma_Y y} \exp\left(-\frac{1}{2}\left(\frac{\ln y - \mu_Y}{\sigma_Y}\right)^2\right), \quad \sigma_Y > 0, \quad y > 0. \tag{4.71}$$

If the empirical mean, μ, and variance, σ^2, of the non-logarithmized values are known, suitable parameter values can be obtained by

$$\mu_Y = \ln\left(\frac{\mu^2}{\sqrt{\mu^2+\sigma^2}}\right), \qquad \sigma_Y = \sqrt{\ln\left(1+\frac{\sigma^2}{\mu^2}\right)}. \tag{4.72}$$

The log-normal distribution is thus well suited for non-negative values.

A continuous uniform distribution $X \sim \mathcal{U}(a, b)$ can be defined by its PDF as

$$f_X(x) = \begin{cases} \dfrac{1}{b-a} & \text{for } a \le x \le b, \\ 0 & \text{for } x < a \text{ or } x > b, \end{cases} \tag{4.73}$$

where a and b are the lower and upper boundaries, respectively.

With the information given above, a log-normal distribution was fitted for all parameters using a maximum likelihood estimation, except for the two aforementioned variables for which a uniform distribution was defined. As can be seen in Fig. 4.9 on top of the histograms, these distributions are a good choice for most variables.

4.2.3 Generation of Virtual Subjects

The databases and analysis presented above are a starting point for the generation of new virtual subjects that follow the known statistical representation of the populations. Note that not all databases cover the total number of variables in the presented metabolic model as not all physiological aspects

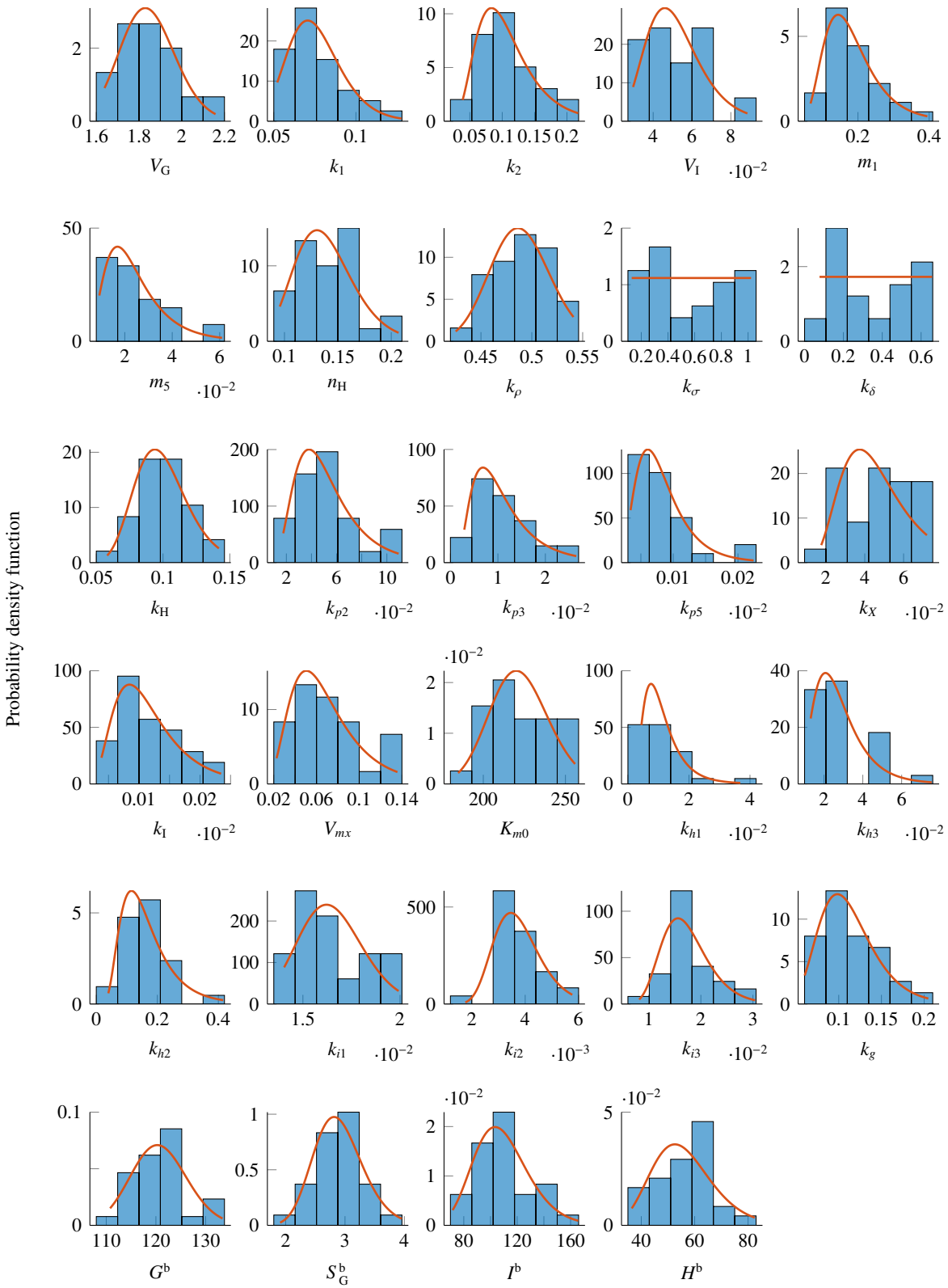

Figure 4.9: Normalized histograms and fitted probability density functions (PDF): Each axis shows a histogram over one parameter of the T1DMS subjects, the fitted PDF is overlayed on top. The distributions are assumed to be log-normal, except for k_σ and k_δ, where they are uniform.

were investigated in the several clinical studies in which these values were obtained. For TNDM and T2DM, the glucagon-related part of the model was not investigated in first publications (Cobelli and Carson 2008) but later reported in Carson et al. (2014). Furthermore, the subcutaneous glucose and insulin kinetics were not considered. On the other hand, in T1DM the complete insulin secretion part was assumed to be absent. And last, the parameters of the gastrointestinal absorption model are not available. For these variables, reasonable assumptions must be made or they have to be estimated from measurement data.

To take into account covariance information, a multivariate parameter generation process must be considered. A multivariate distribution is a generalization of the univariate distribution to more than one variable. Thus, $\boldsymbol{X}$ is a K-dimensional random vector with mean vector $\boldsymbol{\mu}_X$ and covariance matrix $\boldsymbol{\Sigma}_X$. From the multivariate normal distribution

$$f_X(\boldsymbol{x}) = \frac{1}{\sqrt{(2\pi)^K \, |\boldsymbol{\Sigma}_X|}} \exp\left(-\frac{1}{2} \left(\boldsymbol{x} - \boldsymbol{\mu}_X\right)^\top \boldsymbol{\Sigma}_X^{-1} \left(\boldsymbol{x} - \boldsymbol{\mu}_X\right)\right), \tag{4.74}$$

with $|\boldsymbol{\Sigma}_X| \equiv \det(\boldsymbol{\Sigma}_X)$, the log-normal multivariate distribution of the random vector $\boldsymbol{Y} \in \mathbb{R}^K$ can be derived as

$$f_Y(\boldsymbol{y}) = \frac{1}{\sqrt{(2\pi)^K \, |\boldsymbol{\Sigma}_Y|} \prod_{i=1}^K \boldsymbol{y}} \exp\left(-\frac{1}{2} \left(\ln \boldsymbol{y} - \boldsymbol{\mu}_Y\right)^\top \boldsymbol{\Sigma}_Y^{-1} \left(\ln \boldsymbol{y} - \boldsymbol{\mu}_Y\right)\right), \quad \boldsymbol{y} > 0, \tag{4.75}$$

where $\boldsymbol{x}, \boldsymbol{y}, \boldsymbol{\mu}_X$, and $\boldsymbol{\mu}_Y$ are K-by-1 vectors and $\boldsymbol{\Sigma}_X$,$\boldsymbol{\Sigma}_Y$ are K-by-K symmetric, positive definite matrices.

The process of generating new virtual subjects is generally equal for all three groups and shown in Algorithm 1.

Algorithm 1 Function gen() to generate new virtual subjects

Require: $\boldsymbol{\mu}_{\text{T1DMS}}, \boldsymbol{\Sigma}_{\text{T1DMS}}, \boldsymbol{\mu}_{\text{TNDM}}, \boldsymbol{\mu}_{\text{T2DM}}$ from available literature
Calculate the statistical properties such as variance and correlation
Calculate the log-normal distribution parameters from (4.72)
Perform multivariate sampling from a normal distribution
Calculate the cumulative distribution function from the standard normal distribution
Calculate the inverse cumulative distribution function
Transform back to a log-normal distribution

Generation of T1DM Virtual Subjects. The generation of new T1DM virtual subjects is the simplest task, as mean and covariance are already available from the T1DMS database. From that, the algorithm given above leads directly to new virtual subjects $\mathcal{S}$ with

$$\mathcal{S}_{\text{T1DM}} := \text{gen}\left(\boldsymbol{\mu}_{\text{T1DMS}}, \boldsymbol{\Sigma}_{\text{T1DMS}}\right), \tag{4.76}$$

where gen() is a generator function using the T1DMS mean vector, $\boldsymbol{\mu}_{\text{T1DMS}}$, and covariance matrix $\boldsymbol{\Sigma}_{\text{T1DMS}}$. Only parameters of the gastrointestinal tract are not available in the database and must be fitted to experimental records as further described at the end of this section.

For the validation of the generator function, 100 new virtual subjects were created. Their histograms and scatter plots are depicted in Fig. A.1 on page 193. A visual inspection shows good accordance between the T1DMS subjects and the newly created ones.

Generation of TNDM and T2DM Virtual Subjects. To generate TNDM and T2DM virtual subjects, the available mean vectors $\boldsymbol{\mu}_{\text{TNDM}}$ respectively $\boldsymbol{\mu}_{\text{T2DM}}$ are used. As there is no variance given in the literature, the fractional standard deviation of the T1DMS subjects is considered for each parameter, which is

$$c_v = \frac{\sigma_{\text{T1DMS}}}{\mu_{\text{T1DMS}}}, \quad \mu_{\text{T1DMS}} \neq 0, \tag{4.77}$$

where c_v is also known as the coefficient of variation. It shows the extent of variability in relation to the mean of the population. That means, the new variance is multiplicatively connected to the mean value and thus, allows larger deviations for higher means. Variances are given by

$$\sigma^2_{\text{TNDM}} = (c_v \cdot \mu_{\text{TNDM}})^2, \tag{4.78}$$

$$\sigma^2_{\text{T2DM}} = (c_v \cdot \mu_{\text{T2DM}})^2, \tag{4.79}$$

for each parameter in the T1DMS group. For variables not present in the T1DM simulator, a fractional standard deviation of $c_v = 0.35$ and no correlation is assumed for most parameters. The overall variances are computed as

$$\boldsymbol{\Sigma}_{\text{TNDM}} = \begin{bmatrix} \boldsymbol{\Sigma}_{\text{T1DMS}} & \mathbf{0} \\ \mathbf{0} & \boldsymbol{\sigma}^2_{\text{TNDM}} \end{bmatrix}, \tag{4.80}$$

$$\boldsymbol{\Sigma}_{\text{T2DM}} = \begin{bmatrix} \boldsymbol{\Sigma}_{\text{T1DMS}} & \mathbf{0} \\ \mathbf{0} & \boldsymbol{\sigma}^2_{\text{T2DM}} \end{bmatrix}, \tag{4.81}$$

where $\boldsymbol{\Sigma}_{\text{TNDM}}$ and $\boldsymbol{\Sigma}_{\text{T2DM}}$ are the covariance matrices of the TNDM and T2DM subjects, respectively. The lower right sub-matrices have diagonal form with variances σ^2_{TNDM} and σ^2_{T2DM} for each parameter on their main diagonal. From that, new TNDM and T2DM subjects can be generated using

$$\mathcal{S}_{\text{TNDM}} := \text{gen}\left(\boldsymbol{\mu}_{\text{TNDM}}, \boldsymbol{\Sigma}_{\text{TNDM}}\right), \tag{4.82}$$

$$\mathcal{S}_{\text{T2DM}} := \text{gen}\left(\boldsymbol{\mu}_{\text{T2DM}}, \boldsymbol{\Sigma}_{\text{T2DM}}\right). \tag{4.83}$$

For testing, 100 new virtual subjects in each group have been generated and the distribution of their parameters is shown in Fig. A.2 and also reported in Table A.2 on page 192. In general, the means

and distribution of the individual parameters differ, but their ranges overlap, sometimes significantly, so that no variable can be considered on its own. For some parameters, at least one group can be examined separately from the others (e. g., k_ρ, K_{m0}, G^b). For variables k_{i1}, k_{i2}, and k_{ki3}, and also for k_{h1}, k_{h2}, and k_{h3} the same mean and variance was assigned for all groups as can be seen in the quite similar distributions. Parameters k_{G1}, k_{G2} are related to the gastrointestinal tract, and their means have been identified from experimental data as described in the following paragraph. Parameters related to insulin action, both peripheral, V_{mx}, and hepatic, k_{p3}, are lower in T2DM compared to normal subjects. Hepatic glucose effectiveness, k_{p2}, is also lower. Next, variables connected to the insulin secretion part, the dynamic and static β-cell responsivity κ respective β, and also rate constant α are lower in T2DM. In T1DM, they are, along with γ and m_6, not visible in the graph as they are constant. The different parameter configurations reflect changes in the model behavior and can explain pathological alterations of the glucose regulation as can be seen in the simulation studies in Section 4.3.

Furthermore, a log-normal distribution is visible, except for k_σ and k_δ that are uniformly distributed. Note the much higher range due to the higher means, compared to the T1DM data. In addition to the parameters of the system model, also basal values are illustrated here for completeness.

Contrary to parameters, means of the basal values seem to be more meaningful for distinguishing between the groups. Hence, an increased plasma glucose concentration G^b suggests a pathological deviation from the norm. Also, basal insulin concentration, I^b, seems to be higher in diabetic people, which is in accordance with the higher basal insulin secretion rate, S_I^b, in T2DM to compensate for a deteriorated insulin action on glucose changes, visible in lower values for κ, α, and β.

Parameter Estimation of the Gastrointestinal Tract. As explained in Section 4.1.2, the gastrointestinal tract is modeled by two linear compartments representing the amount of glucose in the stomach and intestine, respectively. The rate constants must be estimated to available measurement data as no comparable values are present in the literature. The digestion of a meal highly depends on the composition of macronutrients like glucose, fat, and protein. As this information is seldom, measurements taken from a mixed meal input describe an average but typical scenario and could be a good starting point for a model of meal absorption.

To identify parameters of the gastrointestinal tract experimental data from Dalla Man, Rizza, et al. (2007) was used. In this experiment, the rate of appearance of glucose in blood plasma after a mixed meal test was determined for a population of 204 non-diabetics. The average input was 78 g glucose, which corresponds to 1 g kg^{-1} glucose for the average body weight of 78 kg. The time course is plotted in Fig. 4.10 on the left side, where the black line is the mean function and the gray area represents the $\pm 1\,\sigma$ range. The same protocol was fulfilled for 14 type 2 diabetics (90 g glucose load). Unfortunately, no experimental data has been published but an averaged meal prediction graph was plotted in Dalla Man, Rizza, et al. (2006) as shown in Fig. 4.10 in the middle panel. For T1DM, meal ingestion of 60 g glucose was simulated using the T1DMS. The mean trajectory, $\pm 1\,\sigma$ standard deviation, and upper and lower bounds are shown on the right side of the figure. From the reference data, it can be seen that

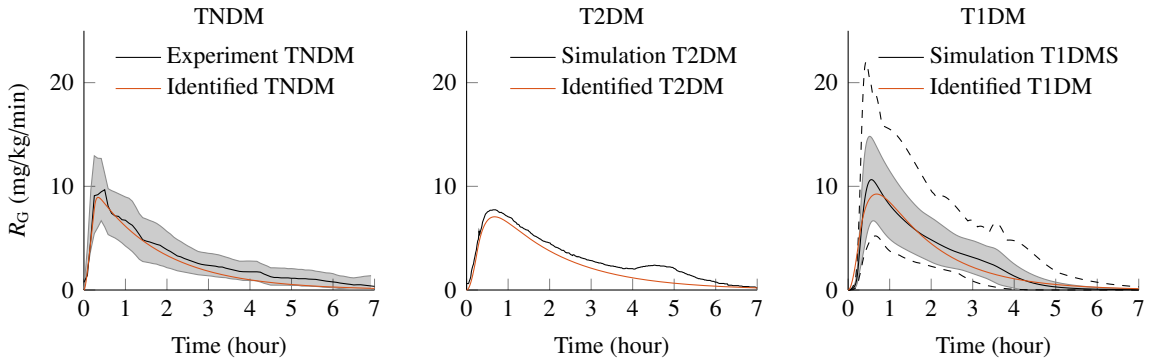

Figure 4.10: Identified rate of appearance of glucose in plasma after a meal for TNDM (left), T2DM (middle), and T1DM (right). References depicted by black solid lines ($\pm 1\sigma$ range in gray, upper and lower bounds by dashed lines), identified trajectories drawn in red. Note that for TNDM, reference is taken from the literature, whereas for T2DM and T1DM, the reference is also simulated.

the absorption rate in T2DM is lower than in the other groups. Whereas the variability for T1DM is much larger than for the healthy ones but comparable in their dynamic.

These three trajectories were taken as references for parameter identification of the model presented in Section 4.1.2. The two-compartment linear model has two rate constants k_{G1} and k_{G2} that determine the dynamics of meal digestion. A nonlinear least-squares estimation was used to identify the two parameters. As can be seen in Fig. 4.10, the model fits well the reference trajectories, though a small underestimation is observable in all three groups. Root mean squared error (RMSE) as given in Eq. (3.17) was calculated with 0.57, 0.81, and 1.23 mg dL^{-1} for TNDM, T2DM, and T1DM, respectively. The identified values, k_{G1} and k_{G2}, are reported in Table A.2. In summary, it can be said that the linear model can mimic the dynamic behavior of the gastrointestinal tract after a mixed meal input.

4.3 Simulation Studies

After the development of the dynamical model of glucose regulation and the creation of virtual subjects, the following section presents several simulation scenarios that have been fulfilled to elicit the static and dynamic model behavior.

Four scenarios are of special interest. This is the steady-state simulation to investigate whether the behavior for all virtual subjects is stable, the OGTT scenario[1] in which all groups receive a meal but no insulin bolus, and the meal tolerance test (MTT) that reflects typical meal ingestion and insulin administration in T2DM and T1DM. The last scenario should incorporate a typical daily-life setting. The first three settings have a simulation duration of 12 h to ensure that most states return to steady-state within simulation time, the last one is 24 h long. Furthermore, the sample time was fixed to 1 min. The inputs to the system are summarized in Table 4.13. In steady-state all state derivatives

[1]The term OGTT typically refers to an oral glucose load of 75 g which rapidly appears in plasma. Here, it is defined as a meal without additional insulin bolus since the gastrointestinal tract was identified for meal ingestion.

Table 4.13: Summary of four simulation scenarios on the three diabetes groups.

Scenario	Group	Meal intake	Bolus insulin	Basal insulin
Steady-state	TNDM	–	–	–
	T2DM	–	–	–
	T1DM	–	–	optimal, acc. to (4.43)
OGTT	TNDM	75 g	–	–
	T2DM	75 g	–	–
	T1DM	75 g	–	optimal, acc. to (4.43)
MTT	TNDM	75 g	–	–
	T2DM	75 g	$1.0\,\mathrm{U\,CU^{-1}}$	–
	T1DM	75 g	optimal CR	optimal, acc. to (4.43)
Daily-life	TNDM	45 g (8 h), 70 g (12 h), 70 g (20 h)	–	–
	T2DM	45 g (8 h), 70 g (12 h), 70 g (20 h)	$1.5\,\mathrm{U\,CU^{-1}}$	–
	T1DM	45 g (8 h), 70 g (12 h), 70 g (20 h)	optimal CR	optimal, acc. to (4.43)

are zero and the system is at its stable operating point. TNDM and T2DM have no inputs, whereas T1DM subjects receive a constant subcutaneous insulin infusion to maintain their steady-state. In the OGTT scenario, all subjects receive a meal of a total of 75 g glucose at simulation start for 15 min, i. e., $5\,\mathrm{g\,min^{-1}}$. The meal input signal is thus not an ideal pulse but a single square wave function that is assumed to be a more realistic excitation in a real-life setting. This scenario does not provide any other inputs to the system. In contrast, the MTT scenario also exploits meal ingestion, but an insulin bolus is given to the diabetic groups to investigate the impact of insulin on the organism. T2DM gets a bolus of 1.0 U per carbohydrate unit (CU), where 1 CU is defined as 10 g of carbohydrates (CHO). T1DM subjects receive an individual optimal insulin bolus according to their predefined carbohydrate ratio (CR) in addition to their basal insulin rate. In both cases, the bolus is given at mealtime. The last case contains multiple MTT scenarios distributed over the whole day to mimic a typical daily life situation. The simulation starts and ends at midnight and includes meal intakes in the morning, at midday, and in the evening, which corresponds to simulation time points of 8 h, 12 h, and 20 h, respectively.

In the following paragraphs, the results for all four scenarios are explained in more detail. For each case a simulation plot is given, showing several characteristic signals: concentrations of glucose, insulin, and glucagon in the top panel; endogenous production of glucose, insulin secretion, and glucagon secretion in the middle panel; uptake and rate of appearance of glucose and also insulin rate of appearance in the last row. Moreover, 100 virtual subjects in each group have been simulated and the ensemble averages have been plotted against each other as can be seen in Figs. 4.11 to 4.14.

Steady-state Simulation. In Fig. 4.11, the results of the steady-state simulation are shown. Generally, all subjects show stable behavior when not excited from the basal level.

Glucose basal value in TNDM is $89.5 \pm 3.9\,\mathrm{mg\,dL^{-1}}$, whereas it is at $119.9 \pm 6.2\,\mathrm{mg\,dL^{-1}}$ for T2DM and at $120.9 \pm 5.5\,\mathrm{mg\,dL^{-1}}$ for T1DM, which reflects the typically elevated glucose concentration in

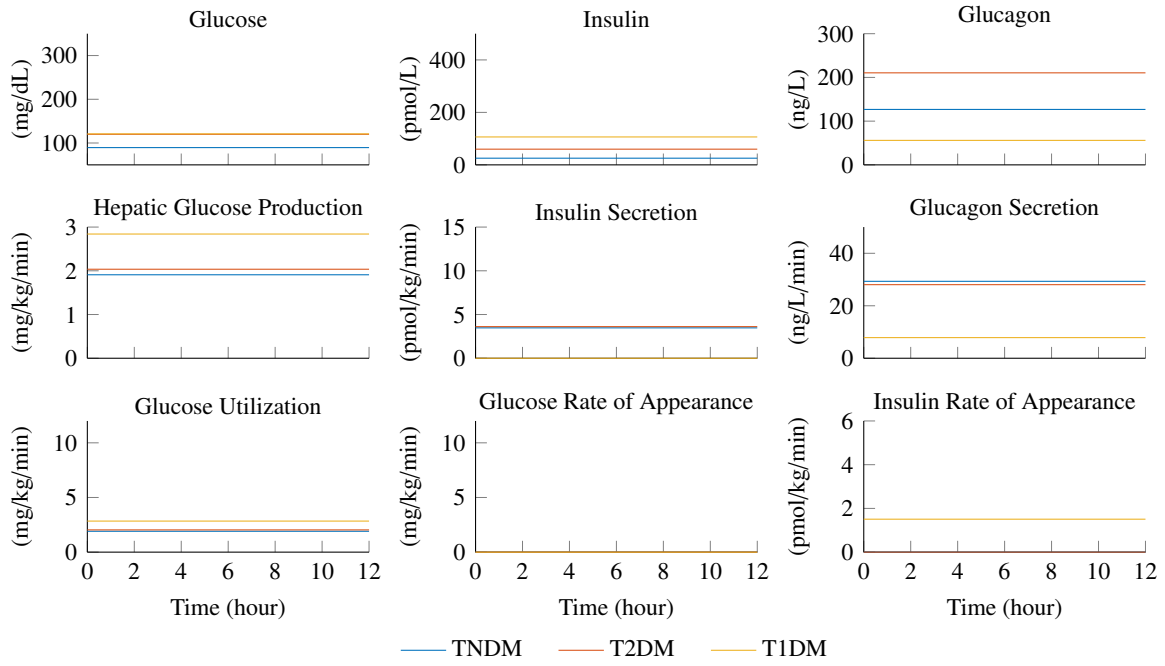

Figure 4.11: Steady-state simulation, averaged over 100 virtual TNDM (blue), T2DM (red), and T1DM (yellow) subjects.

diabetics. Basal insulin concentration is lowest in TNDM with $25.4 \pm 5.1\,\mathrm{pmol\,L^{-1}}$ and also increased with $59.8 \pm 11.4\,\mathrm{pmol\,L^{-1}}$ in T2DM patients, which provides evidence for insulin resistance (Yalow et al. 1960). In T1DM the basal level ($106.4 \pm 18.2\,\mathrm{pmol\,L^{-1}}$) is determined by the basal insulin infusion rate. Glucagon level is at $126.8 \pm 25.4\,\mathrm{ng\,L^{-1}}$ for non-diabetics which is in accordance to measurements (e. g., Unger and Orci (1976), Saccà et al. (1979), and Shah et al. (2000)). In T2DM it is significantly higher with $210.5 \pm 46.9\,\mathrm{pmol\,L^{-1}}$, which is in accordance to Knop et al. (2007). T1DM are assumed to have lower basal glucagon concentrations with $56.0 \pm 10.4\,\mathrm{ng\,L^{-1}}$ as can be seen in Kramer et al. (2014) and Dalla Man, Micheletto, et al. (2014). Hepatic glucose production is in a similar range for TNDM and T2DM with $\approx 2.0 \pm 0.2\,\mathrm{mg\,kg^{-1}\,min^{-1}}$ (DeFronzo 1992), and higher in T1DM with $\approx 2.6 \pm 0.3\,\mathrm{mg\,kg^{-1}\,min^{-1}}$. Insulin secretion does not differ significantly between TNDM and T2DM with $\approx 3.5 \pm 1.5\,\mathrm{pmol\,kg^{-1}\,min^{-1}}$, whereas a complete lack of insulin secretion is assumed in T1DM. Although the glucagon concentration is different between TNDM and T2DM, its secretion rate is similar due to the lower clearance rate, n_{H}, in T2DM. Secretion rate is $\approx 28.5 \pm 9.0\,\mathrm{ng\,L^{-1}\,min^{-1}}$ in TNDM and T2DM and significantly lower in T1DM with $7.9 \pm 2.6\,\mathrm{ng\,L^{-1}\,min^{-1}}$. Glucose utilization closely matches hepatic production which is slightly higher in T1DM with $2.8 \pm 0.4\,\mathrm{mg\,kg^{-1}\,min^{-1}}$ compared to TNDM and T2DM with $1.95 \pm 0.20\,\mathrm{mg\,kg^{-1}\,min^{-1}}$. At steady-state, no meal is given and thus, the rate of appearance of glucose in plasma is zero in all groups. At last, basal insulin is only given to T1DM to maintain steady-state and is $1.5 \pm 0.4\,\mathrm{pmol\,kg^{-1}\,min^{-1}}$.

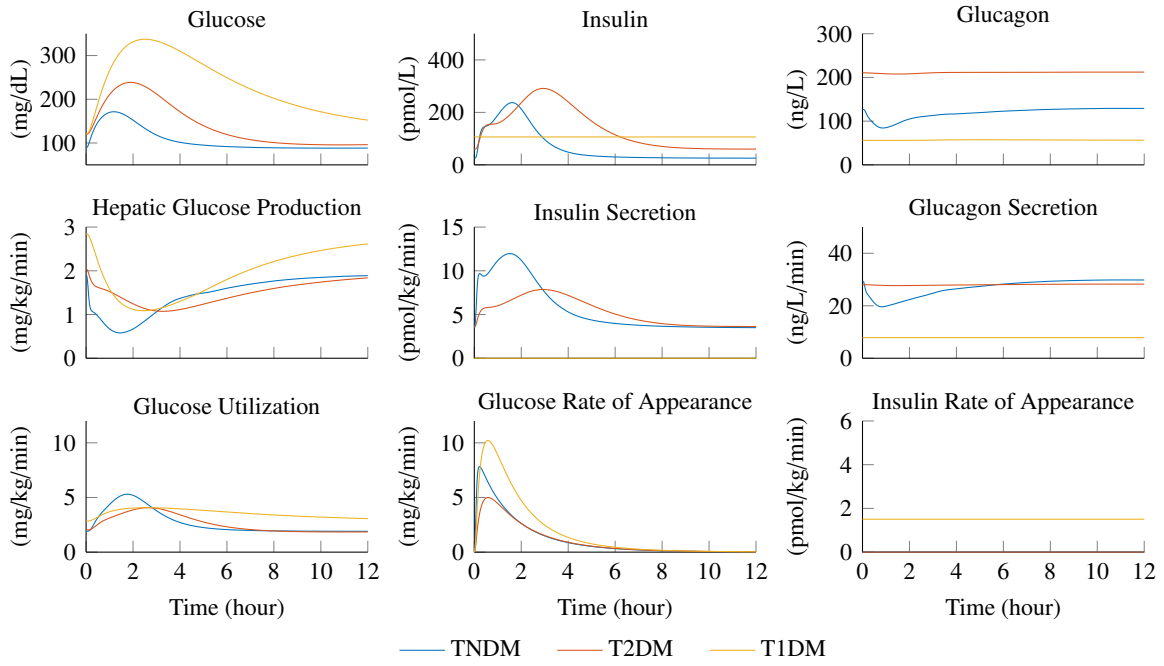

Figure 4.12: Simulation of a meal tolerance test without additional insulin bolus at meal time, averaged over 100 virtual TNDM (blue), T2DM (red), and T1DM (yellow) subjects.

Simulation of a Meal Tolerance Test without Insulin Bolus. In this scenario, a mixed meal containing 75 g glucose without any insulin bolus is simulated and the model outputs are depicted in Fig. 4.12. After meal ingestion, macronutrients are digested, absorbed by the intestine and glucose appears in blood plasma as shown in the middle graph in the last row. Glucose absorption is faster in TNDM than in diabetics with a maximum of 7.7 $\mathrm{mg\,kg^{-1}\,min^{-1}}$ at 22 min, compared to 5 $\mathrm{mg\,kg^{-1}\,min^{-1}}$ at 42 min and 10.1 $\mathrm{mg\,kg^{-1}\,min^{-1}}$ at 41 min for T2DM and T1DM, respectively. Glucose that enters the circulatory system leads to a rise in glucose concentration in all groups.

In healthy subjects, basal glucose is at 98.5 $\mathrm{mg\,dL^{-1}}$ and reaches its maximum value of 171 $\mathrm{mg\,dL^{-1}}$ after 76 min and declines steadily back to basal value after ≈4 h. A rise in plasma glucose levels stimulates insulin secretion and suppresses glucagon secretion. These reciprocal changes suppress hepatic glucose production and enhance glucose utilization. Insulin concentration is visibly biphasic with a maximum of 265.7 $\mathrm{pmol\,L^{-1}}$ at 97 min and returns to basal level of 25.4 $\mathrm{pmol\,L^{-1}}$ after 4 h. Glucagon concentration rapidly decreases from 119.2 $\mathrm{ng\,L^{-1}}$ to a minimum of 85.1 $\mathrm{ng\,L^{-1}}$ at 58 min and rises slowly back to basal level. Hepatic glucose production significantly drops from 1.9 $\mathrm{mg\,kg^{-1}\,min^{-1}}$ to 0.6 $\mathrm{mg\,kg^{-1}\,min^{-1}}$ after 92 min. As endogenous glucose production falls, glucose uptake by muscles is stimulated by the elevated insulin concentration and rises from 1.9 $\mathrm{mg\,kg^{-1}\,min^{-1}}$ to 5.4 $\mathrm{mg\,kg^{-1}\,min^{-1}}$ after 107 min.

In diabetic patients, most signals are delayed and prolonged, compared to TNDM. Basal glucose concentration is elevated with ≈120 $\mathrm{mg\,dL^{-1}}$. In T2DM the slew rate is much slower and reaches its maximum of 238.6 $\mathrm{mg\,dL^{-1}}$ after 120 min. Also, the time to return to basal state is prolonged with

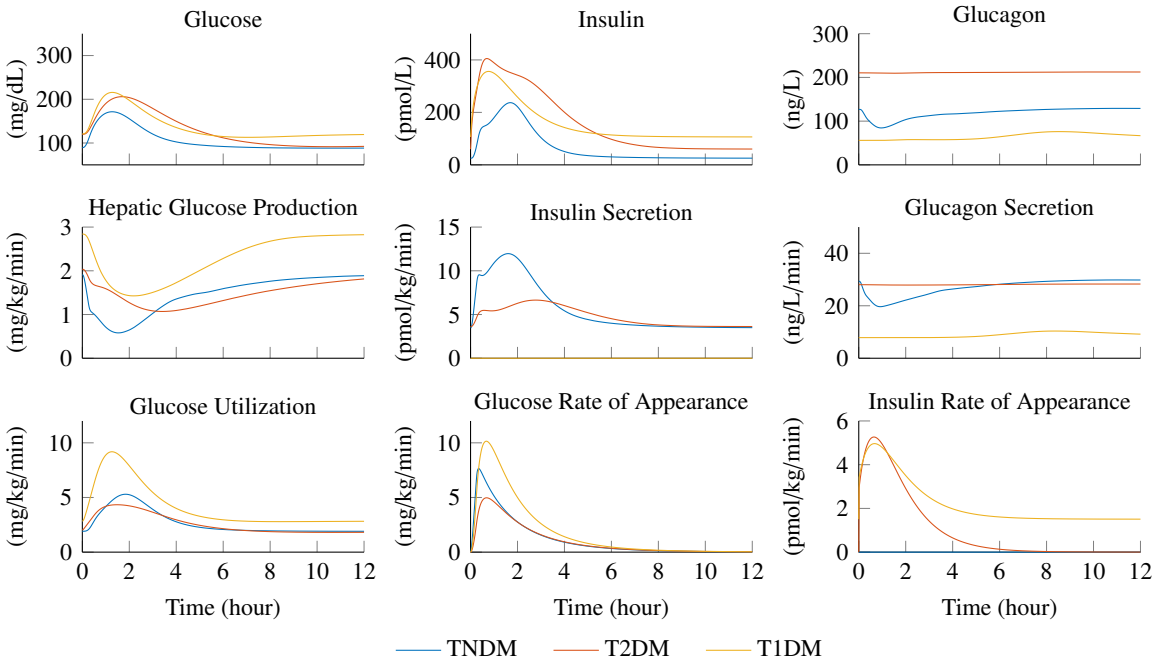

Figure 4.13: Simulation of a meal tolerance test in TNDM (blue), including an additional insulin bolus at meal time in T2DM (red) and T1DM (yellow), each averaged over 100 virtual subjects.

≈8 h. In T1DM this effect is even more distinct as the maximum of 337.2 mg dL^{-1} is not reached before 157 min. Within simulation time glucose concentration does not decline back to basal. The insulin secretion rate in T2DM is not as pronounced as seen in TNDM. Although a biphasic behavior is visible the signal is prolonged, which leads to a delayed rise in insulin concentration. In T1DM no change in the insulin levels is observable as no appropriate secretion exists. Furthermore, glucagon secretion is not suppressed which leads to a delayed and less developed inhibition of endogenous glucose production. Its minimum is ≈1 mg kg^{-1} min^{-1} after 202 min and 152 min for T2DM and T1DM, respectively. This leads, in combination with the diminished postprandial glucose uptake, to an expanded period of hyperglycemia. Lastly, in T1DM when glucose level falls below basal value, glucagon secretion is marginally increased.

Simulation of a Meal Tolerance Test including Insulin Bolus. The results of the MTT scenario are illustrated in Fig. 4.13. In contrast to the meal simulation presented above, an additional insulin bolus is applied to the diabetic subjects at mealtime within the first minute. This is a single 1.0 U per 10 g carbohydrates injection equal for all T2DM and an optimal bolus for each T1DM subject. The effects can be seen in the lower right axis depicting the insulin rate of appearance in plasma. Its occurrence in plasma is delayed due to the s.c. tissue dynamics. For T2DM the appearance rate reaches its maximum of 5.2 pmol kg^{-1} min^{-1} at 39 min and decreases to zero within ≈6 h. In T1DM the peak of 5 pmol kg^{-1} min^{-1} is reached at the same time and declines within ≈4 h back to its basal

rate. These responses are typical for rapid-acting insulin analogs as they are part of a “basal-bolus” regimen or in CSII (Section 2.5) and (Holt et al. 2010, p. 431).

Besides that, the outputs for the non-diabetics do not differ from the results shown in Fig. 4.12 and are again plotted for comparison. Furthermore, as the meal input is the same, the rate of appearance of glucose is equal to the aforementioned signal curves.

As illustrated in the upper left axis, the most apparent changes can be observed in the time course of glucose concentration. The signals of T2DM and T1DM are almost equal with a maximum value of $\approx$210 mg dL^{-1} between 78 min (T1DM) and 107 min (T2DM). Thus, applying a proper insulin dosage at mealtime causes T1DM patients to act similarly to non-diabetic persons, neglecting the higher basal level. In T2DM, this effect is present but not clearly visible. Compared to the OGTT, maximum glucose is reduced by $\approx$30 mg dL^{-1} and is 13 min earlier. That is in accordance with findings that 1 U insulin reduces glucose concentration by 20-60 mg dL^{-1} (Schatz 2006, p. 59).

Insulin secretion rates do not change, as expected. But insulin concentration in plasma is significantly higher due to the insulin bolus with a peak of 402.7 pmol L^{-1} at 37 min in T2DM and 356.2 pmol L^{-1} at 47 min in T1DM. The raised insulin levels do not affect glucagon secretion which is still not suppressed. Similarly, hepatic glucose production is not inhibited properly. In T1DM glucose utilization increases significantly compared to the former scenario and is slightly faster and has a higher maximum than TNDM. In T2DM glucose uptake is comparable with the time course of TNDM.

Since the previous paragraphs only present the ensemble-averaged time responses over all subjects per group, additional single-line plots for each virtual subject are provided in Figs. A.3 to A.5 for the current scenario. Although results are realistic when looking at the whole population, individual signal courses are subject to a large variability due to the broad range of parameters in the mathematical model.

Daily-Life Simulation. The last scenario is a 24 h daily-life simulation of all three groups. Each subject received a 45 g glucose meal after 8 h, a 70 g glucose meal after 12 h, and a 70 g glucose meal after 20 h, which mimics a typical scenario with three meals a day of different amounts. To each meal, diabetic patients received an insulin bolus as reported in Table 4.13. Note that parameters are time-independent and do not vary over the day as it would be typical in most people. Thus, the model predictions do not alter with the time of day. Figure 4.14 shows the model outcomes over 24 h. Effects of the individual meals are linearly superimposed. As can be seen in the rate of appearance of glucose, three peaks exist at the associated meal times. This leads to a rise in the glucose concentration in conjunction with increased insulin levels, forced by higher insulin secretion rates in TNDM respectively external insulin delivery in diabetics. The signal courses of glucagon concentration and glucose production and uptake are appropriate in terms of the subject group.

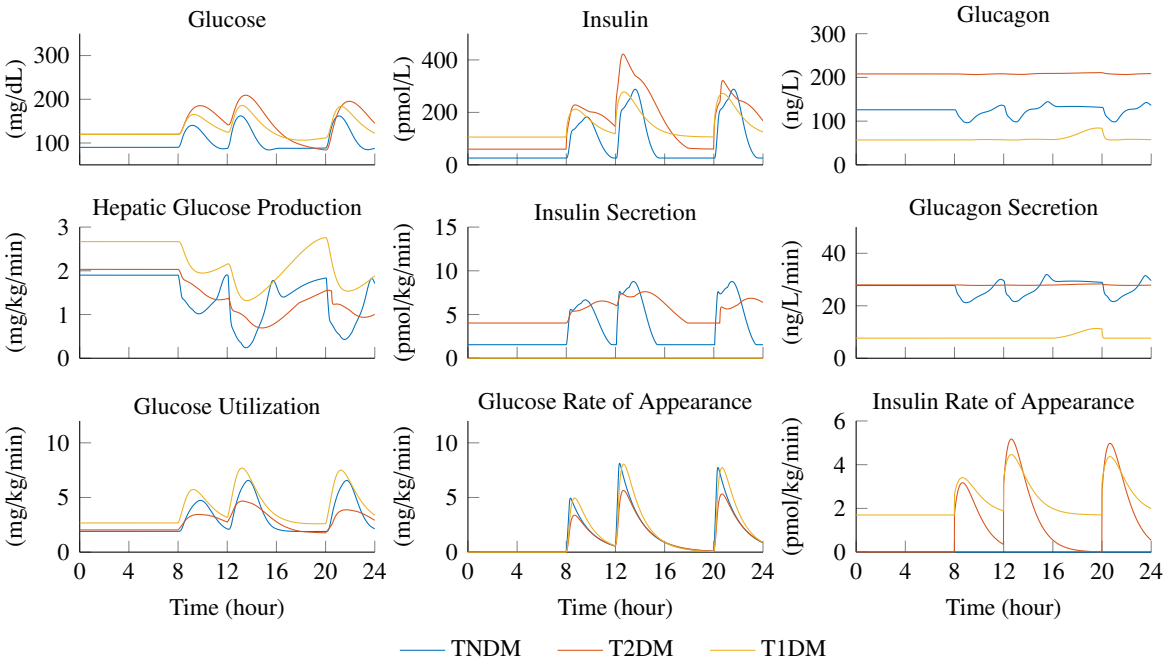

Figure 4.14: Daily-life simulation over 24 h in TNDM (blue), T2DM (red), and T1DM (yellow) subjects.

4.4 Model Evaluation

This section aims to evaluate the behavior of the derived dynamical model and generated virtual subjects, as this is the basis for subsequent development steps. For that, several measurements and approved simulation data sets have been selected from available literature, which are being compared with the outputs of the mathematical model.

The metabolic tests listed in Table 4.14 have been considered for evaluation and are described in more detail in the following paragraphs. The tests take into account different system parts and dynamics, whereas the evaluation focuses on responses to meal ingestion as this is the typical scenario in real life. Since the presented dynamical model is mainly derived from the mixed-meal simulation model by Dalla Man, Rizza, et al. (2007) and the T1DMS (Dalla Man, Micheletto, et al. 2014; The Epsilon Group 2013), results generated by these simulators should be considered for comparison too.

Table 4.14: Experimental data from literature that is used for model evaluation.

Literature	Group	Test	Measurements
Brehm et al. (2006) and Caumo, Bergman, et al. (2000)	TNDM	IMFSIGT	Glucose, insulin
Dalla Man, Rizza, et al. (2007)	TNDM	Mixed-meal	Various substances and fluxes
Dalla Man, Micheletto, et al. (2014), The Epsilon Group (2013)	T1DM	Mixed-meal	Simulation
A. Basu, Dalla Man, R. Basu, et al. (2009)	TNDM	Mixed-meal	Glucose, insulin, glucagon
A. Basu, Dalla Man, R. Basu, et al. (2009)	T2DM	Mixed-meal	Glucose, insulin, glucagon

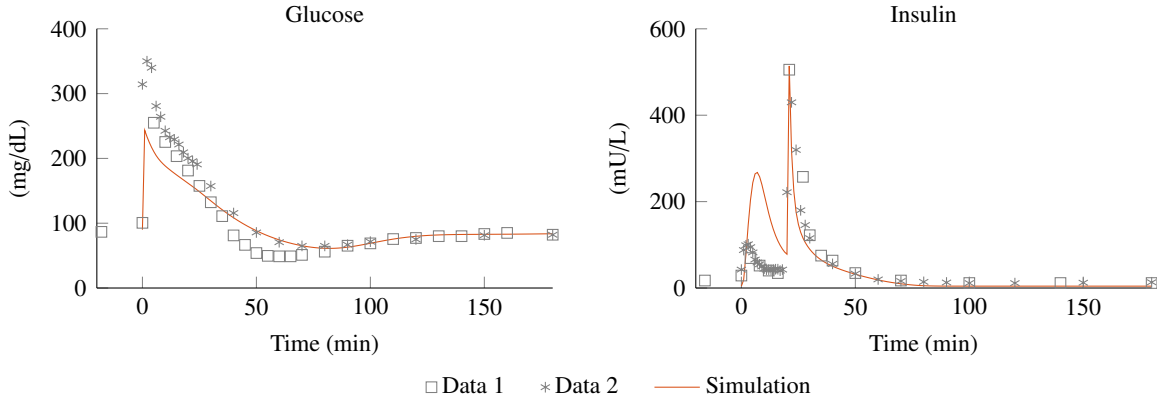

Figure 4.15: Comparison of measurement data (gray markers) and simulation output (red line) after an IMFSIGT in the nominal TNDM subject. Note that measurement errors were omitted for better visibility.

IMFSIGT. Two data sets from publications have been considered: data 1, taken from Brehm et al. (2006), and data 2, taken from Caumo, Bergman, et al. (2000). Both clinical trials fulfilled the same protocol (Section 2.4) on healthy subjects but varying age and body mass. A 0.3 g kg^{-1} i.v. glucose load was given at time zero, followed by an insulin injection of 0.03 U kg^{-1} after 20 min. Glucose and insulin concentrations in plasma have been sampled frequently. Although recorded time courses in both studies differ in maximal amplitude, they are, in overall terms, comparable to each other. Data values and calculated model outputs are shown in Fig. 4.15. For simulation, the nominal TNDM subject with 78 kg body weight was chosen and the input signals were defined as given by the protocol.

On the left side of the plot, glucose trajectories are depicted. Data sets are marked by gray symbols and the simulation output by a red solid line. As can be seen, glucose concentration rises markedly to a maximal peak of 255 mg dL^{-1} in data set 1 and to 350 mg dL^{-1} in data set 2, shortly after administration of the glucose bolus. The time course of the two data sets is similar with a visibly stronger decline after insulin injection at 20 min. Computed glucose output matches the peak value of data set 1. After approx. 75 min the time courses of experiment and simulation do not differ anymore.

The right side of the plot shows the time course of insulin concentration in plasma. Immediately after the glucose bolus insulin level increases from approx. 20 mU L^{-1} to 100 mU L^{-1} in both data sets. It declines rapidly until the administration of insulin after 20 min, where the concentration significantly peaks at approx. 514 mU L^{-1} and falls back to basal level within the next 50 min. The model overestimates the first pancreatic insulin secretion by factor 2.7, whereas the dynamic is comparable. The mismatch between experiment and simulation can be explained by the incretin effect. The insulin response to oral glucose is higher than to i.v. glucose at matching glucose levels (Lindgren et al. 2011; De Gaetano, Panunzi, Matone, et al. 2013). Because the model was identified on the basis of meal data, the incretin effect is thus implicitly included in the model. Since in daily life glucose is never given intravenously it makes sense to have the model identified by meal data rather than i.v. measurements and the modeling error can be neglected. However, the simulation closely matches the time course of insulin concentration after the bolus.

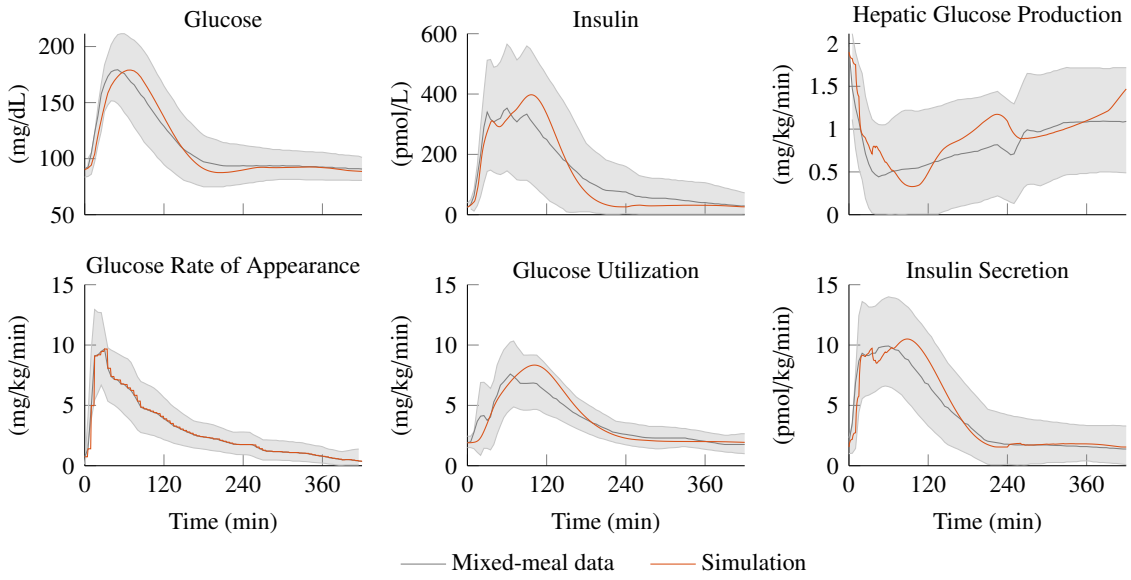

Figure 4.16: Comparison of measurement data (gray line denotes mean, gray area the standard deviation range) and simulation output (red line) after an MTT in the nominal TNDM subject. Note that while glucose rate of appearance was measured during experiment, it is here used as the model input, neglecting the gastrointestinal tract, and thus, gray and red curves are equal (lower left panel).

Comparison to Meal Simulator. Figure 4.16 shows the interpolated measurement data as reported in Dalla Man, Rizza, et al. (2007). The gray solid line depicts the ensemble mean over 204 healthy subjects receiving a mixed-meal of 1 g kg^{-1} body weight of glucose. The gray area represents the standard deviation. Note that plots for insulin secretion and glucagon concentration are not shown here as they have not been investigated in this clinical experiment. After meal ingestion glucose appears in plasma with a mean maximum of 9.7 mg kg^{-1} min^{-1} after 30 min and declines back to zero during the experiment (420 min). Although glucose is still absorbed by the blood over that period, the disturbance to the system is already compensated after approx. 4 h as shown in the upper left axis. Glucose concentration peaks at 180 mg dL^{-1} and is distributed over a range of ±30 mg dL^{-1}. The area shrinks during the experiment and is at ±10 mg dL^{-1} at the end of the study period. Insulin basal level is ≈25 pmol L^{-1} and reaches its averaged maximum of ≈350 pmol L^{-1} after 30 min to 85 min. Besides the average curve, the large standard deviation during transition is noticeable, which lies between 138 pmol L^{-1} to 565 pmol L^{-1}.

The red lines denote simulation output by the nominal TNDM person, who represents the average virtual population. While the glucose rate of appearance was measured during the experiment, it is here used as the input to the model and thus, the influence of the gastrointestinal has been eliminated within the simulation. That leads to better comparability between experimental and calculated outputs. Hence, the red curve equals the gray one in the lower-left panel. Simulation results follow the reference signal accordingly within the standard deviation range. Particularly, the important basal levels are matched reliably. Larger deviations can be observed for the peak area of glucose utilization and during the recovery phase of hepatic glucose production.

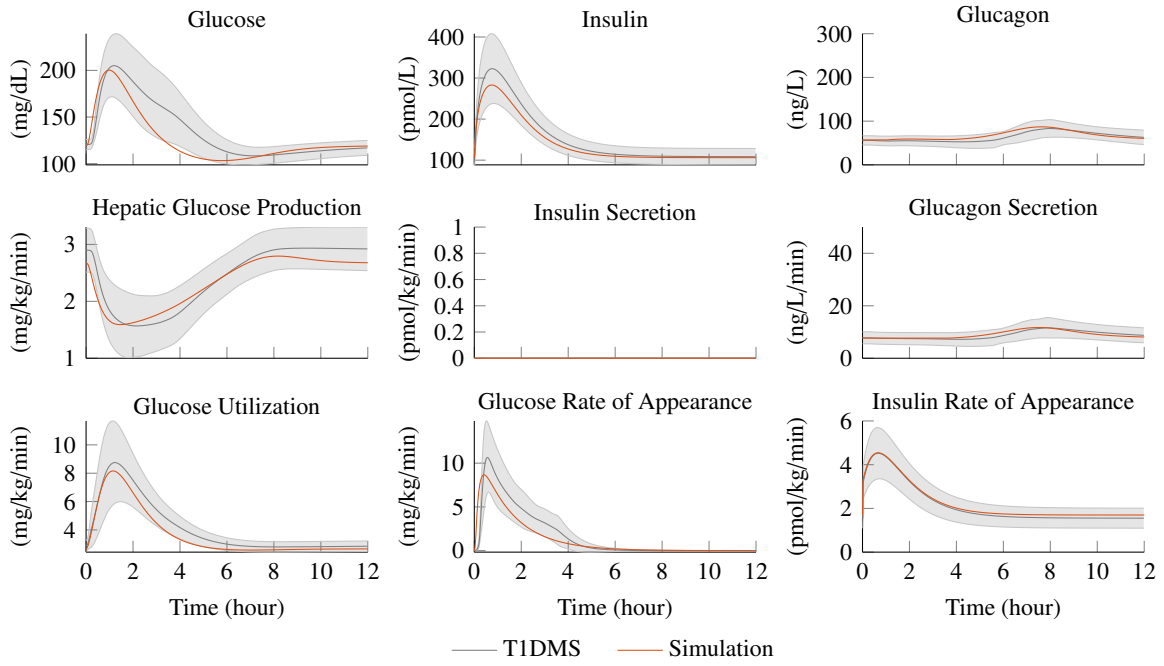

Figure 4.17: Comparison of T1DMS reference model output (gray line denotes mean, gray area the standard deviation range) and simulation output (red line) after an MTT in the nominal T1DM subject.

Comparison to T1DMS. Figure 4.17 shows the time course of several signals created by the T1DMS (Dalla Man, Micheletto, et al. 2014). The gray solid lines represent the average time course over 30 virtual T1DMS subjects and the gray area is the range of the standard deviation. The input to the model was a 60 g glucose load at the simulation start, lasting for 15 min. Additionally, each subject received his optimal basal and bolus insulin injection. In general, the simulation outputs are comparable to those presented in Fig. 4.13 on page 81. The strong increase in glucose and insulin rates of appearance after the respective impulse-shaped input are clearly visible and both appearance rates lead to an elevated glucose and insulin concentration, respectively. As insulin levels rise, endogenous glucose production is suppressed and glucose utilization is promoted. The disturbance is compensated within approx. 6 h. As glucose levels fall temporarily below basal level after 6 h glucagon secretion is initiated to compensate for possible hypoglycemia.

For comparison, the averaged simulation output of the newly defined 100 virtual T1DM subjects is denoted by red lines. The same input signals have been applied to the simulation. First of all, the underestimation of the glucose rate of appearance is noticeable. This is mainly due to the simpler linear model of the gastrointestinal tract in contrast to the highly nonlinear approach that is incorporated in the T1DMS. However, the time courses of glucose and insulin concentration as well as the rate of appearance of insulin in plasma match very closely. Small differences occur in the amplitudes of glucose production and uptake and the glucagon signals, but the simulation shows an overall good accordance. At last, pancreatic insulin secretion is assumed to be absent in both simulators and is depicted here for completeness.

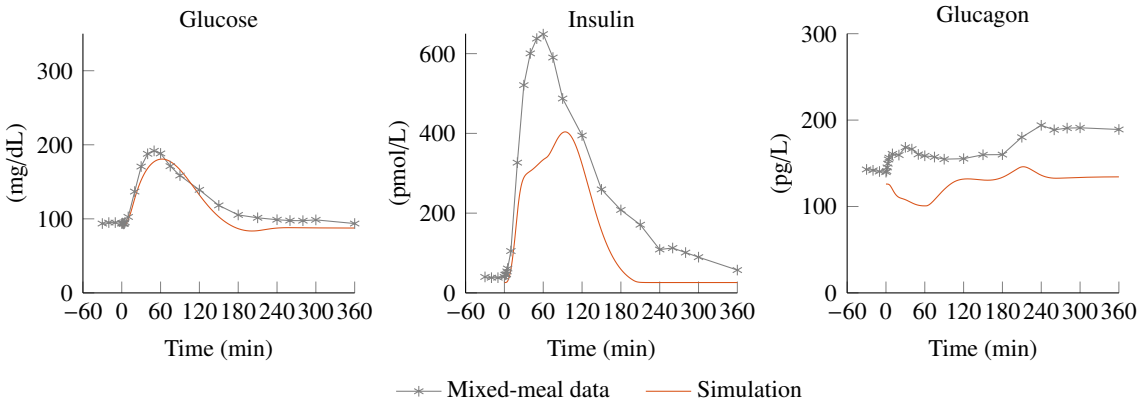

Figure 4.18: Comparison of measurement data (gray markers) and simulation output (red line) after a mixed-meal in the nominal TNDM subject.

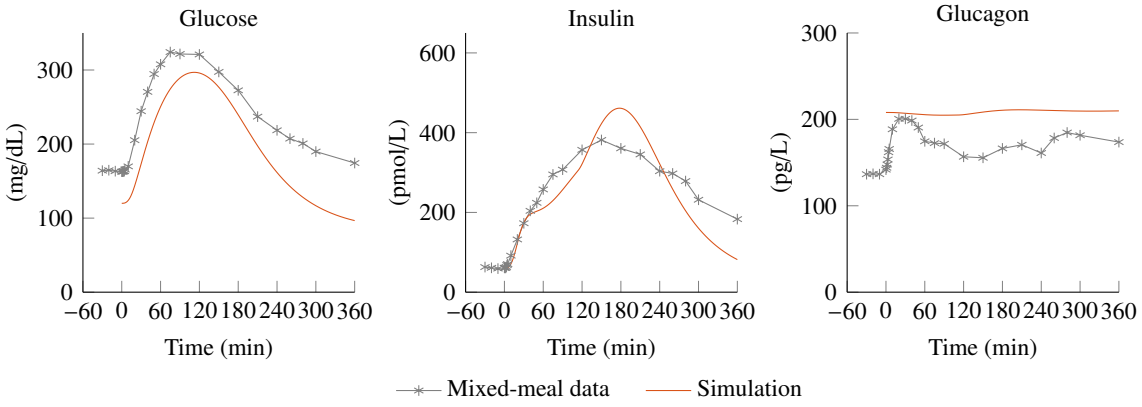

Figure 4.19: Comparison of measurement data (gray markers) and simulation output (red line) after a mixed-meal in the nominal T2DM subject.

Meal Test for TNDM and T2DM. The last test case should take into account the postprandial glucose metabolism in TNDM and T2DM as presented by A. Basu, Dalla Man, R. Basu, et al. (2009), where 11 non-diabetic subjects and 14 type 2 diabetics underwent a mixed-meal test ($1.2\,\mathrm{g\,kg^{-1}}$ body weight of glucose) using triple-tracer technique. The recorded glucose, insulin, and glucagon concentrations are shown in Fig. 4.18 for TNDM and in Fig. 4.19 for T2DM.

In TNDM fasting plasma glucose levels were at $93.6 \pm 1.8\,\mathrm{mg\,dL^{-1}}$ and increased up to a peak of $194.4 \pm 12.6\,\mathrm{mg\,dL^{-1}}$ after the meal (left panel). Fasting insulin concentrations were at $37 \pm 6\,\mathrm{pmol\,L^{-1}}$ with a postprandial peak of $673 \pm 126\,\mathrm{pmol\,L^{-1}}$ at 62 ± 7 min (middle panel). Plasma glucagon concentrations did not differ between the two groups before the meal (approx. $136\,\mathrm{ng\,L^{-1}}$) and increased slightly within the following hour (right panel).

In T2DM fasting plasma glucose levels were higher ($163.8\,\mathrm{mg\,dL^{-1}}$) than in healthy subjects and increased to a higher peak of $325.8\,\mathrm{mg\,dL^{-1}}$ after the meal (left panel). Fasting insulin concentrations did not differ between diabetic ($59 \pm 9\,\mathrm{pmol\,L^{-1}}$) and non-diabetic individuals, but peak postprandial plasma concentrations were lower ($382 \pm 54\,\mathrm{pmol\,L^{-1}}$) and occurred later at 156 ± 16 min (middle

panel). Plasma glucagon concentrations increased more during the first 2 h (right panel), which is in contrast to the typically induced suppression of postprandial glucagon secretion (Aronoff et al. 2004).

For comparison, the simulation outputs of the nominal TNDM and T2DM virtual subjects are plotted as red lines within the respective figures. The nominal glucose basal values (90 mg dL^{-1} in TNDM and 120 mg dL^{-1} in T2DM) match the measured ones in TNDM and are presumed too low in T2DM. Despite that, the time course of glucose is similar to measurements but is slightly delayed in TNDM (peaked 23 min later). Simulated insulin basal values (26 pmol L^{-1} in TNDM and 60 pmol L^{-1} in T2DM) closely match the recorded values. In TNDM, the biphasic time course of the simulated insulin response is apparent, whereas measurements show a significantly higher peak of 673 pmol L^{-1}. This single maximum could be explained by the averaging across all study participants. In T2DM, an increase in insulin concentration is in good accordance within the first 2 h after the meal, but the simulated maximum is higher with 442 pmol L^{-1} at 173 min. Simulated glucagon basal values (126 pmol L^{-1} in TNDM and 208 pmol L^{-1} in T2DM) are in accordance with TNDM and are assumed too high in T2DM. Glucagon secretion is modeled to be inhibited during glucose ingestion in TNDM, respectively to be less present in T2DM subjects. However, the model cannot mimic the observed rises of glucagon levels in the postprandial state.

4.5 Models of Glucose Measurement Devices

In Sections 4.1 and 4.2 mathematical models have been built, that, a) represent the dynamical behavior of the glucose-insulin-glucagon metabolism and b) characterize a virtual subject. Both models serve as a substitute for the real world. For the development of the metabolic model, only the solely physiological relationships have been considered so far. The concentrations of various substances are measurable outputs – and these measurements are subject to technical limitations of the measurement instrumentation, sensor dynamics, or errors like random noise. To complete the process of modeling, first, disturbances and errors in the measurement chain must be identified and quantified. Then, these characteristics must also be incorporated into a mathematical description, which allows its computational simulation. This kind of "virtual sensor" can be useful for the development of subsequent algorithms like data filtering or *in silico* diabetes treatment strategies in open- or closed-loop scenarios.

The acquisition of two substances is of interest. The concentration of glucose in plasma, $G(t)$, and the s.c. tissue, $G_I(t)$. These quantities can be measured by the patient himself or herself in a daily routine. Particularly blood glucose values are the basis for treatment decisions (Sections 2.3 and 2.6). Thus, accurate and reliable glucose values play an important role in maintaining glycemic control in insulin-treated patients (Bergenstal et al. 2005). Measurement of insulin and glucagon concentrations is only feasible in a clinical setting using precise laboratory equipment. Hence, they do not play a role in a model-based scenario and are not considered any further.

Table 4.15: Precision reference according to ISO15197:2013 compared to devices used for measuring glucose concentration: values describe the percentage of measurements that lie within a certain range (in parentheses), data taken from the International Organization for Standardization (2013), Ascensia Diabetes Care Deutschland GmbH (2016), and Dexcom, Inc. (2017).

	ISO15197:2013	**Blood glucose sensor**	**Continuous glucose sensor**
Manufacturer		Ascensia Diabetes Care	Dexcom
Product		Contour Next	G5 Mobile
Correctness for measurement values:			
<100 mg/dL [1]	95 % (±15 mg/dL)	100 % (±10 mg/dL)	
≥100 mg/dL [1]	95 % (±15 %)	97.4 % (±10 %)	
< 80 mg/dL [2]			93 % (±20 mg/dL)
≥ 80 mg/dL [2]			93 % (±20 %)

[1] applicable to all devices used for BGSM
[2] only applicable to Dexcom G5 Mobile

For BGSM devices, the international norm DIN EN ISO 15197:2013 (International Organization for Standardization 2013) is the standard to assess the accuracy of these systems (see the second column in Table 4.15 for details). It can be assumed that all devices available on the market meet the requirements (Freckmann, Baumstark, et al. 2014). For the BGSM device used later in this work, namely the Contour Next (Ascensia Diabetes Care Deutschland GmbH 2016), system accuracy according to the manufacturer is listed in the third column of Table 4.15. Despite the higher precision of that device, compared to the norm, modeling will rely on the standard in order to stay independent of any specific device.

For CGM sensors, no such norm exists yet. However, several studies have assessed the accuracy of these devices, usually compared to reference blood glucose records. A comparison of different generations of CGM sensors from a single manufacturer can be found in Christiansen, Bailey, et al. (2013) and Christiansen, S. K. Garg, et al. (2017); benchmarks comparing different manufacturers in, e. g., Kovatchev, Anderson, et al. (2008), Boscari et al. (2018), and Freckmann, Link, et al. (2018). For the CGM device used later in this work, namely the G5 Mobile (Dexcom, Inc. 2017), system accuracy according to the manufacturer is listed in the last column of Table 4.15. There, the correctness is based on the percentage of CGM values that differ by ±20 % for glucose values larger than 80 mg dL^{-1} or that differ by less than ±20 mg dL^{-1} for glucose values equal to or less than 80 mg dL^{-1}, compared to glucose reference values.

As can be seen for all devices in Table 4.15, measurement errors are not constant over the full glucose range. Instead, for values below a certain threshold, sensor errors are assumed to be absolute. For readings above the threshold, errors are relative in terms of the sensor value. This behavior should also be incorporated into a model.

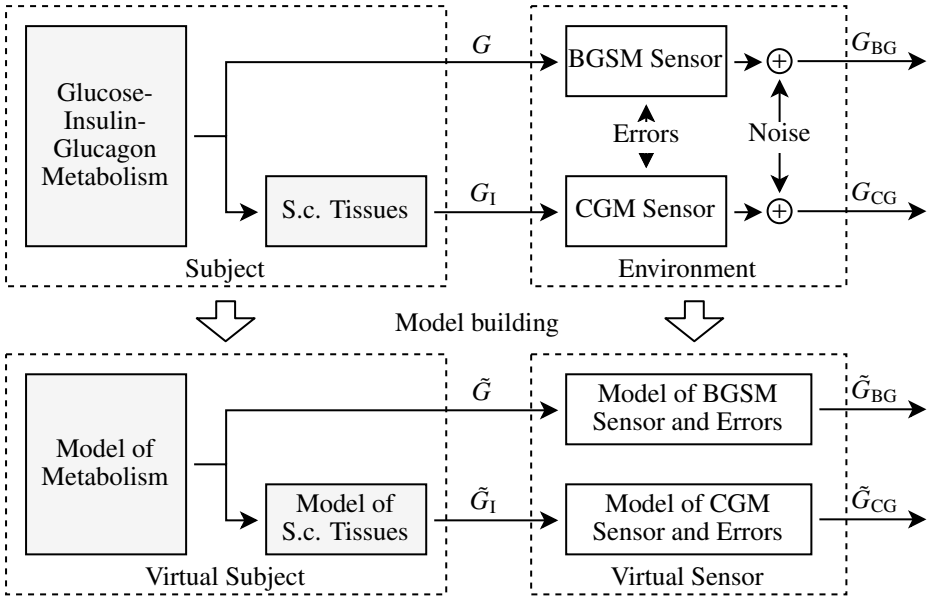

Figure 4.20: Modeling glucose measurement devices: the signals G_{BG} and G_{CG} are distorted and noisy representatives of the glucose concentration in plasma, G, and in the s.c. space, G_{I}, respectively (upper panel). Models of the system (lower panel) must take into account physiology (virtual subject, left side) as well as possible sensor errors and random measurement noise (virtual sensors, right side).

BGSM and CGM devices are affected by measurement errors which can reduce the treatment efficiency because an under- or overestimation of the true glucose value can lead to incorrect treatment decisions, e. g., an insulin administration that is too high or too low for the current situation. Sensor models must mainly consider these errors for realistic *in silico* studies. Furthermore, the error distribution or possible correlation between consecutive measured values has to be considered, if necessary. This complex of problems is shown in the upper part of Fig. 4.20. Starting from the metabolic system of a subject (left side), the concentration of glucose in the plasma, $G(t)$, is measured by the BGSM sensor, and the concentration of glucose within the subcutaneous tissues, $G_{\mathrm{I}}(t)$, by the CGM sensor. Both measuring devices are subject to various sources of errors and additive random measurement noise, summarized as the environment (right side). The lower panel of the graphic depicts the single parts of the virtual system: the model of glucose regulation, in which the kinetics between plasma and the s.c. space is drawn separately. Simulated glucose levels are denoted by $\tilde{G}(t)$, respectively $\tilde{G}_{\mathrm{I}}(t)$, and can be assumed to be perfectly known. Only the sensor models add uncertainty to the simulated signals, leading to virtual sensor readings denoted by $\tilde{G}_{\mathrm{BG}}(t)$ and $\tilde{G}_{\mathrm{CG}}(t)$.

4.5.1 Model of Blood Glucose Measurement Devices

Consecutive measurements collected from blood samples can be assumed to be uncorrelated due to the sparse sampling only a few times a day. Furthermore, the error is assumed to be proportional, i. e., relative, for glucose values greater or equal $100\,\mathrm{mg\,dL^{-1}}$, and to be absolute for glucose values below $100\,\mathrm{mg\,dL^{-1}}$. The error bound is set in such a way that 95 % of all recordings lie within ±15 %,

Table 4.16: Empirical distribution parameters of BGSM sensor errors for the daily-life scenario.

Group	Fraction of data for		Min.	Max.	Data within $z\,\sigma$ for	
	$\mu < 100$	$\mu \geq 100$	($\mathrm{mg\,dL^{-1}}$)	($\mathrm{mg\,dL^{-1}}$)	$\mu < 100$	$\mu \geq 100$
TNDM	0.696	0.304	83	168	0.963	0.949
T2DM	0.114	0.886	84	209	0.902	0.954
T1DM	0	1	103	192	–	0.952

respectively $\pm 15\,\mathrm{mg\,dL^{-1}}$. These assumptions match with the allowed error tolerances according to the International Organization for Standardization (2013).

Findings in Vettoretti, Facchinetti, et al. (2017) showed that a single Gaussian distribution over the entire glucose range is not adequate to describe the sensor errors. They recommended dividing the range into zones of constant absolute and constant relative error standard deviations. For each zone, a suitable PDF was fitted from measurement data. They suggested an unimodal, positively biased, and skewed distribution of the relative sensor errors. To keep the BGSM model simple, two zones are applied here, matching the specifications of the international norm. In both zones, a log-normal distribution with zero error mean is used (4.71). Variables of the log-normal distribution are computed by (4.72), where μ would be the current glucose value and σ^2 the assumed variance. From the assumption that 95 % of all measurements lie within the respective range, the 1 σ standard deviation is calculated by

$$\sigma = \begin{cases} \dfrac{15}{z} & \text{for } \mu < 100\,\mathrm{mg\,dL^{-1}}, \\ \dfrac{0.15}{z} \cdot \mu & \text{for } \mu \geq 100\,\mathrm{mg\,dL^{-1}}, \end{cases} \tag{4.84}$$

where $z = 1.96$ is the associated z-score of the 95 % tolerance interval[2]. From that, a random measurement error can be generated as part of the virtual sensor. To evaluate the computational process the daily-life simulation scenario presented in Section 4.3 is considered. The scenario contains three meals with a duration of 24 h and 1 min sampling time, thus, contains $n = 1441$ blood glucose samples (see the upper left plot in Fig. 4.14 on page 83). The absolute errors, $\epsilon_i^{\mathrm{abs}}$, and the relative errors, $\epsilon_i^{\mathrm{rel}}$, are computed using sensor values, s_i, and reference values, r_i, for measurements $i = 1, \ldots, n$ by

$$\epsilon_i^{\mathrm{abs}} = s_i - r_i\,, \qquad \epsilon_i^{\mathrm{rel}} = \frac{s_i - r_i}{r_i}. \tag{4.85}$$

The noise processes ϵ^{abs} and ϵ^{rel} are plotted as histograms in Fig. 4.21, showing the absolute frequency for each group. Some statistical properties are reported in Table 4.16.

[2] Refer to https://de.wikipedia.org/wiki/Normalverteilung (last visit 07.05.2021).

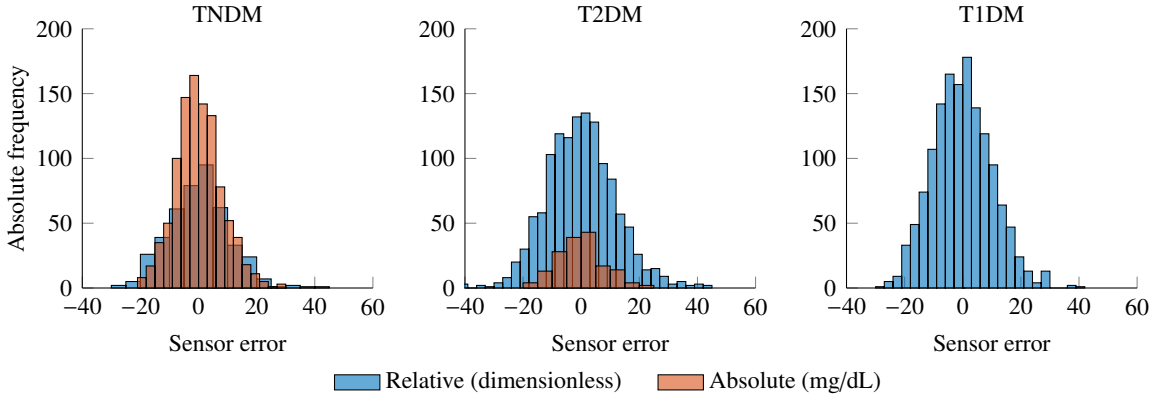

Figure 4.21: Histograms of simulated relative (blue bars) and absolute (red bars) BGSM sensor errors for the daily-life scenario in TNDM (left panel), T2DM (middle panel), and T1DM (right panel).

As can be seen in the left panel for TNDM subjects, the occurrence of absolute errors is higher than for the relative ones, indicating more glucose values below the threshold. Column two in Table 4.16 shows 69.6 % of all readings being below and 30.4 % above the threshold μ. For both zones the number of records within the respective error bounds were computed, which gives 96.3 % within $\pm 15\,\mathrm{mg\,dL^{-1}}$ for glucose concentrations below $100\,\mathrm{mg\,dL^{-1}}$ and 94.9 % within ±15 % for concentrations equal or greater the threshold. Both empirical error bounds are close to the theoretical value of 95 %. For T2DM, shown in the middle panel, only 11.4 % of all glucose values are below the threshold, visible in the far lower amplitude. 90.2 % of these values are within the absolute error bounds, whereas 95.4 % of all relative errors lie within the relative error bound. For T1DM, presented in the right panel, glucose levels did not fall below the threshold, hence, no absolute error can be computed. Relative errors are within the associated error bound at 95.2 %. The results given above show good accordance between the empirical and the theoretical error bounds, both for absolute and for relative errors, as well as for the three subject groups.

One further restriction to mention for BGSM readings is their sparsity. Samples are only taken at a few time points a day, typically before a meal or during physical activities. Thus, representative time courses for a patient are not accessible.

In Fig. 4.22, a representational time course of plasma glucose concentration in the daily-life scenario is shown for each group. Simulated glucose levels at each sampling point are depicted in black. From that, the noisy BGSM measurement signal was generated (gray line). The BGSM sensor reading may significantly deviate from the nominal glucose value, particularly at high levels (e. g., middle panel at 13.5 h where the measured value differs by $42\,\mathrm{mg\,dL^{-1}}$). Furthermore, 20 samples, picked at random time points within the 24 h simulation time, are plotted as red crosses. They stand for possible readings that can be obtained by a patient. However, from these few records, the dynamics of glucose variation may not be apparent. For example, in the left panel, the first peak between 8 h and 10 h would not be visible to a patient when only considering the sparse samples.

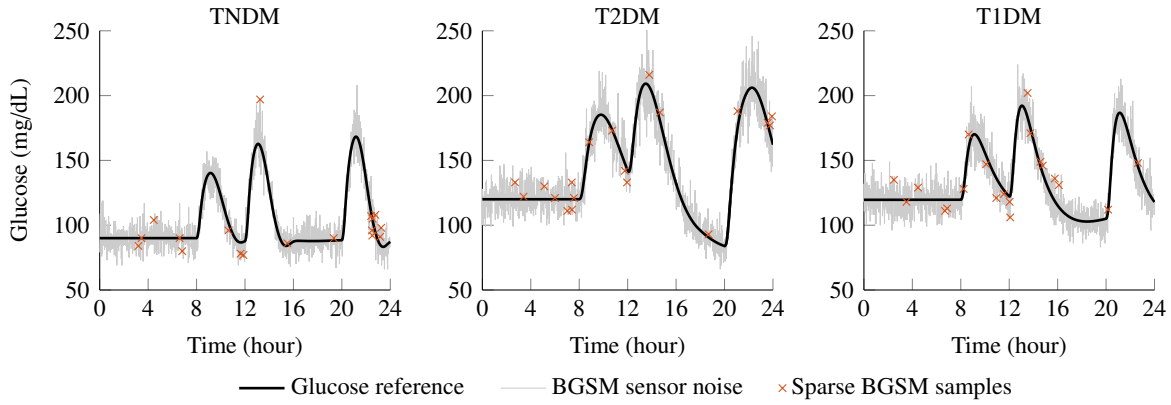

Figure 4.22: Time course of simulated reference glucose values (black lines), BGSM sensor readings (gray lines), and sparsely sampled noisy signal (red crosses) for the daily-life scenario in TNDM (left panel), T2DM (middle panel), and T1DM (right panel).

4.5.2 Model of Continuous Glucose Measurement Devices

In contrast to blood glucose sensors, continuous glucose measurement devices detect glucose concentration in the interstitial fluid with comparably high sampling times of typically 1 to 5 min, which allows for the first time to monitor the dynamical behavior of glucose in real-time. However, these devices have several drawbacks (Breton and Kovatchev 2008):

- A lower precision compared to BGSM devices, with 75 % of all measurement values being within the $\pm 15\,\mathrm{mg\,dL^{-1}}$ respectively ±15 % range (Freckmann, Link, et al. 2018).
- Possible drifts and calibration errors due to unknown or non-modeled physiological effects.
- There exists a physiological time lag between the equilibration of glucose in plasma and the sensor location. Thus, CGM and blood glucose measurements at the same time points cannot be directly compared. But since CGM records are being used to assess blood glucose values, this delay must be incorporated. Furthermore, the delay is neither equal across different subjects nor constant within a single subject over a longer period.

Breton and Kovatchev (2008) were the first to publish a decomposition of CGM sensor errors to assess specific characteristics using linear regression, kernel density estimation, and time series analysis. They identified three major error components: the distribution of sensor readings, the physiological delay, and the time dependency of consecutive sensor readings. First, from sensor measurements compared to references the CGM error mean and standard deviation were determined to be $0.76\,\mathrm{mg\,dL^{-1}}$ and $11\,\mathrm{mg\,dL^{-1}}$, respectively. These findings correspond to the manufacturer's specifications listed in the last column of Table 4.15 for the (close) twofold standard deviation. The histogram revealed a non-Gaussian distribution and was fitted using the Johnson family. Second, continuous and blood glucose data were synchronized using a first-order diffusion model to take into account the physiological delay and also sensor-induced time lags. From the model of subcutaneous glucose kinetics defined in

Section 4.1.5, combining Eqs. (4.25) and (4.26) leads to the common term

$$\dot{G}_{\mathrm{I}}(t) = -\frac{1}{\tau}\left(G_{\mathrm{I}}(t) - G(t)\right) \quad \text{with} \quad k_g = \frac{1}{\tau}, \tag{4.86}$$

with $G(t)$ and $G_{\mathrm{I}}(t)$ denoting the concentrations of glucose in plasma and s.c. space, respectively. Breton and Kovatchev (2008) estimated $\tau = 5\,\mathrm{min}$, which corresponds to reported values in the literature (Rebrin and Steil 2000; Keenan et al. 2009). Hence, the time delay can be estimated when both, a sufficient number of blood glucose and continuous glucose measurements are available. The last issue is related to the time dependency of consecutive CGM data values. For that, Breton and Kovatchev (2008) applied the autocorrelation function (ACF) to compute the correlation of the sensor error over consecutive time points. Their results showed a highly correlated sensor noise across several hours. Using the partial autocorrelation function (PACF), it was apparent that all coefficients for lags greater than 1 were not significant. From that, they concluded that the sensor noise can be best predicted by a linear first-order autoregressive (AR) model and an additive random white-noise term. AR models are linear and discrete-time models for stochastic inputs and are used to approximate more complex processes.

From the findings above, the following model of CGM sensor error is applied:

- Glucose in the interstitial fluid is delayed relative to the blood glucose concentration and is described by the first-order diffusion model in (4.86).
- CGM data from the Dexcom G5 Mobile is sampled at discrete-time points, k, with a sampling time of 5 min.
- The correlated sensor noise, $e(k)$, is described by a first-order AR model driven by a standard normally distributed noise term, $v(k)$, given in (4.87).
- CGM sensor noise, $\epsilon(k)$, is not normally distributed. Instead, a distribution from the Johnson family is chosen to transform signal $e(k)$ given in (4.89). Parameters are listed in Table 4.17.

The general description of a discrete-time AR model of order p with stochastic input $v(k)$ is given by

$$\begin{aligned} e(k) &= b_0 v(k) + \sum_{i=1}^{p} a_i e(k-i), \\ v(k) &\sim \mathcal{N}(0,1)\,. \end{aligned} \tag{4.87}$$

The output signal $e(k)$ is driven by the noise term $v(k)$, normally distributed with zero mean and unit variance, which may be weighted by the factor b_0, and p preceding output signals, where $a_i, i = 1, \ldots, p$ are the weight factors. This process is also known as an infinite impulse response (IIR) filter applied to the white-noise process $v(k)$, which is drawn from the same time-independent standard normal distribution, independent of previous errors (i.i.d, independent and identically distributed). Specifying the order $p = 1$, coefficients $b_0 = a_1 = 0.7$ (Breton and Kovatchev 2008) and applying the

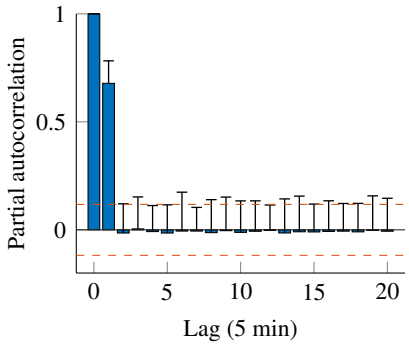

Figure 4.23: Averaged partial autocorrelation function of the simulated CGM sensor noise (lag interval of 5 min). 95 % confidence bounds are plotted as red dashed lines.

Johnson transformation to the error $e(k)$ leads to

$$e(k) = 0.7\,(\nu(k) + e(k-1))\,, \tag{4.88}$$

$$\epsilon(k) = \xi + \lambda \sinh\left(\frac{e(k)-\gamma}{\delta}\right), \tag{4.89}$$

where $\epsilon(k)$ is the CGM error noise process.

The model of CGM error was applied to the daily-life scenario on 100 virtual subjects to confirm the results. Therefore, CGM noise was added to the nominal glucose signal $\tilde{G}_\mathrm{I}(t)$. Note that the diffusion model (4.86) has already been incorporated into the model of virtual subjects, also including representative ranges for τ respectively k_g. From the noisy measurements, PACF was computed and plotted in Fig. 4.23. The blue bars represent the average partial correlation coefficients for the last 20 samples, where each lag represents a period of 5 min; the error bars show the maximum deviations. The coefficient for the current sample point (lag 0) is generally one, the averaged empirical PACF coefficient at lag 1 is 0.68 ± 0.05, which is close to the specified value of 0.7. All coefficients greater than the first lag are close to the 95 % confidence intervals, depicted as red dashed lines. To determine if the manufacturer's confidence bounds are met by the noise process, noisy CGM data was matched with its noise-free blood glucose values, and the relative error between the pairs was calculated for each virtual subject. Results show that 93 ± 4 % of all samples (288 for each subject) have a relative error within ±20 %, which corresponds to the manufacturer's specifications (Table 4.15).

A representational time course of the reference s.c. glucose concentration (black lines), the interpolated CGM sensor noise (continuously plotted lines in gray), and the frequently sampled data points (blue

Table 4.17: Johnson parameters of the CGM error distribution (taken from Breton and Kovatchev (2008)).

Parameters	Family type	λ	ξ	δ	γ
Values	Hyperbolic sine transformation (unbounded)	15.96	−5.471	1.6898	−0.5444

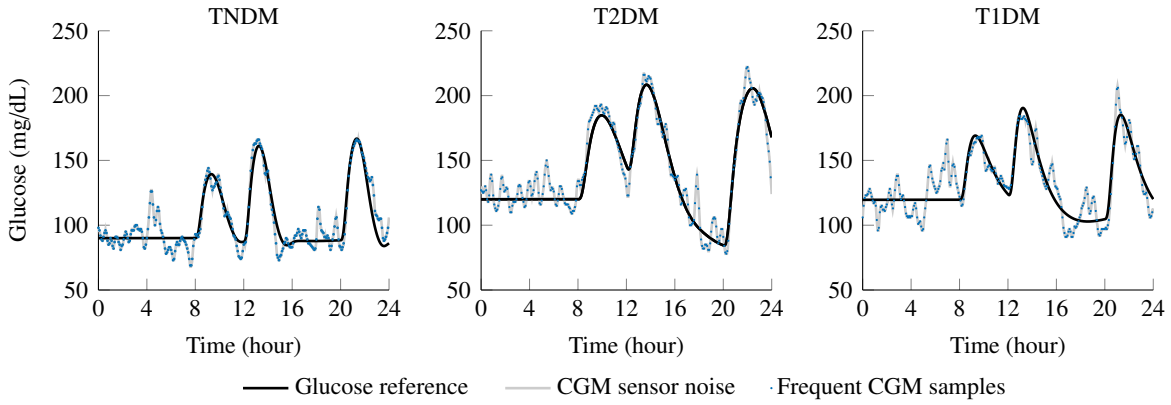

Figure 4.24: Time course of simulated reference s.c. glucose values (black lines), CGM sensor noise signal (gray lines), and frequent samples (blue dots) for the daily-life scenario in TNDM (left panel), T2DM (middle panel), and T1DM (right panel).

dots) are shown in Fig. 4.24 for each group. From the CGM signal the dynamical time course of s.c. glucose concentration is now clearly visible. Hence, compared to sparse blood glucose measurements only, much more information is presented, but also larger sensor noise is added.

4.6 Summary and Conclusion

Mathematical models of glucose-insulin-glucagon regulation and virtual subjects have been presented. They are summarized in Section A. The dynamical model is based on published physiological models derived from clinical data. It consists of 19 nonlinear differential equations reflecting the physiologic knowledge about glucose metabolism in the human body. The model is capable of simulating the time course of glucose, insulin, and glucagon concentrations, as well as various other metabolic fluxes during a meal test. The existing modeling approaches have been unified, which allows a consistent description of the metabolic processes independent of a specific type of diabetes.

Three different groups were considered here: TNDM subjects, T2DM patients with altered metabolic processes, and T1DM subjects in which some control regulations are completely absent. These virtual population models have been generated from published data, that reflect the statistical relationships within the groups. These include mean values, variances, the correlation between parameters, and their underlying distribution. As not all variables have been fully defined in the literature, some of them had to be identified from measurement data in good accordance. Each virtual subject is characterized by a state vector that determines the current metabolic state and a parameter vector that characterizes the health status in a long-term manner. Although the latter is created by a multivariate random process, each population and each subject within show a feasible performance.

Several simulation studies showed a stable steady-state behavior and a physiologically interpretable and meaningful response to single meal ingestion, insulin administration, and daily-life scenarios. The derived dynamical model and the models of virtual subjects were evaluated against measurement data

from several clinical studies, including standard tests such as IVGTT, IMFSIGT, and the more natural mixed-meal tolerance test. The performance of the simulated populations essentially reflects measured data in all test cases. Nevertheless, further enhancements can be expected when suitable parameters of the virtual subjects are identified from individual measurement data as explained in Section 6.2.

To obtain more realistic measurement readings from within the simulation environment, also sensor errors were integrated from standardized norms and available models from the literature. Two sensor types for glucose measurement were incorporated: one to describe random errors from sparse blood glucose measurements and one that takes into account the non-white, non-Gaussian, time-dependent, and dynamical sensor errors that arise from consecutive measurements of subcutaneous glucose concentration. Rigorous modeling of imperfect sensor data allows the *in silico* development of diabetes treatment strategies that may be more robust under realistic conditions. Furthermore, an error model is a helpful tool for online state estimation and will be discussed in Section 6.3.

5 Systems Analysis

After derivation of the dynamical model of glucose regulation (Section 4.1) and the model of virtual subjects (Section 4.2), the question arises which states and parameters can be theoretically determined from observations of a particular output. Two different techniques are introduced here: First, the statistical approach of global sensitivity analysis, which treats parameters of a nonlinear system as stochastic input variables (Section 5.1). Second, the controllability and observability of states, taking into account the internal structure of a linear system. This method can be extended by the concept of empirical Gramians that allows their application on nonlinear systems, too (Section 5.2). The identified influence of certain parameters respectively states on the model outputs is then the basis for subsequent model identification and state estimation procedure (Chapter 6).

5.1 Global Sensitivity Analysis

Parameters identified from experimental data are often subject to a high degree of uncertainty. To be able to deal with these uncertainties, sensitivity analysis (SA) techniques can be used to quantify the influence of parameters on model quality. SA is widely used in systems biology (Marino et al. 2008; Sumner et al. 2012) or environmental modeling (Pianosi et al. 2016). One key area is to identify those input factors that contribute most to the variation in the model output.

When the model equations are too complex to calculate sensitivities analytically by partial derivatives, some sampling-based methods can be applied in which an appropriate number of samples within the input space is taken to estimate the sensitivities numerically.

In contrast to local SA where input factors are only excited within a small range around the nominal value, global SA techniques investigate the effects of simultaneous parameter variations over the entire feasible ranges. This allows the handling of nonlinearities and interactions between input factors.

When the model output is scalar, e. g., an aggregated statistical information, a set of quantitative sensitivity indices describes the variance in that output induced by variation of its input factors. However, in biomedical systems often the dynamic behavior over time is of interest. Thus, the model outputs are functions of time, and consequently, sensitivity indices are also time-dependent. This provides information on how influential parameters are at certain time points.

As an alternative, scalar features can be derived from the model output, and the indices can be calculated thereof. First proposed by K. Campbell et al. (2006) and applied to biological systems by

Sumner et al. (2012), functional principal components (FPCs) seem to be a helpful method to convert vectorial model outputs into an alternative format. It aims to transform functional data into a set of basis functions that represent the most important features in the output. Afterward, a standard SA method can be applied to the coefficients of the FPCs to identify the most relevant factors.

In addition to questions such as local or global SA or qualitative and quantitative SA, computational considerations also play a role. Particularly in biological systems, many parameters are involved that require efficient algorithms. Since quantitative techniques are computationally expensive, the approach presented here is a multi-step SA using a screening technique, a parameter reduction, and a subsequent quantitative SA.

First, some basic considerations are made as described in the next section. Then, Sections 5.1.2 to 5.1.4 explain the aforementioned methods in detail, whereas Section 5.1.5 describes the multi-step approach. Section 5.1.6 defines an overall sensitivity index taking into account the importance of an input factor with regard to its associated FPC. The results obtained by the multi-step approach are reported in detail in Section 5.1.7. Last, as sampling-based sensitivities are not computed exactly, some robustness and convergence deliberations about the estimates are illustrated in Section 5.1.8.

5.1.1 Experimental Setup

Basic considerations include which variables to be subject to the SA techniques, the values of those factors that are kept fixed throughout SA, the definition of the model output, and a proper representation of the input space, regarding the variation within a feasible range, the number of samples, and the sampling scheme (Section 3.2).

Here the input variability space is defined by the physiological range of the parameters in each group. Means were set to the average subject in each group and the range to ±35 % of the corresponding nominal value. In Section 4.2.3 the process of generating virtual subjects has been presented and the same algorithm can be applied here to randomly pick a new set of valid parameters. This has also the advantage that distribution and covariance between parameters are correctly considered.

As mentioned before, two different SA techniques are considered here. The computational fast Elementary Effects Test (EET) for screening purposes (Section 5.1.2) and variance-based sensitivity analysis (VBSA) for a quantified sensitivity index (Section 5.1.4).

The model must be evaluated against sampled input combinations which can be expressed by

$$y = f(\boldsymbol{X}), \tag{5.1}$$

where y is the scalar output and $\boldsymbol{X}$ a matrix of K input factors also referred to as parameters. The dynamical model consists of several model outputs: glucose concentration in plasma and the subcutaneous space, and additionally, concentrations of insulin and glucagon in plasma. The most valuable measurement quantity is the amount of glucose in the subcutaneous tissue since these values can

Table 5.1: Experimental setup for the multi-step sensitivity analysis approach.

Properties	EET	VBSA
Scenarios	STS, OGTT, MTT, IBO	MTT
#Input factors	$K = 35$ (TNDM, T2DM), $K = 28$ (T1DM)	$K = 10$
Sample size	$r = 100$	$n = 20\,000$
#Evaluations per scenario	$r(K+1) = 3600$ (TNDM, T2DM), $r(K+1) = 2900$ (T1DM)	$n(K+2) = 240\,000$
Computational time per scenario[1]	18 min (EET) + 10 min (FPCA)	24 h (VBSA) + 150 min (FPCA)

[1] 4 cores at 3.6 GHz parallel, 32 GB RAM.

be taken by the patients themselves at considerably high sampling rates. Furthermore, this signal is similar to blood glucose but contains one more model parameter that might be important. Insulin and glucagon outputs are only measurable in a laboratory and not in a daily routine. Thus, they are seldom used for treatment decisions and are no longer considered here. Hence, only one model output is observed in the subsequent steps.

The entire procedure is carried out for the three groups and in various scenarios: for screening, four settings were chosen to reflect specific aspects of daily life. Likewise, they excite several parts of the model, so parameters are revealed that are more or less active during the discussed situations. A steady-state (STS) and a meal ingestion (MTT) scenario with 75 g of carbohydrate intake in combination with an additional insulin bolus at mealtime in T2DM and T1DM was performed. The first one is assumed to reveal factors for maintaining basal state, the latter is used to show parameters mainly connected to the digestive tract and the glucose regulation processes. The third scenario (OGTT) equals the second one but omits the insulin bolus in order to discriminate insulin effects. The three settings are equal to the simulation scenarios introduced in Table 4.13. In the last one, only an insulin bolus (IBO) is administered, allowing parameters to be separately determined that are only related to insulin processing. Table 5.1 summarizes some important adjustments. For VBSA, only one scenario was chosen that reflects the common daily life situation. This is the meal ingestion case for TNDM, including an additional insulin bolus at mealtime for T2DM and T1DM. Depending on the SA method used, n parameter sets are sampled and the model is evaluated for each sample.

5.1.2 Factor Screening and Ranking

The Elementary Effects Test or method of Morris is a multiple-start global SA that uses a One-At-a-Time (OAT) sampling scheme (Morris 1991). In this procedure, parameters are sequentially deflected around their nominal value by finite differences one at a time. This is basically a local technique, but if executed r-times with different parameter configurations it becomes a multiple-start method, and

the aggregated individual sensitivities can be taken as a global measure. To determine the r different samples, the radial-based design presented by Campolongo, Saltelli, and Cariboni (2011) is used as it can be shown that it provides several advantages in terms of efficiency and integration with subsequent SA techniques. For the i-th input factor its sensitivity index $\mu_i^\star$ is calculated by

$$\begin{aligned}\mu_i^\star &= \frac{1}{r}\sum_{j=1}^{r}\left|EE_i^{(j)}\right| \\ &= \frac{1}{r}\sum_{j=1}^{r}\left|\frac{f\left(\bar{X}_1^{(j)},\ldots,\bar{X}_i^{(j)}+\Delta_i^{(j)},\ldots,\bar{X}_K^{(j)}\right)-f\left(\bar{X}_1^{(j)},\ldots,\bar{X}_i^{(j)},\ldots,\bar{X}_K^{(j)}\right)}{\Delta_i^{(j)}}c_i\right|,\end{aligned} \tag{5.2}$$

where $EE_i^{(j)}$ is the elementary effect of input factor i at point j, r is the number of grid points, $\Delta_i^{(j)}$ is the perturbation, and c_i a scaling factor to deal with different units of measurements (Sin et al. 2009). In the case of a non-monotonic model the absolute values of an elementary effect must be used to avoid that effects of opposite signs cancel each other out (Campolongo, Cariboni, et al. 2007). The standard deviation for each input factor is given by

$$\sigma_i = \sqrt{\frac{1}{r-1}\sum_{j=1}^{r}\left(EE_i^{(j)}-\mu_i^\star\right)^2}, \tag{5.3}$$

and describes nonlinear effects and interactions between factors.

The computational cost to derive both sets is $r\,(K+1)$, with $r = 100$ sampling points and $K = 35$ (TNDM, T2DM) respectively $K = 28$ (T1DM) factors, which is much lower than for variance-based methods (Table 5.1). The number of samples is consistent with general findings in Pianosi et al. (2016), where r is typically set between 10 and 100, where a larger number increases the possibility of stabilizing factor ranking. The results can be found in Section 5.1.7.1 on page 109.

5.1.3 Transforming the Functional Model Output

The model output is a time series from which the dynamic behavior of the system can be investigated. From that, any SA technique can be applied at each time point to produce a set of time-dependent sensitivity indices that provides insights into those factors that are influential at particular times (Section 5.1.7.2). They can also be integrated over time to identify important parameters in terms of the entire time course of the model output.

An alternative is to define a scalar set of features like the maximum concentration of a substance or the period of oscillations and apply an SA method to these factors. Identifying a scalar feature can be difficult as it is not always clear which is suitable to represent the output. Thus, a method proposed by K. Campbell et al. (2006) and applied to biological systems by Sumner et al. (2012) is adopted. Functional principal component analysis (FPCA) is a popular multivariate analysis technique to extract information from functional data (Ullah et al. 2013). It is used to reduce the dimension

of a set of observations keeping as much of the variation in the data as possible. The methodology aims to transform the functional output into an appropriate coordinate system, i. e., in terms of an appropriate set of basis functions, followed by an SA of the coefficients of the expansion. The new basis set should be able to capture the most important features of the output. An SA technique of choice then identifies parameters that are important to generate these features in terms of triggering the associated model behavior. Transforming the output into a new basis system raises the question of what coordinate system to choose as this is highly problem-specific. Fixed basis functions such as orthogonal polynomials, Haar functions, or wavelets have a consistent fundamental shape across problems and the variability only affects coefficients but may spread the description of simple features across many terms. Data-adaptive basis functions such as principal components and partial least-squares usually concentrate information in the first few terms. Data-driven basis functions are problem-independent and are based on the variation in the data and not on what is believed to be important. A detailed investigation of functional data analysis methodologies can be found in Müller (2008).

FPCA extends the concept of principal component analysis (PCA) to functional outputs. Geometrically, PCA corresponds to a coordinate rotation that maximizes the sample variance, which can be achieved by finding the eigenvectors of the sample covariance matrix. Roughly spoken, one searches the empirical orthonormal basis function that "best fits" the functional data. The first principal component is thus the direction for which the orthogonal projection of the data points has the largest range. The second PC is then the direction orthogonal to the first PC for which the data points have the second largest range, and so forth.

Taken the aspects above, the functional model output $y_j(t)$, $j = 1, \ldots, n$ for a set of n model evaluations can be expanded by an appropriate set of basis functions $\boldsymbol{\Psi}(t) = [\psi_1(t), \ldots]$ such that

$$y_j(t) = \bar{y}(t) + \sum_l d_{jl}\psi_l(t), \quad \text{for } j = 1, \ldots, n, \tag{5.4}$$

where $\bar{y}(t)$ is the mean function across all realizations $y_j(t)$. Different aspects or features of the model outputs are represented by the basis functions $\psi_l(t)$ and the scalar coefficients d_{jl} of the expansion, which weight the basis function for each model output. Their importance is determined by the fraction of variance in the original data accounted for by each FPC. Coefficients d_{jl} for each observation j and each FPC l in $\psi_l(t)$ determine the optimal fit to the function $y_j(t)$ and can be used as a representative for a subsequent sensitivity analysis. Details can be found in Ramsay et al. (2009, Ch. 9.4.5), computational considerations in Fan (2015). The results can be found in Section 5.1.7.1 on page 110 for the EET and in Section 5.1.7.2 on page 120 for the VBSA.

5.1.4 Variance-based Sensitivity Analysis

Variance-based sensitivity analysis (VBSA) belongs to a class of global sensitivity analysis techniques that relies on three assumptions: that input factors are stochastic variables, that the induced variance in the model output can be seen as an approximation of the output uncertainty, and that the influence of

a particular input factor to the output variance is a measure for sensitivity. VBSA is used in a wide range of applications. It is independent of a specific model description and quantitatively assesses the impact of model inputs (Homma et al. 1996; Saltelli, Annoni, et al. 2010; Iooss et al. 2015).

Derivation of Variances from Model Output. Given a general model of the form

$$Y = f(X_1, X_2, \ldots, X_K), \tag{5.5}$$

with K uncertain input factors summarized in $\boldsymbol{X}$. The variance in the model output Y related to a variation of all input factors is $\mathrm{Var}_{\boldsymbol{X}}\{Y\}$, where subscript $\boldsymbol{X}$ denotes that all X_i were allowed to vary. It is now investigated to what extent the variance is reduced when the uncertainty in one input factor is removed by fixing it at a specific value. If the reduction in the output variance is large, it can be assumed that factor X_i is important in determining the output variation.

The variance after fixing the i-th factor X_i at its true value can be expressed by the conditional variance

$$\mathrm{Var}_{\boldsymbol{X}_{\sim i}}\left\{Y \mid X_i = x_i^\star\right\}, \tag{5.6}$$

where subscript $\boldsymbol{X}_{\sim i}$ denotes the matrix of all factors but X_i. As the true value $x_i^\star$ is not known, the expectation value over the conditional variance is built, which gives

$$\mathrm{E}_{X_i}\left\{\mathrm{Var}_{\boldsymbol{X}_{\sim i}}\{Y \mid X_i = x_i\}\right\}. \tag{5.7}$$

That means, the smaller the expected value is for all possible X_i, the greater the influence of this factor on the model output variance.

From the law of total variance (Schmidt 2011), the unexpected variance $\mathrm{Var}\{Y\}$ is given by

$$\mathrm{Var}\{Y\} = \mathrm{Var}_{X_i}\{\mathrm{E}_{\boldsymbol{X}_{\sim i}}\{Y \mid X_i\}\} + \mathrm{E}_{X_i}\{\mathrm{Var}_{\boldsymbol{X}_{\sim i}}\{Y \mid X_i\}\}, \tag{5.8}$$

where $\mathrm{Var}\{\mathrm{E}\{Y \mid X_i\}\}$ is also known as the variance of conditional expectation.

Sobol' (1993) provided a Monte-Carlo variance-based method to efficiently compute the individual factor importance and also the effects of higher-order, i. e., interactions between parameters. It is based on the decomposition of the model (5.5) into a set of functions of increasing dimensionality:

$$f(X_1, \ldots, X_K) = f_0 + \sum_i f_i(X_i) + \sum_i \sum_{j>i} f_{ij}(X_i, X_j) + \cdots + f_{12\ldots K}(X_1, \ldots X_K). \tag{5.9}$$

This expression has 2^K summands. If f is square-integrable over Ω^K, the K-dimensional unit hypercube of K input factors,

$$\Omega^K = (\boldsymbol{X} \mid 0 \leq X_i \leq 1; i = 1, \ldots, K), \tag{5.10}$$

the expansion is unique if f_0 is constant and if each term in the expansion above has zero mean, i. e., $\int f(X_i)\,\mathrm{d}X_i = 0$. From that, these terms can be calculated uniquely using the conditional expectations of the model output Y. In particular,

$$f_0 = \mathrm{E}\{Y\}, \tag{5.11}$$

$$f_i(X_i) = \mathrm{E}_{\boldsymbol{X}_{\sim i}}\{Y \mid X_i\} - \mathrm{E}\{Y\}, \tag{5.12}$$

$$f_{ij}(X_i, X_j) = \mathrm{E}_{\boldsymbol{X}_{\sim ij}}\left\{Y \mid X_i, X_j\right\} - f_i(X_i) - f_j(X_j) - \mathrm{E}\{Y\}, \tag{5.13}$$

and similar for higher orders. The total variance of $f(X)$ can be written as

$$\mathrm{Var}\{Y\} = \int_{\Omega^K} f^2(\boldsymbol{X})\,\mathrm{d}t - f_0^2, \tag{5.14}$$

which can be decomposed as well:

$$\mathrm{Var}\{Y\} = \sum_i \mathrm{Var}_i\{Y\} + \sum_i \sum_{j>i} \mathrm{Var}_{ij}\{Y\} + \cdots + \mathrm{Var}_{12\ldots K}\{Y\}. \tag{5.15}$$

This equation is also known as the ANOVA-HDMR decomposition (Saltelli 2008, p. 162). Dividing both sides of (5.15) by $\mathrm{Var}\{Y\}$ leads to the so-called Sobol' indices defined by

$$1 = \sum_i S_i + \sum_i \sum_{j>i} S_{ij} + \cdots + S_{12\ldots K}, \tag{5.16}$$

where S_i are the first-order indices, also called main effects. Thus, the contribution of each single factor to the output variance. The summands in (5.15) can be derived by calculating the variance of the elements in (5.12)-(5.13):

$$\mathrm{Var}_i\{Y\} = \mathrm{Var}\{f_i(X_i)\} = \mathrm{Var}_{X_i}\{\mathrm{E}_{\boldsymbol{X}_{\sim i}}\{Y \mid X_i\}\} \tag{5.17}$$

$$\begin{aligned}\mathrm{Var}_{ij}\{Y\} &= \mathrm{Var}\left\{f_{ij}(X_i, X_j)\right\} \\ &= \mathrm{Var}_{X_i X_j}\left\{\mathrm{E}_{\boldsymbol{X}_{\sim ij}}\left\{Y \mid X_i, X_j\right\}\right\} - \mathrm{Var}_{X_i}\{\mathrm{E}_{\boldsymbol{X}_{\sim i}}\{Y \mid X_i\}\} - \mathrm{Var}_{X_j}\left\{\mathrm{E}_{\boldsymbol{X}_{\sim j}}\left\{Y \mid X_j\right\}\right\}.\end{aligned} \tag{5.18}$$

Dividing (5.17) by the total variance leads to the first-order indices given by

$$S_i = \frac{\mathrm{Var}_{X_i}\{\mathrm{E}_{\boldsymbol{X}_{\sim i}}\{Y \mid X_i\}\}}{\mathrm{Var}\{Y\}}. \tag{5.19}$$

Equation (5.16) also defines interactions between factors by indices S_{ij}, with $i \neq j$, that are not explained by the sum of the first-order effects of X_i and X_j. Although interactions represent important features of models (Saltelli 2008, p. 161), the number of indices grows exponentially with dimension K. For computational reasons, it is often sufficient to compute the first-order indices only, and the total-order indices which were introduced by Homma et al. (1996). The total effect index represents the whole contribution of the input factor X_i to the output variance, i. e. the first-order effect and all

higher-order effects driven by interactions. Total indices are useful as they contain information on the non-additive features of a model that is visible in the difference between main and total effects. When fixing a factor to an arbitrary value within its input space and the output variance is not affected by this factor then it is non-influential and its total index is zero. The total effects can be calculated by decomposing the output variance again but respecting all factors but one, denoted by $\boldsymbol{X}_{\sim i}$. One gets:

$$\mathrm{Var}\{Y\} = \mathrm{Var}_{\boldsymbol{X}_{\sim i}}\left\{\mathrm{E}_{X_i}\left\{Y \mid \boldsymbol{X}_{\sim i}\right\}\right\} + \mathrm{E}_{\boldsymbol{X}_{\sim i}}\left\{\mathrm{Var}_{X_i}\left\{Y \mid \boldsymbol{X}_{\sim i}\right\}\right\}, \tag{5.20}$$

where $\mathrm{Var}\{Y\} - \mathrm{Var}_{\boldsymbol{X}_{\sim i}}\left\{\mathrm{E}_{X_i}\left\{Y \mid \boldsymbol{X}_{\sim i}\right\}\right\}$ is the remaining variance of Y that would be left, if $\boldsymbol{X}_{\sim i}$ could be fixed to its true values. The outer expectation is the average over all possible combinations in $\boldsymbol{X}_{\sim i}$, as the true values are not known. Dividing by the total variance, $\mathrm{Var}\{Y\}$, the total-order index for X_i is

$$S_{T_i} = \frac{\mathrm{E}_{\boldsymbol{X}_{\sim i}}\left\{\mathrm{Var}_{X_i}\left\{Y \mid \boldsymbol{X}_{\sim i}\right\}\right\}}{\mathrm{Var}\{Y\}} = 1 - \frac{\mathrm{Var}_{\boldsymbol{X}_{\sim i}}\left\{\mathrm{E}_{X_i}\left\{Y \mid \boldsymbol{X}_{\sim i}\right\}\right\}}{\mathrm{Var}\{Y\}}. \tag{5.21}$$

There are some properties of the Sobol' indices worth mentioning. From (5.16) the sum over all indices of all orders is equal to 1 and the sum of the first-order effects $S_i \leq 1$. The difference between S_i and S_{T_i} indicates to which extent a variable interacts with any other input factor. Lastly, the sum over all S_{T_i} will be typically higher than 1 as interactions are counted multiple times. It is equal to 1 if the model would be perfectly additive.

The results are discussed starting in Section 5.1.7.2 for the time-varying sensitivities on page 117 and on page 120 for the indices computed for each functional principal component.

Numerical Computation. Computing the first- and total-order indices derived above can be done numerically using Monte-Carlo simulations. To reduce the computational cost to derive all effects, Saltelli and Tarantola (2002) suggested calculating the total-order indices together with the first-order indices for an additional cost of n model runs. Therefore, they generated two n by K matrices $\boldsymbol{A}$ and $\boldsymbol{B}$ of random input samples a_{ji} and b_{ji}, respectively, where index j runs from 1 to n, the number of samples, and i runs from 1 to K, the number of input factors. From that, the matrix $\boldsymbol{A}_{\boldsymbol{B}}^{(i)}$ is constructed, where all columns are from $\boldsymbol{A}$ except the i-th column, that is from $\boldsymbol{B}$. The model is then evaluated $n + n$ times for matrices $\boldsymbol{A}$ and $\boldsymbol{B}$, plus $K \cdot n$ for the matrices $\boldsymbol{A}_{\boldsymbol{B}}^{(i)}$. Thus, the total computational cost is $n\,(K + 2)$. For the simultaneous estimate of the indices, Jansen's formula is used (Jansen et al. 1994; Jansen 1999), which is also proposed as best practice (Saltelli, Annoni, et al. 2010). The first-order indices are computed as

$$S_i = 1 - \frac{\frac{1}{2n}\sum_{j=1}^{n}\left(f\left(\boldsymbol{B}\right)_j - f\left(\boldsymbol{A}_{\boldsymbol{B}}^{(i)}\right)_j\right)^2}{\frac{1}{n}\sum_{j=1}^{n}\left(f\left(\boldsymbol{A}\right)_j\right)^2 - f_0^2}, \tag{5.22}$$

where

$$f_0^2 = \left(\frac{1}{n} \sum_{j=1}^{n} f(\boldsymbol{A})_j \right)^2$$

is the ensemble mean over the outputs in $\boldsymbol{A}$, and $f(\cdot)$ is the scalar model output with respect to the various input matrices. Similarly, the total-order effects can be estimated by

$$S_{T_i} = \frac{\frac{1}{2n} \sum_{j=1}^{n} \left(f(\boldsymbol{A})_j - f\left(\boldsymbol{A}_{\boldsymbol{B}}^{(i)}\right)_j \right)^2}{\frac{1}{n} \sum_{j=1}^{n} \left(f(\boldsymbol{A})_j \right)^2 - f_0^2}. \tag{5.23}$$

Typical values for n range from a few hundred to thousands or even more (Saltelli 2008, p. 164).

5.1.5 Concept of the Multi-Step Sensitivity Analysis

The model of glucose regulation has a large number of parameters. Moreover, the model output is a function of time that cannot be handled by standard methods for sensitivity analysis, which require scalar outputs. To overcome these issues, the single methodologies introduced so far have been integrated into a multi-step SA algorithm, presented by Tolks, Ament, and Eberle (2020). This approach allows a) a computational fast screening of a large parameter space in order to identify candidates for subsequent analysis, b) offers a solution for dynamical models by using FPCA that aggregates the functional outputs to a small set of scalars, from which c) quantitative indices can be computed by a variance-based analysis method, providing an overall sensitivity measure. The multi-step approach is depicted in Fig. 5.1 and includes the following items:

1. The whole parameter set is sampled using an appropriate sampling technique (1) and the Elementary Effects Test (2) is carried out for screening (Section 5.1.2). As the model output is not a scalar, FPCA is used to explain the variance in the output with a minimal set of orthonormal basis functions (3, Section 5.1.3). For each of the principal components, the elementary effects can then be calculated (4).
2. From that, only factors with a high EE are chosen. Thus, only a reduced parameter set is used for the following steps (5).
3. The main sensitivity analysis is fulfilled using a VBSA technique (Section 5.1.4) with an appropriate representation of the input space (6). Again, the model must be evaluated for all generated samples (7). Sensitivity indices are calculated at each time step (8) of the functional output and provide insights into the dynamics of the indices during the entire time course.
4. Moreover, the output variance can be described by a set of basis functions and their associated coefficients (9). For each component, VBSA is fulfilled (10), resulting in the first-order and total-order effects (11).
5. From the indices for each PC the overall sensitivities provide an aggregated scalar representation of the global importance of a factor (12, Section 5.1.6).

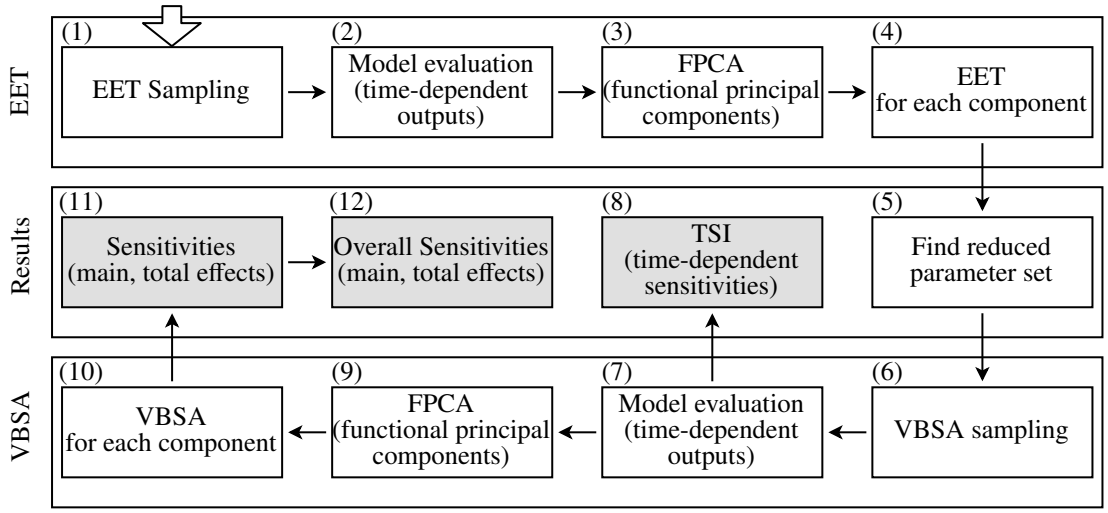

Figure 5.1: Proposed workflow illustrating the multi-step SA, which combines screening, parameter reduction, and quantitative SA to derive time-dependent and overall sensitivity indices.

5.1.6 Overall Sensitivity Indices

Elementary effects and quantitative indices presented in Section 5.1.2 respectively Section 5.1.4 are scalar representations derived from techniques that are based on a scalar model output. Including FPCA to reduce the time-dependent model output to a set of scalar scores for each functional principal component results in a set of indices for each FPC. To obtain an overall importance measure, results are weighted by their associated fraction of variance explained, FVE, which means, the contribution of each FPC to the total variability in the output.

The overall mean elementary effect, $\bar{\mu}_i^\star$, is defined by

$$\bar{\mu}_i^\star = \sum_{h=1}^{q} \mu_i^{\star(h)} \cdot FVE^{(h)}, \tag{5.24}$$

where $\mu_i^{\star(h)}$ is the elementary effect of parameter i, derived from the h-th out of q functional PCs.

The overall main effect $\bar{S}_i$ and the overall total effect $\bar{S}_{T_i}$ are defined by

$$\bar{S}_i = \sum_{h=1}^{q} S_i^{(h)} \cdot FVE^{(h)}, \tag{5.25}$$

$$\bar{S}_{T_i} = \sum_{h=1}^{q} S_{T_i}^{(h)} \cdot FVE^{(h)}, \tag{5.26}$$

where $S_i^{(h)}$ respectively $S_{T_i}^{(h)}$ are the sensitivity indices of the i-th input factor associated with the h-th FPC. This is a measure for the overall first-order respectively total-order effect of factor i on the model output, weighted by the relative importance of its FPC. As the variance described by the FPCs decreases quickly, the first q components already provide a good approximation of the overall indices.

5.1.7 Results and Discussion

The Elementary Effects Test and the variance-based technique, both in extension with functional component analysis, were applied to the model of glucose-insulin-glucagon regulation. After the generation of the sampling matrix, the model was evaluated for each input configuration. The sensitivities for both techniques were calculated from the scalar scores of the derived functional principal components.

This procedure was fulfilled for different scenarios listed in Table 5.1 on page 101. For EET, four scenarios were considered to get an overall view of the input factors when different model parts are active. During VBSA, only the meal ingestion scenario was taken into account since this is the most common in daily life.

5.1.7.1 Screening

Visual Inspection. To get a first overall view of the influence of all parameters the model was separately evaluated for each single input factor with $r = 25$, which leads to $2r \cdot K$ model runs. That allows a visual inspection of the variability in the output if only one single parameter is perturbed and any others are fixed at their nominal values. It gives hints on factors that have to be investigated further. The results for each group are reported in Figs. B.1 to B.3 for only the MTT scenario:

- An inspection of Fig. B.1 for TNDM reveals parameters $k_{G2}, V_G, k_1, k_2, m_5, m_6, \beta, G^b$, and I^b to induce the most variance to the output. From those, G^b seems to shift the whole time course vertically, whereas m_6 determines the shape when glucose decreases back to basal. Parameters k_1 and k_2 mainly influence the rise of glucose after the meal. The other factors determine falling glucose values after the peak to a lesser extent.
- For T2DM shown in Fig. B.2, the most influential factors are similar to those in TNDM. Some parameters like I^b, S_G^b and m_5 seem to add extra variance in steady-state. Furthermore, parameters related to insulin absorption $k_{i1} \ldots k_{i3}$ do not have a visible influence on the output.
- Results for T1DM are given in Fig. B.3. As not all parameters are present in this group the respective axes were left empty. Besides G^b and V_G, both directly related to glucose levels, parameters $k_{i1} \ldots k_{i3}$ add variability to the time course, particularly when glucose decreases after the peak. Furthermore, k_{p2} and V_{mx} seem to increase variance over a prolonged time.

A visual inspection of the influence of single factors can only be a starting point for subsequent analysis using EET and VBSA techniques.

Elementary Effects Test. EET was applied for the whole set of independent parameters. That is $K = 35$ for TNDM and T2DM, while in T1DM $K = 28$ as some parameters are always assumed to be zero in the insulin secretion parts of the model (Section 4.1.8). Suggestions about the number of repetitions range from $r = 10$ (Campolongo and Saltelli 1997) to 25, which was shown to be sufficient for screening purposes, but not enough to stabilize factor ranking (Pianosi et al. 2016). A

robustness and convergence analysis was carried out and revealed that a discrimination between the first ten and any other input factors is possible for $r \geq 30$ and further stabilization occurs until $r = 100$ (Section 5.1.8). Thus, to be on the safe side, r was fixed at 100 for all investigations, although it raises the computational cost from ≈5 min to 28 min for each scenario.

Figure 5.2 shows the mean functions including standard deviation for all groups and considered scenarios. The first row shows the two cases for TNDM, whereas the second and third rows depict the cases for T2DM and T1DM, respectively. The output signal is always the concentration of glucose in the subcutaneous space.

- In steady-state, there is no input to the system, except for T1DM, where basal insulin is given in order to guarantee a stable behavior. A deviation of the parameters from their nominal values leads to a dynamical reaction in which a new balanced state will be reached.
- Given a meal of 75 g of glucose plus an additional insulin bolus of 1.5 U CU^{-1} in the diabetic subjects leads to the transient behavior as shown in column 2. In TNDM, the variance around the mean function is smaller than in the other groups. In T2DM, an undershoot below basal glucose concentration can be seen.
- The OGTT is the same as the meal test in case 2, except that no insulin bolus was given. In both diabetic groups, variance does not differ significantly but mean functions increased slightly in T2DM and highly in T1DM.
- The IBO scenario reveals that the model is stable under mild hypoglycemia. A clear descent in glucose levels is visible with a higher variance in T2DM which could be an indicator for mechanism active to better compensate for lowering glucose levels.

In the following, only the most common MTT scenario is further investigated.

Functional Principal Components. To extract more information from variations in the model output functional principal components were calculated using the *PACE* toolbox (Fan 2015). Computation in each group and scenario took around 10 min. The resulting FPCs are plotted in the upper panels of Figs. 5.3 to 5.5 for TNDM, T2DM, and T1DM, respectively. As the interpretation of these time-courses is not always straightforward it is convenient to plot the average function of the output sample plus and minus some multiples of the FPCs (Ramsay et al. 2009), too. These plots are given in the lower panels of the same figures.

In TNDM (Fig. 5.3), the first three principal components account for 99 % of the variability in the glucose s.c. signal. It indicates that these components are enough to describe the major variance in the data. All FPCs start from zero suggesting that there is no variance at the simulation start.
The first PC accounts for 76 % of the variance. It is positive over the whole time course with a peak after 3 h and a steady-state value different from zero after the transient behavior. That means this FPC shifts the glucose signal vertically with the greatest increase at peak time. This is better visible in the bottom panel of the first FPC. At the beginning, no variance is added to the mean function but with

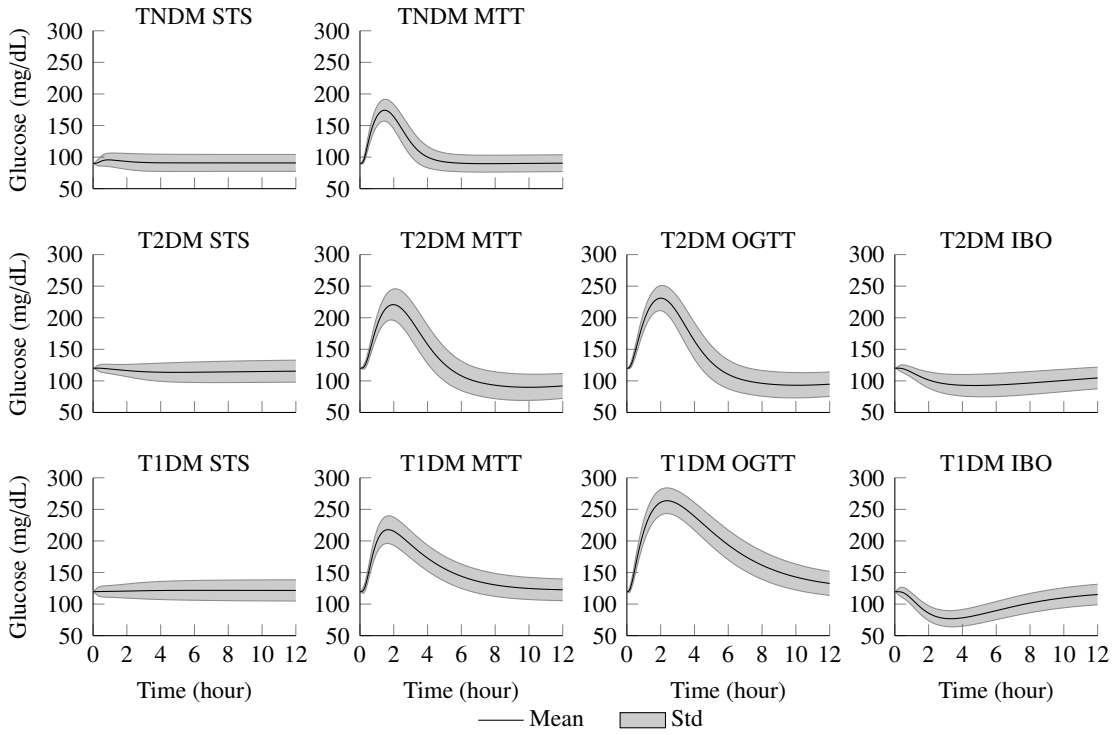

Figure 5.2: Ensemble mean functions (black lines) and standard deviation (gray area) of s.c. glucose model output for all considered groups (rows) and scenarios (columns).

ongoing time the concentration is shifted up and down over the entire course. A single model run with a high related score results in a higher-than-average time course and a higher steady-state value, whereas runs with negative scores will value smaller.

The second FPC still accounts for 14 % variance and is positive within the first two hours, then it decreases to a negative steady-state. Positive scores on this FPC mainly induce a faster fall in glucose concentration after meal ingestion and a lower-than-average glucose level at steady-state. This is also supported when observing the mean function in the bottom panel of this FPC. Furthermore, as its values vanish to zero only a little variance is added in steady-state.

The third FPC describes 9 % variance in the data with a positive course within the first hour and negative values after 2.5 h shrinking back to zero in steady-state. Its main effect appears during glucose changes after a meal. Thus, higher scores on this FPC generate faster rises and falls in glucose levels and higher peaks, too.

In T2DM (Fig. 5.4), the first three FPCs account for 99 % of the total variance which is portioned to 82 %, 13 %, and 4 % for the first, second, and third FPC, respectively. They can be analyzed as shown for the TNDM group.

The first FPC starts at zero and is positive but its time course has a delayed peak and the decrease to steady-state is prolonged. However, after a rise within the first four hours, it declines steadily but does not reach a stable value within simulation time. Pointing to the mean function below the FPC mainly adds the same amount of variance after the glucose concentration peaked.

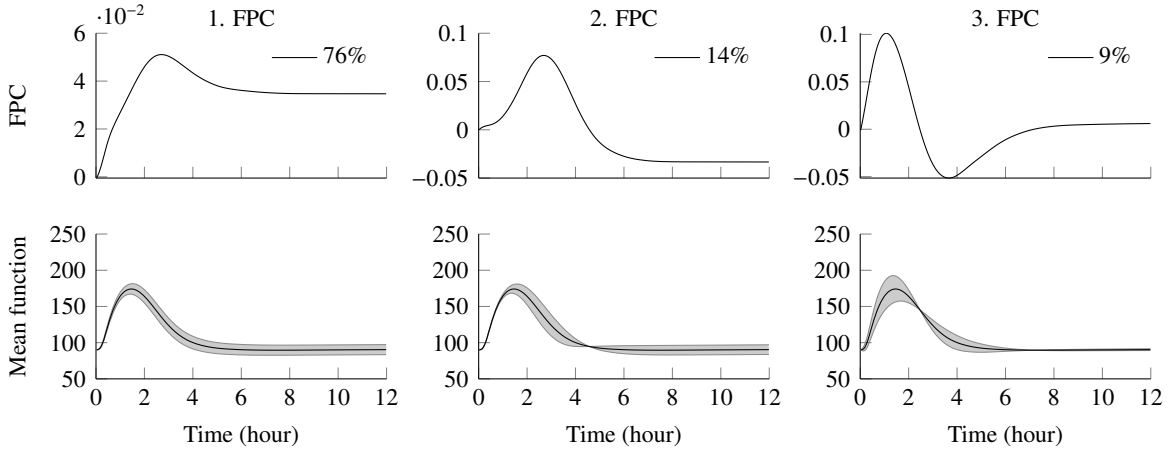

Figure 5.3: First three functional principal components (FPC) of glucose model output (upper panels) and mean function plus and minus multiples of each FPC (lower panels) for TNDM.

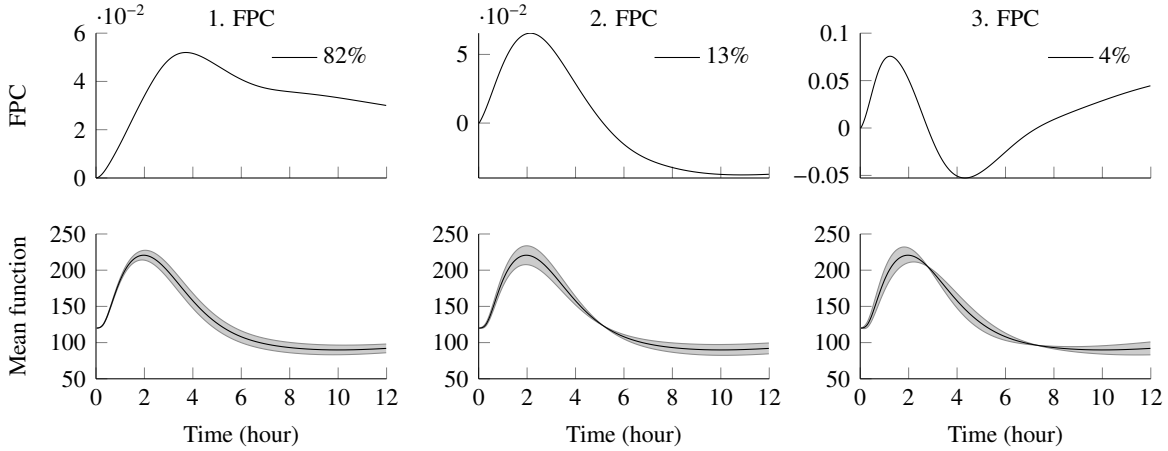

Figure 5.4: First three functional principal components (FPC) of glucose model output (upper panels) and mean function plus and minus multiples of each FPC (lower panels) for T2DM.

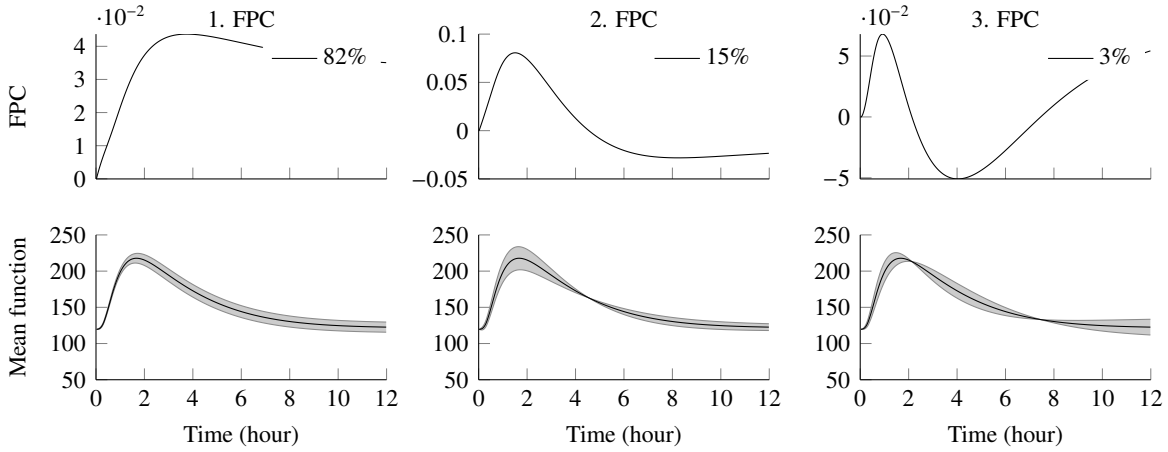

Figure 5.5: First three functional principal components (FPC) of glucose model output (upper panels) and mean function plus and minus multiples of each FPC (lower panels) for T1DM.

The second FPC is positive for the first five hours, i. e., during the majority of the transient behavior. Thus, inducing variability in the peak glucose concentration. Positive coefficients will force the output function to change steeper and to peak higher. After that, the FPC course is negative and adds variance at the end of the simulation.
The third FPC has pronounced positive and negative peaks after one and four hours, respectively, and mainly adds variance when glucose rises and decreases back to basal. Positive scores generate faster ascents and descents and induce higher-than-average time courses when the simulation ends.

The first three functional principal components in T1DM (Fig. 5.5) account for almost 100 % of the total variance in the model output. As the time courses of all FPCs and their related variance plots are similar to those in T2DM it is referred to the interpretation given there.

In this paragraph, FPCA was fulfilled to extract the dominant features of the subcutaneous glucose model output, derived by Monte-Carlo simulations. The scores associated with each FPC can now serve as a scalar input to compute the elementary effects (Section 5.1.2), as well the overall indices (Section 5.1.6). The effect of each input factor must be taken in relation to the variance explained by each of the FPCs.

Elementary Effects. As the current method is used for screening purposes, one is interested in distinguishing between factors that are important to drive the different features in the model output and those that can be neglected in subsequent steps. Thus, only the mean value $\mu_i^\star$ of each input factor is investigated. Figures 5.6 to 5.8 show the results as a stacked bar plot for each of the three groups. For all parameters, their mean is plotted on the vertical axis for the first, second, and third functional PC, colored in blue, red, and yellow, respectively. Thus, the height of the bars in one color is the relative importance of a factor with respect to their FPCs. Parameters with high values in only one FPC are important in inducing variability to this particular feature described by the FPC. Parameters with a high value within all FPCs are important for all features represented by them.

In TNDM (Fig. 5.6), particularly one factor stands out. Parameter G^b is the basal glucose level and thus, variance in G^b directly induces variability in the output. It is the major determinant in the first and to a lesser extent in the third functional PC and is mainly visible in steady-state. The high variance can also be seen in Fig. B.1. Other major factors are m_5, m_6, related to hepatic insulin extraction, and β, related to static insulin secretion. All three are involved in the process of how fast glucose is cleared from plasma.
The second FPC mainly accounts for variability between the first and fourth hour, thus, in the postprandial fall of glucose concentration. This feature is mainly driven by m_5, m_6, and β, and to a lesser extent V_{mx} and I^b which determine glucose clearance from plasma due to lower hepatic insulin extraction after a meal, higher insulin secretion, and glucose utilization. This makes sense as the amount and action of insulin mainly determine glucose disposal. All these factors are involved in the dynamical behavior of the model.
The third FPC accounts for 9 % variability, mainly when glucose levels change. The most important

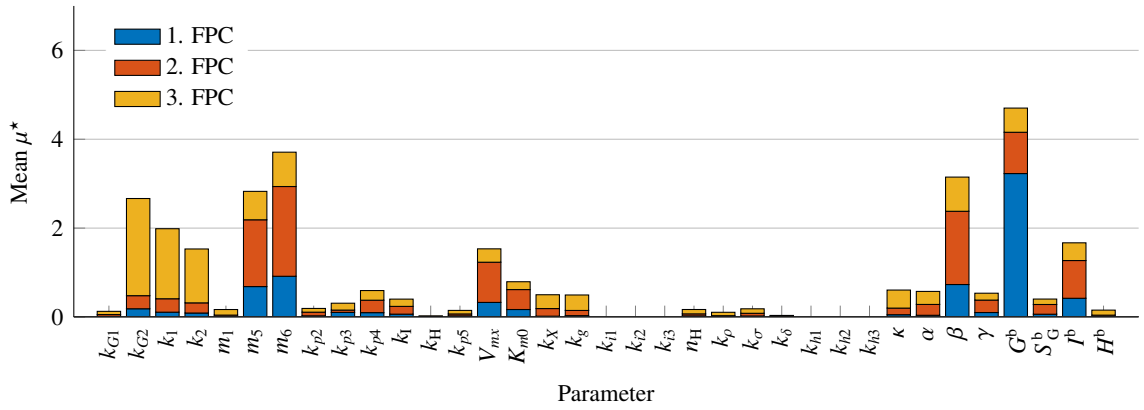

Figure 5.6: Mean $\mu^\star$, of the elementary effects of each parameter on s.c. glucose output for group TNDM ($K = 35$). The sensitivities are separately drawn for the first, second, and third functional principal component (FPC) in blue, red, and yellow, respectively.

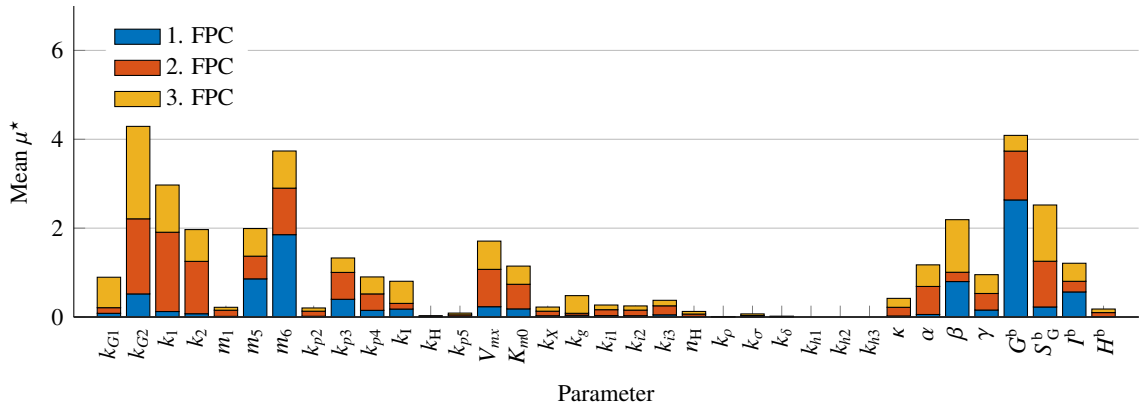

Figure 5.7: Mean $\mu^\star$, of the elementary effects of each parameter on s.c. glucose output for group T2DM ($K = 35$). The sensitivities are separately drawn for the first, second, and third functional principal component (FPC) in blue, red, and yellow, respectively.

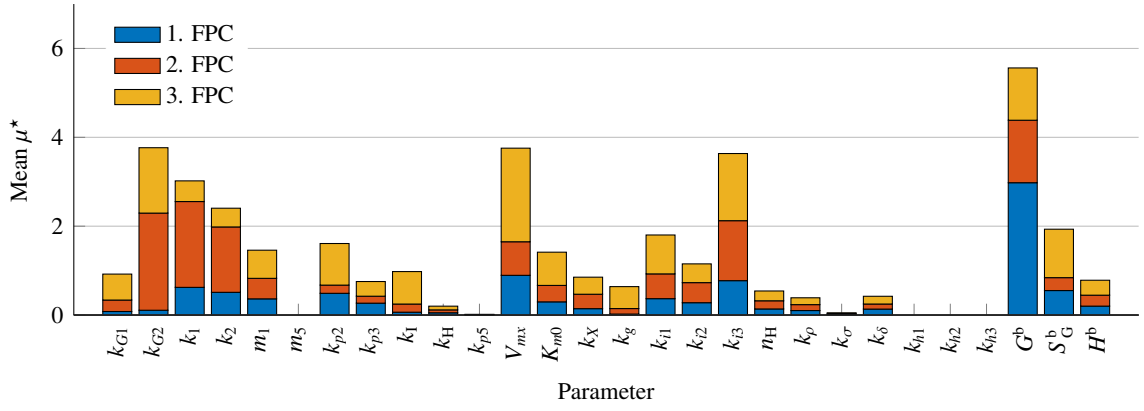

Figure 5.8: Mean $\mu^\star$, of the elementary effects of each parameter on s.c. glucose output for group T1DM ($K = 28$). The sensitivities are separately drawn for the first, second, and third functional principal component (FPC) in blue, red, and yellow, respectively.

parameters involved in controlling glucose rise are k_{G2}, k_1, and k_2, all associated with glucose appearing in plasma and glucose kinetics. Less active are m_5, m_6, and β, as well as k_X, k_g, κ, and α.
Parameters k_{i1} to k_{i3} and k_{h1} to k_{h3} are zero as they are not affected by the meal input signal. Furthermore, parameters related to glucagon compartments play only a minor role.

In T2DM (Fig. 5.7), the main determinant in inducing variability into the first FPC is G^{b}, too. Thus, the same interpretation given for TNDM holds. Also, m_5, m_6, and β drive the feature explained by the first FPC. Parameters describing variance by the second FPC are similar to those for the third FPC in TNDM, whereby most of these factors also drive the third FPC. Thus, most of the variance that occurs around the glucose peak cannot be assigned to a single principal component. More emphasis is given to α, a rate constant related to static insulin action on glucose level above basal and thus, important for the delay of insulin action, as well as to the endogenous glucose production rate $S_{\mathrm{G}}^{\mathrm{b}}$, which mainly influences the output behavior at simulation end (see Fig. B.2 too).
Parameters k_{p3}, k_{p4}, and k_{I}, all related to hepatic glucose production, weight higher than others. Their values lie in similar ranges compared to TNDM but since in T2DM insulin fluxes are significantly higher, their influence on glucose production is increased.
Furthermore, V_{mx}, K_{m0}, and k_g do not differ significantly between the two groups. Since an insulin bolus was given in this group, parameters related to insulin absorption in plasma, k_{i1} to k_{i3} were active, but at a low level.

Although T2DM and T1DM both describe diabetic subjects the effects of normal and type 2 are quite similar to each other. The mean values of T1DM subjects (Fig. 5.8) show different behavior. Again, G^{b} is the major factor in the first FPC, inducing variance during the transient and, to a lesser extent, in the steady-state phase of the scenario.
Parameters inducing most variance in the second FPC are comparable to those in T2DM, namely k_1, k_2, and k_{G2}. Besides that, insulin absorption rates k_{i1} to k_{i3} are more important than in the other groups, particularly for the third FPC, and are related to the phase of decreasing glucose levels (see Fig. B.2 too). As insulin secretion is completely absent in T1DM, external delivery and absorption of insulin gains much more importance to the variability of the output. Despite higher values of most parameters for the third FPC, it must be noted that the overall fraction of variance explained is only 3 %, and thus, the absolute importance is low.

Overall Indices. Interpretation of the importance of different input factors related to a functional component is not a straightforward task. To simplify interpretation, the overall effect defined in (5.24) can be considered, where the individual effects are weighted by the fraction of variance in the associated functional component.

The resulting mean effect, $\bar{\mu}^\star$, for all parameters and groups is given in Fig. 5.9. The following parameters have none or minimal effect on glucose output: k_{h1} to k_{h3}, $k_\sigma, k_\rho, k_\delta, n$, H^{b}, as well as k_{H} and k_{p5}, all related to glucagon kinetics, its secretion, or action on hepatic glucose production. Additionally, insulin action on glucose production, k_{I}, and the delay between changes in insulin

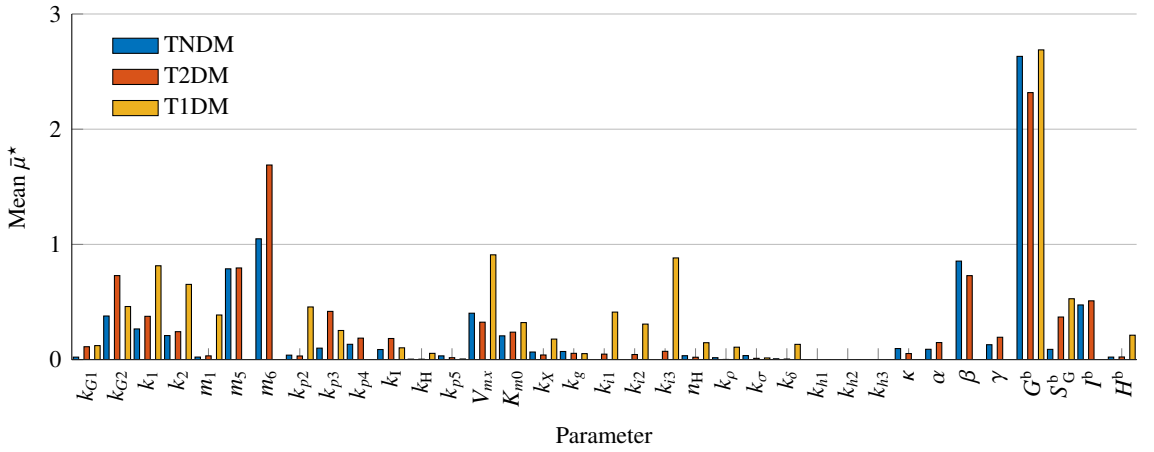

Figure 5.9: Overall mean, $\bar{\mu}^\star$, of the elementary effects of each parameter on s.c. glucose output for TNDM (blue bars), T2DM (red bars), and T1DM (yellow bars) subjects.

concentration and insulin action, k_X, can be neglected. Looking at parameters related to insulin secretion reveals that β is most important since it is involved in the control of static insulin secretion. In contrast, the assumption that κ, the dynamic glucose control that weights glucose rate of change, has overall importance does not hold. As insulin secretion is absent in T1DM the related effects are set to zero. To compensate for the lack of action, however, parameters responsible for insulin absorption into plasma, k_{i1} to k_{i3}, become apparent. As mentioned earlier the dominant parameter in all groups is the basal glucose concentration as variance in this factor directly induces variability in the output. Furthermore, parameters k_1, k_2, and k_{G2} are not dominant but are obviously needed to describe glucose kinetics, particularly when glucose levels are rising after a meal. Lastly, m_5 and m_6 are related to hepatic insulin extraction and thus, indirectly control the amount of insulin released into the circulatory system. They regulate glucose clearance from plasma in combination with the hepatic glucose production, $S_{\mathrm{G}}^{\mathrm{b}}$, and glucose utilization parameters V_{mx} and K_{m0}.

The interpretation given above shows that the importance of certain factors during a meal depends on the group of diabetes and should be considered in a subsequent quantitative sensitivity analysis.

Reducing the Parameter Space. To reduce the computational cost when computing the variance-based sensitivity indices, only a reduced parameter set is used. Taking into account the findings above, only those 10 parameters with the highest overall mean effect in each group are considered. They are reported in Table 5.2.

5.1.7.2 Variance-based Sensitivity Analysis

The section above has shown that the Elementary Effects Test is a computational cheap technique for effective screening over a large range of input factors to distinguish between important and non-influential parameters. It has also been shown how functional principal component analysis can be

Table 5.2: Reduced parameter set in each group, sorted by descending values of $\bar{\mu}^\star$.

Group	Parameter set									
TNDM	G^b	m_6	β	m_5	I^b	V_{mx}	k_{G2}	k_1	k_2	K_{m0}
T2DM	G^b	m_6	m_5	k_{G2}	β	I^b	k_{p3}	k_1	S_G^b	V_{mx}
T1DM	G^b	V_{mx}	k_{i3}	k_1	k_2	S_G^b	k_{G2}	k_{p2}	k_{i1}	m_1

used to find dominant modes in the variability of the model output and how effects on their scores can be determined. On that basis, the parameter space could be reduced to only those parameters having a large influence on the dominant features of the functional model outcome.

Now, variance-based sensitivity analysis is applied to the reduced parameter set of size $K = 10$ to compute quantitative sensitivity indices. To generate stable and reliable estimates of the indices a large number of input samples is needed. Here, n is set to 20 000. The calculation of the main and total indices can be done based on $n(K + 2)$ model runs, leading to a total of 240 000 evaluations. At a computational time of 10 000 runs per hour, this requires approximately 24 h plus an additional cost of 150 min to compute the functional PCs (Table 5.1 on page 101).

The whole procedure is carried out for all three groups and the MTT scenario. Figure 5.10 shows the single model outcomes of the subcutaneous glucose concentration for each group. The time courses are similar to those obtained by the Elementary Effects Test (MTT scenario in Fig. 5.2). The time average standard deviations introduced by the parameter variations are 14.75, 22.77, and 17.92 mg dL^{-1} for TNDM, T2DM, and T1DM, respectively.

Time-varying Sensitivity Indices. One possibility to deal with time-dependent model outputs without computing functional principal components is to calculate sensitivities at each discrete time step or at specified time points in the output signal. From this kind of plot, one could visually derive

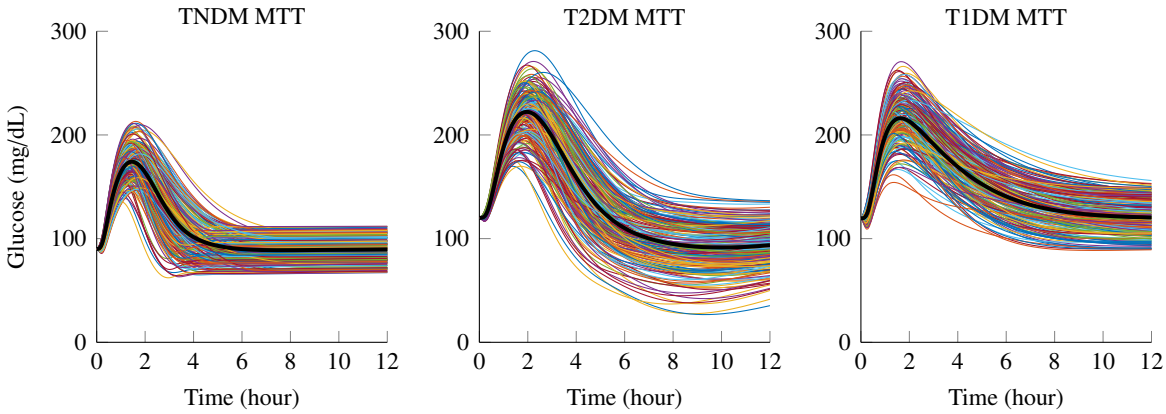

Figure 5.10: Single s.c. glucose model outputs (colored lines, only 200 realizations shown) and mean function (black line) for TNDM (left), T2DM (middle), and T1DM (right) subjects.

the importance of a factor evolving with time when specific events occur that are of interest. The resulting indices at each time step (1 min) are plotted in Figs. 5.11 to 5.13 for TNDM, T2DM, and T1DM, respectively, and are sorted in descending order by their overall elementary effect. Note that at the simulation start, the variance in the output is zero, and thus, indices cannot be computed.

In TNDM the visibly dominant input factor over the whole time course is G^{b} (Fig. 5.11). Its sensitivity is zero at simulation start and rises steadily to a first maximum after 104 min when the average glucose signal has its peak. When the glucose level falls back to basal, sensitivity gets weaker but rises again after three hours. Sensitivity is at its maximum after all dynamics in the system decayed and reached steady-state. Seemingly, G^{b} is less sensitive when the system is in a transient phase and most variance is induced in steady-state.
Parameters k_1 and k_2 describing glucose kinetics are most sensitive at simulation beginning and decline rapidly to zero within the first two hours. This is in accordance with the variance course plotted in Fig. B.1, where the rise in glucose is mainly subject to variability.
Another important parameter in the initial phase is k_{G2}, the rate at which ingested glucose is digested and thus, reaches plasma. It has its first maximum after one hour and a second but far lower peak after four hours. While the first is a direct contribution of glucose variability due to its appearance in plasma the latter seems to be indirectly related to the dynamical behavior of other substances.
All other parameters are more or less sensitive when glucose reaches its peak concentration and when decreasing back to basal level.

A comparable behavior can be seen in T2DM (Fig. 5.12). Note that the output does not reach steady-state within simulation time. It is still in a transient phase. As in TNDM, k_1 is the most important parameter at the start of the simulation and decreases to zero within four hours. Note that factor k_2 was fixed in VBSA, which explains the high value of k_1 of nearly one, inducing most of the variance alone. Although the time course of k_{G2} is similar to the TNDM group, the second peak is delayed and prolonged taking into account the overall slower dynamic when glucose turns back to basal.
In contrast to TNDM, m_6 induces more variance in the output between glucose peak and simulation end, which indicates prolonged dynamical action within the system. Additionally, the sensitivity of the basal hepatic glucose production rate, $S^{\mathrm{b}}_{\mathrm{G}}$, plays a role from 9 h on when glucose rises slightly after the undershot (see single output courses in the middle panel of Fig. 5.10). This is consistent with findings from the IBO scenario, where it plays, besides m_6 and G^{b}, a major role when glucose levels regenerate after induced mild hypoglycemia (results not shown here).
Moreover, G^{b} rises steadily from zero to 0.65 at the end of the simulation, which is similar to TNDM subjects. All remaining parameters have a sensitivity below 0.1 and a similar time course.

The time courses of sensitivities in T1DM are also similar to those in the other groups (Fig. 5.13). Most of the variance at the simulation start is induced by variations in k_1, k_2, and k_{G2}, again.
Since factors of insulin secretion are absent in T1DM, V_{mx}, related to glucose utilization, is most important during the phase of glucose transition. The whole time course is delayed and prolonged.
Sensitivities for parameters of insulin absorption into plasma, k_{i1}, k_{i3}, have an almost equal time course

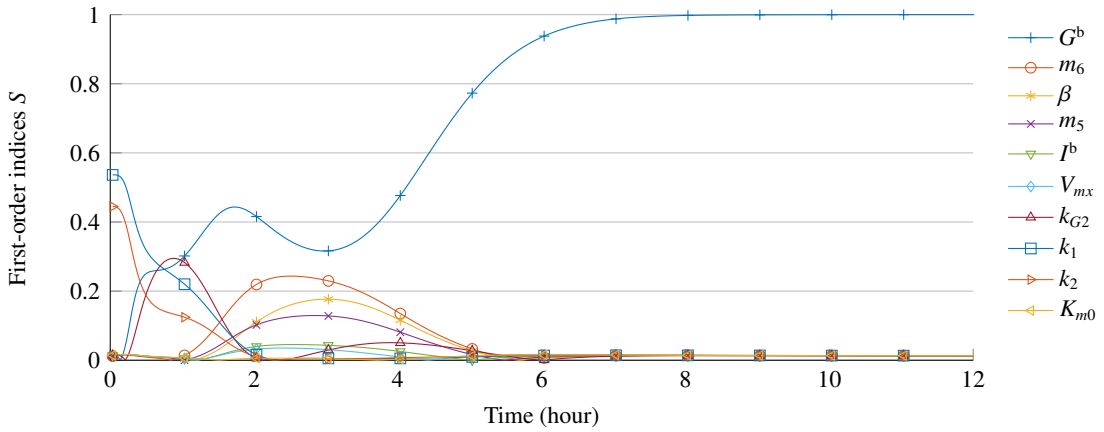

Figure 5.11: Time-varying first-order sensitivities $S(t)$ for TNDM, computed at each time step. Note that the markers have been added only for a better distinguishability of the lines.

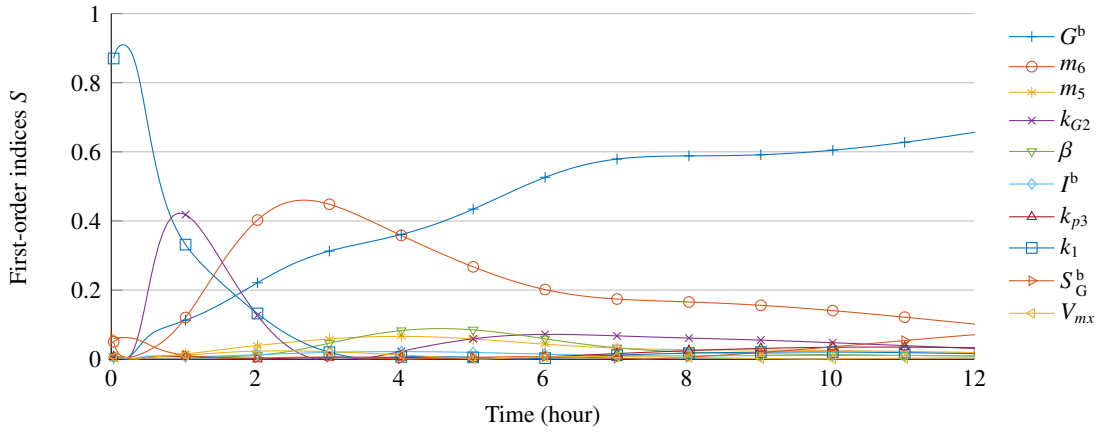

Figure 5.12: Time-varying first-order sensitivities $S(t)$ for T2DM, computed at each time step.

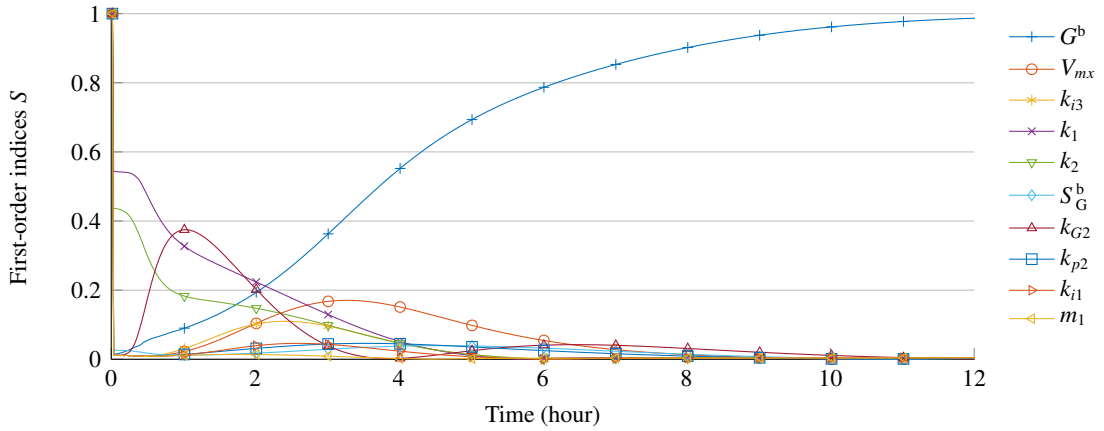

Figure 5.13: Time-varying first-order sensitivities $S(t)$ for T1DM, computed at each time step.

but differ in amplitude. They are active between the first and fifth hour and therefore, during the main transient behavior.
Furthermore, m_1, the rate constant with which insulin is exchanged between liver and plasma has only a small but constant effect over the entire simulation.

In summary, time-dependent sensitivity indices reveal contributions of factors to the output variability of a dynamical system at specific time points. This improves the understanding of when particular parameters are more or less active. One major drawback is that it could lead to false assumptions about the overall importance of a factor. This could be the case if a parameter has a high sensitivity at a particular time step but the overall contribution to the output variation is low. The effect can be seen, e. g., for parameters k_1 and k_2 at simulation start. Although their importance is high, there is only minimal variance in the model output and therefore the effect on the overall variability is low. However, using functional principal component analysis could provide additional information on how to interpret these measurements correctly.

Functional Principal Components. Section 5.1.3 showed how functional principal components could be used to describe the main modes of variability in the model output. Section 5.1.7.1 described the results obtained after applying FPCA on the functional model output for the Elementary Effects Test. Here, FPCA is fulfilled on the model output generated by the variance-based design. The number of FPCs was again fixed to $q = 3$, which is enough to describe nearly all of the variance.

The results are illustrated in Figs. B.4 to B.6 for TNDM, T2DM, and T1DM subjects, respectively. The general time course of functional components is almost equal to the ones derived by the Elementary Effects Test (compare to Figs. 5.3 to 5.5). Hence, the explanation given there still holds. In TNDM, the first three FPCs account for 78 %, 14 %, and 7 % explained variability. In T2DM, the FPCs explain 86 %, 11 %, and 3 % of variability and in T1DM they give 79 %, 18 %, and 3 %. The dominant modes in the s.c. glucose signal are described by only 10 parameters, whereas during EET the full parameter set was used. This confirms that the EET can be used as an effective screening technique to reduce the number of possible influential factors without losing too much information in the observed signal. This directly leads to a possible disadvantage of this method. If several model outputs must be considered, e. g., insulin concentration in plasma, the interpretation effort increases rapidly. Parameters identified to be important for one output are not necessarily relevant for other outputs. In that case, another methodology must be found to consider the relative importance of parameters on multiple outputs.

First-order and Total-order Sensitivity Indices. After calculating the functional principal components, sensitivity indices can be computed from the coefficients of each functional basis set (Section 5.1.4 on page 106). The resulting first-order indices, S_i, and total-order sensitivities, S_{Ti}, are reported in Tables B.1 to B.3 for TNDM, T2DM, and T1DM, respectively. First, in all groups the total-order sensitivities are only marginally higher than the first-order, indicating only minimal interaction between parameters. From that, it is not necessary to compute second-order or higher-order indices as

it would be needed if one wants to investigate particular interactions between input factors. Second, some main effects have values slightly lower than zero or the main effect is higher than the total effect (e. g., K_{m0} in TNDM, first FPC). Theoretically, these results cannot occur but can be explained by various approximation errors when building the FPCs, especially when the indices are low within one component. Besides that, the relative importance of each parameter in each FPC is comparable to the respective mean elementary effect (Figs. 5.6 to 5.8):

In TNDM, the dominant parameter in the first FPC is G^{b}, whereas all other factors are weakly represented. This is in accordance with the corresponding elementary effect and also visible when considering its time course. In the second FPC, parameters m_6, β, and m_5 are most influential. All these factors are related to the insulin part of the model. Finally, parameters k_{G2}, k_1, and k_2 induce the most variability explained by the third FPC. These findings confirm the results obtained with the Elementary Effects Test. The sensitivity of K_{m0} is negligible in all FPCs. Hence, only 9 out of 10 investigated parameters in the variance-based analysis are important. In this group, the different input factors can be easily associated with a particular functional principal component and thus, to a dominant feature in the output variance.

In T2DM, most variance is induced by parameters G^{b} and m_6 for the first component. The second component is mainly driven by parameters k_1 and k_{G2}, related to glucose appearance and kinetics in plasma. This is in contrast to the ones in TNDM, where the second FPC is associated with insulin-related factors. However, this behavior is understandable since the insulin system has deteriorated in type 2 diabetics and thus, its importance on the model output is weaker than in normal subjects. The third FPC is mainly driven by k_{G2}, β, and $S_{\mathrm{G}}^{\mathrm{b}}$, but also V_{mx} and G^{b} are involved. The assignment of individual parameters to a specific component is no longer clear-cut. Furthermore, I^{b} and k_{p3} have only little influence on the basis functions.

Sensitivities in the T1DM group are similar to those for T2DM. Parameter G^{b} is again the single important factor to drive variance in the first FPC, whereas the second FPC is dominated by the glucose-related parameters k_1, k_2, and k_{G2}. Parameter m_1 has only minimal effect. Insulin absorption rates k_{i1} and k_{i3} are both related to a lesser extent to the second and also the third FPC. For the latter, the most variance is introduced by V_{mx}, related to glucose utilization, k_{G2}, and $S_{\mathrm{G}}^{\mathrm{b}}$, inducing variance when glucose level rises and falls, respectively.

Overall Sensitivity Indices. To derive an overall sensitivity measure for each parameter, Eqs. (5.25)-(5.26) are used. Sensitivity index $S_i^{(h)}$ ($S_{T_i}^{(h)}$) of parameter i belonging to principal component h is weighted by its fraction of variance explained, $FVE^{(h)}$, and summarized to the overall index $\bar{S}_i$ ($\bar{S}_{T_i}$). Results are shown in Fig. 5.14 for the first-order effects only, as the total-order indices do not differ significantly. In the figure, 16 parameters are plotted which are common in all three groups.

The overall most important parameter in all groups is G^{b}. Parameters m_5, m_6, and β are involved in how much and how fast insulin is secreted into the system, and thus, it makes sense that they are

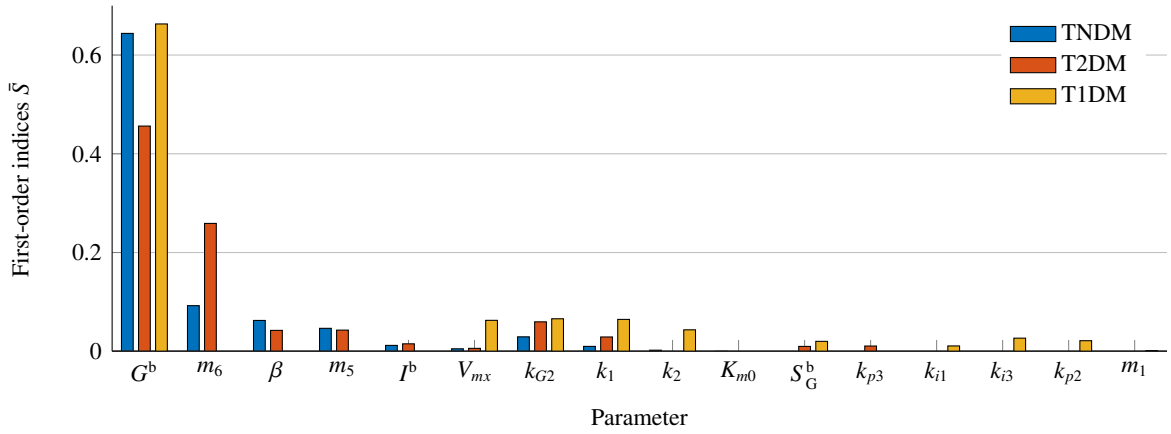

Figure 5.14: Overall first-order sensitivities, $\bar{S}_i$, for TNDN (blue), T2DM (red), and T1DM (yellow). In total, 16 parameters are shared by the three groups. A bar height of zero indicates that the respective factor is not active within the group.

important. As insulin secretion is assumed to be absent in T1DM their values are zero in this group. There, V_{mx}, related to insulin sensitivity, and k_{p2}, the liver glucose effectiveness, contribute more to the variance in the system. Parameters k_{i1} and k_{i3} come into play when subjects have to inject insulin subcutaneously as they regulate its absorption into plasma. Without any other insulin-related process in T1DM, they are important in this group. However, T2DM subjects also have to inject insulin but since secretory processes are still present, factors do not induce enough variance in the output to become apparent. Parameters k_1 and k_{G2} are important in all groups as they mainly determine how fast glucose appears in plasma after a meal and how fast it is distributed within the circulatory system. Furthermore, k_{p3} and S_G^b are more important in the diabetic groups, mainly when glucose concentration rises from levels below basal. In relation to other factors, m_1 and K_{m0} are not relevant and could be neglected.

5.1.8 Robustness and Convergence

Sampling-based sensitivity analysis techniques have been proven to be good alternatives if sensitivities cannot be computed analytically. As they do not provide exact solutions, the robustness and convergence of the estimates should be assessed.

Two aspects are of interest here. First, robustness analysis aims to investigate whether the indices are independent of a particular input-output sample (Pianosi et al. 2016). That means, an estimate is assumed to be robust if its value is similar for different subsets of samples of the same size. Bootstrapping provides a simple method without involving additional model evaluations (Efron et al. 1986; Yang 2011). Second, convergence analysis is used to assess whether an index is stable for different sizes of the input-output samples. A simple approach would be to re-estimate the sensitivities for an increasing size of samples drawn from the original sample. If the indices do not stabilize

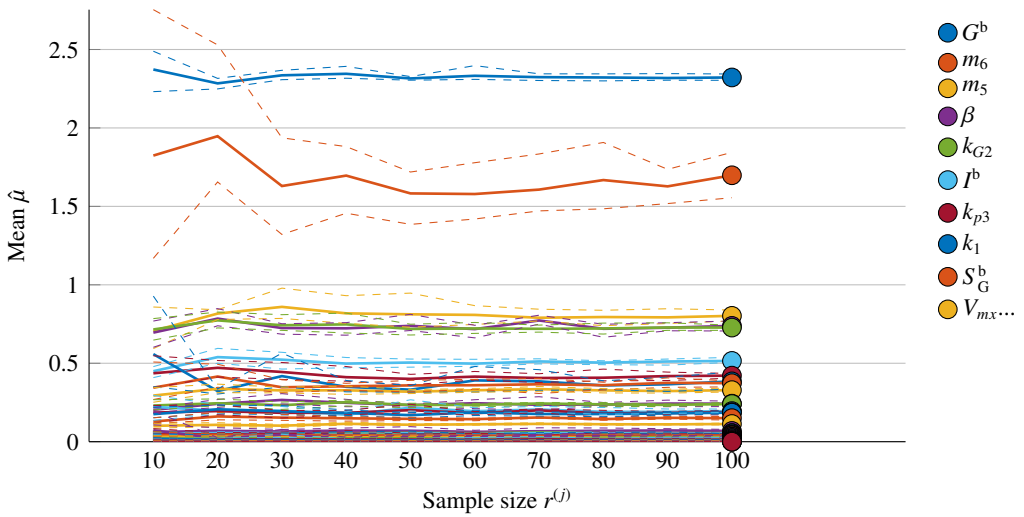

Figure 5.15: Results of convergence and robustness analysis exemplarily shown for the T2DM subject and the MTT scenario. Mean effect, $\hat{\mu}_i$, computed for an increasing number of model evaluations (one solid line per factor). Dashed lines represent robustness obtained at each subset $r^{(j)}$ by bootstrapping.

additional model runs and a re-computation of the extended sample size might be necessary to improve convergence (Pianosi et al. 2016).

Although it is not common to assess robustness and convergence for the Elementary Effects Test but variance-based techniques, the analysis is illustrated exemplarily for one case on the overall indices $\hat{\mu}_i$. Therefore, they are not computed using the mean values over all elementary effects as given in (5.24), but for every single effect by

$$\hat{\mu}_i^{(j)} = \sum_{h=1}^{q} EE_i^{(j,h)} \cdot FVE^{(h)}, \tag{5.27}$$

where $EE_i^{(j,h)}$ is the effect for factor i, the finite difference j computed for principal component h, and q is the number of FPCs. This returns a matrix of overall effects from which convergence can be assessed. Repeating for varying randomly selected subsets of elementary effects allows the assessment of the robustness by building averages and standard deviations.

Results for the type 2 diabetic group and the MTT scenario are shown in Fig. 5.15. Mean effect $\hat{\mu}_i^{(j)}$ and its confidence interval were calculated for sample sizes $r^{(j)}$ from 10 up to 100 and bootstrapping with 10 repetitions. At low sample sizes ($r < 40$), the error is higher for some factors but lower and upper confidence bounds shrink with increasing sample sizes. All factors but G^b and m_6 lie between zero and one and thus, are near to each other. Although confidence bounds overlap, factor ranking is possible for those effects with larger means as their values stabilize quickly.

To assess the robustness and convergence of the variance-based analysis, the first-order sensitivity indices $S_i^{(j)}$ were computed for $j = 1 \ldots 10$ times with increasing sample sizes from 2000 to 20 000.

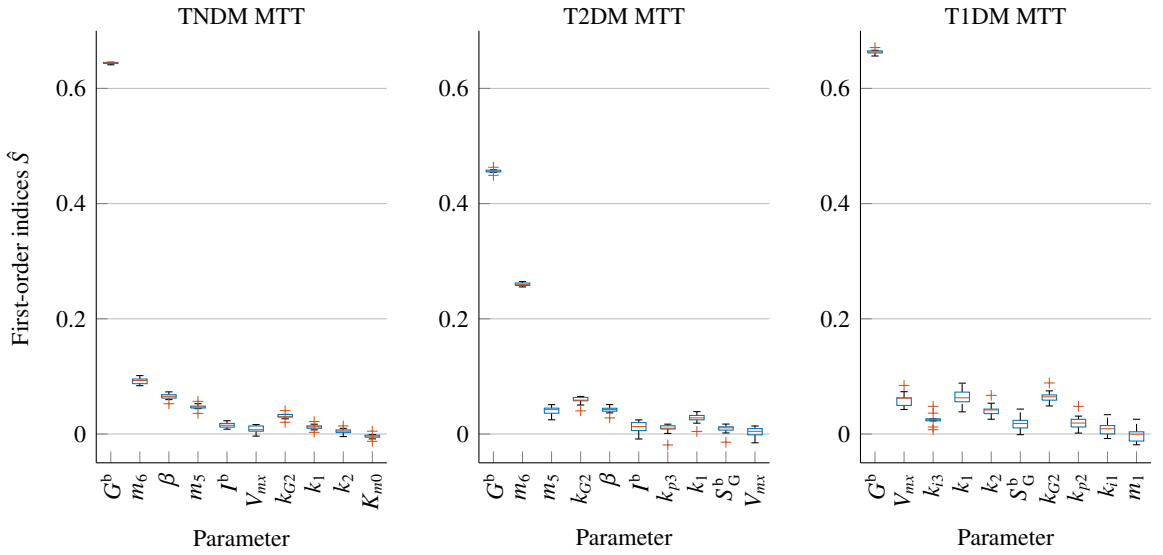

Figure 5.16: Robustness analysis of the variance-based overall first-order sensitivity indices. Each overall index was computed several times on a randomly chosen subset drawn from the original sample. The boxplot shows the median, 25th and 75th percentiles, extreme points, and outliers for each parameter and for TNDM, T2DM, and T1DM in the left, middle, and right panel, respectively.

Each run was repeated 100 times for a randomly chosen subset of that fixed size and statistics were computed. The overall indices $\hat{S}_i^{(j)}$ are derived from (5.25) but applied to each j, which results in

$$\hat{S}_i^{(j)} = \sum_{h=1}^{q} S_i^{(j,h)} \cdot FVE^{(h)}. \tag{5.28}$$

Index $S_i^{(j,h)}$ is the sensitivity of parameter i, computed on subset j and related to the functional principal component h. $FVE^{(h)}$ denotes the fraction of variance explained by the h-th FPC.Repeating over all subsets allows the calculation of the average and standard deviation at each j. The results for $j = 10$ are shown as a box plot in Fig. 5.16, where only small errors in all parameters and across all groups are visible, and thus, the sensitivity estimates can be trusted.

Summary. In the preceding section, a multi-step global sensitivity analysis technique has been presented that is capable of identifying those parameters that induce the most variance in the model output. Therefore, multiple statistical information was aggregated into a quantitative overall sensitivity index (Fig. 5.14). Although these indices identify candidates for subsequent model identification, they do not reveal whether the parameters can be actually determined by observing the output, especially several at once. However, controllability and observability analysis, which are introduced in the following chapter, can do this.

5.2 State and Parameter Analysis

The following section addresses the analysis of dynamic and static states of the glucose regulation system. A dynamical state defines the behavior of a quantity in the system over time, here by a set of ordinary differential equations. System parameters can be regarded as static, i. e., time-invariant states. That is particularly useful for parameter identification or online state estimation (Chapter 6). Controllability and observability are basic properties of dynamical systems and affect the feasibility of control tasks. System Gramian matrices embody these attributes in a condensed manner. They serve as the main determinant for the following investigations.

A linear, continuous, time-invariant MIMO (multiple-input multiple-output) system in state-space form is given by

$$\begin{cases} \dot{\boldsymbol{x}} = \boldsymbol{A}\boldsymbol{x} + \boldsymbol{B}\boldsymbol{u}, \\ \boldsymbol{y} = \boldsymbol{C}\boldsymbol{x}, \end{cases} \tag{5.29}$$

with state vector $\boldsymbol{x}(t) \in \mathbb{R}^N$, input vector $\boldsymbol{u}(t) \in \mathbb{R}^M$, and output vector $\boldsymbol{y}(t) \in \mathbb{R}^O$. Matrix $\boldsymbol{A} \in \mathbb{R}^{N\times N}$ transforms the states, input matrix $\boldsymbol{B} \in \mathbb{R}^{N\times M}$ maps the inputs to the states and output matrix $\boldsymbol{C} \in \mathbb{R}^{O\times N}$ maps the states to the outputs. The system is called stable if the eigenvalues in $\boldsymbol{A}$ are strictly negative.

A general nonlinear input-output system in state-space form, Σ, can be defined by

$$\Sigma : \begin{cases} \dot{\boldsymbol{x}} = \mathbf{f}\left(t, \boldsymbol{x}, \boldsymbol{u}, \boldsymbol{p}\right), \\ \boldsymbol{y} = \mathbf{g}\left(t, \boldsymbol{x}, \boldsymbol{p}\right), \end{cases} \tag{5.30}$$

with a set of state equations $\mathbf{f}(\cdot)$ and output equations $\mathbf{g}(\cdot)$. Both functions depend on time t, state vector $\boldsymbol{x}(t)$ with initial condition $\boldsymbol{x}_0 = \boldsymbol{x}(0)$, input vector $\boldsymbol{u}(t)$, and a constant parameter vector $\boldsymbol{p} \in \mathbb{R}^P$.

The whole model of glucose-insulin-glucagon metabolism in state-space representation can be found in Eqs. (A.1) and (A.2). All states and their initial values for all groups are reported in Table A.1. The model consists of a set of $N = 19$ ODEs, $M = 5$ inputs, and $O = 4$ outputs. The input-output definitions can be found in Section 4.1. The state equations are nonlinearly coupled, but the output equations are linear. Thus, $\mathbf{g}\left(t, \boldsymbol{x}, \boldsymbol{p}\right) = \boldsymbol{C}\boldsymbol{x}$ with $\boldsymbol{C} \in \mathbb{R}^{4\times 19}$. This property will have some implications for the design of the state observer explained in Chapter 6.

To give a general overview of the state trajectories, simulation results are shown in Fig. 5.17 for TNDM, T2DM, and T1DM subjects. The simulation consists of a meal of 75 g glucose at $t = 0$ for the first 15 min for all groups. Hence, the oral glucose amplitude is $5000\,\mathrm{mg\,min^{-1}}$. Inputs $u_{\mathrm{G}}^{\mathrm{iv}}(t)$, $u_{\mathrm{I}}^{\mathrm{sc}}(t)$, and $u_{\mathrm{H}}^{\mathrm{sc}}(t)$ are zero. T2DM receive an insulin bolus at $t = 0$, and T1DM additionally receive their optimal basal insulin. Hence, insulin s.c. signal $u_{\mathrm{I}}^{\mathrm{sc}}(t)$ is zero in TNDM, impulse-shaped with magnitude $11.25\,\mathrm{U\,min^{-1}}$ at $t = 0$ in T2DM, and impulse-shaped with $4.69\,\mathrm{U\,min^{-1}}$ at $t = 0$ plus a constant basal insulin dose of $19.73\,\mathrm{mU\,min^{-1}}$ for $-1 \leq t \leq 12\,\mathrm{h}$ in T1DM (see MTT scenario on

page 81). Hence, the same explanations for plasma glucose, s.c. glucose, plasma insulin, and plasma glucagon signals hold. The input and output signals and state trajectories are shown in Fig. 5.17.

The first two states $Q_{\mathrm{Gas},1}(t)$, $Q_{\mathrm{Gas},2}(t)$ are linear and describe the amount of glucose in the stomach and intestine, respectively. The trajectories are impulse-shaped but delayed with a low time constant in the first and a high value in the second state. States $G_{\mathrm{P}}(t)$, $G_{\mathrm{T}}(t)$, and $G_{\mathrm{Sc}}(t)$ determine the amount of glucose in plasma, slowly-equilibrating tissues, and the subcutaneous space, respectively. From the first and latter states, glucose concentration can be directly derived as the output signals. The state trajectories have the typical shape, a rise from the basal value after the glucose load, and a decline back to basal, which is delayed and prolonged in diabetic groups. The amount of insulin in plasma, liver, and portal vein are given by the states $I_{\mathrm{P}}(t)$, $I_{\mathrm{L}}(t)$, and $I_{\mathrm{Po}}(t)$, respectively. In TNDM the typical first and second insulin responses are apparent, which are deteriorated in T2DM. In T1DM insulin in the portal vein is zero as no insulin is secreted by the pancreas. Insulin in the other two states is determined by the amount of s.c. administered insulin as seen in states $I_{\mathrm{Sc},1}(t)$ and $I_{\mathrm{Sc},2}(t)$. An insulin injection can be regarded as an impulse input and thus, the typical impulse response of two linear first-order systems is clearly visible. In T2DM the amount of insulin declines back to zero, whereas in T1DM a basal insulin infusion rate is needed to maintain steady-state. Glucagon amount in plasma and s.c. space is denoted by states $H_{\mathrm{P}}(t)$, $H_{\mathrm{Sc},1}(t)$, and $H_{\mathrm{Sc},2}(t)$, respectively. Only in TNDM glucagon secretion rate $S^{\mathrm{s}}_{\mathrm{H}}(t)$ falls in reaction to elevated glucose values. Glucagon in the s.c. site is zero in all groups as no glucagon is given in this setting.

From the state trajectories shown in Fig. 5.17 it is obvious that it is impossible to drive all states by just a meal input. For example, states $H_{\mathrm{Sc},1/2}(t)$ are zero in all groups since no glucagon was administered. Also, states $I_{\mathrm{Sc},1/2}(t)$ are only non-zero in the diabetic groups as they received an insulin bolus. Hence, different input perturbations will affect the states in a variety of ways. Moreover, it can be assumed that it is not possible to determine all states from observation of only a few output signals.

To systematically investigate to which extent input signals influence the states respectively state trajectories can be calculated from output measurements controllability and observability are suitable methodologies well known from control theory (J. Lunze 2014, Ch. 3).

5.2.1 Concept of Controllability

Controllability of a system is a basic property that allows determining to which extent states $\boldsymbol{x}(t)$ can be affected by the input $\boldsymbol{u}(t)$[1]. It is an analytical concept that only depends on the structure of the state equations, i. e., in linear systems on matrices $\boldsymbol{A}$ and $\boldsymbol{B}$. But it is independent of time and input sequence.

An asymptotically stable system is controllable if it is possible to steer it from an arbitrary initial state $\boldsymbol{x}_0$ into an arbitrary final state $\boldsymbol{x}_{\mathrm{f}} = \boldsymbol{x}(T_{\mathrm{f}})$ by an appropriately chosen control input $\boldsymbol{u}_{[0,T_{\mathrm{f}}]}(t)$ within a finite time horizon $0 \leq t \leq T_{\mathrm{f}}$.

[1] The term controllability is used equivalently to the term reachability.

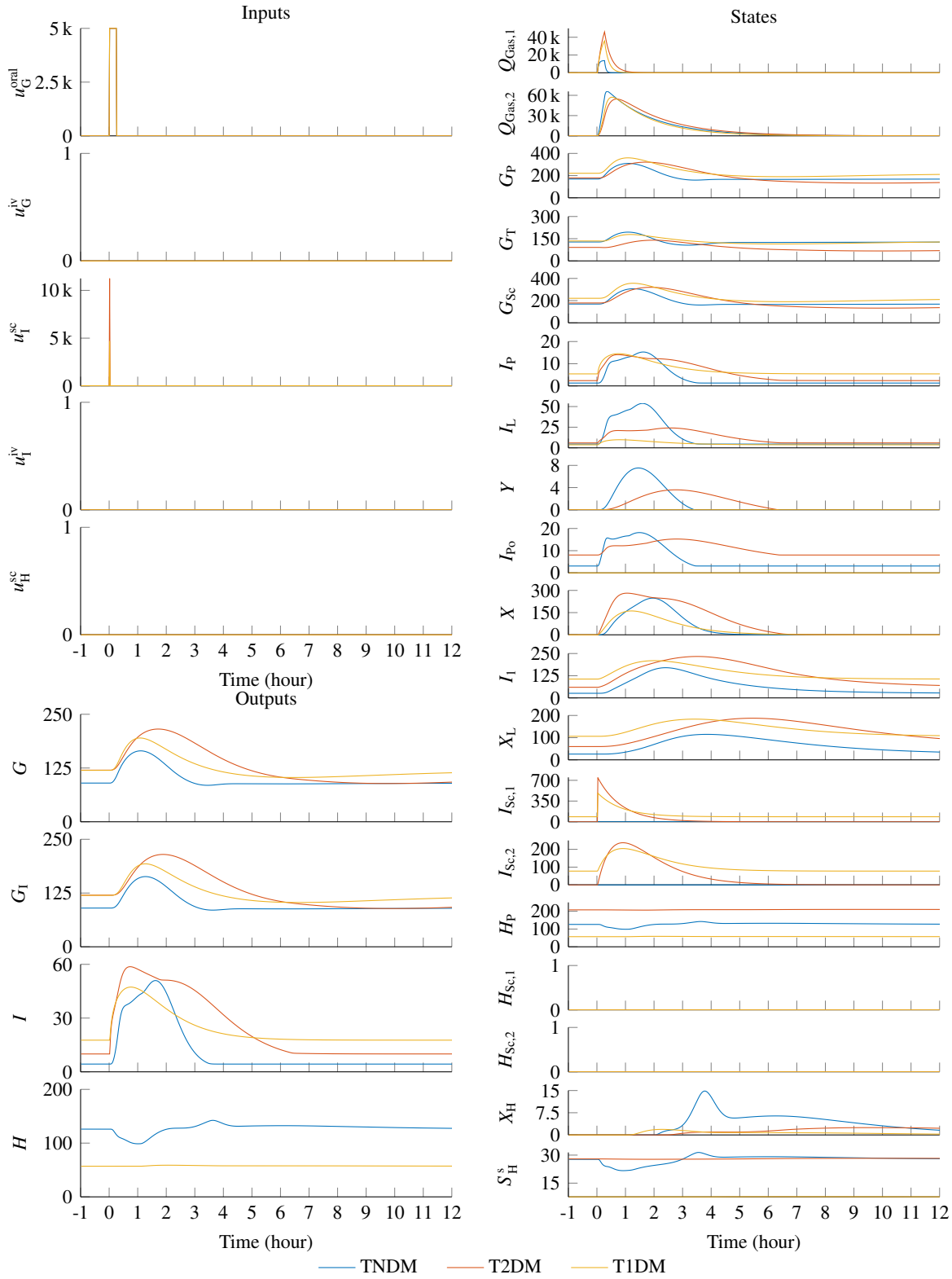

Figure 5.17: Simulation of a meal of 75 g glucose at $t = 0$ for TNDM (blue), T2DM (red), and T1DM (yellow). Left panel shows the input and output signals, right panel state trajectories. Note that variable k is here used as a substitute for 1×10^3.

The general solution of (5.29) is given by

$$\boldsymbol{x}(t) = \boldsymbol{\Phi}(t)\boldsymbol{x}_0 + \int_0^t \boldsymbol{\Phi}(t-\tau)\boldsymbol{B}\boldsymbol{u}(\tau)\,\mathrm{d}\tau, \tag{5.31}$$

with $\boldsymbol{\Phi}(t) = \mathrm{e}^{\mathbf{A}t}$ being the transition matrix. It is sufficient to only consider the movement from the zero state to the final state, thus, without loss of generality $\boldsymbol{x}_0 = \mathbf{0}$. Setting $t = T_\mathrm{f}$ and using the power series of the matrix exponential gives

$$\begin{aligned}\boldsymbol{x}_\mathrm{f} &= \int_0^{T_\mathrm{f}} \boldsymbol{\Phi}(T_\mathrm{f}-\tau)\boldsymbol{B}\boldsymbol{u}(\tau)\,\mathrm{d}\tau,\\ &= \int_0^{T_\mathrm{f}} \sum_{l=0}^{\infty} \boldsymbol{A}^l \frac{(T_\mathrm{f})^l}{l\,!}\boldsymbol{B}\boldsymbol{u}(\tau)\,\mathrm{d}\tau,\\ &= \sum_{l=0}^{\infty} \boldsymbol{A}^l\boldsymbol{B}\hat{\boldsymbol{u}}_l,\end{aligned} \tag{5.32}$$

with

$$\hat{\boldsymbol{u}}_l = \int_0^{T_\mathrm{f}} \frac{(T_\mathrm{f}-\tau)^l}{l\,!}\boldsymbol{u}(\tau)\,\mathrm{d}\tau$$

a constant vector of dimension M. The sum in (5.32) is a linear combination of the columns of $\boldsymbol{B}$, $\boldsymbol{A}\,\boldsymbol{B}$, $\boldsymbol{A}^2\,\boldsymbol{B}, \ldots$. In order to be able to reach any arbitrary point $\boldsymbol{x}_\mathrm{f} \in \mathbb{R}^N$ these column vectors must span the N-dimensional space. If the system is controllable there exists a control sequence

$$\boldsymbol{u}_{[0,T_\mathrm{f}]}(t) = \boldsymbol{B}^\top\,\mathrm{e}^{\mathbf{A}^\top(T_\mathrm{f}-t)}\boldsymbol{W}_\mathrm{C}^{-1}\left(\boldsymbol{x}_\mathrm{f} - \mathrm{e}^{\mathbf{A}T_\mathrm{f}}\boldsymbol{x}_0\right), \tag{5.33}$$

that steers the system from $\boldsymbol{x}_0$ to $\boldsymbol{x}_\mathrm{f}$ for a given final time T_f, where matrix $\boldsymbol{W}_\mathrm{C}$ denotes the controllability Gramian.

Controllability Gramian. In stable linear systems, controllability matrix $\boldsymbol{W}_\mathrm{C}$ can be found by using a linear input-to-state map which represents a generalized energy transfer from inputs to states and is a measure for how well a state can be driven by a perturbation of the inputs. Matrix $\boldsymbol{W}_\mathrm{C}$ is defined as

$$\boldsymbol{W}_\mathrm{C} = \int_0^{T_\mathrm{f}} \mathrm{e}^{\mathbf{A}t}\boldsymbol{B}\boldsymbol{B}^\top\,\mathrm{e}^{\mathbf{A}^\top t}\,\mathrm{d}\tau, \tag{5.34}$$

which is called the finite controllability Gramian. For an infinite time horizon $T_\mathrm{f} = \infty$ this matrix is the smallest semi-positive solution to the Lyapunov equation

$$\boldsymbol{A}\boldsymbol{W}_\mathrm{C} + \boldsymbol{W}_\mathrm{C}\boldsymbol{A}^\top = -\boldsymbol{B}\boldsymbol{B}^\top, \tag{5.35}$$

that is symmetric and positive definite if the system is controllable (Moore 1981; Lall et al. 1999).

There exists an infinite number of control inputs $\boldsymbol{u}_{[0,T_\mathrm{f}]}(t)$ to steer the system from $\boldsymbol{x}_0$ to $\boldsymbol{x}_\mathrm{f}$. However, (5.33) is optimal in terms of the energy required to transition the system within the time interval $[0,\ T_\mathrm{f}]$ as it minimizes the cost functional

$$J\left(\boldsymbol{u}_{[0,T_\mathrm{f}]}\right) = \int_0^{T_\mathrm{f}} \boldsymbol{u}(\tau)^\top \boldsymbol{u}(\tau)\,\mathrm{d}\tau = \boldsymbol{x}_\mathrm{f}^\top \boldsymbol{W}_\mathrm{C}^{-1} \boldsymbol{x}_\mathrm{f}. \tag{5.36}$$

(Antoulas 2005, p. 71). That means states which have a low degree of controllability require more energy to be reached. This is related to small eigenvalues in the controllability Gramian and thus, larger value in its inverse, which also increases amplitudes in the control input $\boldsymbol{u}_{[0,T_\mathrm{f}]}(t)$ in (5.33).

If the system is perturbed from $\boldsymbol{x}_0 = \boldsymbol{0}$ by a series of unit impulses to all inputs $\boldsymbol{u}(t) = \boldsymbol{\delta}(t)$, the solution to the state differential equation is

$$\boldsymbol{x}(t) = \int_0^t \mathrm{e}^{\mathbf{A}(t-\tau)} \boldsymbol{B}\boldsymbol{u}(\tau)\,\mathrm{d}\tau = \mathrm{e}^{\mathbf{A}t}\boldsymbol{B}. \tag{5.37}$$

The generalized energy transfer, E_C, from the inputs into the states can be defined as the sum over the squared states integrated over an infinite time horizon:

$$\begin{aligned} E_\mathrm{C} &= \int_0^\infty \boldsymbol{x}^\top(\tau)\,\boldsymbol{x}(\tau)\,\mathrm{d}\tau, \\ &= \mathrm{Tr}\left(\int_0^\infty \boldsymbol{x}(\tau)\,\boldsymbol{x}^\top(\tau)\,\mathrm{d}\tau\right), \\ &= \mathrm{Tr}\left(\boldsymbol{W}_\mathrm{C}\right), \end{aligned} \tag{5.38}$$

which is the sum over the main diagonal in matrix $\boldsymbol{W}_\mathrm{C}$. Each element $\boldsymbol{W}_{\mathrm{C}_{ii}}$ can be seen as the energy intake into state x_i. The off-diagonal elements define the coupling between states. Analysis of the eigenvalues and associated eigenvectors shows the directions in which the system can be steered easily. It is characterized by large eigenvalues. A state with an eigenvalue of zero cannot be reached. Thus, this state is not controllable. In this case, it could be possible to find a subspace of the original state-space that is still controllable and for which the controllability Gramian is still regular.

Empirical Controllability Gramian. For nonlinear systems, the empirical controllability Gramian is a data-driven extension of the linear system Gramian. For that, extensive numerical simulations can be fulfilled for a given set of input perturbations to excite the system around a nominal trajectory. The Gramian matrix is then systematically computed and averaged over all runs. Note that the empirical Gramian is only valid within a limited region around the chosen trajectory and is not a global approximation. Input perturbations are defined by non-empty sets of directions $\mathcal{E}_u$ of standard unit

vectors, rotations by orthogonal matrices $\mathcal{R}_u$, and positive scalar scale factors $\mathcal{Q}_u$:

$$\begin{aligned}\mathcal{E}_u &= \left\{\boldsymbol{e}_i \in \mathbb{R}^M; \|e_i\| = 1; \boldsymbol{e}_i \boldsymbol{e}_{j\neq i} = 0;\ i = 1, \ldots, M\right\},\\ \mathcal{R}_u &= \left\{\boldsymbol{S}_i \in \mathbb{R}^{M\times M}; \boldsymbol{S}_i^{\top}\boldsymbol{S}_i = \boldsymbol{I};\ i = 1, \ldots, S\right\},\\ \mathcal{Q}_u &= \{c_i \in \mathbb{R}; c_i > 0;\ i = 1, \ldots, Q\},\end{aligned} \tag{5.39}$$

where M is the number of inputs, S the number of desired combined input excitation, and Q the number of scale factors (Himpe and Ohlberger 2013). In general, $\mathcal{R}_u$ would be a full factorial design plan as it combines all possible input excitation. To reduce the computational costs it is often sufficient to simplify the rotations to the positive and negative unit matrix, $\mathcal{R}_u = \{\boldsymbol{I}, -\boldsymbol{I}\}$, as suggested by Lall et al. (1999). Hence, only one input is deflected simultaneously. In the case of the glucose-insulin-glucagon model, the set of rotations is further reduced to only the positive unit matrix $\boldsymbol{I}$ because no negative control signals can be applied to the system. Moreover, certain input combinations at once could lead to unphysiological model behavior, e. g., when glucose is given orally combined with an i.v. injection of glucose or an s.c. administration of glucagon at the same time.

The empirical controllability Gramian $\widehat{\boldsymbol{W}}_{\mathrm{C}}$ can be computed using the non-empty sets $\mathcal{E}_u$, $\mathcal{R}_u$, and $\mathcal{Q}_u$, input signal $\boldsymbol{u}(t)$ around a nominal input trajectory $\bar{\boldsymbol{u}}(t)$, and monitoring the corresponding state trajectory $\bar{\boldsymbol{x}}(\bar{\boldsymbol{u}})$:

$$\begin{aligned}\widehat{\boldsymbol{W}}_{\mathrm{C}} &= \frac{1}{Q\,S}\sum_{h=1}^{Q}\sum_{i=1}^{S}\sum_{j=1}^{M}\frac{1}{c_h^2}\int_0^{T_{\mathrm{f}}}\boldsymbol{\Psi}^{(hij)}(t)\,\mathrm{d}t,\\ \boldsymbol{\Psi}^{(hij)}(t) &= \left(\boldsymbol{x}^{(hij)}(t) - \bar{\boldsymbol{x}}\right)\left(\boldsymbol{x}^{(hij)}(t) - \bar{\boldsymbol{x}}\right)^{\top} \in \mathbb{R}^{N\times N}.\end{aligned} \tag{5.40}$$

Inputs to derive a specific state vector $\boldsymbol{x}^{(hij)}(t)$ are generated by the configuration

$$\boldsymbol{u}^{(hij)}(t) = \bar{\boldsymbol{u}} + c_h\,\boldsymbol{S}_i\,\boldsymbol{e}_j\,\boldsymbol{u}(t). \tag{5.41}$$

Note that the algebraic solution (5.35) is defined with an infinite time horizon. For computational purposes, a final time T_{f} must be chosen that is large enough for all states to reach steady-state.

To assess the empirical controllability Gramian, a suitable nominal trajectory and input excitation must be chosen in order to perturb the system from steady-state. For that, the MTT scenario is selected again. The specific input amplitudes can be found in Section 5.2.6. The resulting empirical Gramians for the three groups are given in (B.1)-(B.3) on page 201. As the matrices are symmetric only the upper right or lower left triangular matrix must be taken into account. The diagonal elements contain the energy intake into the i-th state. Off-diagonal elements with arbitrary values are denoted by $(*)$. When no connection exists between two states the respective element is denoted by zero.

Obviously, no structural connection exists between the gastrointestinal tract (states $x_{1/2}$), insulin in the s.c. space (states $x_{13/14}$), and glucagon in the s.c. space (states $x_{16/17}$). Hence, it is impossible to drive

these states in common when only a single input is excited. Moreover, there is no link between insulin concentration in the s.c. space (states $x_{13/14}$) and its concentration within the portal vein (state x_9). State x_9 is driven by static and dynamic insulin secretion which is only active when glucose is above basal or rising. Hence, as insulin in the s.c. tissue lowers glucose concentration below basal no direct or indirect effect on insulin in the portal vein exists in the model.
A different picture arises when looking at the controllability in T1DM subjects (B.3). The structural interconnections between states are the same as in the other groups, but as parameters related to insulin secretion are assumed to be zero (Table A.2), some connections are virtually broken. This is reflected by several zero elements in the Gramian matrix. In general, states x_8 and x_9, related to the provision of new insulin to the β-cells and the insulin concentration in the portal vein, respectively, are not controllable. Furthermore, insulin concentrations in plasma, $I_\mathrm{P}(t)$ (state x_6), and in the interstitial fluid, $X(t)$ (state x_{10}), are not linked to the gastrointestinal tract.

In TNDM and T2DM, controllability matrices $\widehat{\boldsymbol{W}}_{\mathrm{C_{TNDM}}}$ and $\widehat{\boldsymbol{W}}_{\mathrm{C_{T2DM}}}$ have both full rank, whereas in T1DM, $\operatorname{rank}\left(\widehat{\boldsymbol{W}}_{\mathrm{C_{T1DM}}}\right) = 17$ and thus, the system is not fully controllable.

5.2.2 Concept of Observability

Observability is a second basic property in systems analysis that allows to determine to which extent the outputs of a system can be driven by the states. In most systems not all state variables are measurable and thus, the question arises, if it is possible to compute the current state $\boldsymbol{x}(t)$ from the output vector $\boldsymbol{y}(t)$. Typically, the dimension of the output vector is smaller than the dimension of the state vector ($O < N$). From this, there could exist several possible combinations of states that all produce the same output. However, a state can be determined by observing the motion of the system not only at a certain time point but over a time interval and reconstructing the current system state from the trajectory $\boldsymbol{y}(t)$ for $0 \leq t \leq T_\mathrm{f}$ using the model. If the system is additionally driven by an external input $\boldsymbol{u}(t)$, it is necessary to incorporate it into state reconstruction. A system is called observable if the state can be determined in this way (J. Lunze 2014, Ch. 3.2). As for the concept of controllability, observability is a structural property of the underlying system and depends only on matrices $\boldsymbol{A}$ and $\boldsymbol{C}$ in linear systems.

From the equation of motion,

$$\boldsymbol{y}(t) = \underbrace{\boldsymbol{C}\,\mathrm{e}^{\mathbf{A}t}\boldsymbol{x}_0}_{\boldsymbol{y}_\mathrm{free}(t)} + \int_0^t \boldsymbol{C}\mathrm{e}^{\boldsymbol{A}(t-\tau)}\boldsymbol{B}\boldsymbol{u}(\tau)\,\mathrm{d}\tau, \tag{5.42}$$

it can be seen that the initial state $\boldsymbol{x}_0$ only affects the free motion $\boldsymbol{y}_\mathrm{free}(t)$. To solve the observability problem, only the undisturbed system without additional inputs must taken into account. If it is observable, the disturbed system is also observable.

Observability Gramian. The observability Gramian $\boldsymbol{W}_{\mathrm{O}}$ can be derived by the state-to-output map which represents the generalized energy transfer from states into outputs and quantifies how well a change in a state can be measured by the outputs. It is defined as

$$\boldsymbol{W}_{\mathrm{O}} = \int_0^{T_{\mathrm{f}}} \mathrm{e}^{\mathbf{A}^\top \tau} \boldsymbol{C}^\top \boldsymbol{C}\, \mathrm{e}^{\mathbf{A}\tau}\, \mathrm{d}\tau, \tag{5.43}$$

for an arbitrary finite time $T_{\mathrm{f}} < \infty$ (Antoulas 2005, p. 76). If the system is observable, this matrix is positive definite and thus, invertible. The initial state can then be derived by

$$\boldsymbol{x}_0 = \boldsymbol{W}_{\mathrm{O}}^{-1} \int_0^{T_{\mathrm{f}}} \mathrm{e}^{\mathbf{A}^\top \tau} \boldsymbol{C}^\top \boldsymbol{y}_{\mathrm{free}}(\tau)\, \mathrm{d}\tau. \tag{5.44}$$

For an infinite horizon $T_{\mathrm{f}} = \infty$, $\boldsymbol{W}_{\mathrm{O}}$ is the smallest semi-positive solution to the Lyapunov equation

$$\boldsymbol{A}^\top \boldsymbol{W}_{\mathrm{O}} + \boldsymbol{W}_{\mathrm{O}} \boldsymbol{A} = -\boldsymbol{C}^\top \boldsymbol{C} \tag{5.45}$$

(Lall et al. 1999). A system is said to be observable if $\boldsymbol{W}_{\mathrm{O}} > 0$ and (5.45) has a unique solution.

The generalized energy transfer, E_{O}, from the states into the outputs can be defined by the sum over the squared outputs integrated over an infinite time horizon $T_{\mathrm{f}} \to \infty$:

$$\begin{aligned} E_{\mathrm{O}} &= \int_0^{T_{\mathrm{f}}} \boldsymbol{y}^\top(\tau)\, \boldsymbol{y}(\tau)\, \mathrm{d}\tau, \\ &= \boldsymbol{x}_0^\top \int_0^{T_{\mathrm{f}}} \mathrm{e}^{\mathbf{A}^\top \tau} \boldsymbol{C}^\top \boldsymbol{C}\, \mathrm{e}^{\mathbf{A}\tau}\, \mathrm{d}\tau\, \boldsymbol{x}_0, \\ &= \boldsymbol{x}_0^\top \boldsymbol{W}_{\mathrm{O}}\, \boldsymbol{x}_0, \end{aligned} \tag{5.46}$$

where the main diagonal element $\boldsymbol{W}_{\mathrm{O}_{ii}}$ is a metric for the energy transfer from state x_i into the outputs when the system freely evolves towards steady-state. Likewise controllability Gramian, elements with $\boldsymbol{W}_{\mathrm{O}_{ii}} = 0$ cannot be observed. Off-diagonal components denote interconnections between states. Furthermore, if states are not observable one can still find a subspace of the original state-space for which the observability Gramian is still regular.

Empirical Observability Gramian. The empirical observability Gramian is calculated by systematically perturbing the initial states around steady-state and observing the output trajectory $\boldsymbol{y}(t)$ for each numerical experiment. State perturbations are defined by non-empty sets of directions of standard unit vectors $\mathcal{E}_x$, rotations by orthogonal matrices $\mathcal{R}_x$, and positive scale factors $\mathcal{Q}_x$:

$$\begin{aligned} \mathcal{E}_x &= \left\{ \boldsymbol{f}_i \in \mathbb{R}^N; \|f_i\| = 1; \boldsymbol{f}_i \boldsymbol{f}_{j\neq i} = 0;\ i = 1, \ldots, N \right\}, \\ \mathcal{R}_x &= \left\{ \boldsymbol{T}_i \in \mathbb{R}^{N\times N}; \boldsymbol{T}_i^\top \boldsymbol{T}_i = \boldsymbol{I};\ i = 1, \ldots, T \right\}, \\ \mathcal{Q}_x &= \{ d_i \in \mathbb{R}; d_i > 0;\ i = 1, \ldots, R \}, \end{aligned} \tag{5.47}$$

where N is the number of states, T is the number of desired state excitation, and R is the number of scale factors (Himpe and Ohlberger 2014). The Gramian matrix can then be computed and averaged over all runs. Some initial states are zero and cannot be perturbed in a negative range. Thus, rotation matrices $\boldsymbol{T}_i$ reduce to the unit matrix $\boldsymbol{I}$, and only one state is excited at a time.

The empirical observability matrix $\widehat{\boldsymbol{W}}_{\mathrm{O}}$ can be obtained using the non-empty perturbation sets $\mathcal{E}_x$, $\mathcal{R}_x$, and $\mathcal{Q}_x$ around a nominal state $\bar{\boldsymbol{x}}$ and monitoring the output $\bar{\boldsymbol{y}}(\bar{\boldsymbol{x}})$:

$$\begin{aligned} \widehat{\boldsymbol{W}}_{\mathrm{O}} &= \frac{1}{RT} \sum_{u=1}^{R} \sum_{v=1}^{T} \frac{1}{d_u^2} \boldsymbol{T}_v \int_0^{T_\mathrm{f}} \boldsymbol{\Psi}^{(uv)}(t)\, \mathrm{d}t\, \boldsymbol{T}_v^\top, \\ \boldsymbol{\Psi}_{ab}^{(uv)}(t) &= \left(\boldsymbol{y}^{(uva)}(t) - \bar{\boldsymbol{y}}\right)^\top \left(\boldsymbol{y}^{(uvb)}(t) - \bar{\boldsymbol{y}}\right), \end{aligned} \tag{5.48}$$

where $\boldsymbol{y}^{(uva)}(t)$ is the system output for the initial state configuration

$$\boldsymbol{x}_0^{(uva)} = \bar{\boldsymbol{x}} + d_u \boldsymbol{T}_v \boldsymbol{f}_a, \tag{5.49}$$

and $\bar{\boldsymbol{y}}$ may be the average or steady-state output. Note that the final time T_f must be chosen large enough for all states to return to steady-state.

To obtain the empirical observability Gramian, a suitable state configuration has to be found. For that, the MTT scenario is selected again. Specific input perturbations can be found in Section 5.2.6. The resulting empirical Gramians for all three groups are reported in (B.4)-(B.6) on page 202. Only the diagonal elements and states which are not observable are shown. Off-diagonal elements with arbitrary values are denoted by $(*)$. In TNDM and T2DM all states are observable, whereas in T1DM states x_8 and x_9, the insulin action on glucose changes, $Y(t)$, and insulin in the portal vein, $I_{\mathrm{Po}}(t)$, respectively, are not observable. Any induced changes in these states cannot influence the rest of the system as their related parameters α and γ are zero, and no motion exists in these states. Hence, $\operatorname{rank}\left(\widehat{\boldsymbol{W}}_{\mathrm{O}_{\mathrm{T1DM}}}\right) = 17$.

5.2.3 Controllable and Observable Subspace

From the Gramian matrices given in (B.1)-(B.6), it can be seen that in T1DM two states are neither controllable nor observable. In linear systems written in Jordan canonical form, this usually occurs if the i-th row in the input matrix $\boldsymbol{B}$ or the i-th column in the output matrix $\boldsymbol{C}$ are null vectors. This means the input $\boldsymbol{u}$ does not drive state x_i respectively the state x_i is not connected to the output. Hence, the motion of this affected state cannot be controlled or observed and this part of the system is structurally neither controllable nor observable.

In the nonlinear model investigated here, this is not the case. Although there exist null vectors in input and output matrices (Section A) the motion of the corresponding states itself is nonexistent as their related parameters are zero and thus, these states remain zero over time. Hence, controllability and observability mainly depend on the concrete parameter configuration.

In general, the motion of $\boldsymbol{x}(t)$ can be dissected into a part that is controllable/observable and into a part that is not controllable/not observable:

$$\boldsymbol{x}(t) = \boldsymbol{x}_{\text{cntr}}(t) + \boldsymbol{x}_{\widetilde{\text{cntr}}}(t), \qquad \boldsymbol{x}(t) = \boldsymbol{x}_{\text{obsv}}(t) + \boldsymbol{x}_{\widetilde{\text{obsv}}}(t).$$

It is also possible to decompose the Gramian matrices $\boldsymbol{W}_{\text{C}}$ and $\boldsymbol{W}_{\text{O}}$ as

$$\boldsymbol{W}_{\text{C}} = \left[\begin{array}{c|c} \boldsymbol{W}_{\text{C}_{\text{cntr}}} & \boldsymbol{0} \\ \hline \boldsymbol{0} & \boldsymbol{0} \end{array}\right], \qquad \boldsymbol{W}_{\text{O}} = \left[\begin{array}{c|c} \boldsymbol{W}_{\text{O}_{\text{obsv}}} & \boldsymbol{0} \\ \hline \boldsymbol{0} & \boldsymbol{0} \end{array}\right], \tag{5.50}$$

that means, in an upper left sub-matrix of controllable states, $\boldsymbol{W}_{\text{C}_{\text{cntr}}}$, with $\mathbb{R}^{\text{cntr}} \subseteq \mathbb{R}^N$ and the null space respectively a sub-matrix of observable states, $\boldsymbol{W}_{\text{O}_{\text{obsv}}}$, with $\mathbb{R}^{\text{obsv}} \subseteq \mathbb{R}^N$ in matrix $\boldsymbol{W}_{\text{O}}$.

5.2.4 Extension to Parameters

In Sections 5.2.1 and 5.2.2, the concept of controllability and observability of states was introduced. As a measure for the generalized energy transfer from the inputs into the outputs empirical controllability and observability Gramians were defined that can be determined based on extensive numerical computations. The concept of observability can be extended to the parameters of the system. For that, the identifiability Gramian matrix can be defined for the augmented system $\widehat{\Sigma}$ given by

$$\widehat{\Sigma}: \begin{cases} \dot{\hat{\boldsymbol{x}}} = \begin{bmatrix} \dot{\boldsymbol{x}} \\ \dot{\boldsymbol{p}} \end{bmatrix} = \begin{bmatrix} \mathbf{f}(t, \boldsymbol{x}, \boldsymbol{u}, \boldsymbol{p}) \\ \boldsymbol{0} \end{bmatrix}, \quad \hat{\boldsymbol{x}}_0 = \begin{bmatrix} \boldsymbol{x}_0 \\ \boldsymbol{p} \end{bmatrix}, \\ \boldsymbol{y} = \mathbf{g}(t, \boldsymbol{x}, \boldsymbol{p}), \end{cases} \tag{5.51}$$

with $\boldsymbol{x}(t) \in \mathbb{R}^N$ and $\boldsymbol{p} \in \mathbb{R}^P$. Thus, $\hat{\boldsymbol{x}}(t)$ has the dimension $N + P = \hat{N}$. In the augmented system, parameters are treated as constant states that are appended to the prior state vector. Their derivative $\dot{\boldsymbol{p}}(t)$ is therefore zero.

Identifiability Gramian. The concept of identifiability can be regarded as an observability-based parameter investigation. This approach is about observing the system's parameters of the augmented system (5.51) as stated in Geffen et al. (2008).

The augmented observability Gramian $\boldsymbol{W}_{\text{O}}^{\star}$ can be computed following Section 5.2.2, where the perturbation of states must be appended by a suitable parameter excitation. The matrix has the following block structure:

$$\boldsymbol{W}_{\text{O}}^{\star} = \left[\begin{array}{c|c} \boldsymbol{W}_{\text{O}} & \boldsymbol{W}_{\text{OP}} \\ \hline \boldsymbol{W}_{\text{PO}} & \boldsymbol{W}_{\text{P}} \end{array}\right] \in \mathbb{R}^{\hat{N} \times \hat{N}}. \tag{5.52}$$

The upper left block contains the state observability Gramian matrix $\boldsymbol{W}_{\mathrm{O}}$, the lower right sub-matrix contains the parameter-space observability information, and $\boldsymbol{W}_{\mathrm{PO}} = \boldsymbol{W}_{\mathrm{OP}}^{\top}$ is a mixed state and parameter block. The Gramian identifiability matrix $\boldsymbol{W}_{\mathrm{I}}$ can then be extracted via the Schur complement (Carlson 1986) for the lower right block:

$$\boldsymbol{W}_{\mathrm{I}} = \boldsymbol{W}_{\mathrm{P}} - \boldsymbol{W}_{\mathrm{PO}} \boldsymbol{W}_{\mathrm{O}}^{-1} \boldsymbol{W}_{\mathrm{OP}}, \tag{5.53}$$

allowing to isolate the parameter identifiability information (Geffen et al. 2008). The matrix has full rank if all parameters are identifiable, whereas null elements point to non-observable factors.

5.2.5 A Priori and a Posteriori Observability

The eigenvalues of the Gramian, $\lambda(\boldsymbol{W})$, determine the degree of observability of the system, where lower values quantify a weaker energy transfer into the outputs. Particularly, an eigenvalue of zero indicates a state that can be considered structurally (*a priori*) not observable. Structural observability provides information on if it would be possible at least in principle to observe certain states, which depends on the system formulation and includes the stimuli, dynamic equations, and the measured outputs. Often, structural observable states or parameters cannot be practically determined with precision, e. g., due to a lack of available observations, measurement errors, or interdependencies among states. If only because of the dimensionality reduction between states and outputs, it will not be possible to estimate all states from the measurement of a smaller number of outputs. Interdependence among states and parameters describes that the effects of changes in one component are being compensated by changes in other components and thus, both parts cannot be identified separately. Practical (*a posteriori*) observability tries to take into account at least some of these limitations.

5.2.6 Setup of Numerical Experiments

The experimental setup follows the definitions and considerations given in Section 5.1.1 for the global sensitivity analysis. Here, only the steady-state scenario (STS) and the meal tolerance test (MTT) are fulfilled. Moreover, as s.c. glucose concentration is the main measurement quantity, the experimental setup and results are shown for model output G_{I}. However, the entire procedure can also be carried out for all other outputs like insulin concentration. Given the model in state-space representation (A.1)-(A.2), output matrix $\boldsymbol{C}$ becomes the row vector

$$\boldsymbol{C} = \begin{bmatrix} 0 & 0 & 0 & 0 & \frac{1}{V_{\mathrm{G}}} & 0 & 0 & 0 & 0 & 0 & 0 & 0 & 0 & 0 & 0 & 0 & 0 & 0 \end{bmatrix}, \quad y(t) \in \mathbb{R}^1,$$

with $y(t) = \frac{1}{V_{\mathrm{G}}} x_5(t) = G_{\mathrm{I}}(t) = \frac{1}{V_{\mathrm{G}}} G_{\mathrm{Sc}}(t)$. The Gramians have been calculated using the *emgr* framework presented in Himpe (2018) and Himpe (2020b).

For controllability analysis, the following settings are defined: The nominal input function for TNDM and T2DM is $\bar{\boldsymbol{u}}(t) = \boldsymbol{0}$, i. e., no steady-state input exists. For T1DM, the steady-state input is

$\bar{\boldsymbol{u}}(t) = \left[0, 0, 0, u_{\mathrm{I}}^{\mathrm{sc}}(t), 0\right]^{\mathrm{T}}$ with $u_{\mathrm{I}}^{\mathrm{sc}}(t) = 19.73\,\mathrm{mU\,min^{-1}}$, that means, a constant subcutaneous insulin infusion. The perturbation function for each input j is $u_j(t) = \delta(t)$, which is an impulse at $t = 0$ with a magnitude of $\left[10\,\mathrm{g}, 0.3\,\mathrm{g\,kg^{-1}\,min^{-1}}, 5\,\mathrm{U\,min^{-1}}, 30\,\mathrm{mU\,kg^{-1}\,min^{-1}}, 100\,\mathrm{ng\,kg^{-1}\,min^{-1}}\right]^{\mathrm{T}}$. The impulse amplitudes are equally spaced from 25 % to 100 % of the reported values, hence, $Q = 4$. As only one input at a time is perturbed, rotations $\boldsymbol{S}_i$ reduce to positive unit matrices, hence $S = 1$. With $M = 5$ different inputs, a total of $Q \cdot S \cdot M = 20$ simulations have to be fulfilled. In the MTT scenario, a meal bolus of 75 g is given orally, and diabetic subjects receive their suitable insulin boluses. The computational time for all runs was 2 s in each scenario.

For investigating observability, the following settings are defined: The nominal state $\bar{\boldsymbol{x}}$ is set to the typical initial state $\boldsymbol{x}_0$ for each group (Table A.1). Scale factors d_i around the nominal state are set to 25 %, 50 %, 75 %, and 100 % of half of the nominal values, hence $R = 4$. For initial states being zero, the following scales are chosen: $x_1 = 10\,000$, $x_2 = 30\,000$, $x_8 = 7.5$, $x_{10} = 250$, $x_{13} = 700$, $x_{14} = 250$, $x_{16} = 1 \times 10^{-3}$, $x_{17} = 1 \times 10^{-3}$, $x_{18} = 15$ to account for typical physiological excursions in every individual state. As only one input at a time is perturbed, rotation $\boldsymbol{T}_i$ reduces to a positive unit matrix, hence $T = 1$. With $N = 19$ states, a total of $R \cdot T \cdot N = 76$ simulations have to be fulfilled. In the MTT scenario, a meal bolus of 75 g is given orally, and diabetic subjects receive their suitable insulin boluses. The computational time for all runs was 1.7 s in each scenario.

After derivation of the Gramian matrices, a metric to assess practical observability respectively identifiability must be defined. Therefore, the observability of dynamical states of system (5.30) respectively the identifiability of constant states of the augmented system (5.51) are now summarized under the name observability and the Gramian is denoted by $\boldsymbol{W}$. Controllability will not be discussed further as it is not needed for the subsequent identification and estimation procedures. An iterative state selection algorithm presented in Eberle et al. (2012a) is used. It requires a positive definite Gramian and thus, all states must be structurally observable. If this is not the case the algorithm can be applied to the observable sub-matrix of $\boldsymbol{W}$ where the non-observable states are excluded. Practical observability is hereby defined by the smallest eigenvalue $\underline{\lambda}$ of a set of states for which observability should be determined and characterizes the allowed least amount of energy transfer. To find out which combinations of states satisfy this condition a set $\mathcal{E}$ is defined. Beginning with state $x_i \in \mathcal{E}$, the smallest eigenvalue $\underline{\lambda}$ is derived from Gramian $\boldsymbol{W}_{ii}$. That means all rows and columns of $\boldsymbol{W}$ have been deleted, except for the i-th. A second state or parameter may be added to the set $\mathcal{E}$ and the smallest eigenvalue of the Gramian submatrix $\boldsymbol{W}_{\mathcal{E}}$ is determined again. If the result is still satisfactory with $\underline{\lambda} > \varepsilon$, this procedure can be iteratively continued until the condition fails or all relevant states and parameters are contained in the set (Algorithm 2).

Moreover, a full factorial design plan can be passed through in order to derive information on all possible state and parameter combinations. Thus, the eigenvalues of each corresponding Gramian sub-matrix have to be calculated, leading to 2^{N-1} respectively $2^{\hat{N}-1}$ eigenvalue decompositions, with N and $\hat{N}$ the number of states in the regular respectively in the augmented system. This analysis could also be helpful to determine the largest set of states and parameters that is practically observable.

Algorithm 2 Iterative state and parameter selection

Require: Gramian $\boldsymbol{W}$
Ensure: $\boldsymbol{W} > 0$
  Initialize $\mathcal{E} = \varnothing$
  while not all relevent states in $\mathcal{E}$ **do**
    Add next most relevant state to set: $x_i \in \mathcal{E}$
    Determine $\boldsymbol{W}_{\mathcal{E}}$
    Calculate smallest eigenvalue $\underline{\lambda}(\boldsymbol{W}_{\mathcal{E}})$
    if $\underline{\lambda} \leq \varepsilon$ **then**
      Remove current state
    end if
  end while
  Design completed

To make the computation of the eigenvalues numerically more stable the system states can be scaled in such a way that the diagonal elements of the Gramian are equal to one. This can be done by computing the matrix twice. In a first run, diagonal elements in $\boldsymbol{W}$ can be used to determine the transformation

$$\boldsymbol{x}_S := \sqrt{\operatorname{diag}(\boldsymbol{W})}, \quad \boldsymbol{V} = \operatorname{diag}^{-1}(\boldsymbol{x}_S), \tag{5.54}$$

that rotates the states into a new basis $\tilde{\boldsymbol{x}} = \boldsymbol{V}\boldsymbol{x}$ (Eberle et al. 2012a), with $\boldsymbol{V}$ being invertible. The scaled system $\widetilde{\Sigma}$ is then given by

$$\widetilde{\Sigma}: \begin{cases} \dot{\tilde{\boldsymbol{x}}} = \boldsymbol{V}\mathbf{f}\left(t, \boldsymbol{V}^{-1}\tilde{\boldsymbol{x}}, \boldsymbol{u}, \boldsymbol{p}\right), \\ \tilde{\boldsymbol{y}} = \mathbf{g}\left(t, \boldsymbol{V}^{-1}\tilde{\boldsymbol{x}}, \boldsymbol{p}\right). \end{cases} \tag{5.55}$$

The transformation will alter the physical meaning of the states but not the input-output properties. The second run will then be fulfilled using the scaled system (5.55) which yields a Gramian with diagonal elements equal to one. The total energy transfer is then the sum over all diagonal elements $\boldsymbol{W}_{ii}$, that is equal to the number of states N respectively $\hat{N}$. Moreover, since the transformation is linear it is always possible to switch between both state representations.

5.2.7 Results and Discussion

The following section presents the results of state observability and parameter identifiability for steady-state and mixed-meal scenarios in TNDM, T2DM, and T1DM subjects.

State Observability. All scenarios and all state excitations generated stable system responses. Each state was subsequently perturbed one at a time and the output signal $G_{\mathrm{I}}(t)$ was recorded. The resulting 76 different trajectories for each group are depicted in Fig. 5.18 for the steady-state scenario and in Fig. 5.19 for the MTT scenario.

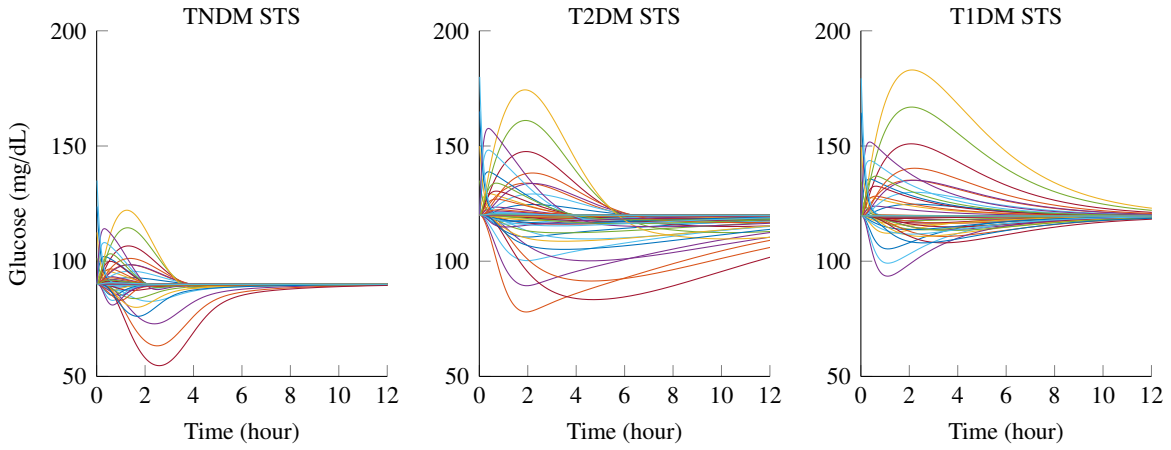

Figure 5.18: Output trajectories after subsequent single state perturbations from steady-state derived by observability analysis for TNDM (left panel), T2DM (middle), and T1DM (right). No inputs were applied to the system, except the steady-state basal insulin infusion in T1DM.

Comparing the time courses between the groups reveals a much faster dynamic in TNDM. The steady-state glucose concentration is determined by parameter $G_{\mathrm{P}}^{\mathrm{b}}$ and is lower in TNDM. Steady-state is reached after 8 h in TNDM, whereas in T2DM and T1DM it is not completely reached within simulation time. Thus, an extended final time needs to be necessary for these groups. A test case with a simulation time of 24 h did not alter the resulting Gramian matrices significantly, so the original interval of 12 h is retained. The higher output amplitudes can be explained by: first, larger state perturbations, as they depend on the initial state which is higher in the diabetic groups; and second, by the fact that no insulin bolus was given. Particularly, an excitation of states $Q_{\mathrm{Gas},1/2}(t)$ $(x_{1/2})$, the glucose amount in the gastrointestinal tract, can be interpreted as a meal. Without additional insulin bolus, diabetic groups suffer from a prolonged hyperglycemic excursion. In the MTT scenario (Fig. 5.19), the free movement of the system is superimposed by the forced response due to the given inputs. Within the first half hour after the start of the simulation, a movement towards the stationary value is visible. After that, the glucose load takes effect and the system trajectories are located around the nominal meal response signal. As the input value is the same in all runs deviations from the nominal trajectory are induced by the different initial state configurations. The major variation in all groups takes place when glucose concentration reaches its maximum. With ongoing simulation time, variations are minimized until steady-state is reached.

The associated observability Gramian was computed twice using (5.54) to scale the system properly, hence, all diagonal elements $\boldsymbol{W}_{\mathrm{O}_{ii}}$ are equal to one. The resulting scaled eigenvalues for each group are depicted in Fig. 5.20 and Fig. B.7 for the STS respectively MTT scenario. As can be seen, the eigenvalues decrease exponentially from 10^0 down to $\mathcal{O}\left(10^{-8}\right)$ for TNDM, respectively $\mathcal{O}\left(10^{-11}\right)$ for the diabetic groups. Note that in T1DM two states are not observable and hence, observability was determined for only the observable subspace in $\mathbb{R}^{17}$. The eigenvalues of the remaining non-observable states are zero. The decline of the eigenvalues in TNDM is slightly flatter, suggesting overall better state observability as in the diabetic cases. The progression of the eigenvalues in the MTT scenario is

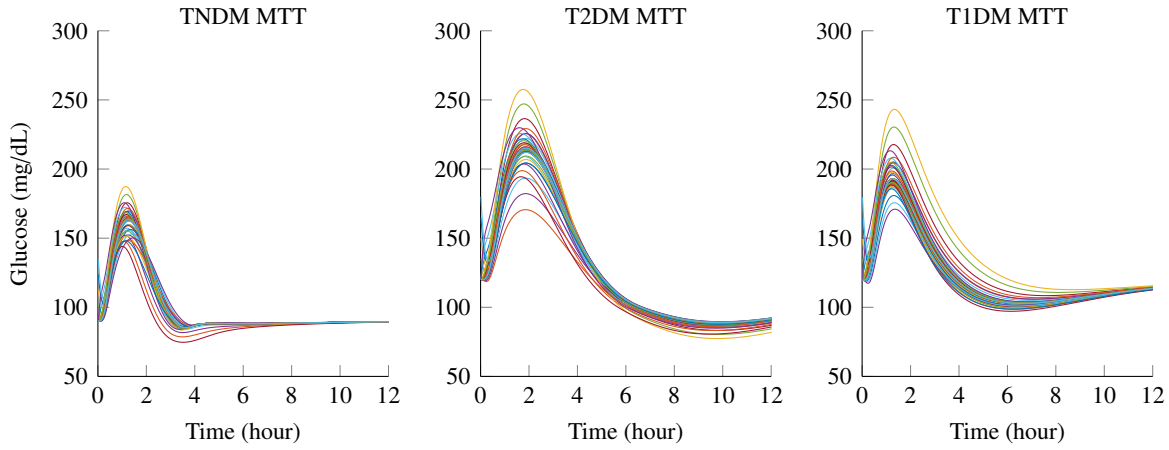

Figure 5.19: Output trajectories after subsequent single state perturbations from steady-state derived by observability analysis for TNDM (left panel), T2DM (middle), and T1DM (right). Inputs as defined for the MTT scenario were applied to the system.

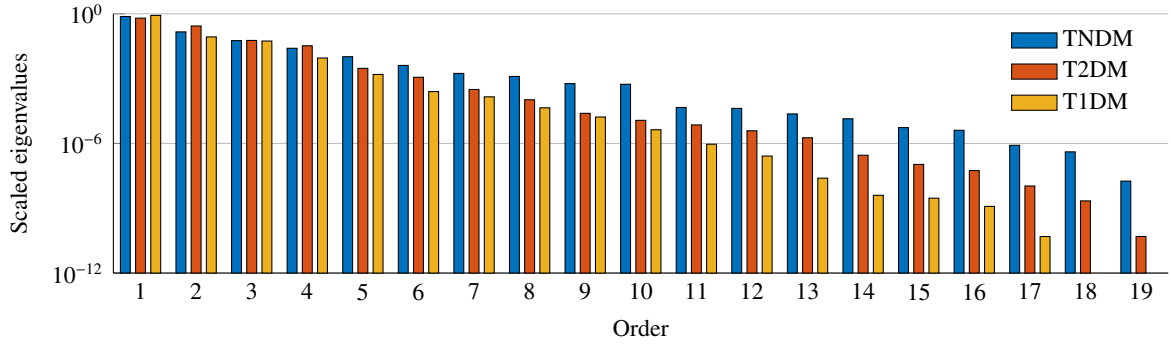

Figure 5.20: Scaled eigenvalues of observability Gramian $\boldsymbol{W}_{\mathrm{O}}$ in the STS scenario for TNDM (blue), T2DM (red), and T1DM (yellow) subjects.

comparable to the STS setting shown here but indicates overall better observability as their values are about an order of magnitude higher. Furthermore, eigenvalues for T2DM are closer to TNDM, suggesting improved observability in this group and for this scenario.

To quantify the joint observability of states, the procedure following Algorithm 2 is executed for several state combinations for TNDM, T2DM, and T1DM subjects and the two scenarios (Table 5.3). A threshold of $\underline{\lambda} > \epsilon = 0.1$ has been chosen for practical observability, which has turned out to be a good choice for state observability in glucose-insulin models (Eberle et al. 2012a).
Since the diagonal elements in $\boldsymbol{W}$ are equal to one, the decomposition of a single state Gramian sub-matrix will result in an eigenvalue of one in both scenarios (cases (a) and (b) stand exemplarily for all single state observations). One major aim is to prove if it is possible to observe the substance concentrations of glucose, insulin, and glucagon in plasma, from the measurement of only $G_{\mathrm{I}}(t)$.
Cases (c) and (d) present the observation of plasma glucose, $G_{\mathrm{P}}(t)$, in combination with plasma insulin, $I_{\mathrm{P}}(t)$, respectively plasma glucagon concentration, $H(t)$. Case (c) is observable as the corresponding eigenvalue is larger than the threshold. Case (d) reveals that glucagon cannot be observed as its

Table 5.3: Observability defined by the smallest eigenvalue $\underline{\lambda}(\boldsymbol{W}_{O_\varepsilon})$ for a set of states in $\mathcal{E}$ computed from Gramians in steady-state (STS) and the mixed-meal (MTT) scenario for TNDM, T2DM, and T1DM.

		STS			MTT		
Case	**Set $\mathcal{E}$ of states to be observed**	**TNDM** $\underline{\lambda}(\boldsymbol{W}_{O_\varepsilon})$	**T2DM** $\underline{\lambda}(\boldsymbol{W}_{O_\varepsilon})$	**T1DM** $\underline{\lambda}(\boldsymbol{W}_{O_\varepsilon})$	**TNDM** $\underline{\lambda}(\boldsymbol{W}_{O_\varepsilon})$	**T2DM** $\underline{\lambda}(\boldsymbol{W}_{O_\varepsilon})$	**T1DM** $\underline{\lambda}(\boldsymbol{W}_{O_\varepsilon})$
(a)	$[G_P]$	1.0000	1.0000	1.0000	1.0000	1.0000	1.0000
(b)	$[I_P]$	1.0000	1.0000	1.0000	1.0000	1.0001	1.0000
(c)	$[G_P, I_P]$	0.1704	0.6780	0.1323	0.2487	0.2385	0.2061
(d)	$[G_P, H]$	0.0615	0.0581	0.0450	0.0385	0.0579	0.0687
(e)	$[G_P, I_P, H]$	0.0286	0.0540	0.0184	0.0351	0.0440	0.0307
(f)	$[G_P, G_{Sc}]$	0.6160	0.7104	0.7301	0.6502	0.6975	0.6689
(g)	$[G_P, G_{Sc}, I_P]$	0.1169	0.5789	0.0988	0.1892	0.1995	0.1523
(h)	$[G_{Sc}, I_P]$	0.9118	0.9755	0.9723	0.9509	0.9408	0.9634
(i)	$[G_P, Q_{Gas,2}]$	0.3618	0.2964	0.1806	0.2311	0.2966	0.2700
(j)	$[Q_{Gas,1}, Q_{Gas,2}]$	0.0073	0.0144	0.0018	0.0043	0.0203	0.0032
(k)	$[I_{Sc,1}, I_{Sc,2}]$	0.1272	0.0112	0.0228	0.1004	0.0814	0.0296
(l)	$[H_{Sc,1}, H_{Sc,2}]$	0.0145	0.0047	0.0030	0.0338	0.5261	0.0051
(m)	$[G_P, I_P, Q_{Gas,2}]$	0.2839	0.2516	0.1465	0.1901	0.2513	0.2141
(n)	$[G_P, Y]$	0.1967	0.7127	0.0000	0.5503	0.6384	0.0000
(o)	$[G_P, G_{Sc}, I_1, H_{Sc,1}]$	0.1514	0.2194	0.0780	0.3561	0.4898	0.1303

eigenvalue is around one order of magnitude lower than necessary. Thus, it will not be possible to observe all three substances at the same time as shown in case (e).

Cases (f)–(h) show state combinations including observation of s.c. glucose. As $G_{Sc}(t)$ is directly proportional to the measured output $G_I(t)$, the smallest eigenvalue does not decrease significantly (compare, e. g., cases (c) and (g)). Furthermore, a comparison between the scenarios in cases (c) and (g) shows a slightly higher smallest eigenvalue in TNDM and a lower one in T2DM for the MTT scenario. Since the eigenvalues in the other test cases do not differ significantly between the two scenarios, the observability of insulin seems to depend on the test scenario and should be kept in mind when it comes to state estimation in practice.

Cases (i) and (j) take into account glucose amount in the gastrointestinal tract which could be useful for a meal recognition system. The smallest eigenvalue shows that a simultaneous observation of $G_P(t)$ and $Q_{Gas,2}(t)$ would be possible. A combined observation of $Q_{Gas,1}(t)$ and $Q_{Gas,2}(t)$ is not applicable, neither for the steady-state nor the MTT scenario. That makes sense as both states are connected in series and thus, one is not able to distinguish between the two, when only measuring the output of this chain. The same behavior can be noticed in cases (k) and (l). The chains of s.c. insulin, $I_{Sc,1/2}(t)$, and s.c. glucagon, $H_{Sc,1/2}(t)$ can not be uniquely distinguished (except in case (k), where it is fairly possible for TNDM). Case (m) is an extension of case (i) that shows observability for glucose and insulin in plasma, simultaneously with $Q_{Gas,2}(t)$.

Case (n) reveals that it is also possible to estimate $G_P(t)$ and the provision of new insulin, $Y(t)$, in TNDM and T2DM. As $Y(t)$ can be seen as a kind of control signal for new insulin release, it could have

a diagnostic value. All other factor combinations are less important or have their smallest eigenvalue below the defined threshold.

Further analysis of the steady-state scenario in TNDM shows, that there exist 356 state combinations that satisfy $\underline{\lambda} > 0.1$ with a maximum of four simultaneously observable states, e. g., case (o). In T2DM, 284 (also case (o)) and in T1DM, 138 combinations are valid. In the MTT scenario, particularly for T2DM, the number of valid observable state combinations rises to 571.

Finally, the major states of interest, plasma glucose, $G_{\mathrm{P}}(t)$, and plasma insulin, $I_{\mathrm{P}}(t)$, are observable in all three groups when only $G_{\mathrm{I}}(t)$ is measured (case (c)). Case (m) is worth mentioning, too, as good observability of glucose in the gastrointestinal tract can be a starting point for an (unknown) meal input estimation. Furthermore, the smallest eigenvalues only differ marginally between the groups. And last, observability does not seem to highly depend on the examined scenario, except for T2DM, where $I_{\mathrm{P}}(t)$ is better observable under steady-state conditions.

Observability can be enhanced if more than one or other outputs are considered. E. g., when plasma insulin would be measured in addition to glucose, improved observability of the insulin subsystem could be expected. In Eberle et al. (2012a), it has been shown that, besides glucose measurements, recording insulin significantly improves the identifiability of diagnostic parameters.

Parameter Identifiability. Now, observability analysis is extended to the problem of identifiability of parameters. For that, the augmented system $\widehat{\Sigma}$ given by (5.51) is considered, where parameters are defined as constant states, and observability analysis can then be performed for the extended state vector. With $N = 19$ dynamical states and $P = 34$ constant parameters, the augmented state vector $\hat{\boldsymbol{x}}$ has dimension $\hat{N} = 53$.

To perturb the augmented states within a suitable range the same configuration as given in Section 5.2.6 is used. That means the maximum excitation for each state and parameter is 50 % of its nominal value. One exception must be made to parameter m_6 in T2DM subjects, where an initial value of this height leads to simulation failures. This parameter perturbation is restricted to only 25 % of its nominal value to avoid such behavior.

Another aspect to mention is the choice of a unit matrix for the rotation in set $\mathcal{R}_x$. That means each state is individually perturbed. When in joint state and parameter observability this simplified but fast screening approach could return misleading results. Whenever a parameter is perturbed that belongs to a state that is stationary, a change in its value is not apparent in the state trajectory. Hence, this parameter will be considered non-identifiable. To avoid non-identifiability in steady-state, a full factorial design plan should be carried out to include every possible joined perturbation of states and parameters. However, this would lead to a considerable number of $2^{\hat{N}-1} = O\left(10^{15}\right)$ simulation runs that cannot be handled properly. As an alternative, a suitable input trajectory must be chosen to obtain a proper system response, such as the MTT scenario. The approach has the advantage that only $T \cdot R \cdot \hat{N} = 212$ (number of scale factors $T = 4$, $R = 1$) simulation runs are necessary to compute the

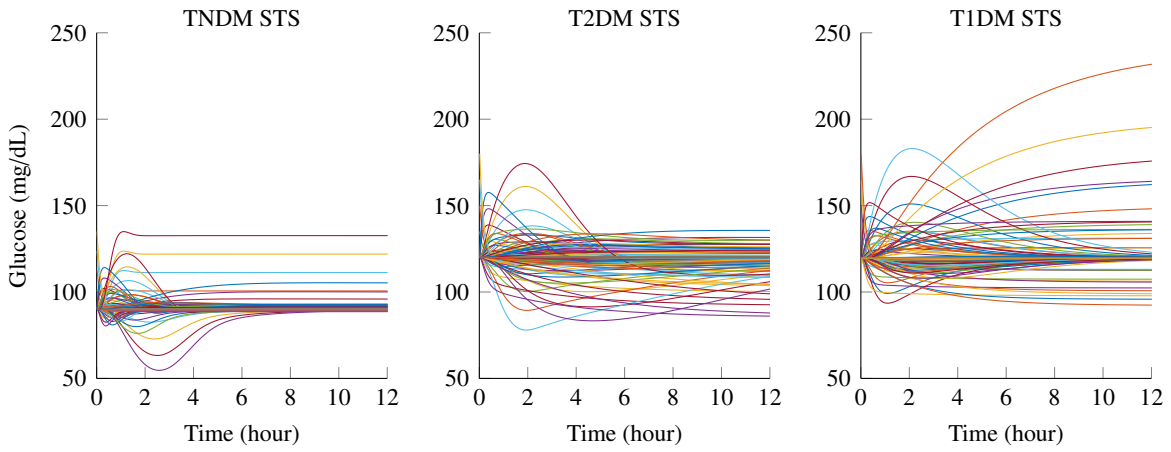

Figure 5.21: Output trajectories derived by a single (augmented) state perturbation identifiability analysis in the STS scenario for TNDM (left panel), T2DM (middle), and T1DM (right).

Gramian for each group. The resulting output trajectories are depicted in Figs. 5.21 and 5.22 for the STS and MTT scenarios, respectively.

Comparing the time courses of the steady-state scenario with the ones retrieved by state observability (Fig. 5.18) reveals the large influence of the parameters as they can shift the steady-state of the model output. This behavior is similar to the trajectories produced by global sensitivity analysis (Fig. 5.2 for EET or Fig. 5.10 for VBSA). Most of the signal sequences that generate an offset to the nominal s.c. glucose value can be explained by the parameter $G_{\mathrm{P}}^{\mathrm{b}}$, the basal glucose concentration. Other state perturbations lead to a rise in the glucose output, and yet others to significant drops. They have in common that the nominal basal value is reached again. These behavioral patterns are particularly well visible for TNDM in the left panel of Fig. 5.21. A slightly different picture arises for T1DM on the right side, where larger deviations from the nominal steady-state are clearly apparent. This deviant behavior can be mainly explained by the mismatch of basal insulin administration required to maintain a nominal steady-state and the new amount of insulin necessary for the altered parameter sets.

For the MTT scenario (Fig. 5.22), the meal response is clearly visible, as well as the shifted stationary points, which become apparent as offsets in the model output. In TNDM mainly the offset and not the dynamic of the output signal changes for the different state and parameter perturbations. However, in the diabetic groups, the rate at which glucose is reduced from plasma depends considerably on the initial state vector.

The associated observability Gramian, $\boldsymbol{W}_{\mathrm{O}}^{\star}$ (5.52), was computed twice using (5.54) to scale the system properly. Hence, all diagonal elements $\boldsymbol{W}_{\mathrm{O}_{ii}}^{\star}$ are equal to one. If a state or parameter is not observable the corresponding rows and columns in the matrix are zero. In this case, only the observable part of the Gramian is further used. Table B.4 on page 204 lists the identifiable parameters. Identifiability depends on the investigated group and the applied scenario for which the Gramian was computed. In the steady-state scenario, only 12 out of 34 parameters were determined to be identifiable (left

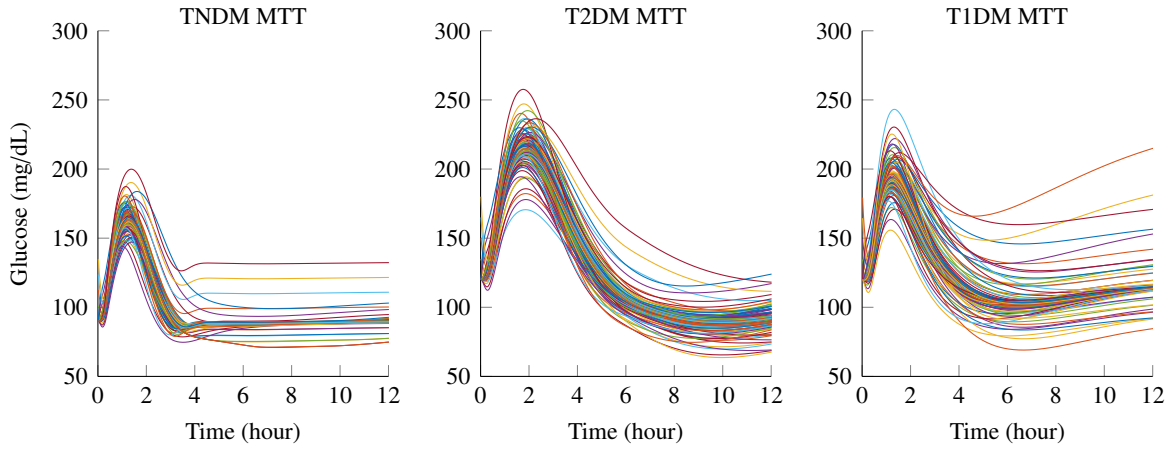

Figure 5.22: Output trajectories derived by a single (augmented) state perturbation identifiability analysis in the MTT scenario for TNDM (left panel), T2DM (middle), and T1DM (right).

part of the table). All non-identifiable parameters are associated with states that remain constant in this setting. Particularly, important parameters associated with the insulin response (e. g., β), the time delay between glucose in plasma and s.c. space, k_g, or the digestion time (e. g., k_{G2}) cannot be identified within steady-state. In T1DM, three more parameters associated with insulin secretion are not identifiable, whereas parameters $k_{i,1..3}$ are identifiable, as their related states are stimulated by the s.c. insulin infusion, which does not occur in TNDM and T2DM.
For the MTT scenario (right part of Table B.4), the number of identifiable parameters improves. In TNDM, their number rises to 28 of 34. Only the s.c. insulin, $k_{i,1..3}$, and s.c. glucagon-related parameters, $k_{h,1..3}$, are not identifiable as their related states are neither perturbed nor affected by an input signal. In T2DM, the three s.c. insulin-related parameters, $k_{i,1..3}$, have now become identifiable since an insulin bolus is given in the MTT scenario and thus, a response is induced in the related states. In T1DM, all parameters linked to insulin secretion (e. g., κ, α, β, γ) and $k_{h,1..3}$ remain unidentifiable.

To obtain information about the joint state and parameter observability, the eigenvalues of the full Gramian $\boldsymbol{W}_{\mathrm{O}}^{\star}$ are computed. In both scenarios, the eigenvalues decline exponentially from 10^0 down to $O\left(10^{-18}\right)$ in the steady-state scenario and down to $O\left(10^{-11}\right)$ in the MTT scenario. Under steady-state, for TNDM and T2DM, 31 augmented states are observable, i. e., 19 dynamical states and 12 parameters; for T1DM 17 dynamical states and also 12 parameters have non-zero eigenvalues. In the MTT scenario, TNDM has 47 observable states in total, T2DM 49 states, and T1DM 42. Moreover, the smallest observable eigenvalue is at least about an order of 11 magnitudes higher. In both cases, TNDM subjects have slightly better overall observability. The resulting scaled eigenvalues are depicted in Figs. B.8 and B.9, respectively.

The observability of dynamical states has already been reported in Table 5.3. Now, to quantify the joint observability of states and parameters, Algorithm 2 is executed for several augmented state combinations for TNDM, T2DM, and T1DM subjects and the two scenarios. The setup is the same as for the state observability analysis in Section 5.2.6. Also, a threshold of $\underline{\lambda} > \epsilon = 0.1$ has been chosen

Table 5.4: Joint observability defined by the smallest eigenvalue $\underline{\lambda}(\boldsymbol{W}_{\mathrm{O}_\varepsilon})$ for a set of states in $\mathcal{E}$ computed from Gramians in steady-state (STS) and mixed-meal (MTT) scenario for TNDM, T2DM, and T1DM.

		STS			MTT		
Case	**Set $\mathcal{E}$ of states to be observed**	**TNDM** $\underline{\lambda}\left(\boldsymbol{W}^{\star}_{\mathrm{O}_\varepsilon}\right)$	**T2DM** $\underline{\lambda}\left(\boldsymbol{W}^{\star}_{\mathrm{O}_\varepsilon}\right)$	**T1DM** $\underline{\lambda}\left(\boldsymbol{W}^{\star}_{\mathrm{O}_\varepsilon}\right)$	**TNDM** $\underline{\lambda}\left(\boldsymbol{W}^{\star}_{\mathrm{O}_\varepsilon}\right)$	**T2DM** $\underline{\lambda}\left(\boldsymbol{W}^{\star}_{\mathrm{O}_\varepsilon}\right)$	**T1DM** $\underline{\lambda}\left(\boldsymbol{W}^{\star}_{\mathrm{O}_\varepsilon}\right)$
(a)	$\left[G_\mathrm{P}, I_\mathrm{P}, G^\mathrm{b}\right]$	0.1198	0.0799	0.0974	0.2391	0.1046	0.1863
(b)	$\left[G_\mathrm{P}, I_\mathrm{P}, I^\mathrm{b}\right]$	0.1237	0.0193	0.1037	0.2154	0.1134	0.1597
(c)	$\left[G_\mathrm{P}, I_\mathrm{P}, G^\mathrm{b}, I^\mathrm{b}\right]$	0.0084	0.0049	0.0062	0.0516	0.0812	0.0192
(d)	$[G_\mathrm{P}, I_\mathrm{P}, m_6]$	0.1404	0.0643	0.1053	0.2235	0.1066	0.1353
(e)	$[G_\mathrm{P}, I_\mathrm{P}, \beta]$	0.0000	0.0000	0.0000	0.2020	0.1032	0.0000
(f)	$[G_\mathrm{P}, I_\mathrm{P}, m_5]$	0.1354	0.1211	0.0000	0.1945	0.0996	0.0000
(g)	$[G_\mathrm{P}, I_\mathrm{P}, V_{mx}]$	0.0000	0.0000	0.0000	0.1825	0.1447	0.0547
(h)	$[G_\mathrm{P}, I_\mathrm{P}, k_{G2}]$	0.0000	0.0000	0.0000	0.0885	0.1912	0.1952
(i)	$[G_\mathrm{P}, I_\mathrm{P}, k_1]$	0.1670	0.0560	0.0992	0.0744	0.0513	0.0829
(j)	$\left[G_\mathrm{P}, I_\mathrm{P}, k_{p3}\right]$	0.1266	0.0750	0.0969	0.2401	0.1436	0.1441
(k)	$[G_\mathrm{P}, I_\mathrm{P}, k_{i3}]$	0.0000	0.0000	0.0209	0.0000	0.2223	0.1186
(l)	$[G_\mathrm{P}, k_{G2}]$	0.0000	0.0000	0.0000	0.1921	0.3284	0.4356
(m)	$[G_\mathrm{P}, k_1]$	0.2680	0.9554	0.3819	0.2625	0.6842	0.4232
(n)	$\left[G_\mathrm{P}, I_\mathrm{P}, k_g\right]$	0.0000	0.0000	0.0000	0.1001	0.1468	0.1113
(o)	$\left[G_\mathrm{P}, I_\mathrm{P}, G^\mathrm{b}, m_6\right]$	0.0120	0.0006	0.0011	0.1934	0.0381	0.0358
(p)	$\left[G_\mathrm{P}, I_\mathrm{P}, G^\mathrm{b}, \beta\right]$	0.0000	0.0000	0.0000	0.2009	0.0697	0.0000
(q)	$\left[G_\mathrm{P}, I_\mathrm{P}, G^\mathrm{b}, k_{G2}\right]$	0.0000	0.0000	0.0000	0.0464	0.0124	0.1851
(r)	$\left[G_\mathrm{P}, I_\mathrm{P}, k_{p3}, I^\mathrm{b}, \beta\right]$	0.0000	0.0000	0.0000	0.1087	0.0158	0.0000
(s)	$\left[G_\mathrm{P}, Y, G^\mathrm{b}, m_6\right]$	0.0107	0.0007	0.0000	0.1884	0.0380	0.0000
(t)	$[G_\mathrm{P}, m_6]$	0.9915	0.8524	0.7014	0.7314	0.7382	0.7555
(u)	$\left[G_\mathrm{P}, k_{p3}\right]$	0.7569	0.8843	0.5835	0.9034	0.7441	0.7511
(v)	$\left[G^\mathrm{b}, m_6\right]$	0.9915	0.8524	0.7014	0.7314	0.7382	0.7555
(w)	$\left[G^\mathrm{b}, \beta\right]$	0.0000	0.0000	0.0000	0.6746	0.6991	0.0000
(x)	$\left[G^\mathrm{b}, m_6, \beta\right]$	0.0000	0.0000	0.0000	0.1528	0.1193	0.0000

for practical observability. The main focus is on the estimation of plasma glucose, $G_\mathrm{P}(t)$, and insulin, $I_\mathrm{P}(t)$, in conjunction with several parameters. In total, 13 augmented states were selected, resulting in $2^{13} - 1 = 8191$ feasible combinations. From that, 284 in TNDM, 287 in T2DM, and 175 in T1DM have the smallest singular value larger than the threshold when considering the more meaningful MTT scenario. A maximum of five augmented states is simultaneously observable. The results are listed in Table 5.4.

Cases (a) and (b) show that it is possible to either identify $G_\mathrm{P}(t)$, $I_\mathrm{P}(t)$, and the glucose basal value G^b, or $G_\mathrm{P}(t)$, $I_\mathrm{P}(t)$, and the basal insulin concentration I^b, but not both parameters in combination (case (c)). Furthermore, either can only be estimated during the MTT scenario.

Cases (d)–(k) each contains one parameter in addition to the aforementioned substance concentrations: $m_6, \beta, m_5, V_{mx}, k_{G2}, k_1, k_{p3}$, and k_{i3}, which are most influential according to their first-order sensitivity indices (Fig. 5.14). Parameters that only take effect during transient behavior of the system can not be

identified in steady-state, like β or k_{G2} (cases (e), (h)). Insulin-related parameters, β and m_5 (cases (e) and (f)) can not be estimated in T1DM, due to the absence of insulin secretion. Whereas k_{i3} (case (k)) generally leads to an eigenvalue of zero in TNDM, and in T2DM only in steady-state, as no insulin is administered in these cases. Parameter k_{G2} (case (h)) is not practically identifiable in TNDM, while this occurs for k_1 (case (i)) in all groups; the smallest eigenvalue is lower than the chosen threshold $\epsilon > 0.1$.

To assess if identifiability is enhanced when fewer variables have to be estimated in common, cases (l) and (m) are introduced. There, only eigenvalues of $G_{\mathrm{P}}(t)$ besides the named parameters were computed. In both cases, $\underline{\lambda}$ increases, particularly for k_1 in case (m). Furthermore, k_1 is one of the few parameters observed well in steady-state.

Case (n) introduces parameter k_g, which is involved in the diffusion of glucose from plasma into the s.c. space. This variable is not sensitive at all, regarding the overall time course of glucose measurements but has an important role when estimating plasma glucose from s.c. records. Hence, it will also be included here. The smallest eigenvalues show identifiability just above the threshold value in all three groups when the system is in a transient state.

Cases (o)–(s) include one or two more parameters to be observed in common, up to a maximum number of five augmented states. The reported cases exemplify a wider range of possible valid configurations that can be assumed observable using the selected threshold.

Cases (t) and (u) are further examples to show that a significant improvement in the eigenvalues can be achieved when only state $G_{\mathrm{P}}(t)$ is observed with one additional parameter in common.

Finally, in cases (v)–(x), only the most sensitive parameters (compare with Fig. 5.14) are identified in combination. The cases reveal that two parameters can be observed at once, but identifiability decreases rapidly for all factors in common (case (x)). Moreover, β can only be determined during an MTT and not T1DM subjects, which is in accordance with the results obtained by the sensitivity analysis.

5.3 Summary and Conclusion

The preceding chapter introduced two different techniques for state and parameter analysis and their applicability to a model of glucose-insulin-glucagon regulation.

The statistical approach treats states and parameters as varying input factors that induce variability in the system outputs. The computationally cheap Elementary Effects Test (Section 5.1.2) allowed reducing the full parameter vector to a subset of only 10 sensitive variables. Moreover, the subsequent variance-based sensitivity analysis (Section 5.1.4) enabled the quantification of these results into a total sensitivity index. For this, the transformation from a functional to a set of scalar model outputs also had to be conducted. The whole procedure was implemented as a multi-step sensitivity analysis. The findings showed differences between type 1 and type 2 diabetics, as well as non-diabetic subjects that result from alterations of the underlying glucose-insulin metabolism. Particularly, basal glucose

concentration and parameters involved in insulin secretion and glucose control have been shown to be the most important factors.

Controllability, observability, and its extension to identifiability are common methods for analyzing the input-output behavior of linear, dynamical systems. The concept of Gramians was applied to determine the generalized energy transfer from the inputs to the states, respectively from the states into the outputs. Its extension to empirical Gramians allowed for determining the energy transfer for nonlinear systems within a large working range. By using the smallest eigenvalues of the computed Gramian matrices, observability and identifiability could be quantified. Results show that not all states are controllable or observable, particularly the insulin secretion part of the model in T1DM. It was further quantified that only a small subset of states and parameters can be theoretically identified from glucose observations in the subcutaneous space, which is the essential measurement variable (Section 6.1.1). However, it has been shown that glucose concentration in plasma and its basal level can be estimated. Hence, this process should be restricted to those factors that are "important", respectively those which have shown to be observable or identifiable. How states and parameters can be identified from measurement data will be shown in the following chapter.

Global sensitivity analysis considers parameters as stochastic input factors acting on the model outputs, often used for static models. The concept of controllability and observability is well known for dynamical systems. As an outlook, both techniques could be linked to each other. First by extending GSA by declaring initial states as input factors and computing their sensitivities on the output. Hence, it becomes the stochastic analog to observability. Second, one could also declare states as model outputs in order to compute the parameter's sensitivities on the new outputs, which would correspond with the sensitivity Gramian matrix when the parameters are treated as external inputs (compare with (3.13) on page 37 for this concept).

6 Model Identification and State Estimation

In Section 4.1 a mathematical model of the glucose-insulin-glucagon metabolism has been presented. Moreover, in Section 4.2 models for virtual subjects have been derived. These consist of a set of parameters that characterize the health condition of a subject in a long-term manner and a set of dynamical states that describe the current metabolic condition of a subject. Chapter 5 introduced techniques to identify those variables that can be theoretically determined from observation of a particular model output. In the following, two complementary methods address how these variables can be determined: Model or parameter identification is here defined as adapting model parameters in such a way that simulated model outputs and experimental data match closely, typically by solving an optimization problem offline (Section 6.2). On the other hand, state estimation is performed online, i. e., in real-time, and updates of the model states of a subject based on current measurements (Section 6.3). The development of these methods can be carried out based on simulated data for which the models of virtual sensors are helpful (Section 4.5). Additionally, clinical data from the literature, as well as experimental data recorded under everyday-life conditions is considered (Section 6.1).

This two-sided approach aims to personalize the generic model to a particular subject that may support a physician in diagnosing the progression of diabetes over a longer period. Once the model is adapted, online estimation could provide real-time information on the current health status.

6.1 Database of Patient Records

A database of personal patient measurement records is the basis for all subsequent experimental analyses. The database consists of blood glucose samples, continuous glucose samples, the amount and time point of meal ingestion, and the amount and time points of insulin administration. Six subjects provided data: a single TNDM person who reflects a healthy condition, two T2DM subjects under conventional insulin therapy, and three T1DM patients under CSII (Section 2.5). TNDM and T2DM patients gave their written consent for data acquisition and analysis, and T1DM patient data was kindly provided by The Nightscout Data Commons Committee (2018) obtained via the Open Humans platform (Open Humans 2018). All data has been recorded between January 2016 and September 2018 under real-life conditions, i. e., all participants underwent their daily life routine and followed their regular treatment plans. In Table 6.1 the number of BGSM and CGM measurements and some key statistics related to these intervals are summarized.

Table 6.1: Statistical information about the recorded experimental data.

Group	Subject	Days	Number of measurements			Basic statistics	
			BGSM	BGSM per day	CGM	Mean ± Std. ($mg\,dL^{-1}$)	Min. / Max. ($mg\,dL^{-1}$)
TNDM	814	70	1542	22.0	18 747	93.6 ± 18.9	39 / 251
T2DM	126	12	82	2.3	3339	145.4 ± 40.9	39 / 267
T2DM	385	18	109	6.1	4716	172.4 ± 34.3	62 / 289
T1DM	20330028	94	1096	11.5	25 182	115.9 ± 45.7	26 / 401
T1DM	39561557	60	550	9.2	15 867	130.0 ± 50.0	38 / 331
T1DM	76423578	234	2776	11.9	54 436	133.2 ± 45.6	22 / 447

6.1.1 Input and Output Measurements

Blood glucose was measured using commercially available sensors several times a day according to the patient's needs. Subcutaneous glucose concentration was measured using two different sensors (G4 Platinum or G5 Mobile, Dexcom, San Diego, CA, USA), measurement range 40-400 $mg\,dL^{-1}$ (Dexcom, Inc. 2017). CGM devices calculate and save the mean s.c. glucose values over a 5 min interval and require calibration twice a day by corresponding blood glucose pairs. The sensor lifetime is 7 consecutive days, it must be replaced afterward. T1DM subjects under CSII wore an insulin pump (640g, 530g, or Veo, Medtronic Minimed, Northridge, CA, USA). All devices were operated as described by the manufacturer's handbooks. Daily basal insulin infusion rates for each T1DM subject are shown in Fig. C.1 on page 205.

In contrast to clinical studies that are fulfilled within tight conditions and exact protocols, data obtained under everyday-life settings may be subject to larger uncertainty like missing values due to, e. g., loss of sensor connection. Furthermore, permanent or temporary physiological conditions such as strong physical activity, illness, or medication cannot be excluded. All these factors may influence glucose metabolism and measurements and must be regarded as unknown disturbances. Last to mention are uncertainties in acquiring the input signals. The amount of insulin injected by pen or pump can be precisely adjusted and thus regarded to be exactly known without error. However, the amount and rate of digestion of ingested glucose highly depend on the meal and the quantities of carbohydrates and sugars in combination with other macro-nutrients such as fat. This complex is illustrated in Fig. C.2 where two completely different responses to meals of a similar amount of CHO/glucose are highlighted. The rise of glucose in blood and ISF to a high CHO meal (left) is far lower and prolonged, compared to a meal rich in sugar (right). This behavior is visible in the CGM signal and confirmed by the frequent BGSM samples. Hence, the same glucose input to the system does not generally imply the same postprandial glucose excursion (Freckmann, Hagenlocher, et al. 2007). In fact, the assumed meal input is determined by the patient and his or her ability to estimate the correct quantity of glucose within the meal. As a support for the patient, a food database (myFitnessPal, Under Armour, Baltimore, MD, USA) can be queried, too, which returns most of the macro-nutrients in a particular product.

From that, two of the five introduced model inputs can be utilized in daily life: oral glucose input, $u_{\mathrm{G}}^{\mathrm{oral}}(t)$, and s.c. insulin infusion input, $u_{\mathrm{I}}^{\mathrm{sc}}(t)$. Moreover, two out of four model outputs can be measured in this way: concentration of glucose in the blood, $G(t)$, and in the interstitial fluid, $G_{\mathrm{I}}(t)$, respectively (Section 4.1).

In controlled clinical trials, a series of physiological tests can be applied to investigate particular responses of glucose metabolism. Here, only daily-life measurement data over large periods is available, which can be regarded as a discrete-time series of mixed-meal tests with or without insulin administration. To locate suitable intervals from which a parameter identification or state estimation can be fulfilled, the period of interest is automatically separated into sequences that satisfy the following properties (Fig. 6.1):

- A sequence must consist of a meal input in order to induce a proper response to the metabolism. That is important as some parameters can not be identified in steady-state.
- The sequence must be long enough to capture most of the transient behavior. A default duration of 4 hours was chosen.
- A sufficient number of data points must be recorded for identification. For BGSM data, a sampling rate $s_{\mathrm{BG}} = 1\,\mathrm{h}^{-1}$ and for the CGM signal $s_{\mathrm{CG}} = 6\,\mathrm{h}^{-1}$ was chosen. Hence, within one measurement sequence, at least 4 BGSM and 24 CGM records must exist.
- The correlation coefficient between BGSM and CGM signals must be higher than 0.5 to exclude periods of diverging measurement curves.

However, these specifications are a trade-off between a sufficient amount of data that represents the true time course of glucose and the fact that patients typically perform BGSM only a few times a day.

Since measurement of insulin is not possible within the daily-life protocol, experimental data from A. Basu, Dalla Man, R. Basu, et al. (2009) was additionally considered to show the general applicability of parameter optimization. The protocol was a mixed-meal test in TNDM and T2DM subjects (Table 4.14). Concentrations of glucose and insulin in blood have been plotted in Figs. 4.18 and 4.19.

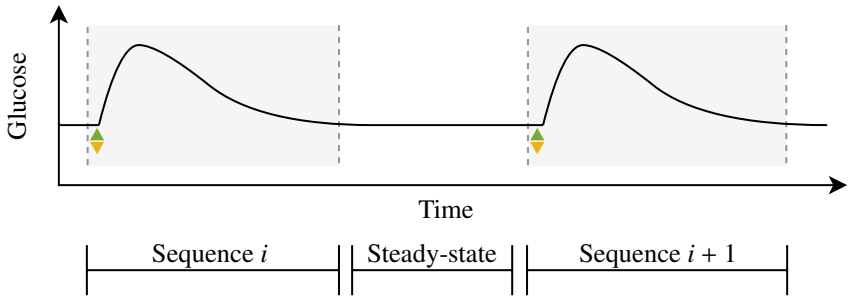

Figure 6.1: Partition of a continuous-time signal into single sequences of fixed length and predefined properties.

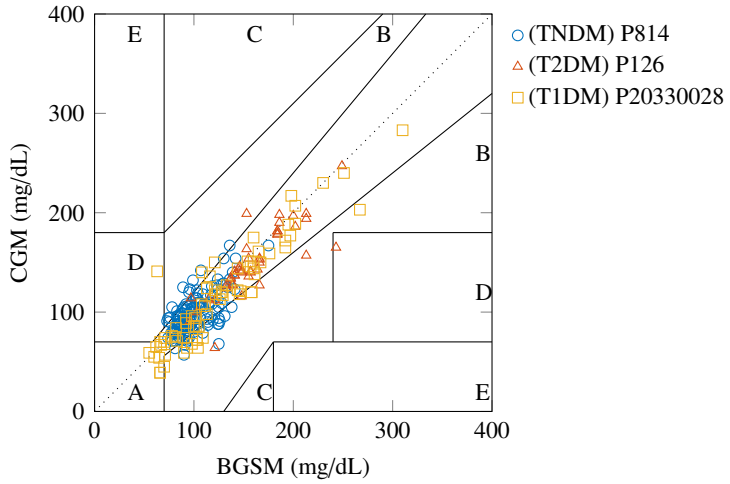

Figure 6.2: Error grid analysis (EGA) of paired blood glucose (BGSM) and continuous glucose (CGM) measurements for one subject in each group over 7 consecutive days.

6.1.2 Measurement Analysis

To assess the quality of the measurement records, an error grid analysis (EGA) is performed (Section 3.3.4) between BGSM and CGM data pairs. The evaluation of the sensor performance is limited to the observations during the trials. It does not claim to be generally valid. EGA plot is shown in Fig. 6.2 for a randomly chosen measurement interval of seven consecutive days, i. e., for one sensor lifetime, for the TNDM (blue), one T2DM (red), and one T1DM (yellow) subject. The number of measurement pairs, n, and the calculated performance for each zone are reported in Table 6.2. The percentage of values within the clinically accurate zones A and B is close to 100 % and almost similar to reported values in Freckmann, Link, et al. (2018). Other performance evaluations of discontinued CGM devices report similar results (Damiano et al. 2014; Freckmann, Pleus, et al. 2013). Note the higher error in zone D for the T2DM subject which can be attributed to a single measured value. Since there are only $n = 45$ data pairs present in this subject, the error has a stronger effect on the performance metric. EGA plots for all subjects over the whole measurement period are shown in Fig. C.4 on page 206.

Table 6.2: Results of the EGA performance evaluation shown in Fig. 6.2 with a total number of n measurements.

Subject	n	% of data pairs in zone					MARD
		A	B	C	D	E	(%)
814	137	78.8	21.2	0.0	0.0	0.0	11.7
126	45	86.7	11.1	0.0	2.2	0.0	8.6
20330028	74	82.4	16.2	0.0	1.4	0.0	14.3

Moreover, the mean absolute relative difference (MARD), introduced in Eqs. (3.15) and (3.16), is calculated as

$$\mathrm{MARD} = 100\% \cdot \frac{1}{n} \sum_{k=1}^{n} \left| \frac{G_{\mathrm{BG}}(k) - G_{\mathrm{CG}}(k)}{G_{\mathrm{BG}}(k)} \right|, \tag{6.1}$$

where $G_{\mathrm{BG}}(k)$ is the k-th measured blood glucose (BG) and $G_{\mathrm{CG}}(k)$ the continuous glucose (CG) concentration. MARD varies between 8.6 % in T2DM and 14.3 % in the T1DM subject (Table 6.2), which is slightly higher than findings in Freckmann, Link, et al. (2018), where MARD was estimated with approx. 11 % during a 14-day study.

Last, BGSM and CGM signals, along with discrete-time points of meal ingestion and insulin injection, are shown in Fig. 6.3 for two consecutive days taken from the measurement period above. CGM data is frequently sampled every 5 min, whereas BGSM data is sparse. Most BGSM data points are available in the TNDM participant, from which glucose dynamics are also visible. Moreover, a time delay between BG and CG records is noticeable (e. g., the glucose rise after 12:00 or 33:00 hours). Particularly in the T2DM patient, BG samples were only taken to calibrate the CGM device. Hence, the dynamic time course of glucose only becomes apparent by CGM data. Meal inputs clearly correlate with a rise in glucose levels. In the TNDM subject, periods of elevated postprandial glucose concentration are comparatively short, followed by a prolonged steady-state phase until the next meal. In the diabetic patients, s.c. insulin is usually given at mealtimes (meal bolus) or to correct elevated glucose levels (correction bolus). Furthermore, glucose profiles are characterized by a larger variability, a prolonged postprandial period, and reach higher maxima, compared to the TNDM subject. Most of the time, CGM data agrees well with BGSM references.
However, there are also large deviations in the absolute values and the gradients. Even diverging signal courses occurred quite a few times during the observation period. Moreover, sensor drifts can occur, which is apparent when the CGM signal is calibrated on new BGSM samples. Typical artifacts are plotted in Fig. C.3 on page 205.

In summary, the acquired CGM data was compared with corresponding BGSM reference values. The achieved MARD is 8.6-14.3 % for the investigated periods and across all subjects and thus in the expected range. EGA revealed that almost all data is located within clinically accurate zones A and B. Hence, it can be assumed that the records are appropriate for the following identification and estimation procedures.

6.2 Model Personalization

Model personalization means adapting the parameters of a nominal model in such a way that the simulated model outputs closely match the measured experimental data of an individual, which can be referred to as the system (Fig. 3.6). Here, the model inputs, $\boldsymbol{u}(k)$, are meal ingestions and insulin administrations that a subject has noted for that particular experiment. The unknown disturbances $\boldsymbol{z}(k)$

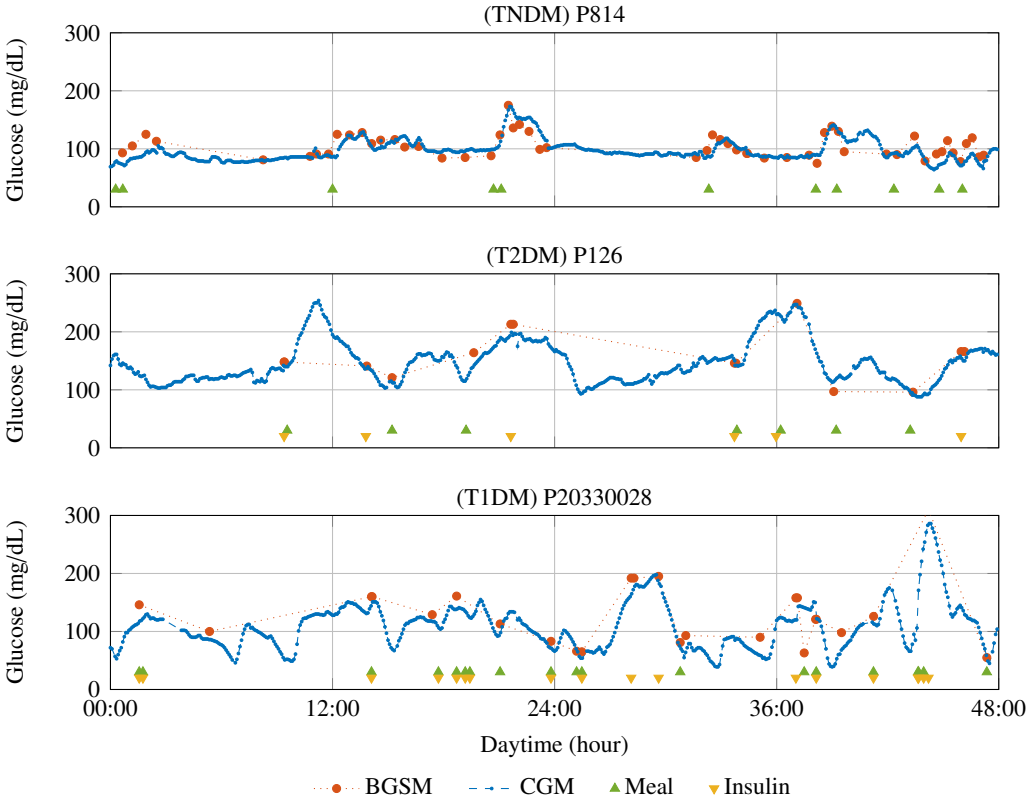

Figure 6.3: Representative time courses of blood glucose (red markers connected by dashed line) and continuous glucose measurements (blue), discrete meal times (green), and discrete bolus insulin administrations (yellow) in TNDM (top), T2DM (middle), and T1DM (bottom) during an 48 h interval. Note that amounts of ingested glucose and administered insulin have been omitted for better visibility.

may be physical activities or other factors not incorporated into the model. Simulated and measured outputs are compared in terms of the cost function Q, which is defined by the sum of the squared error between system output $G_{\mathrm{CG}}(k)$ and model output $G_{\mathrm{I}}(k)$ given by (3.14). All optimizations have been conducted using the Matlab function *lsqnonlin* that is based on the interior-reflective Newton method (Coleman et al. 1996) and solves a nonlinear but constraint vector-valued data-fitting problem of the form

$$\min_{\boldsymbol{p}} \|Q(\boldsymbol{p})\|_2^2 = \min_{\boldsymbol{p}} \left(f_1(\boldsymbol{p})^2 + f_2(\boldsymbol{p})^2 + \ldots + f_O(\boldsymbol{p})^2 \right), \tag{6.2}$$

where $f_1(\boldsymbol{p}), \ldots, f_O(\boldsymbol{p})$ are the considered object functions $f_i = \boldsymbol{y}_i(k) - \hat{\boldsymbol{y}}_i(k, \hat{\boldsymbol{p}})$, $i = 1, \ldots, O$, with $\boldsymbol{y}_i$ and $\hat{\boldsymbol{y}}_i$ being the model output respectively the measured reference trajectory.

The total parameter vector $\boldsymbol{p}$ is not identifiable. Indeed, the subset of sensitive parameters, as discussed in Section 5.1.7, can be considered in order to optimize those variables that contribute most to the output variability. Hence, an identified subject $\hat{\mathcal{S}}$ consists of a set of nominal parameters $\boldsymbol{p}$ that are kept at their default values and a set of adapted parameters $\hat{\boldsymbol{p}} \subset \boldsymbol{p}$.

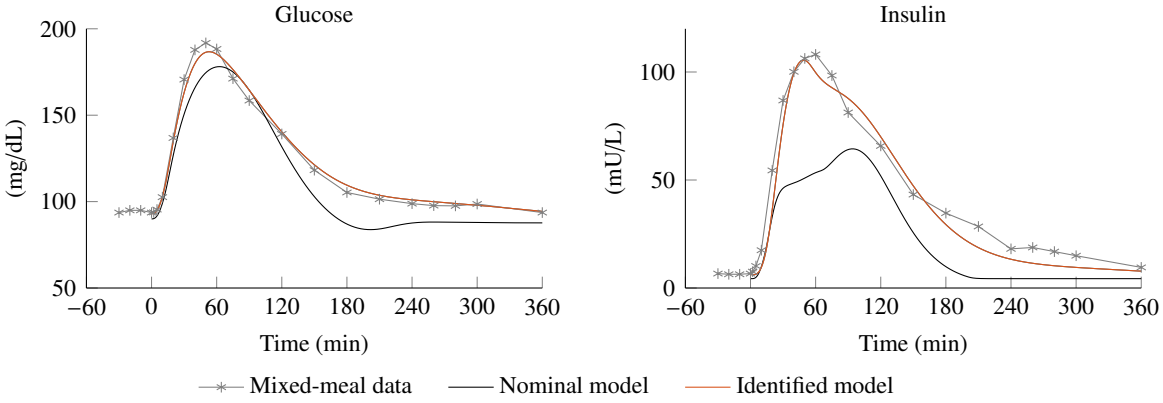

Figure 6.4: Comparison of measurement data (gray markers, data taken from A. Basu, Dalla Man, R. Basu, et al. (2009)) and outputs of nominal (black line), and identified model (red line) after an MTT in TNDM subjects.

6.2.1 Parameter Identification from Blood Glucose and Insulin Measurements

To show the general applicability of the parameter identification process, experimental blood glucose and insulin records taken from A. Basu, Dalla Man, R. Basu, et al. (2009) are considered first. The data has already been presented in Section 4.4 for the nominal TNDM subject (Fig. 4.18) and the nominal T2DM subject (Fig. 4.19). Now, a subset of sensitive parameters should be adapted in order for the model to adequately represent the time courses of glucose and insulin. The parameters are listed in Tables C.1 and C.2 for TNDM and T2DM subjects, respectively, and are identified according to (6.2) for $O = 2$. Note that basal glucose and insulin values, G^{b} respectively I^{b} are excluded from the identification as these values were also reported in the publication. In the same tables mean and standard deviation derived from the virtual population are reported, together with the optimized values, obtained by $r = 25$ repetitions of the optimization process starting from different initial conditions. The measured courses of blood glucose and insulin, along with the nominal and optimized model outputs, are shown in Figs. 6.4 and 6.5 for the TNDM and T2DM subjects, respectively.

For TNDM, time courses of the nominal trajectories deviate strongly from the measured signals, particularly insulin. Hence, it can be assumed that parameters must be varied considerably. The optimization process always finds the same minimum, indicated by the standard deviation of zero in each parameter. The two-sample t-test[1] for a 95 % confidence bound is calculated according to (3.18) and also reported in Table C.1. The assumed null hypothesis that the means of the nominal and optimized parameters are equal is clearly rejected by the high t-values, compared to the 95 % reference. Furthermore, the 95 % F-values for each parameter, calculated using (3.19) are of order 10^7 and above due to the zero variance in the optimized parameters. A visual inspection of the model outputs shows good accordance with the data. RMSE (3.17) between measured and simulated outputs improved from 19.3 mg dL^{-1} for the nominal model to 5.2 mg dL^{-1} for the optimized one.

[1] As the variance of nominal and optimized parameter samples are not equal, the test is also known as Welch-test.

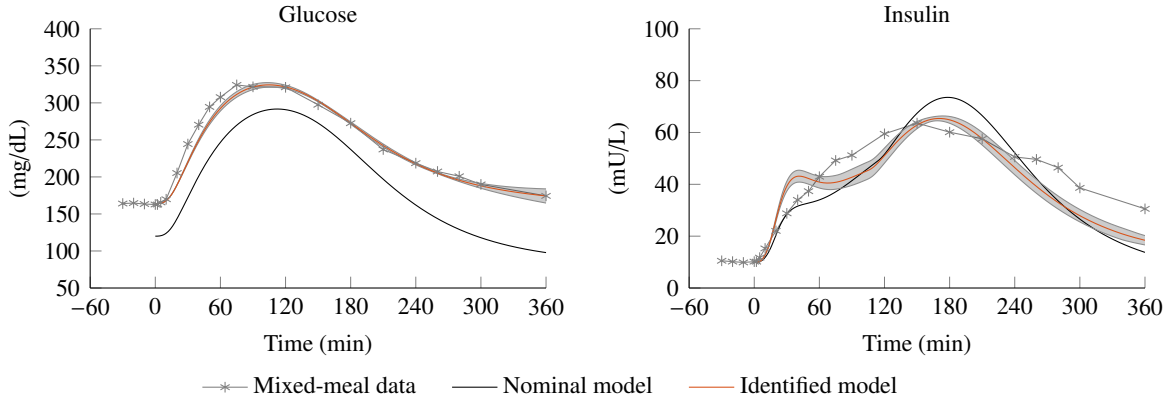

Figure 6.5: Comparison of measurement data (gray markers, data taken from A. Basu, Dalla Man, R. Basu, et al. (2009)) and outputs of nominal (black line), and identified model (red line and gray area denote mean and ± standard deviation range, respectively) after an MTT in T2DM subjects.

For T2DM, the time course of glucose mainly deviates from data due to a mismatch of the basal glucose concentration, which generates an offset error. Time courses of insulin do not differ much, particularly the prolonged elevation is already well represented by the nominal model (Fig. 6.5). Optimized parameters significantly differ from the nominal values, indicated by the 95 % t-value higher than the reference (Table C.2). Compared to the TNDM case, there are deviations in the optimized parameters after $r = 25$ repetitions of the optimization process. In 5 out of 9 parameters, the variance is lower than for the nominal values. Since the 95 % F-value is higher than the reference, the null hypothesis that the variance in the nominal parameters is lower must be rejected. Hence, it can be stated that most of the parameters can be identified with precision. Moreover, model adaptation improved the RMSE between measured and simulated outputs from 39.7 mg dL^{-1} to 7.9 mg dL^{-1}.

The experiment given above shows that it is generally possible to identify sensitive parameters from experimental data obtained in a clinical trial under controlled settings. Hence, a physiological model can be adapted to an individual for a personalized glucose and insulin simulation.

6.2.2 Parameter Identification from Daily-Life CGM Data

During a daily-life scenario, measuring insulin is not feasible for an individual. Moreover, BGSM records are taken too sparsely for optimization. Thus, only frequent CGM data provides enough information over a longer observation interval. If not stated otherwise, it will be the only signal reference on the basis of which the identification procedure is performed. Furthermore, meals and insulin injections are available as inputs to the system. In contrast to controlled studies which satisfy equal physiological conditions, several drawbacks arise from data obtained during daily life:

- Insulin sensitivity and β-cell responsivity are not constant during the day (Saad et al. 2012). Since these parameters are modeled to be time independent altered responses of a subject to a meal at different times a day may not be properly incorporated.

- Optimization is applied to certain sequences of data. However the initial metabolic state of a subject at the beginning of a sequence is unknown, e. g., a meal or insulin dose could have been taken recently before. Hence, these inputs are unknown to the model and their impact may not be correctly represented. To overcome this problem only intervals in the morning could be considered, where a steady-state condition may be assumed.
- The model of the gastrointestinal tract was identified from a standardized mixed-meal. In daily life, meals may have another combination of macro-nutrients which may change the rate of ingestion and thus the rate of appearance of glucose in the blood.
- The mean standard deviation of the s.c. glucose signal, $G_{\mathrm{I}}(t)$, induced by parameter variations as shown for the variance-based sensitivity analysis is 14.75 to 22.77 $\mathrm{mg\,dL^{-1}}$ (Section 5.1.7.2). The standard deviation introduced by the CGM sensor is approx. 10.5 $\mathrm{mg\,dL^{-1}}$ (Section 4.5.2). Thus, parameter identification from single measurement intervals will not be with precision as the variability caused by the parameters is, to a large extent, superimposed by the sensor error.

These factors have a significant impact on the model to adequately follow the measured CGM data. Due to these limitations, the same quality of results as in the identification from blood glucose and insulin data (Section 6.2.1) can not be expected.

Identification of the Physiological Time Delay. Parameter $\tau = \frac{1}{k_g}$ is the physiological time delay between glucose in the blood and interstitial fluid (Section 4.1.5). According to (4.25), it is modeled by a first-order delay. It is further independent of other parameters and can be identified from a sufficient number of both, glucose values in blood, $G_{\mathrm{BG}}(t)$, and continuous measurements, $G_{\mathrm{CG}}(t)$, from the s.c. space, where $G_{\mathrm{BG}}(t)$ is the input and $G_{\mathrm{CG}}(t)$ is the output of the model. Moreover, this parameter cannot be identified during steady-state, thus, an interval of transient behavior such as during an MTT must be provided. Optimization is first performed on noisy simulation data to verify its general applicability. Second, τ is identified from experimental records. As both, simulated and experimental data are noisy, it will not be possible to determine the parameter consistently from only one measurement interval. Therefore, τ is identified using a growing number of sequences in order to investigate averaging effects.

Algorithm 3 is applied for the identification by simulation. For this purpose, $L = 10$ out of 300 virtual subjects in all groups are randomly selected, i. e., L different nominal time delays $\tau_l, l = 1, \ldots, L$ exist. For each subject, the time courses of glucose in plasma and ISF are simulated using the MTT scenario and independent noise processes are added (Sections 4.5.1 and 4.5.2). To assess the repeatability accuracy of the identification, this process is repeated for a growing number of repetitions. For this, the set $\mathcal{R} = \{1, 10, 25, 50\}$ is defined. Each element in $\mathcal{R}$ stands for a certain number of repetitions. That means, τ is identified from $r_1 = 1$ to $r_4 = 50$ independent glucose sequences, which allows segregating the noise terms in the signals.
Furthermore, the nominal sampling rate of CGM signals is $s_{\mathrm{CG}} = 12\,\mathrm{h^{-1}}$. Although BGSM data is sparse, their sampling rate s_{BG} is also set to this value and both signals are then interpolated with

Algorithm 3 Identification of time delay τ by simulation

Require: Number of subjects L, set $\mathcal{R} = \{1, 10, 25, 50\}$
  for $l = 1, 2, \ldots, L$ **do**
    Randomly pick a virtual subject $\mathcal{S}_l$ from within all groups
    Simulate the desired scenario
    for $i = 1, 2, 3, 4$ **do**
      Create r_i independent noisy processes $\tilde{G}_{\mathrm{BG}}(t)$ and $\tilde{G}_{\mathrm{CG}}(t)$ from simulated signals $\tilde{G}(t)$ respectively $\tilde{G}_{\mathrm{I}}(t)$
    end for
    Estimate $\hat{\tau}_{l,i}$ from r_i noisy measurements
  end for
  Calculate the error between nominal τ_l and optimized $\hat{\tau}_{l,i}$

a sampling time of 1 min. Parameter τ is then identified on the basis of each of the r_i measurement sequences in $\mathcal{R}$ and for each subject $\mathcal{S}_l$. Finally, the differences between the nominal τ_l and each optimized $\hat{\tau}_{l,i}$ are calculated. The results are shown in Fig. 6.6. It can be seen that the error (mean depicted as red dots within the bars) decreases while the number of considered repetitions increases. For $r_1 = 1$, the median error is 4.4 min but τ cannot be identified with precision, indicated by the large error bar. For $r_4 = 50$, the estimation error reduces to 0.72 ± 0.69 min (when neglecting the outlier) while the repeatability accuracy significantly increases, indicated by the shrinking error bars. For all r_i, the mean error is higher than the median due to outliers. Generally, it is possible to identify the physiological time delay from BGSM and CGM simulation data with noise. Moreover, the correctness and precision of the estimate improve with a growing number of repetitions included in the identification procedure.

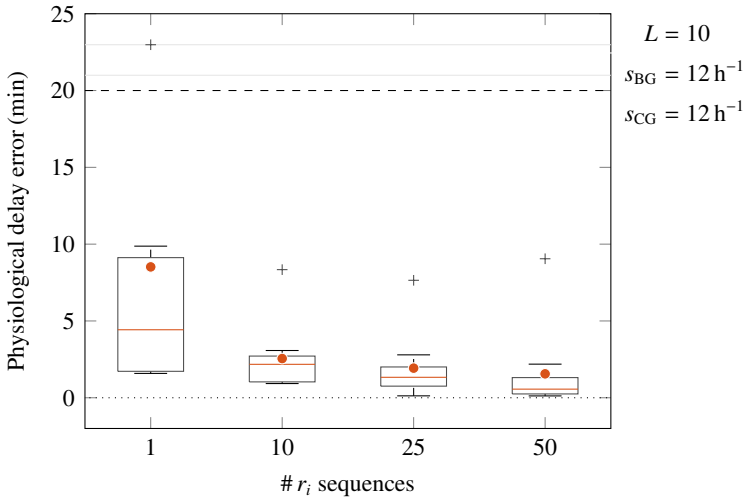

Figure 6.6: Error of the identified physiological time delay from noisy simulation data: The columns show the difference between nominal τ_l and identified values, $\hat{\tau}_{l,i}$, when a single, 10, 25, and 50 sequences are considered for the identification process. Bars show the median (red lines within the boxes) and mean (red circles) of the error.

Table 6.3: Identified physiological time delay $\hat{\tau}$ (min) for different subjects and a growing number of considered sequences, up to the total count m. Standard deviations estimated by $r = 25$ repetitions.

Group	Subject	# Sequences				
		1 (min)	**10** (min)	**25** (min)	**Set (m)** (min)	m
TNDM	814	26.2 ± 20.1	30.1 ± 15.7	24.7 ± 6.3	19.5 ± 0.0	138
T1DM	20330028	18.9 ± 20.6	13.8 ± 7.7	13.5 ± 3.8	15.1 ± 0.0	58
T1DM	39561557	11.4 ± 10.7	6.8 ± 2.8	6.4 ± 1.8	6.2 ± 0.0	47
T1DM	76423578	8.2 ± 10.7	6.2 ± 8.2	5.1 ± 3.3	4.7 ± 0.0	321

To identify τ from experimental data, suitable sequences must be found using the design presented in Fig. 6.1, where an interval contains a meal input, begins 30 min before and ends 4 h after the meal. An example set of intervals that consists of five sequences of BGSM and CGM samples after a meal of 50 ± 2 g CHO for the TNDM subject is shown in Fig. C.5 on page 207. A total number of m sequences are found in the TNDM and T1DM subjects (last column in Table 6.3). In both T2DM subjects, not enough BGSM records are available and thus, the identification could not be performed. The process itself is fulfilled in the same manner as for the simulation. That means, τ is identified taking into account 1, 10, 25, and m randomly chosen intervals taken from m available sequences. All optimizations are repeated $r = 25$ times to evaluate the repeatability accuracy. Results are reported in Table 6.3 for each subject. It can be seen that the standard deviations of the identified values decrease for a growing number of sequences. Considering $m = 25$, the delay can be estimated within a ±6 min range. Taking into account all available data, $\hat{\tau}$ is approx. 20 min in the TNDM subject, which is higher than in the T1DM patients, for which $\hat{\tau}$ is between 4.7 and 15.1 min.

When taking into account that the records were taken under real-life conditions, including measurement errors and other unknown disturbances, it can be stated that the identified values are within the physiological range and can be estimated with precision. Note that errors of only a few minutes are not important here as the sampling time of the CGM sensor is 5 min. However, an identified delay of up to 20 min may affect a subsequent blood glucose estimation process (Section 6.3). Furthermore, repeatability accuracy improves when considering more and more sequences. Hence, it can be assumed that τ can be adapted to a particular subject during an observation period of a few days.

Identification of the Basal Glucose Concentration. The basal glucose concentration G^{b} is the long-term steady-state glucose level. It is typically determined by clinicians in the morning after an overnight fast. In a daily-life scenario, periods of fasting are seldom. Hence, G^{b} is identified on the one hand from the mean of the overall CGM data and otherwise from CGM data obtained in the morning hours, between 07:00 and 08:00. Furthermore, it is identified from steady-state sequences using an optimization algorithm. A steady-state interval is here defined by a duration of at least 2 h, no meal or insulin input, and a maximum deviation in the CGM signal of 25 mg dL^{-1}. No such sequences could be found in diabetic patients, hence, the identification is only performed for the TNDM subject.

Table 6.4: Basal glucose concentration G^{b}, determined from n overall CGM data, n CGM data points recorded between 07:00 and 08:00 in the morning, and identified from m steady-state sequences.

Group	Subject	Overall		07:00-08:00		Identified	
		n	Mean ± Std. ($\mathrm{mg\,dL^{-1}}$)	n	Mean ± Std. ($\mathrm{mg\,dL^{-1}}$)	m	Mean ± Std. ($\mathrm{mg\,dL^{-1}}$)
TNDM	814	18 747	92.9 ± 18.2	795	87.3 ± 10.5	67	86.8 ± 9.7
T2DM	126	3303	144.8 ± 40.5	135	127.6 ± 22.4		–
T2DM	385	4716	172.4 ± 34.4	203	146.2 ± 23.0		–
T1DM	20330028	25 181	115.9 ± 45.3	1088	113.6 ± 35.4		–
T1DM	39561557	15 776	130.0 ± 49.9	637	127.5 ± 46.5		–
T1DM	76423578	54 415	133.6 ± 44.8	2218	121.6 ± 20.6		–

The results are reported in Table 6.4 for each subject, where n is the number of CGM records and m is the number of sequences from which means and standard deviations are computed. The mean values are the lowest in the TNDM subject, also having the smallest standard deviations. Across all test cases, the values deviate from each other by less than $7\,\mathrm{mg\,dL^{-1}}$. In the morning and during steady-state, standard deviations are almost halved, compared to the overall values. In the T2DM diabetics means are the highest with also higher standard deviations. In the T1DM patients, means during fasting are within 113.6-127.5 $\mathrm{mg\,dL^{-1}}$, which conforms to the desired target value of $120\,\mathrm{mg\,dL^{-1}}$ for most diabetic patients. Across all subjects, basal glucose during fasting has a lower variability than in the overall case. However, it cannot be determined with confidence from the obtained CGM records, particularly in the T1DM patients. Hence, for all subjects, parameter G^{b} is fixed to the mean CGM value computed for the morning hours.

Identification of the Sensitive Parameters. The identification of the remaining sensitive parameters is fulfilled for several types of sequences, including single meal intervals of 4.5 h duration (Fig. 6.1) and 12 h and 24 h sequences in three subjects, one in each group. Optimization not only from a single measurement sequence but also across several intervals would allow finding a global parameter estimate that satisfies the individual glucose excursions in a long-term manner. Another opportunity would be to average over multiple parameter vectors, each identified from a single sequence, in order to determine a kind of average model of the subject under investigation.

From all sequences mentioned above, meal ingestion, as well as basal and bolus insulin administration, are extracted. From that, simulation inputs are generated by linear interpolation. The previously identified variables are set to their new values. In addition to the considered sensitive parameter set, the basal insulin infusion rate IIR^{b} is adjusted in order to meet the T1DM patient's needs, too (nominal $IIR^{\mathrm{b}} = 1.18\,\mathrm{U\,h^{-1}}$). For this, (4.43) is rearranged for $I_{\mathrm{P}}^{\mathrm{b}}$ (open-loop design) to allow IIR^{b} to be the set point. Since the infusion rate is time-dependent, but the model allows only time-independent parameters, IIR^{b} is set to the daily mean (Fig. C.1). A set of parameters is identified for each out of $r = 10$ different sequences for each subject.

Table 6.5: Mean and standard deviation of MARD (%) between CGM data and simulated model outputs for $r = 10$ randomly chosen sequences. Simulation outputs are generated by the nominal, the identified, and the averaged model, which was further validated on r full 24 h intervals.

Group	Subject	Model			Validation
		Nominal (%)	Identified (%)	Averaged (%)	(%)
TNDM	814	24.38 ± 10.07	7.81 ± 3.13	13.06 ± 5.11	15.30 ± 9.53
T2DM	385	28.17 ± 7.80	14.93 ± 6.70	18.05 ± 7.50	27.12 ± 11.39
T1DM	76423578	70.95 ± 31.31	16.16 ± 3.52	27.87 ± 10.34	38.43 ± 15.71

For validation, errors (6.1) between experimental CGM and simulated CG data are computed. EGA (Fig. 3.8) is used to assess the clinical relevance of the results. Moreover, identified parameter sets are compared to the empirical distribution computed for the 100 generated virtual subjects (Fig. A.2). Furthermore, the average parameter set for each subject is computed and validated on r further full-day intervals to assess general applicability.

Errors for the three subjects are reported in Table 6.5. In diabetics, MARD is higher with a higher standard deviation, too. In all subjects, the MARD of the averaged model has at least halved, compared to the nominal model error. Moreover, it is obvious that the averaged model performs weaker than the identified single models. MARD increases in all subjects and is between 13.1 % and 27.9 %. The performance further deteriorates for the 24 h validation sequences. However, the average model remains superior compared to the nominal simulation.

The identified parameter sets compared to the nominal virtual patients are depicted in Fig. C.6 on page 209. From that, it is obvious that parameters cannot be identified with precision as the errors for most values are larger than the assumed distribution of the nominal parameters.

Exemplarily, the time courses of three 24 h validation sequences are illustrated in Fig. 6.7, one for each subject. The plots show the measured BGSM and CGM data, as well as the nominal, and the averaged identified model outputs for the TNDM (top panel), a T2DM (middle), and a T1DM subject (bottom panel). Colored markers denote meal and bolus insulin time points, respectively. The best results are visible for the TNDM subject, as the simulations adequately represent most of the postprandial glucose excursions. Furthermore, basal glucose concentration matches the CGM signal obtained at night and early hours. MARD for this sequence is reduced to 9.2 %. For the diabetic subjects, particularly the T2DM one, simulation follows the glucose signal in a global scope but neither represents faster glucose changes nor the measured amplitudes. Despite that, For this interval, MARD is calculated as 10.9 %. In the T1DM subject, the large mismatch of the nominal model is noticeable at first, which is mainly due to a wrong assumption of the basal insulin infusion rate ($IIR^{\mathrm{b}} = 1.18\,\mathrm{U\,h^{-1}}$). Subject P7642357 receives insulin with a rate of 0.2-0.5 $\mathrm{U\,h^{-1}}$ in the morning (Fig. C.1), which is not enough to maintain steady-state in simulation, and thus, glucose concentration rises slowly. Adjusting to the daily mean ($IIR^{\mathrm{b}} = 0.48\,\mathrm{U\,h^{-1}}$) leads to acceptable steady-state behavior at night (00:00-07:00). The MARD could be reduced from 79.1 % to 22.8 %.

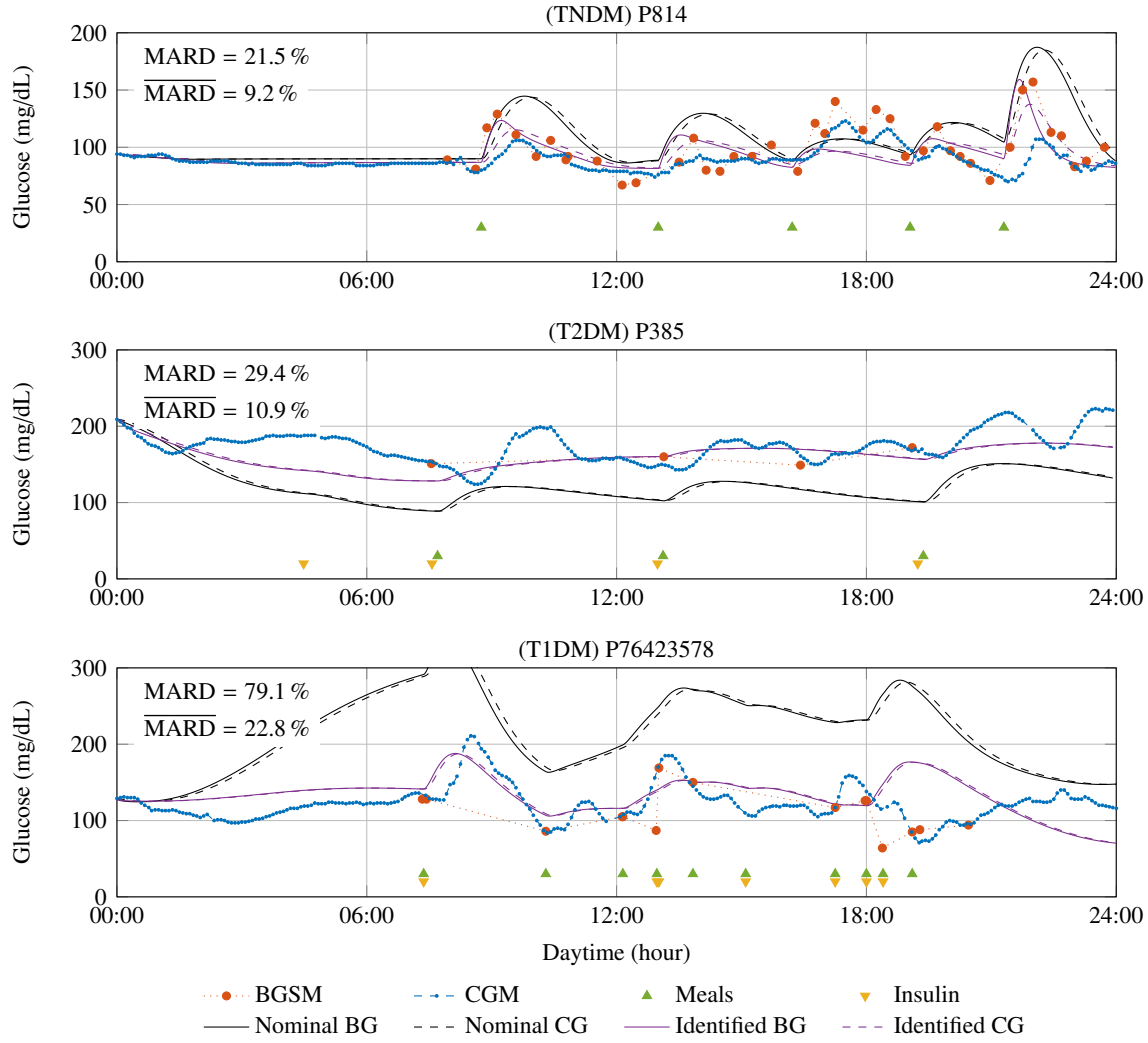

Figure 6.7: Time course of experimental BGSM (red markers) and CGM (blue markers) data versus nominal model outputs (BG in solid black, CG in dashed black) and identified model outputs (BG in solid purple, CG in dashed purple). Meals (green triangles) and bolus insulin injections (yellow triangles) at discrete-time points are inputs to both, experiment and simulation. Data is shown for 24 h validation sequences in TNDM (top), T2DM (middle), and T1DM (bottom panel). Error between CGM and CG is given for the nominal (MARD) and for the identified ($\overline{\text{MARD}}$) model. Note that the basal insulin rate for P76423578 (Fig. C.1) is not printed here for better visibility.

Finally, EGA is shown in Fig. C.7 on page 210. The plots show the reference experimental CGM data against simulated continuous glucose levels for the nominal model (black dots), the optimized models for each sequence they were identified from (blue squares), and the mean model for the same sequences (red triangles), all shown on the left side. The right side depicts the performance of the nominal (black dots) and the mean identified model (green triangles) for all validation sequences.
For the TNDM subject (top subplots), recorded values are concentrated between 75 and 140 mg dL^{-1}. The nominal model overestimates the reference measurements (46 % respectively 50 % in zones A and B), whereas the identified model results lie, for most values, within zone A (95.6 %), close to the

diagonal. For the averaged model, 98 % are within A and B. For the validation intervals (upper right subplot), the number of data pairs within zone A improves from 68 % to 77 %, mainly shifting from zone B (25 % to 17 %) when comparing the nominal and the mean identified model. The number of values within zone D decreased only slightly (6.5 % to 5.8 %).
In the T2DM subject (middle subplots), almost all of the nominal simulation data is within zones A and B (30 % respectively 68 %), a few values also reaching zones C and D. The mean identified model increases the number of values within zone A up to 62 %. The nominal model shows almost the same behavior for the validation sequences (middle right subplot) (98 % within zones A and B). Although the number of values in zone A increases from 33 % to 48 %, there are also some outliers in zones C, D, and E (in sum 6 %).
In the T1DM subject (bottom subplots), the nominal model strongly overestimates glucose measurements, mainly due to the mismatch of the basal insulin infusion rate. Only 66 % of CG data is within zones A and B, 32 % within zone C. Model adaptation significantly improves simulation results to 55 % and 41 % within zones A and B, respectively, for the averaged model. For the validation intervals (bottom right subplot) more than half of the data is within zone C (54 %) and only 15 % and 28 % in zones A and B, respectively. Optimization significantly improved the results, leading to 91 % within zones A and B.
Comparing the three subjects with each other, the averaged model shows comparable results for the validation sequences with 94 %, 94 %, and 91 % of simulated CG values within zones A and B, for TNDM, T2DM, and T1DM, respectively. However, the model performs best in the non-diabetic case since 77 % of all values lie within zone A. For each subject there exist 6-9 % outliers within zones C-E, which could not be reduced by the identified models.

In summary, parameters can be determined by identification from single meals of 4.5 h duration. However, a consistent adaptation with precision is impossible as the postprandial glucose behavior is mainly determined by the type of the ingested meal. Hence, one gets a kind of meal-dependent parameter set that is not valid in a global scope. Moreover, an identification by 24 h intervals leads to parameter sets that allow the simulated CG output to smoothly follow the glucose trajectory over the whole day, but its capability to adequately represent specific postprandial glucose excursions is limited. This behavior is apparent in Fig. 6.7, particularly for the two diabetic subjects. Overall, the MARD between experimental CGM data and simulated CG pairs could be reduced significantly. Furthermore, EGA shows that over 90 % of all data points lie within the clinically relevant zones.

The previous analyses referred to the CGM signal only, since it is available as a quasi-continuous measurement variable. To further improve the model capabilities to correctly determine the current glucose concentration online state estimation is a suitable approach since it allows updates of the model states during run-time. It also enables the estimation of other non-measurable variables.

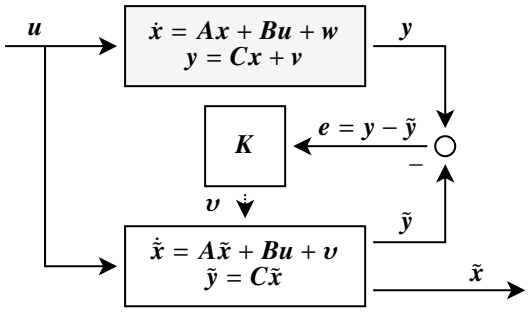

Figure 6.8: Structure of the linear Kalman filter for estimating state $\tilde{\boldsymbol{x}}$.

6.3 Online State Estimation

Online state estimation aims to determine the current states of the system during run-time. For this purpose, an observer must be designed and the desired states must be observable by measurements (Section 5.2.7).

6.3.1 Derivation of the Model-based Observer

Model-based state observation aims to reconstruct the internal state vector $\tilde{\boldsymbol{x}} \in \mathbb{R}^N$, $\tilde{\boldsymbol{x}}(0) = \tilde{\boldsymbol{x}}_0$ using a model of the underlying system. For that, the same input vector $\boldsymbol{u} \in \mathbb{R}^M$ must be applied to the system, and likewise, the simulated and experimental measurements $\boldsymbol{y} \in \mathbb{R}^{O<N}$ must be taken. The internal states can then be corrected by the feedback of the error between measured and simulated outputs $\boldsymbol{e} = \boldsymbol{y} - \tilde{\boldsymbol{y}}$ using a suitable observer matrix $\boldsymbol{K}$ (Fig. 6.8). Taking the linear system (5.29), one gets the state-space form of the observer:

$$\begin{cases} \dot{\tilde{\boldsymbol{x}}} = \boldsymbol{A}\tilde{\boldsymbol{x}} + \boldsymbol{B}\boldsymbol{u} + \boldsymbol{K}\left(\boldsymbol{y} - \tilde{\boldsymbol{y}}\right), \\ \tilde{\boldsymbol{y}} = \boldsymbol{C}\tilde{\boldsymbol{x}}. \end{cases} \tag{6.3}$$

The basic concepts and assumptions of the Kalman filter (KF) are introduced in the following paragraph. Since the model is continuous-time, nonlinear, and has colored measurement noise, some enhancements succeed. An elaborated derivation of all equations, modifications, and generalizations can be found in, e. g., Simon (2006) and Grewal et al. (2008).

The Linear Kalman Filter. The deterministic model (5.29) is extended by the stochastic disturbances $\boldsymbol{w}$ and $\boldsymbol{v}$, which leads to

$$\begin{cases} \dot{\boldsymbol{x}} = \boldsymbol{A}\boldsymbol{x} + \boldsymbol{B}\boldsymbol{u} + \boldsymbol{w}, \\ \boldsymbol{y} = \boldsymbol{C}\boldsymbol{x} + \boldsymbol{v}, \end{cases} \tag{6.4}$$

where $\boldsymbol{w}$ and $\boldsymbol{v}$ can be interpreted as process and measurement noises, respectively. Since filters are typically implemented on a digital platform, the system dynamics are often discretized and then a

discrete-time KF can be applied. Thus, the filter equations are first derived for the discrete-time case, and then some modifications for continuous-time systems are introduced.

The continuous-time system (6.4) is discretized as follows:

$$\begin{cases} \boldsymbol{x}_k = \boldsymbol{A}_d \boldsymbol{x}_{k-1} + \boldsymbol{B}_d \boldsymbol{u}_{k-1} + \boldsymbol{w}_{k-1}, \\ \boldsymbol{y}_k = \boldsymbol{C}_d \boldsymbol{x}_k + \boldsymbol{v}_k, \end{cases} \tag{6.5}$$

where $\boldsymbol{A}_d$, $\boldsymbol{B}_d$, and $\boldsymbol{C}_d$ are the discrete-time state transition, input, and output matrices, respectively. Further, $\boldsymbol{x}_k$ and $\boldsymbol{y}_k$ are the state and output vectors at a discrete-time point $k \in \mathbb{N}$ with $\boldsymbol{x}_k = \boldsymbol{x}(k) = \boldsymbol{x}(t = k \cdot \Delta T)$ and sampling time ΔT.

The stochastic processes can be described by their probability density or distribution function. It is assumed that these processes are normally distributed (4.70), white, uncorrelated, and have zero mean. Thus, the following statements hold:

$$\begin{aligned} \boldsymbol{w} &\sim \mathcal{N}(0, \boldsymbol{Q}_k), \\ \boldsymbol{v} &\sim \mathcal{N}(0, \boldsymbol{R}_k), \\ \mathrm{E}\left\{\boldsymbol{w}_k \cdot \boldsymbol{w}_j^\top\right\} &= \boldsymbol{Q}_k \cdot \delta_{k-j}, \\ \mathrm{E}\left\{\boldsymbol{v}_k \cdot \boldsymbol{v}_j^\top\right\} &= \boldsymbol{R}_k \cdot \delta_{k-j}, \\ \mathrm{E}\left\{\boldsymbol{v}_k \cdot \boldsymbol{w}_j^\top\right\} &= \boldsymbol{0}, \end{aligned} \tag{6.6}$$

where $\boldsymbol{Q}_k$ and $\boldsymbol{R}_k$ are known covariance matrices of process respectively measurement noise and δ_{k-j} is the Kronecker delta function, i. e., $\delta_{k-j} = 1$ if $k = j$ and $\delta_{k-j} = 0$ if $k \neq j$.

The goal is now to derive an estimate $\tilde{\boldsymbol{x}}_k$ of the state $\boldsymbol{x}_k$ based on the propagation of the dynamical system and noisy measurements $\boldsymbol{y}_k$. For that, the *a priori* state vector, i. e., the estimated state at time k based on $k-1$ measurements is introduced with $\tilde{\boldsymbol{x}}_k^-$, the covariance of the estimation error with $\boldsymbol{P}_k^-$. The *a posteriori* state vector, i. e., the corrected state after the measurement $\boldsymbol{y}_k$ was taken is denoted by $\boldsymbol{x}_k^+$ and its covariance matrix with $\boldsymbol{P}_k^+$.

The estimate at time k is calculated as

$$\begin{aligned} \tilde{\boldsymbol{x}}_k^- &= \mathrm{E}\left\{\boldsymbol{x}_k \mid \boldsymbol{y}_1, \boldsymbol{y}_2, \ldots, \boldsymbol{y}_{k-1}\right\}, \\ &= \mathrm{E}\left\{\boldsymbol{A}_d \boldsymbol{x}_{k-1} + \boldsymbol{B}_d \boldsymbol{u}_{k-1} + \boldsymbol{w}_{k-1}\right\}, \\ &= \boldsymbol{A}_d \tilde{\boldsymbol{x}}_{k-1}^+ + \boldsymbol{B}_d \boldsymbol{u}_{k-1}. \end{aligned} \tag{6.7}$$

That means the *a priori* estimate is the conditional expectation of $\boldsymbol{x}_k$, based on all measurements before, but not including time k. From the propagation of the mean of $\boldsymbol{x}_k$ over time, given by (6.5), the term (6.7) can be derived, i. e., the *a priori* estimate at time k depends on the *a posteriori* estimate $\boldsymbol{x}_{k-1}^+$ at the last time step $k-1$. Quantity $\boldsymbol{x}_k^+$ is the conditional expectation of $\boldsymbol{x}_k$ up to and including

measurement $\boldsymbol{y}_k$ and is given by

$$\tilde{\boldsymbol{x}}_k^+ = \mathrm{E}\left\{\boldsymbol{x}_k \mid \boldsymbol{y}_1, \boldsymbol{y}_2, \ldots, \boldsymbol{y}_k\right\}, \tag{6.8}$$

$$\tilde{\boldsymbol{x}}_0^+ = \mathrm{E}\left\{\boldsymbol{x}_0\right\}, \tag{6.9}$$

where $\tilde{\boldsymbol{x}}_0^+$ is the initial estimate at $k = 0$ when no measurements are available yet. The same holds for the update equation for $\boldsymbol{P}$, the covariance of the estimation error. The uncertainty $\boldsymbol{P}_0^+$ in the initial guess is given by

$$\boldsymbol{P}_0^+ = \mathrm{E}\left\{\left(\boldsymbol{x}_0 - \tilde{\boldsymbol{x}}_0^+\right)\left(\boldsymbol{x}_0 - \tilde{\boldsymbol{x}}_0^+\right)^\top\right\}. \tag{6.10}$$

From the propagation of the covariance of a state of a discrete-time system (Simon 2006, Ch. 4.1), the time update for the covariance $\boldsymbol{P}$ can be derived using Eqs. (6.5) and (6.7), which leads to:

$$\begin{aligned}
\boldsymbol{P}_k^- &= \mathrm{E}\left\{\left(\boldsymbol{x}_k - \tilde{\boldsymbol{x}}_k^-\right)\left(\boldsymbol{x}_k - \tilde{\boldsymbol{x}}_k^-\right)^\top\right\}, \\
&= \boldsymbol{A}_d \cdot \mathrm{E}\left\{\left(\boldsymbol{x}_{k-1} - \tilde{\boldsymbol{x}}_{k-1}^+\right)\left(\boldsymbol{x}_{k-1} - \tilde{\boldsymbol{x}}_{k-1}^+\right)^\top\right\} \cdot \boldsymbol{A}_d^\top + \mathrm{E}\left\{\boldsymbol{w}_{k-1} \cdot \boldsymbol{w}_{k-1}^\top\right\}, \\
&= \boldsymbol{A}_d \boldsymbol{P}_{k-1}^+ \boldsymbol{A}_d^\top + \boldsymbol{Q}_{k-1}.
\end{aligned} \tag{6.11}$$

For each iteration step $k := k + 1$, the observer gain $\boldsymbol{K}_k$ is determined along with the correction of the state estimate and its covariance:

$$\boldsymbol{K}_k = \boldsymbol{P}_k^- \boldsymbol{C}_d^\top \left(\boldsymbol{C}_d \boldsymbol{P}_k^- \boldsymbol{C}_d^\top + \boldsymbol{R}_k\right)^{-1}, \tag{6.12}$$

$$\tilde{\boldsymbol{x}}_k^+ = \tilde{\boldsymbol{x}}_k^- + \boldsymbol{K}_k\left[\boldsymbol{y}_k - \boldsymbol{C}_d \tilde{\boldsymbol{x}}_k^-\right], \tag{6.13}$$

$$\boldsymbol{P}_k^+ = \left(\boldsymbol{I} - \boldsymbol{K}_k \boldsymbol{C}_d\right) \boldsymbol{P}_k^- \left(\boldsymbol{I} - \boldsymbol{K}_k \boldsymbol{C}_d\right)^\top + \boldsymbol{K}_k \boldsymbol{R}_k \boldsymbol{K}_k^\top, \tag{6.14}$$

with $\boldsymbol{I}$ being the unit matrix of appropriate dimension. These are known as the measurement-update equations of $\tilde{\boldsymbol{x}}_k$ and $\boldsymbol{P}_k$. The Kalman gain in (6.12) is optimal under the conditions given in (6.6). It is optimal in the sense that the estimation error has not only a zero mean but also a minimum variance. The Kalman filter is therefore also referred to as an optimal filter.

Incorporating Colored Measurement Noise. To derive the KF process and measurement noise were both supposed to be white. In the case of colored measurement noise, the system and output equations are again given by (6.5). However, the discrete noise process $\boldsymbol{v}_k$ itself is the output of the linear system

$$\boldsymbol{v}_k = \boldsymbol{\psi}_d \boldsymbol{v}_{k-1} + \boldsymbol{\eta}_{k-1}, \tag{6.15}$$

with the statistical properties:

$$\begin{aligned} \boldsymbol{w}_k &\sim \mathcal{N}(0,\, \boldsymbol{Q}_k), \\ \boldsymbol{\eta}_k &\sim \mathcal{N}(0,\, \boldsymbol{Q}_{k,\eta}), \\ \mathrm{E}\left\{\boldsymbol{w}_k \cdot \boldsymbol{w}_j^\top\right\} &= \boldsymbol{Q}_k \cdot \delta_{k-j}, \\ \mathrm{E}\left\{\boldsymbol{\eta}_k \cdot \boldsymbol{\eta}_j^\top\right\} &= \boldsymbol{R}_{k,\eta} \cdot \delta_{k-j}, \\ \mathrm{E}\left\{\boldsymbol{w}_k \cdot \boldsymbol{\eta}_j^\top\right\} &= \boldsymbol{0}, \end{aligned} \tag{6.16}$$

where $\boldsymbol{\psi}_d$ is the constant system matrix of the noise process driven by the zero-mean, white, and uncorrelated noise term $\boldsymbol{\eta}_k$ with covariance matrix $\boldsymbol{Q}_{k,\eta}$. To solve this problem, $\boldsymbol{v}_k$ can be incorporated into the system as an augmented state as shown in Bryson et al. (1965) for continuous-time systems. This leads to system

$$\widehat{\Sigma}: \begin{cases} \hat{\boldsymbol{x}}_k = \begin{bmatrix} \boldsymbol{x}_k \\ \boldsymbol{v}_k \end{bmatrix} = \begin{bmatrix} \boldsymbol{A}_d & \boldsymbol{0} \\ \boldsymbol{0} & \boldsymbol{\psi}_d \end{bmatrix} \begin{bmatrix} \boldsymbol{x}_{k-1} \\ \boldsymbol{v}_{k-1} \end{bmatrix} + \begin{bmatrix} \boldsymbol{B}_d & \boldsymbol{0} \\ \boldsymbol{0} & \boldsymbol{0} \end{bmatrix} \begin{bmatrix} \boldsymbol{u}_{k-1} \\ \boldsymbol{0} \end{bmatrix} + \begin{bmatrix} \boldsymbol{w}_{k-1} \\ \boldsymbol{\eta}_{k-1} \end{bmatrix}, \\ \boldsymbol{y}_k = \begin{bmatrix} \boldsymbol{C}_d & \boldsymbol{I} \end{bmatrix} \begin{bmatrix} \boldsymbol{x}_k \\ \boldsymbol{v}_k \end{bmatrix} + \boldsymbol{0}, \end{cases} \tag{6.17}$$

which can be written as

$$\begin{cases} \hat{\boldsymbol{x}}_k = \hat{\boldsymbol{A}}_d \hat{\boldsymbol{x}}_{k-1} + \hat{\boldsymbol{B}}_d \hat{\boldsymbol{u}}_{k-1} + \hat{\boldsymbol{w}}_{k-1}, \\ \boldsymbol{y}_k = \hat{\boldsymbol{C}}_d \hat{\boldsymbol{x}}_k + \hat{\boldsymbol{v}}_k. \end{cases} \tag{6.18}$$

The augmented system is equivalent to the original system but with modified state $\hat{\boldsymbol{x}}$, transition matrix $\hat{\boldsymbol{A}}_d$, input matrix $\hat{\boldsymbol{B}}_d$, input $\hat{\boldsymbol{u}}$, process noise $\hat{\boldsymbol{w}}$, output matrix $\hat{\boldsymbol{C}}_d$, and measurement noise $\hat{\boldsymbol{v}}$. Moreover, the covariance matrices of process and measurement noise are computed by

$$\begin{aligned} \mathrm{E}\left\{\hat{\boldsymbol{w}}_k \cdot \hat{\boldsymbol{w}}_k^\top\right\} &= \mathrm{E}\left\{\begin{bmatrix} \boldsymbol{w}_k \\ \boldsymbol{\eta}_k \end{bmatrix} \cdot \begin{bmatrix} \boldsymbol{w}_k^\top & \boldsymbol{\eta}_k^\top \end{bmatrix}\right\} \\ &= \begin{bmatrix} \boldsymbol{Q}_k & \boldsymbol{0} \\ \boldsymbol{0} & \boldsymbol{Q}_{k,\eta} \end{bmatrix}, \end{aligned} \tag{6.19}$$

$$\mathrm{E}\left\{\hat{\boldsymbol{v}}_k \cdot \hat{\boldsymbol{v}}_k^\top\right\} = \boldsymbol{0}. \tag{6.20}$$

Extension to Continuous-time Systems. Since the model of glucose metabolism is continuous-time but measurements are only available at discrete-time points, a hybrid approach is appropriate (Simon 2006, Ch. 13.2.2), which avoids the discretization step in (6.5). Extending (6.4) with the

continuous-time process noise $\boldsymbol{w}$ and discrete-time measurement noise $\boldsymbol{v}_k$, one gets

$$\begin{cases} \dot{\boldsymbol{x}} = \boldsymbol{A}\boldsymbol{x} + \boldsymbol{B}\boldsymbol{u} + \boldsymbol{w}, \\ \boldsymbol{y}_k = \boldsymbol{C}\boldsymbol{x}_k + \boldsymbol{v}_k, \end{cases} \tag{6.21}$$

where $\boldsymbol{y}_k$ and $\boldsymbol{x}_k$ are the output respectively state vectors at time k. Vector $\boldsymbol{x}_k$ can be derived by solving the continuous-time equation with an integration technique such as the Runge-Kutta method. Process noise $\boldsymbol{w}(t)$ is continuous-time with covariance $\boldsymbol{Q}$ and measurement noise $\boldsymbol{v}_k$ is discrete-time with covariance $\boldsymbol{R}_k$:

$$\begin{aligned} \boldsymbol{w}(t) &\sim \mathcal{N}(0, \boldsymbol{Q}), \\ \boldsymbol{v}_k &\sim \mathcal{N}(0, \boldsymbol{R}_k), \end{aligned} \tag{6.22}$$

The filter is initialized using Eqs. (6.9) and (6.10). For $k = 1, 2, \ldots$, the state estimate $\tilde{\boldsymbol{x}}$ is propagated from $\tilde{\boldsymbol{x}}_{k-1}^{+}$ to $\tilde{\boldsymbol{x}}_k^{-}$ by

$$\dot{\tilde{\boldsymbol{x}}} = \boldsymbol{A}\tilde{\boldsymbol{x}} + \boldsymbol{B}\boldsymbol{u} + \boldsymbol{w}_0, \tag{6.23}$$

with $\boldsymbol{w}_0$ being the nominal process noise, that is $\boldsymbol{w}_0(t) = 0$. At time k, the measurement noise is incorporated as given in (6.12)-(6.14).

Extension to Nonlinear Systems. The extended Kalman filter is based on a linearization of a nonlinear system in each iteration step. For that, a linearization around the last estimate is performed before prediction and before correction, respectively; and the Kalman filter estimate is based on that linearized system.

Combining the nonlinear system (5.30) with the hybrid filter approach in (6.21) gives

$$\begin{cases} \dot{\boldsymbol{x}} = \mathbf{f}\,(t, \boldsymbol{x}, \boldsymbol{u}, \boldsymbol{p}) + \boldsymbol{w}, \\ \boldsymbol{y}_k = \mathbf{g}\,(k, \boldsymbol{x}_k, \boldsymbol{p}) + \boldsymbol{v}_k, \end{cases} \tag{6.24}$$

with the same statistical properties as defined in (6.22). The propagation of states is continuous-time, whereas the output equation is discrete-time. Moreover, the same initialization as given in Eqs. (6.9) and (6.10) can be used. To linearize the system, the partial derivatives of state function $\mathbf{f}$ and output function $\mathbf{g}$ are calculated as

$$\begin{aligned} \boldsymbol{F} &= \left.\frac{\partial \mathbf{f}}{\partial \boldsymbol{x}}\right|_{\tilde{\boldsymbol{x}}}, \\ \boldsymbol{G} &= \left.\frac{\partial \mathbf{g}}{\partial \boldsymbol{x}}\right|_{\tilde{\boldsymbol{x}}}, \end{aligned} \tag{6.25}$$

leading to the linearized system and output matrices $\boldsymbol{F}$ and $\boldsymbol{G}$. However, these must now be recomputed at each time step k, resulting in the time-varying matrices $\boldsymbol{F}_k$ and $\boldsymbol{G}_k$. The remaining filter equations

Algorithm 4 Hybrid extended Kalman filter

Require: $\tilde{\boldsymbol{x}}_0^+, P_0^+$
  for $k = 1, 2, \ldots$ **do**
    Integrate $\dot{\tilde{\boldsymbol{x}}}$ from time $(k-1)^+$ to k^- using $\dot{\tilde{\boldsymbol{x}}} = \mathbf{f}\left(t, \tilde{\boldsymbol{x}}, \boldsymbol{u}, \boldsymbol{p}\right)$ resulting in $\tilde{\boldsymbol{x}} = \tilde{\boldsymbol{x}}_k^-$ (6.23)
    Estimate $\boldsymbol{P}_k^- = \boldsymbol{F}_k \boldsymbol{P}_{k-1}^+ \boldsymbol{F}_k^\top + \boldsymbol{Q}$ using Eqs. (6.11) and (6.25)
    Incorporate measurement $\boldsymbol{y}_k$ into state and covariance estimation:
    Compute Kalman gain: $\boldsymbol{K}_k = \boldsymbol{P}_k^- \boldsymbol{G}_k^\top \left(\boldsymbol{G}_k \boldsymbol{P}_k^- \boldsymbol{G}_k^\top + \boldsymbol{R}_k\right)^{-1}$ using (6.12)
    Correct state: $\tilde{\boldsymbol{x}}_k^+ = \tilde{\boldsymbol{x}}_k^- + \boldsymbol{K}_k \left[\boldsymbol{y}_k - \mathbf{g}\left(k, \tilde{\boldsymbol{x}}_k^-, \boldsymbol{u}, \boldsymbol{p}\right)\right]$ using (6.13)
    Correct covariance: $\boldsymbol{P}_k^+ = \left(\boldsymbol{I} - \boldsymbol{K}_k \boldsymbol{G}_k\right) \boldsymbol{P}_k^- \left(\boldsymbol{I} - \boldsymbol{K}_k \boldsymbol{G}_k\right)^\top + \boldsymbol{K}_k \boldsymbol{R}_k \boldsymbol{K}_k^\top$ using Eqs. (6.14) and (6.25)
  end for

correspond to those of the linear filter as given in (6.11) and (6.12)-(6.14), where the constant matrices $\boldsymbol{A}_d$ and $\boldsymbol{C}_d$ are replaced by $\boldsymbol{F}_k$ and $\boldsymbol{G}_k$, respectively. Furthermore, the linear model output $\boldsymbol{C}_d \tilde{\boldsymbol{x}}_k^-$ is substituted by the nonlinear output equation $\mathbf{g}\left(k, \tilde{\boldsymbol{x}}_k^-, \boldsymbol{u}, \boldsymbol{p}\right)$. The whole procedure is summarized in Algorithm 4.

EKF for Blood Glucose Estimation from CGM Data. Now, the goal is to continuously estimate the current blood glucose concentration based on glucose measurements within the interstitial fluid using a CGM device. Although blood glucose measurements can and should be performed several times a day, model-based estimation of this quantity would allow continuous BG monitoring which enriches the sparse samples.

Sections 5.2.2 and 5.2.4 introduced the concept of observability and identifiability. Results in Section 5.2.7 showed that it is practically not possible to estimate all states or parameters with precision from observations of the glucose concentration in the subcutaneous space, G_I. Moreover, the analysis was based on an ideal system, i. e., without considering any measurement noise, which is indeed induced by CGM sensors (Section 4.5.2). However, an estimation of the blood glucose level G from CGM data should be possible. Hence, two states are estimated which have shown to be observable (Table 5.3): glucose masses in plasma $\tilde{G}_\mathrm{P}$ and in the interstitial fluid $\tilde{G}_\mathrm{Sc}$, summarized into vector $\tilde{\boldsymbol{x}}$. The estimated output vector $\tilde{\boldsymbol{y}}$ consists of the glucose concentrations in the blood, $\tilde{G}$, and the interstitial fluid, $\tilde{G}_\mathrm{I}$, respectively.

The nonlinear set of system equations (A.1) and the linear output equation (A.2) are used to design the observer. Thus, linearization is needed only for calculating the state covariance $\boldsymbol{P}_k^-$. To update the covariance $\boldsymbol{P}_k^+$, the linear filter approach (6.14) is sufficient using the constant output matrix $\boldsymbol{C}$.
The filter is initialized with a randomly chosen state estimate $\tilde{\boldsymbol{x}}_0 = \nu$, with $\nu \sim \mathcal{N}(\boldsymbol{x}_0, \sqrt{\boldsymbol{x}_0})$ and $\boldsymbol{x}_0$ the nominal initial state. Furthermore, appropriate initial state uncertainty $\boldsymbol{P}_0^+$ and process noise covariance matrices $\boldsymbol{Q}$ were both defined for each group (Table C.3).
Meal ingestion $u_\mathrm{G}^\mathrm{oral}$ and insulin administration u_I^sc are the typical inputs to the system. The scalar CGM measurement is $y = G_\mathrm{CG}$, its covariance is assumed to be constant with $R = \left(10\,\mathrm{mg\,dL^{-1}}\right)^2$.
The filter runs with a sampling time of $\Delta T = 1\,\mathrm{min}$. States are calculated using a Runge-Kutta

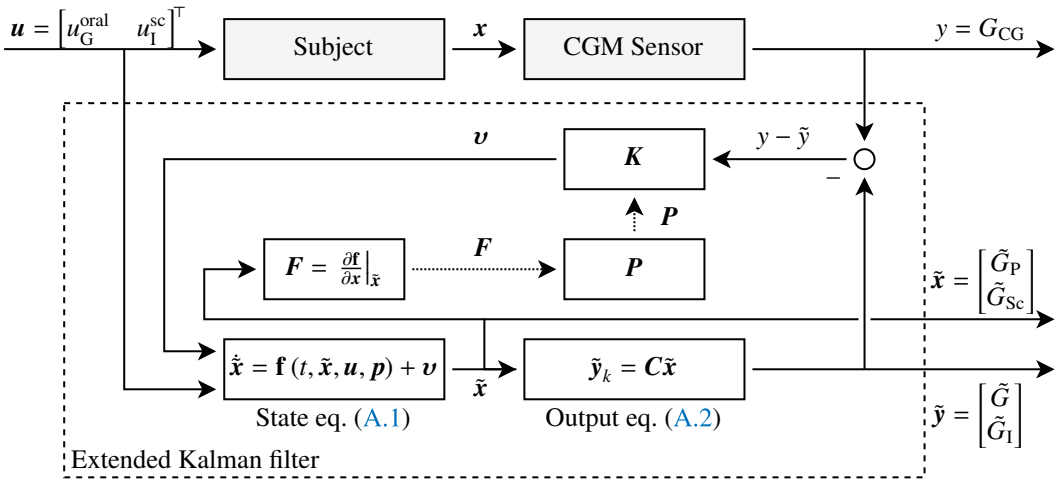

Figure 6.9: Structure of the extended Kalman filter for continuous glucose estimation from CGM data.

integration method, whereas the measurements are sampled discretely at 5 min. Between the samples, no information is available about the covariance, hence, $\boldsymbol{P}_k^+ = \infty \boldsymbol{I}$, which can be achieved by arbitrarily large numbers on the diagonal. Figure 6.9 summarizes the model-based estimation approach. Moreover, missing CGM data could occur during the experiment due to sensor connection faults. In these cases, the observer performs a prediction of the current state, which is described in the next paragraph.

Short-term Prediction. The EKF is based on an update of the current state using the model equations and a correction step using measurement data, fulfilled in each time step. In case of a missing measurement at time k, the state estimate relies on only the update step (6.7) as no knowledge about the data is available and $\boldsymbol{P}_k^+ = \infty \boldsymbol{I}$. This concept can be extended by predicting the future state trajectory for times $k+1, \ldots, k+t_{\mathrm{h}}$, where t_{h} is the prediction horizon, which is typically between 30 and 60 min, allowing the patient to modify treatment decisions in order to prevent possible harmful glycemic excursions. In contrast to time series analyses based on ARMA(X) models (auto-regressive-moving-average with exogenous inputs), which can also be used for short-term predictions, a model-based approach has the advantage that future values do not inherently depend on only past measurements but on the internal state dynamics of the model and its response to possible new system excitation. Hence, providing an adequate model may increase the prediction horizon.

To assess the prediction capabilities, Algorithm 4 is adapted as shown in Fig. 6.10. Within an arbitrary data sequence, the EKF estimates the internal model states based on measurement data for a time horizon t_{w}. Since the initial state estimates are not known exactly, setting $t_{\mathrm{w}} = 12\,\mathrm{h}$ allows the filter to converge accordingly. After reaching the end of t_{w}, states are predicted on only the model update equations and system inputs for the prediction horizon of $t_{\mathrm{h}} = 4\,\mathrm{h}$. The process is repeated by shifting the total filter window, $t_{\mathrm{w}} + t_{\mathrm{h}}$, by $t_{\mathrm{s}} = 30\,\mathrm{min}$ along the entire measurement sequence. In retrospect, the predictions made in each window can be compared with the measurements recorded within this interval.

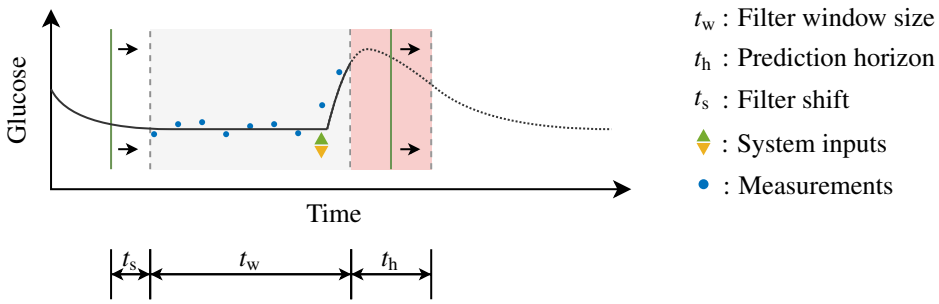

Figure 6.10: Process of the short-term prediction of future blood glucose levels: The filter runs within the nominal window size, t_w, where time-update and correction steps are fulfilled at each time step using measured inputs and outputs. The prediction follows for the time horizon t_h, based on only the state updates. The procedure is repeated successively by shifting the complete filter window, $t_w + t_h$, by t_s along the entire measurement sequence.

6.3.2 Experimental Design, Results, and Discussion

After the derivation and configuration of the observer, its feasibility in estimating blood glucose levels from experimental CGM data is evaluated. For that, several key properties of the experimental design must be defined:

- One subject in each group (the same as shown in Table 6.5 and Fig. 6.7) was chosen.
- Since BGSM records are sparse, sequences of a duration of one week were simulated at once, in order to have a suitable amount of records available for validation.
- To test repeatability, the estimation procedure was repeated for different intervals. In subjects P814 and P385, all sequences were considered ($r = 10$ respectively $r = 3$), in P76423578, $r = 10$ out of a total of 25 one-week intervals were randomly selected.
- The estimation was further processed for the model using the nominal parameters, as well as with the identified parameter vector, to evaluate possible improvements made by the optimization.
- Meal ingestion and basal and bolus insulin administrations were incorporated into the simulation as described for the parameter identification process.

Online State Estimation. An exemplary time course of 24 h duration is shown in Fig. 6.11 for each subject. There, experimental BGSM and CGM records, meal intakes, and insulin administrations are plotted in conjunction with BG and CG estimates, using the identified model.
First, in the diabetic subjects, BGSM and CGM data pairs are close to each other. In subject P814, a larger deviation can be seen in the stationary regions (e. g., at 18:00–21:00), as well as during dynamic phases (e. g., at 12:00). This behavior can be explained by the larger time constant in this subject, which was identified to be almost four-fold higher than in the diabetic subjects (Table 6.3). Thus, the CGM signal is more delayed compared to the glucose concentration in the blood. Second, the CG estimates adequately follow the CGM signal.
In P814, $n = 22$ BGSM samples are available for validating the BG signal. At most times BG estimates are comparable with measurements. Especially the earlier change in blood glucose compared to the

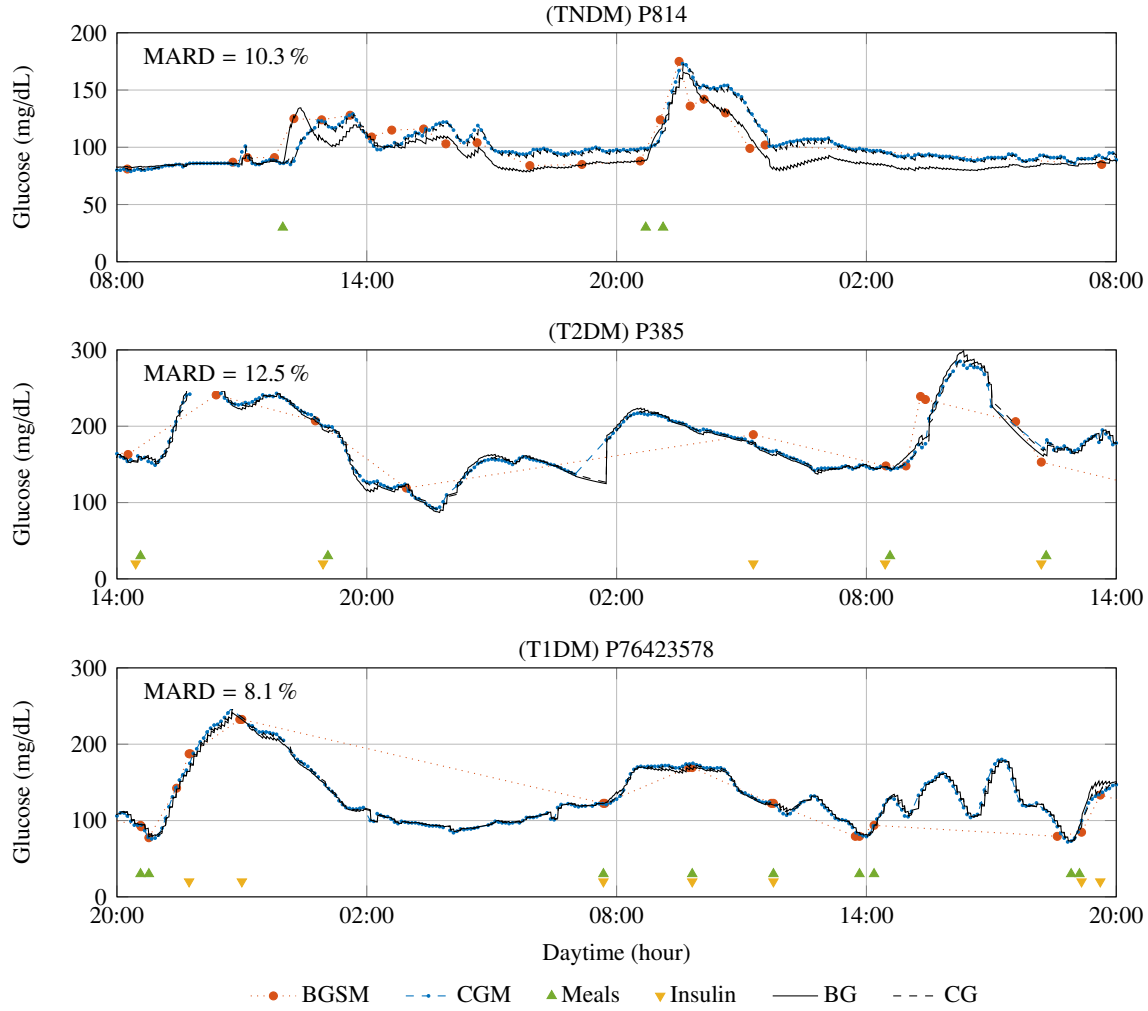

Figure 6.11: Time course of experimental BGSM (red markers) and CGM (blue markers) data versus estimated glucose values (BG in solid black, CG in dashed black). Inputs to experiment and simulation were meals (green triangles) and bolus insulin injections (yellow triangles) at discrete-time points. Data is shown during a 24 h sequence for a TNDM (top), T2DM (middle), and T1DM (bottom panel) subject. Error between BGSM and BG is given as MARD. Note that the basal insulin rate for P76423578 (Fig. C.1) is not printed here for better visibility.

CGM signal is well represented. The MARD for this sequence is calculated with 10.3 %.

In P385, this interval was selected as it contains much more BGSM values than the average for this subject ($n = 11$). Moreover, it also contains two periods of missing CGM data, at 01:00 and 11:00, which allows for investigating the observer performance for short-time predictions. Most times, the BG estimate closely precedes the CGM signal. Some over- or undershoots are apparent when glucose dynamics change. In cases of missing measurements, BG estimates rely on state predictions only. At 01:00 a comprehensible state prediction can be seen. Furthermore, the state is updated correctly as soon as measurement data is available again, which leads to the step in the estimates at 02:00. At the end of the interval, CGM is missing for at least one hour during a rapid fall of glucose. There, the model predicts a safe and reliable glucose time course. The MARD for this sequence is 12.5 %.

Table 6.6: Error (MARD in %) between BGSM measurements and BG estimates for one subject in each group. MARD is calculated between n data pairs derived by i) simulation of nominal and identified model, and ii) online estimation of nominal and identified model.

Subject	n	Simulation		Estimation	
		Nominal (%)	Identified (%)	Nominal (%)	Identified (%)
814	1428	19.9 ± 2.9	15.8 ± 1.3	13.0 ± 1.3	11.8 ± 0.8
385	99	31.2 ± 2.4	20.1 ± 4.1	11.4 ± 2.4	10.2 ± 1.6
76423578	930	172.2 ± 35.1	55.0 ± 13.7	19.8 ± 7.7	15.1 ± 6.4

In P76423578, $n = 20$ BGSM records exist (most times two values directly follow each other). The time course of estimated blood glucose closely precedes the CGM measurement, the same way as for the T2DM subject. The MARD for this sequence is calculated with 8.1 %.

To assess the repeatability of the observer and to further investigate how much the model personalization improves the estimation results, the procedure is repeated for r different sequences. The overall MARD (mean and standard deviation) for each subject and n BG pairs is reported in Table 6.6. The number of data pairs available ranges from $n = 99$ for P385 up to $n = 1428$ for P814, allowing a valid interpretation of the results. First, the error between BGSM and BG values coming from a naive simulation of the nominal model is calculated, followed by a simulation of the optimized model. Second, nominal and identified models are used for the BG estimation.
For all subjects, the simulation of the identified model significantly improves the BG signal. The error is reduced by 20 % in TNDM up to 62 % in the T1DM subject. Further, the standard deviation of the error has reduced considerably, which is likely due to the adjustment of the basal insulin dose. Switching from naive simulation to model-based estimation still reduces the mean and standard deviation of the error. Here, the T1DM subject benefits the most, and the non-diabetic subject the least. This suggests that the identified model for the non-diabetic is quite good in itself, whereas for the T1DM many mechanisms do not yet seem to be adequately represented by the model.
Last, the state observer using the identified parameter set produces the best results, with a MARD of 10.21 % and 11.83 % for the TNDM and T2DM subject, respectively; and 15.10 ± 6.43 % for P76423578. Moreover, P814 has the lowest standard deviation which allows a stable BG estimation over longer periods and under various conditions.

To assess the implications when BG estimates are utilized for treatment decisions, an EGA is performed. The results for each subject and zones A–E, as well as the total MARD for all considered sequences are reported in Table 6.7, the related EGA plots can be found in Fig. 6.12 on page 173. For all subjects, over 90 % of all BG data pairs are within zones A and B, indicating an overall accurate estimation performance.
In P814, records are more compact, most ranging between 80 and 180 mg dL^{-1}. 99.3 % of all data lie in zones A and B, and only 0.7 % in zone D. Compared to results obtained by the naive model simulation (black markers in Fig. 6.12), where 97.1 % are within zones A and B, the results improved

Table 6.7: Results of the EGA performance evaluation between BGSM measurements and BG estimates for one subject in each group with a total number of n values. EGA plots are shown in Fig. 6.12.

Subject	n	% of data pairs in zone					MARD
		A	B	C	D	E	(%)
814	1428	82.2	17.1	0.0	0.7	0.0	11.8
385	99	90.0	10.0	0.0	0.0	0.0	10.2
76423578	930	79.5	13.7	0.3	6.5	0.0	15.1

by only 2.2 percentage points. However, a significant number of values shifted from zone B (from 32.6 % to 17.1 %) into zone A (from 64.5 % to 82.2 %). The EGA confirmed that the state observer is able to reduce the BG error, compared to the naive simulation. Anyway, also the nominal and identified models return computations that are valid most times.

In P385, BG values within zone A improved from 31.2 % over 63.6 % up to 90 % for the nominal and identified model simulations, respectively state estimation. In total, all estimated BG estimates lie within the clinically relevant zones A and B. Note that only $n = 99$ BGSM samples were available, which is significantly fewer than for the other two subjects.

In P76423578, the naive simulation is not able to generate any reliable output, mainly due to the mismatch of the basal insulin infusion rate. The nominal EGA results are 4.7, 22.5, 60.6, 2.6, and 9.6 % for zones A-E, respectively. The observer approach increases the values within zones A and B to 93.1 % which is significantly more than the simulation approach, but lower than in the other groups. 6.5 % of all values fall into zone D, which means, glucose measurements below $\approx$60 mg dL^{-1} were often overestimated. A closer investigation of the time course of BGSM and CGM samples revealed that the CGM device was not able to properly track the BG excursions. This could be related to some physiological effects that occur too rapidly to be apparent in the subcutaneous tissue where the measurement takes place or it is due to errors in the BGSM device itself. Furthermore, BG records have the highest variability, ranging from 50 mg dL^{-1} up to 380 mg dL^{-1}. It is noticeable, that also the very high BGSM values are estimated accordingly, indicated by their low deviation from the diagonal.

Online State Prediction. The observer prediction capabilities are assessed for one subject in each group and r weeks of measurement data as listed in Section 6.3.2 and further explained in Fig. 6.10. Thus, leading to an ensemble of n intervals of measurement data and associated state predictions derived from the identified models. From that, CGM records, G_{CG}, are taken as reference, which is then compared with the predictions of continuous glucose $\tilde{G}_{\mathrm{I}}$ at different prediction horizons t_{h} ranging from 0 min up to 240 min. For each point in the set $\mathcal{W} = \{0, 30, 60, 90, 12, 150, 180, 210, 240\}$, the mean absolute error (MAE) across the whole ensemble is computed by

$$\mathrm{MAE}_{t_{\mathrm{h}}} = \frac{1}{n} \sum_{i=1}^{n} \left| G_{\mathrm{CG}}(i) - \tilde{G}_{\mathrm{I}}(i) \right|, \tag{6.26}$$

where $n = [2533,\ 659, \text{and } 3026]$ for subject P814, P385, and P76423578, respectively.

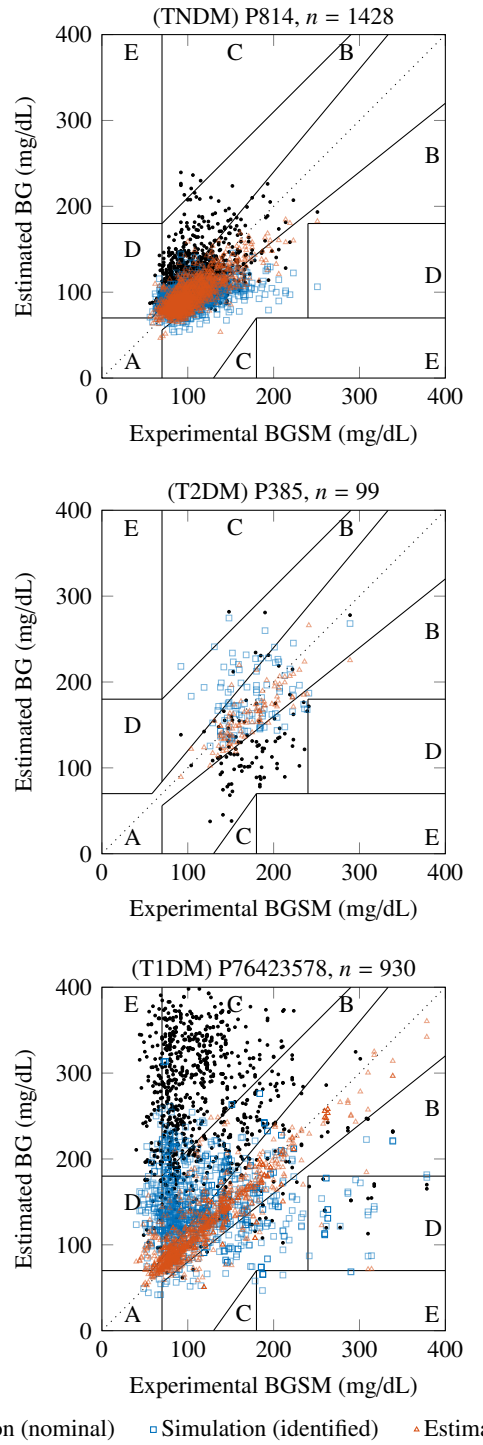

Figure 6.12: EGA of paired experimental BGSM data and estimated blood glucose (BG) values in three subjects: P814 (upper), P385 (middle), and P76423578 (lower panel). Experimental BGSM records are obtained from $r = 10$ sequences ($r = 3$ in T2DM) of 1 week duration each. BG data is calculated from naive simulation of the nominal model (black) and the mean identified model (blue); estimated BG values (red) are derived from the identified model. EGA results are reported in Table 6.7.

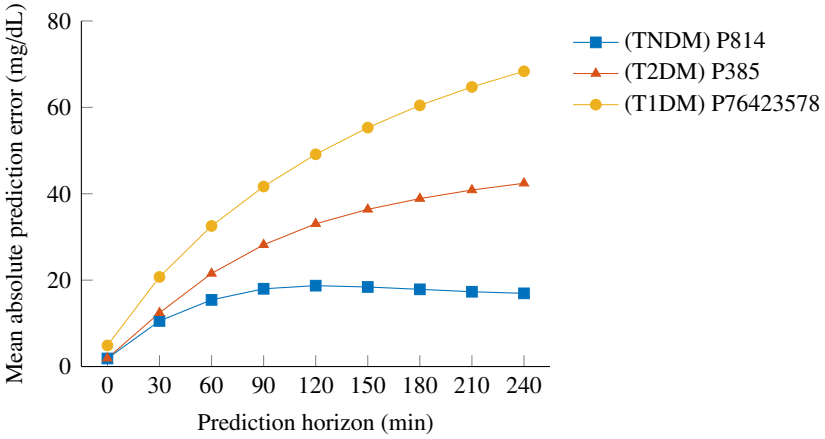

Figure 6.13: Mean absolute prediction error for time horizons increasing from 0 to 240 min for subjects P814 (blue), P385 (red), and P76423578 (yellow).

The prediction error depending on the prediction horizon is depicted in Fig. 6.13 for each participant. There, it can be seen that the error develops quite differently depending on the subject group and hence, the ability of the simulation model to adequately represent the subject it was identified from. From Table 6.5 on page 159, it is known that the identified model for the non-diabetic subject performs superior compared to the diabetic cases. This behavior is confirmed by the results in Fig. 6.13, where the prediction error for the T2DM and T1DM subjects is at least 2 respectively 3 times higher than for the TNDM subject.

In P814, after a rise of the MAE from 1.9 mg dL^{-1} up to 18 mg dL^{-1} at 90 min, it stabilizes and does not exceed 20 mg dL^{-1} over the entire prediction horizon. In contrast, in T2DM and T1DM, the error rises with increasing window size, although the gradient becomes less steep over time.

The RMSE$_{t_h=0}$ at $t_h = 0$ min, i. e., the estimation error at run-time, is calculated with 3.1, 3.4, and 7.8 mg dL^{-1} for subject P814, P385, and P76423578, respectively. The typical 30 min ahead RMSE$_{t_h=30}$ is 15.6, 17.1, and 27.1 mg dL^{-1}.

The EGA performance analysis for the three subjects and prediction horizons of 0, 30, and 60 min is shown in Fig. 6.14. At $t_h = 0$ min, almost all predicted values are close to the main diagonal and, thus, have minimal errors. At $t_h = 30$ min, the data pairs of subjects P814, P385, and P76423578 are within the clinically relevant zones A and B with 99.9, 100, and 99.9 %, respectively, and none in zone E. When setting $t_h = 60$ min, the majority of points still fall into zones A and B, but the number of errors increases. In the TNDM subject, 71, 24.6, 0.27, 4.1, and 0 % of pairs are within zones A-E, respectively. The best prediction is obtained for the T2DM subject, where 80.9, 18.5, 0.3, 0.3, and 0 % are within zones A-E, respectively. The T1DM subject performs worse, with 47.6, 50, 1.1, 1.1, and 0.2 % of data pairs within zones A-E, respectively. Hence, values indicated in zone C would lead to an overreaction, whereas glucose predictions within zone D seem to be accurate and would typically not be corrected. The critical zone E, whose occurrence would lead to a converse treatment decision, occurs with 0.2 % in P76423578.

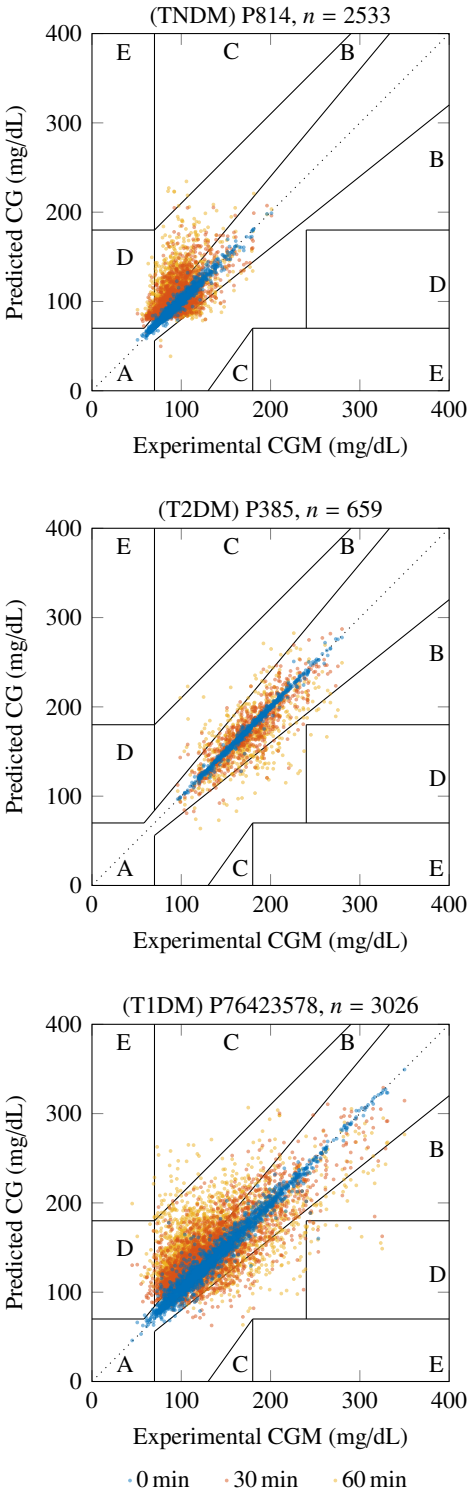

Figure 6.14: EGA of paired experimental CGM data and predicted continuous glucose (CG) values in three subjects: P814 (upper), P385 (middle), and P76423578 (lower panel). Experimental CGM records are obtained from $r = 10$ sequences ($r = 3$ in T2DM) of 1 week duration each. Predicted CG values are shown for a horizon of 0 min (blue), 30 min (red), and 60 min (yellow).

6.4 Summary and Conclusion

This chapter introduced a collection of daily-life measurement data obtained by several diabetic and non-diabetic persons. The records contain meal intakes and insulin administrations, which are inputs to a mathematical model of glucose regulation. They further contain blood and continuously measured glucose values, which are the main outputs of the model.

Section 6.2.1 showed the general applicability of a model identification approach from blood glucose and insulin measurements if enough and precise records are available, e. g., obtained in a clinical setting. Moreover, only those parameters were adapted which have shown to be important, which was quantified by their sensitivity index (Section 5.1.6).

Besides that, statistical approaches for sensitivity analysis, observability, and identifiability analysis (Section 5.2) have shown which states and parameters are, theoretically, observable by CGM data. In practice, consistent parameter identification for several subjects and different measurement sequences is currently not possible. This can be primarily explained by the high measurement noise in the CGM signal, which is in a similar order of magnitude as the variability in the model output when parameters are varied within their physiological range. Hence, variance induced by parameter changes cannot be distinguished from measurement noise which makes a precise identification of all sensitive parameters practically impossible. Nevertheless, at least the basal glucose concentration and the physiological time lag could be determined. However, the ongoing technological improvements in CGM data acquisition, signal processing, and data integration from other sources may help to overcome these limitations in the near future (Vettoretti, Cappon, et al. 2018).

Although parameter identification was not successful at all for the reasons mentioned above, an online state estimation of the major clinical factor, the concentration of glucose in the blood, is feasible. For that purpose, a state observer was designed, taking into account several statistical properties of process and sensor noise. Blood glucose is not continuously measurable but can be estimated in real-time from experimental CGM data, providing integrated monitoring. Results show a MARD between measured and estimated blood glucose values of 10.2 % and 15.1 %, including almost 2500 records obtained from different diabetic and non-diabetic patients during several months. Furthermore, the observer design was extended for short-term predictions of future glucose excursions. Error metrics and an EGA were computed for prediction horizons ranging from 0 min up to 240 min. The RMSE between CGM data and predicted CG values for a prediction horizon of 30 min includes between 659 and 3026 data pairs and is calculated with 15.6, 17.1, and 27.1 $\mathrm{mg\,dL^{-1}}$ for the TNDM, the T2DM, and the T1DM subject, respectively. EGA performance shows that almost all predictions in all subjects fall within the clinically relevant zones A and B. Hence, allowing a patient to properly correct treatment decisions for a time horizon up to 60 min.

7 MoDiM – Model-based Diabetes Monitoring

MoDiM (Model-based Diabetes Monitoring) is an extensible web-based service for real-time glucose monitoring, acquisition of insulin delivery and meal ingestion, and model-based state estimation. It connects to an open-source mobile application that implements interfaces to several sensors and a repository for data storage. The main feature is a simulation environment that makes use of a mathematical model of glucose-insulin-glucagon regulation and the available measurement data. Hence, it provides real-time information of the patient's current metabolic status to gain new insights into the personal health progression and can help to achieve better therapeutic decisions to support patients in their daily diabetes management (Fig. 7.1).

Use Cases. For patients, the use of a model-based system in daily life has several benefits:

- Diabetics have to measure their blood glucose values several times a day. A reliable estimate of the current concentration may reduce the number of painful finger pricks.
- A continuous estimate of glucose levels would allow a patient to react earlier to deviations from euglycemia and could reduce times of severe metabolic conditions.
- A simulation model not only allows estimating the current state of a patient but also enables short-time predictions of future glucose levels. Compared to the sole evaluation of the past time course of glucose measurements, a model-based prediction has the advantage of generating considerably more precise predictions. It also allows taking into account possible future events if provided by patients.

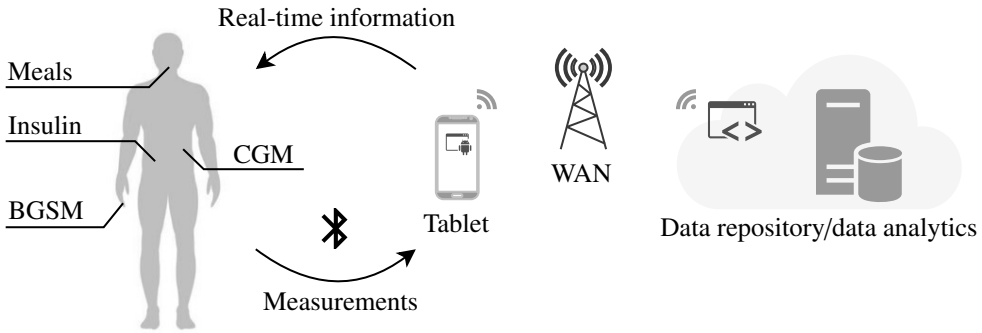

Figure 7.1: *MoDiM* concept: Mobile glucose measurement devices and insulin pumps are wirelessly connected to a tablet via Bluetooth. The tablet serves as a user interface and is connected to a web service. This online service consists of a web server, a database for data storage, and a data analytics platform.

- Moreover, this would allow a kind of management game mode in which a patient could simulate different scenarios of meal ingestion, insulin injection, or physical activity and their influence on future metabolic states.

Components and General Structure. *MoDiM* consists of a series of hardware and software components (Table 7.1). It implements interfaces to the blood glucose sensor Contour Next One, the continuous glucose sensor G5 Mobile, and several insulin pumps via the open-source Android app xDrip+. Meal ingestion must be provided manually within this application. These records define the major inputs and outputs of a patient in a daily-life diabetes setting which are needed for the model-based diabetes monitoring. All recordings are converted into JSON (JavaScript Object Notation) format, a collection of name/value pairs that is human-readable and easy for machines to parse and generate. Moreover, measurement values are automatically transmitted to a non-relational database (MongoDB) in real-time. The database is free, easy to install and maintain, and can be run on various platforms. There also exist several APIs (Application Programming Interface) with which the database can be accessed from other services. It is running on a Raspberry Pi, a low-cost, low-energy embedded device, that could also serve as a server for at-home-usage. For online and offline data analysis and algorithm development, the database can be accessed from Matlab via a Java-API (MongoDB Java driver). Since Java is natively supported by Matlab only some wrapper classes had to be designed to encapsulate the database API. The whole toolchain is shown in the lower part of Fig. 7.2.

MoDiM service is the main component that reacts to user requests and new database entries and calls subsequent methods for data processing. It is written in JavaScript and is executed within a JavaScript

Table 7.1: Hard- and software components used to build up the *MoDiM* service and application.

Components	Device/Version	Reference
Hardware		
Blood glucose sensor	Contour Next One	Ascensia Diabetes Care Deutschland GmbH (2016)
Continuous glucose sensor	G5 Mobile	Dexcom, Inc. (2017)
Tablet	Android 8.1	https://www.android.com
Embedded device	Raspberry Pi 3B	https://www.raspberrypi.org/
Software		
Development	Matlab 2019b Matlab Coder 2019b	The MathWorks, Inc. (2019), McVittie (2020)
Database	MongoDB 4.2.8	https://www.mongodb.com
Database driver	MongoDB Java driver 3.9.1	https://mongodb.github.io/mongo-java-driver/
BAN hardware driver	xDrip+ d8e7079-2018.01.22	The Nightscout Foundation (2018)
LLVM-to-JavaScript Compiler	Emscripten 1.39.18	Zakai (2011), https://emscripten.org/
Web server	Nginx	https://www.nginx.com
JavaScript Runtime	Node.js 12.18.2	https://nodejs.org

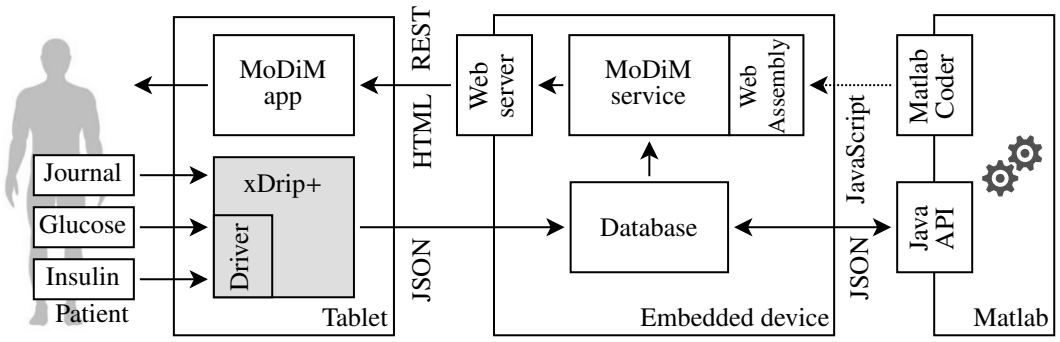

Figure 7.2: *MoDiM* structure: Glucose sensors and insulin pumps communicate with the open-source Android app xDrip+ (gray box). Meals must be manually entered within the app. Records are saved in JSON format in a database accessible by Matlab via a Java-API. Algorithms developed in Matlab can be compiled into C++ code and from there into JavaScript. An embedded device runs the database and a JavaScript runtime environment which provides the core web services by an HTML and a RESTful-API. This interface can be accessed from any (mobile) device.

runtime environment (Node.js) also running on the embedded device (upper part of Fig. 7.2). Algorithms for model-based monitoring and data analysis can be developed in Matlab/Simulink. Matlab Coder provides functionalities for converting these procedures into generic C++ code. From this point, an LLVM-to-JavaScript Compiler (Emscripten) compiles the code into byte-code as a WebAssembly, which can be called from the *MoDiM* main component. Finally, a user can access the service by the MoDiM Android application or any web browser. For that, a web server (Nginx) provides an HTML (HyperText Markup Language) and RESTful (Representational State Transfer) interface that allows graphical outputs and data readings in a standardized and convenient manner.

From a development view, new algorithms can be tested against real-time data delivered by the *MoDiM* service. Therefore, it is irrelevant whether the data was obtained by a real patient or generated from a virtual subject by simulation. In both cases, the data repository will be written with records in a standardized way. The system architecture with all interfaces remains the same.

The current hardware setup is depicted in Fig. 7.3, where the *MoDiM* application can be seen in the background showing a set of patient data. CGM sensor and receiver, blood glucose device, and embedded computer are visible in the foreground.

Figure 7.3: *MoDiM* hardware consists of a tablet device (back), Dexcom G5 Mobile CGM sensor and receiver (front right), Contour Next One blood glucose sensor (front center), and Raspberry Pi (front left).

8 Summary and Future Research

Thesis Summary

Diabetes technology is towards a fully automated “artificial pancreas” (AP). These systems currently consist of a pump for insulin delivery (the actor in a closed-loop system), continuous glucose measurements (the sensor), and a control algorithm that determines the required insulin dose based on the current glucose measurements and personal needs (Fig. 1.2). Control algorithms such as model predictive control (MPC) greatly benefit from a personalized model of glucose-insulin-glucagon metabolism as the patient’s individual characteristics and current metabolic states can be taken into account.

To create these personalized models and gather more insights into internal metabolic states, three tasks were fulfilled within this work: derivation of a unified model of glucose-insulin-glucagon metabolism, analysis of important variables in the system, and a model adaptation utilizing parameter identification and state estimation.

The physiological-based compartment model of glucose regulation was derived from available approaches in the literature. It takes into consideration the plasma concentrations of glucose and the two antagonistic hormones insulin and glucagon (Chapter 4). The model is divided into parts for substance secretion or external delivery, their distribution within the body including the subcutaneous space, and their utilization and disposal. The model is unified in terms of its capability to describe the normal physiological case, as well as the pathophysiological conditions in type 1 and type 2 diabetic patients (T1DM respective T2DM). For healthy subjects (TNDM), glycemic control is reached by an increase in insulin secretion which raises glucose uptake in the cells. Simultaneously, an increased glucagon release suppresses endogenous glucose production in the liver. In T2DM, the feedback loops are still intact but deteriorated, leading to prolonged elevated postprandial glucose levels. Insulin administration through the subcutaneous route causes a normalization of metabolism. In T1DM, insulin secretion is absent and the steady-state is maintained by basal insulin administration. Postprandial glucose excursion is near normal by additional bolus insulin at mealtimes. The different behavior patterns are dictated by differences in the subject’s parameters. Therefore, a database of virtual subjects was generated which allows the investigation of various metabolic conditions. Several comparative simulation studies followed, to evaluate the ability of the model to predict substance excursions in steady-state and after a meal with and without insulin bolus. Moreover, the model was evaluated against measurement data taken from the literature to assess the limits of the design. Furthermore, to

be able to correctly simulate the inherent measurement noise of glucose devices, published sensor models were integrated into the simulation environment. Hence, a dynamical, nonlinear model of ordinary differential equations with 19 states and over 40 parameters, a population of 100 virtual subjects in each of the three groups, and virtual BGSM (blood glucose self-management) and CGM (continuous glucose measurements) devices are available for now.

For systems analysis (Chapter 5), two different techniques were applied to the model. Global sensitivity analysis (GSA) was performed to determine which parameters induce a high variability in the outputs, thus, which may be identifiable in a subsequent optimization procedure. Second, empirical controllability, observability, and identifiability Gramians were computed to determine (augmented) states that are controllable or observable from measurements of the s.c. glucose output. Both methods serve as a basis for the subsequent model adaptation and state estimation.
As the model has many input factors and GSA is computationally expensive since the whole input space must be sampled appropriately, a multi-step approach was introduced. The procedure includes the Elementary Effects Test used as a screening technique in order to identify 10 out of 37 independent parameters with the highest mean elementary effect. For the reduced parameter set, a variance-based sensitivity analysis followed. Both techniques can only be applied to scalar model outputs. In order to allow the time-dependent s.c. glucose output to be investigated, they were extended by the concept of functional principal component analysis, which led to overall sensitivity indices. GSA was fulfilled for several scenarios and all three groups, allowing the investigation of group-dependent differences. The analysis showed superior importance of basal glucose concentration, G^{b}, in all groups. In TNDM and T2DM, m_5 and m_6, related to insulin secretion, and β, related to glucose control, play a major role. Moreover, k_{G2}, which determines the rate of digestion has a higher index. In T1DM, parameters k_1, V_{mx}, and k_{i3} became apparent.
Section 5.2 introduced the concept of controllability and observability of dynamical states in linear systems. Gramian matrices were used to quantify these properties. As the model is nonlinear, the methods were extended using empirical Gramians, hence, allowing investigation of the system behavior around a particular nominal trajectory. The mixed-meal ingestion scenario including insulin bolus for diabetic patients was chosen as this is most common in daily life. Moreover, the concept of observability was extended to the identifiability of parameters, allowing an observability-based parameter identification. Results show, especially for the T1DM subjects, that not all states are controllable respectively observable due to missing insulin secretion. Furthermore, when only the s.c. glucose signal is measured, just a small subset of states and parameters can be observed in practice. This was determined by the smallest eigenvalue of the empirical Gramian of the given subset. However, glucose concentration is observable in all groups, in steady-state as well as in the postprandial phase.

Chapter 6 has two objectives. First, to adapt sensitive parameters to individual measurement data, thus, personalize the model. And second, to estimate the current blood glucose concentration on the basis of experimental CGM data in real-time.
Therefore, measurements of several diabetic patients and healthy subjects were collected. The database includes six people who provided BGSM and CGM records, as well as their meals and

insulin injections over several months. Three of them were T1DM patients who wore an insulin pump for automatic basal insulin delivery. Two other individuals were long-time T2DM patients under conventional therapy. The last participant was healthy. Input and output records were statistically evaluated and EGA (error grid analysis) between CGM and BGSM was performed. The number of considered days varied between 12 and 234, leading to 3303 respectively up to 54 427 CGM records. MARD (mean absolute relative difference) was calculated to be between 8.4 and 14.3 %.
Parameter identification was fulfilled using an optimization-based method, for which the error between measured CGM and model output was minimized. The methodology was first shown using frequent blood glucose and insulin data from the literature. Output RMSE (root mean squared error) was reduced from 19.3 down to 5.2 mg dL^{-1} in TNDM and from 39.7 to 7.9 mg dL^{-1} in T2DM subjects. Sensitive parameters were identified with precision indicated by results from the t-test and F-test. The main focus was to identify parameters from frequent CGM records as these data are available for all patients in daily-life. First, basal glucose concentration and the time delay between glucose in the blood and interstitial fluid were determined. Second, all remaining sensitive parameters were identified from various measurement sequences. In general, a precise adaptation to individuals was not possible at all. This is mainly because measurement noise is in the same order as the variability in the model output during sensitivity analysis. Hence, from only observing the s.c. glucose signal it is not possible to distinguish between parameter alterations and sensor noise using the current generation of CGM devices. Nevertheless, an adaptation to single sequences like a meal is quite feasible, but the obtained parameter values are not valid for other intervals. To still be able to use the advantages of model adaptation, an average identified model for one subject in each group was built. MARD and EGA, built from validation data revealed a significant model improvement in TNDM and T1DM, but not in the T2DM subject.
Based on the personalized models, a nonlinear state observer was designed. The extended Kalman filter is suitable for nonlinear systems, was further adapted for continuous-discrete state and measurement updates, and also colored measurement noise was incorporated as an additional state. Blood glucose (BG) concentration was successfully estimated from CGM data in real-time for interval lengths up to several weeks. MARD was calculated between estimated BG and measured BGSM values for validation, where the number of considered pairs varied between 99 and 1428. In the TNDM, T2DM, and T1DM subject, MARD is 11.8 %, 10.2 %, and 15.1 %, respectively. Hence, BG can be estimated with a similar uncertainty as for the CGM signal itself. Moreover, EGA was performed with 99.3 %, 100 %, and 93.2 % of all BG data pairs within the clinically relevant zones A and B. Finally, a short-term prediction of continuous glucose values for a time horizon up to 240 min was evaluated. The mean absolute prediction error 30 min ahead was 10.6 mg dL^{-1}, 12.4 mg dL^{-1}, and 20.7 mg dL^{-1} for the TNDM, T2DM, and T1DM subject, respectively.

The methods obtained in this work were incorporated into a web-based platform for continuous model-based glucose monitoring. The application makes use of an existing open-source app for smartphones to communicate with several glucose sensors available on the market. Model-based algorithms developed in Matlab can be automatically compiled into C++ and from there to WebAssembly

components. The web service runs in a JavaScript environment, has access to measurement records that were uploaded into a database, and processes the data. Results are provided by a web server that is accessible via an HTML and RESTful API by any (mobile) web browser. Hence, allowing a user to continuously monitor the current health status and to access other personalized diagnostics.

On-going and Future Directions

Besides technological improvements in sensing and signal processing of possible future CGM devices (Vettoretti, Cappon, et al. 2018), a rich spectrum of further advances arises:

Model Extensions. Extending the model means mathematical description and implementation of further physiological effects, substances, or interactions between different components. Conditions such as stress, illness, medication, or physical activity have a significant influence on everyday hormone levels and their metabolism, which makes tight glucose control with exogenous insulin administration challenging. Most of those environmental effects cannot be measured easily and must be regarded as model uncertainty. However, physical activity has a major impact on energy exchange and can be determined using heart rate or skin resistance. Several clinical trials on activity tracking and CGM monitoring exist (Kapitza et al. 2010; Zecchin et al. 2013), which resulted in model approaches also incorporated into a glucose-insulin model (Dalla Man, Breton, et al. 2009).

Estimation of Additional States and Time-varying Parameters. In this work, blood glucose concentration was estimated from CGM data. One further step would incorporate additional internal states such as the insulin concentration, which would allow the design of more sophisticated control strategies. Moreover, current models rely on the announcement of a meal to correctly predict post-prandial glucose excursions. In a closed-loop system, the controller could initiate an insulin bolus on a meal announcement. Using CGM data, meals could be detected using the rate of change of BG (Dassau et al. 2008). In a model-based approach, the observer could be extended by the meal input as an additional state to be estimated in order to handle unannounced meals. Last, some parameters (e. g., insulin sensitivity, and glucose utilization) are assumed to be time-dependent (Visentin et al. 2018). Their daily pattern could be integrated as additional states too. In all cases, practical observability or identifiability must be proven to estimate these states with precision.

Model Order Reduction. The system presented here has already 19 states and over 40 parameters in total. Incorporating more and more physiological effects further increases the complexity of the model and not all of them are measurable or otherwise known *a priori*. Besides model simplification approaches such as linearization or Padé approximation, model order reduction (MOR) is a model-driven technique to reduce the number of (augmented) states in linear as well as nonlinear systems. It is a method of choice as it simplifies the design of state observers (Misgeld et al. 2017) or controllers

for closed-loop insulin control. In a model of reduced order, only a subspace of the state-space system is considered, which contains only those states that contribute most to the input-output behavior. The subset can be found when the system is balanced, i. e., the generalized energy transfer from inputs into states and from states into outputs are weighted equally and the states are decoupled. Then, the order can be reduced by truncation of those states with the lowest energy transfer (Tolks and Ament 2017b). The balancing information can be obtained by using the concept of (empirical) Gramians for controllability and observability shown in this thesis. Hence, this procedure allows for a continuous model-based design.

Individualized Closed-loop Control Strategies. Using CGM data, a personalized model, and state estimation allows continuous monitoring of individual blood glucose excursions and maybe a step further towards an "artificial pancreas." Beginning with simple PID (proportional-integral-derivative) control, the current state-of-the-art technique is model predictive control. MPC relies on a model of the underlying process to predict the future system behavior depending on the input signals. This allows the calculation of an optimal input signal by minimizing a cost function s.t. various constraints in order to produce optimal outputs. The performance of an MPC is related to the prediction capabilities of the model. Thus, the achievable glucose control performance would benefit from a personalized model without increasing the computational costs of the algorithm (Messori et al. 2018). Moreover, the model of glucose-insulin-glucagon regulation, in combination with a virtual population of diabetic patients, enables model-driven controller design and *in silico* testing and performance evaluation, even before clinical trials. Finally, a portable AP system with limited computational power and battery life would also benefit from a reduced-order design of the simulation model and controller.

Appendices

A Mathematical Models

Input vector $\boldsymbol{u}(t)$:

$$\boldsymbol{u}(t) = \begin{bmatrix} u_{\mathrm{G}}^{\mathrm{oral}}(t) & u_{\mathrm{G}}^{\mathrm{iv}}(t) & u_{\mathrm{I}}^{\mathrm{sc}}(t) & u_{\mathrm{I}}^{\mathrm{sc}}(t) & u_{\mathrm{H}}^{\mathrm{sc}}(t) \end{bmatrix}^{\top}$$

Output vector $\boldsymbol{y}(t)$:

$$\boldsymbol{y}(t) = \begin{bmatrix} G(t) & G_{\mathrm{I}}(t) & I(t) & H(t) \end{bmatrix}^{\top}$$

Nonlinear state equations $\boldsymbol{x}(t)$:

$$\begin{aligned}
\dot{x}_1(t) &= -k_{G1}x_1(t) + u_{\mathrm{G}}^{\mathrm{oral}}(t) \\
\dot{x}_2(t) &= -k_{G2}x_2(t) + k_{G1}x_1(t) \\
\dot{x}_3(t) &= S_{\mathrm{G}}(t) + R_{\mathrm{G}}(t) - U_{\mathrm{ii}}(t) - E(t) - k_1x_3(t) + k_2x_4(t) + u_{\mathrm{G}}^{\mathrm{iv}}(t) \\
\dot{x}_4(t) &= -U_{\mathrm{id}}(t) + k_1x_3(t) - k_2x_4(t) \\
\dot{x}_5(t) &= -k_g x_5(t) + k_g x_3(t) \\
\dot{x}_6(t) &= -\left(m_2 + m_4\right)x_6(t) + m_1x_7(t) + R_{\mathrm{I}}(t) + u_{\mathrm{I}}^{\mathrm{sc}}(t) \\
\dot{x}_7(t) &= -\left(m_1 + m_3(t)\right)x_7(t) + m_2x_6(t) + S_{\mathrm{I}}(t) \\
\dot{x}_8(t) &= \begin{cases} -\alpha\left(x_8 - \beta\left(G(t) - G^{\mathrm{b}}\right)\right) & \text{if } \beta\left(G(t) - G^{\mathrm{b}}\right) \geq -S_{\mathrm{I}}^{\mathrm{b}} \\ -\alpha x_8 - \alpha S_{\mathrm{I}}^{\mathrm{b}} & \text{if } \beta\left(G(t) - G^{\mathrm{b}}\right) < -S_{\mathrm{I}}^{\mathrm{b}} \end{cases} \\
\dot{x}_9(t) &= -\gamma x_9(t) + S_{po}(t) \\
\dot{x}_{10}(t) &= -k_X x_{10}(t) + k_X\left(I(t) - I^{\mathrm{b}}\right) \\
\dot{x}_{11}(t) &= -k_{\mathrm{I}} \cdot \left(x_{11}(t) - I(t)\right) \\
\dot{x}_{12}(t) &= -k_{\mathrm{I}} \cdot \left(x_{12}(t) - x_{11}(t)\right) \\
\dot{x}_{13}(t) &= -(k_{i1} + k_{i2})x_{13}(t) + u_{\mathrm{I}}^{\mathrm{sc}}(t) \\
\dot{x}_{14}(t) &= k_{i1}x_{13}(t) - k_{i3}x_{14}(t) \\
\dot{x}_{15}(t) &= -n_{\mathrm{H}}x_{15}(t) + S_{\mathrm{H}}(t) + R_{\mathrm{H}}(t) \\
\dot{x}_{16}(t) &= -\left(k_{h1} + k_{h2}\right)x_{16}(t) + u_{\mathrm{H}}^{\mathrm{sc}}(t) \\
\dot{x}_{17}(t) &= k_{h1}x_{16}(t) - k_{h3}x_{17}(t) \\
\dot{x}_{18}(t) &= -k_{\mathrm{H}} \cdot x_{18}(t) + k_{\mathrm{H}} \cdot \max\left(x_{15}(t) - H^{\mathrm{b}}, 0\right) \\
\dot{x}_{19}(t) &= \begin{cases} -k_\rho\left[x_{19}(t) - S_{\mathrm{H}}^{\mathrm{b}}\right] & \text{if } G(t) \geq G^{\mathrm{b}} \\ -k_\rho\left[x_{19}(t) - \max\left(\dfrac{k_\sigma \cdot \left(G^{\mathrm{b}} - G(t)\right)}{I(t) + 1} + S_{\mathrm{H}}^{\mathrm{b}}, 0\right)\right] & \text{if } G(t) < G^{\mathrm{b}} \end{cases}
\end{aligned} \tag{A.1}$$

Input matrix $\boldsymbol{B}$:

$$\boldsymbol{B}^{\top} = \begin{bmatrix} 1 & 0 & 0 & 0 & 0 & 0 & 0 & 0 & 0 & 0 & 0 & 0 & 0 & 0 & 0 & 0 & 0 & 0 & 0 \\ 0 & 0 & 1 & 0 & 0 & 0 & 0 & 0 & 0 & 0 & 0 & 0 & 0 & 0 & 0 & 0 & 0 & 0 & 0 \\ 0 & 0 & 0 & 0 & 0 & 0 & 0 & 0 & 0 & 0 & 0 & 0 & 1 & 0 & 0 & 0 & 0 & 0 & 0 \\ 0 & 0 & 0 & 0 & 0 & 1 & 0 & 0 & 0 & 0 & 0 & 0 & 0 & 0 & 0 & 0 & 0 & 0 & 0 \\ 0 & 0 & 0 & 0 & 0 & 0 & 0 & 0 & 0 & 0 & 0 & 0 & 0 & 0 & 0 & 1 & 0 & 0 & 0 \end{bmatrix}$$

Linear output equation $\boldsymbol{y}(t)$:

$$\boldsymbol{y}(t) = C\boldsymbol{x}(t) \tag{A.2}$$

Output matrix $\boldsymbol{C}$:

$$\boldsymbol{C} = \begin{bmatrix} 0 & 0 & \frac{1}{V_{\mathrm{G}}} & 0 & 0 & 0 & 0 & 0 & 0 & 0 & 0 & 0 & 0 & 0 & 0 & 0 & 0 & 0 & 0 \\ 0 & 0 & 0 & 0 & \frac{1}{V_{\mathrm{G}}} & 0 & 0 & 0 & 0 & 0 & 0 & 0 & 0 & 0 & 0 & 0 & 0 & 0 & 0 \\ 0 & 0 & 0 & 0 & 0 & \frac{1}{6V_{\mathrm{I}}} & 0 & 0 & 0 & 0 & 0 & 0 & 0 & 0 & 0 & 0 & 0 & 0 & 0 \\ 0 & 0 & 0 & 0 & 0 & 0 & 0 & 0 & 0 & 0 & 0 & 0 & 0 & 0 & 1 & 0 & 0 & 0 & 0 \end{bmatrix}$$

Table A.1: States, basal and initial values, and essential signals of the unified model.

Description	Symbol	State	Basal	Initial states $\boldsymbol{x}_0$			Unit
				TNDM	T2DM	T1DM	
Glucose amount in stomach	$Q_{\mathrm{Gas},1}(t)$	x_1	0	0	0	0	mg
Glucose amount in intestine	$Q_{\mathrm{Gas},2}(t)$	x_2	0	0	0	0	mg
Glucose rate of appearance	$R_{\mathrm{G}}(t)$						$\mathrm{mg\,kg^{-1}\,min^{-1}}$
Glucose production rate	$S_{\mathrm{G}}(t)$		$S_{\mathrm{G}}^{\mathrm{b}}$				$\mathrm{mg\,kg^{-1}\,min^{-1}}$
Glucose utilization	$U(t)$		U^{b}				$\mathrm{mg\,kg^{-1}\,min^{-1}}$
Glucose plasma	$G_{\mathrm{P}}(t)$	x_3	$G_{\mathrm{P}}^{\mathrm{b}}$	169.2	178.8	221.0	$\mathrm{mg\,kg^{-1}}$
Glucose tissue	$G_{\mathrm{T}}(t)$	x_4	$G_{\mathrm{T}}^{\mathrm{b}}$	127.9	91.2	134.7	$\mathrm{mg\,kg^{-1}}$
Glucose subcutaneous	$G_{\mathrm{Sc}}(t)$	x_5	$G_{\mathrm{P}}^{\mathrm{b}}$	169.2	178.8	221.0	$\mathrm{mg\,kg^{-1}}$
Glucose concentration plasma	$G(t)$		G^{b}				$\mathrm{mg\,dL^{-1}}$
Insulin plasma	$I_{\mathrm{P}}(t)$	x_6	$I_{\mathrm{P}}^{\mathrm{b}}$	1.3	2.4	5.4	$\mathrm{pmol\,kg^{-1}}$
Insulin liver	$I_{\mathrm{L}}(t)$	x_7	$I_{\mathrm{L}}^{\mathrm{b}}$	4.6	5.9	3.7	$\mathrm{pmol\,kg^{-1}}$
Insulin concentration plasma	$I(t)$		I^{b}				$\mathrm{pmol\,L^{-1}}$
Insulin rate of appearance	$R_{\mathrm{I}}(t)$						$\mathrm{pmol\,kg^{-1}\,min^{-1}}$
Insulin secretion rate	$S_{\mathrm{I}}(t)$						$\mathrm{pmol\,kg^{-1}\,min^{-1}}$
Static insulin secretion rate	$Y(t)$	x_8	0	0	0	0	$\mathrm{pmol\,kg^{-1}\,min^{-1}}$
Insulin portal vein	$I_{\mathrm{Po}}(t)$	x_9	$I_{\mathrm{Po}}^{\mathrm{b}}$	3.1	8.0	0	$\mathrm{pmol\,kg^{-1}}$
Insulin interstitial fluid	$X(t)$	x_{10}	0	0	0	0	$\mathrm{pmol\,L^{-1}}$
Delayed insulin action on EGP	$I_1(t)$	x_{11}	I^{b}	25.9	59.8	106.0	$\mathrm{pmol\,L^{-1}}$
Insulin action on EGP	$X_{\mathrm{I}}(t)$	x_{12}	I^{b}	25.9	59.8	106.0	$\mathrm{pmol\,L^{-1}}$
Insulin subcutaneous	$I_{\mathrm{Sc},1}(t)$	x_{13}	$I_{\mathrm{Sc},1}^{\mathrm{b}}$	0	0	84.8	$\mathrm{pmol\,kg^{-1}}$
Insulin subcutaneous	$I_{\mathrm{Sc},2}(t)$	x_{14}	$I_{\mathrm{Sc},2}^{\mathrm{b}}$	0	0	77.6	$\mathrm{pmol\,kg^{-1}}$
Glucagon plasma	$H(t)$	x_{15}	H^{b}	126.0	208.0	57.0	$\mathrm{ng\,L^{-1}}$
Glucagon rate of appearance	$R_{\mathrm{H}}(t)$						$\mathrm{ng\,L^{-1}\,min^{-1}}$
Glucagon secretion rate	$S_{\mathrm{H}}(t)$						$\mathrm{ng\,L^{-1}\,min^{-1}}$
Glucagon subcutaneous	$H_{\mathrm{Sc},1}(t)$	x_{16}	$H_{\mathrm{Sc},1}^{\mathrm{b}}$	0	0	0	$\mathrm{mg\,kg^{-1}}$
Glucagon subcutaneous	$H_{\mathrm{Sc},2}(t)$	x_{17}	$H_{\mathrm{Sc},2}^{\mathrm{b}}$	0	0	0	$\mathrm{mg\,kg^{-1}}$
Glucagon action on EGP	$X_{\mathrm{H}}(t)$	x_{18}	0	0	0	0	$\mathrm{ng\,L^{-1}}$
Static glucagon secretion rate	$S_{\mathrm{H}}^{\mathrm{s}}(t)$	x_{19}	$S_{\mathrm{H}}^{\mathrm{b}}$	27.7	27.9	7.7	$\mathrm{ng\,L^{-1}\,min^{-1}}$

Table A.2: Statistical values of parameters of TNDM, T2DM, and T1DM subjects. Distribution (Dist) is either log-normal ($\mathcal{LN}$) showing mean and standard deviation (Std.) or uniform ($\mathcal{U}$) with minimum and maximum. If a variable is constant or dependent, no distribution is noted.

Sign	Dist	TNDM		T2DM		T1DM		Unit
		Mean/Min.	Std./Max.	Mean/Min.	Std./Max.	Mean/Min.	Std./Max.	
V_G	$\mathcal{LN}$	1.8800	0.1328	1.4900	0.1033	1.8480	0.1413	$\mathrm{dL\,kg^{-1}}$
k_1	$\mathcal{LN}$	0.0650	0.0128	0.0420	0.0110	0.0731	0.0160	$\mathrm{min^{-1}}$
k_2	$\mathcal{LN}$	0.0790	0.0295	0.0710	0.0277	0.1077	0.0456	$\mathrm{min^{-1}}$
k_{G1}	$\mathcal{LN}$	0.3649	0.1164	0.0717	0.0214	0.1145	0.0207	$\mathrm{min^{-1}}$
k_{G2}	$\mathcal{LN}$	0.0102	0.0041	0.0097	0.0034	0.0116	0.0043	$\mathrm{min^{-1}}$
f_G		0.9000	0.0000	0.9000	0.0000	0.9000	0.0000	–
BW	$\mathcal{LN}$	78.0000	8.4995	90.0000	7.2349	69.7098	20.4504	kg
k_{p1}		2.6596	0.5043	3.0900	0.5278	4.9866	1.1117	$\frac{\mathrm{mg}}{\mathrm{kg\,min}}$
k_{p2}	$\mathcal{LN}$	0.0021	0.0009	0.0007	0.0003	0.0055	0.0022	$\mathrm{min^{-1}}$
k_{p3}	$\mathcal{LN}$	0.0090	0.0043	0.0050	0.0027	0.0105	0.0055	$\frac{\mathrm{mg}}{\mathrm{kg\,min}} / \frac{\mathrm{pmol}}{\mathrm{L}}$
k_{p4}	$\mathcal{LN}$	0.0550	0.0197	0.0786	0.0250	0.0000	0.0000	$\frac{\mathrm{mg}}{\mathrm{kg\,min}} / \frac{\mathrm{pmol}}{\mathrm{kg}}$
k_{p5}	$\mathcal{LN}$	0.0500	0.0228	0.0087	0.0060	0.0087	0.0047	$\frac{\mathrm{mg}}{\mathrm{kg\,min}} / \frac{\mathrm{ng}}{\mathrm{L}}$
k_I	$\mathcal{LN}$	0.0079	0.0027	0.0066	0.0031	0.0109	0.0056	$\mathrm{min^{-1}}$
k_H	$\mathcal{LN}$	0.0930	0.0182	0.0991	0.0183	0.0991	0.0185	$\mathrm{min^{-1}}$
F_{ii}		1.0000	0.0000	1.0000	0.0000	1.0000	0.0000	$\frac{\mathrm{mg}}{\mathrm{kg\,min}}$
V_{m0}		2.4884	0.9892	6.3097	4.4589	4.4740	1.6032	$\frac{\mathrm{mg}}{\mathrm{kg\,min}}$
V_{mx}	$\mathcal{LN}$	0.0470	0.0232	0.0340	0.0173	0.0715	0.0318	$\frac{\mathrm{mg}}{\mathrm{kg\,min}} / \frac{\mathrm{pmol}}{\mathrm{L}}$
K_{m0}	$\mathcal{LN}$	225.5900	16.8902	466.2100	38.6765	226.6101	17.8879	$\mathrm{mg\,kg^{-1}}$
k_X	$\mathcal{LN}$	0.0331	0.0108	0.0840	0.0299	0.0470	0.0156	$\mathrm{min^{-1}}$
k_g	$\mathcal{LN}$	0.1053	0.0335	0.1053	0.0380	0.1053	0.0352	$\mathrm{min^{-1}}$
k_{e1}		0.0005	0.0000	0.0007	0.0000	0.0005	0.0000	$\mathrm{min^{-1}}$
k_{e2}		339.0000	0.0000	269.0000	0.0000	339.0000	0.0000	$\mathrm{mg\,kg^{-1}}$
V_I	$\mathcal{LN}$	0.0500	0.0131	0.0400	0.0132	0.0511	0.0169	$\mathrm{L\,kg^{-1}}$
m_1	$\mathcal{LN}$	0.1900	0.0924	0.3790	0.1817	0.1850	0.0619	$\mathrm{min^{-1}}$
m_2		0.4771	0.8241	0.6728	0.3967	0.3130	0.0944	$\mathrm{min^{-1}}$
m_4		0.1908	0.3296	0.2691	0.1587	0.1252	0.0378	$\mathrm{min^{-1}}$
m_5	$\mathcal{LN}$	0.0304	0.0034	0.0526	0.0052	0.0263	0.0105	$\frac{\mathrm{min\,kg}}{\mathrm{pmol}}$
m_6	$\mathcal{LN}$	0.6471	0.0504	0.8118	0.0583	0.6000	0.0000	–
HE^b		0.6000	0.0000	0.6000	0.0000	0.6000	0.0000	–
κ	$\mathcal{LN}$	2.3000	0.7021	0.9900	0.3419	0.0000	0.0000	$\frac{\mathrm{pmol}}{\mathrm{kg}} / \frac{\mathrm{mg}}{\mathrm{dL}}$
α	$\mathcal{LN}$	0.0500	0.0168	0.0140	0.0052	0.0000	0.0000	$\mathrm{min^{-1}}$
β	$\mathcal{LN}$	0.1100	0.0476	0.0500	0.0167	0.0000	0.0000	$\frac{\mathrm{pmol}}{\mathrm{kg\,min}} / \frac{\mathrm{mg}}{\mathrm{dL}}$
γ	$\mathcal{LN}$	0.5000	0.1755	0.5000	0.1680	0.0000	0.0000	$\mathrm{min^{-1}}$
k_{i1}	$\mathcal{LN}$	0.0162	0.0017	0.0162	0.0019	0.0162	0.0018	$\mathrm{min^{-1}}$
k_{i2}	$\mathcal{LN}$	0.0038	0.0010	0.0038	0.0009	0.0038	0.0009	$\mathrm{min^{-1}}$
k_{i3}	$\mathcal{LN}$	0.0177	0.0060	0.0177	0.0051	0.0177	0.0044	$\mathrm{min^{-1}}$
n_H	$\mathcal{LN}$	0.2200	0.0491	0.1344	0.0279	0.1344	0.0318	$\mathrm{min^{-1}}$
k_ρ	$\mathcal{LN}$	0.8600	0.0472	0.4955	0.0322	0.4955	0.0288	$\mathrm{min^{-1}}$
k_σ	$\mathcal{U}$	20.5000	7.7510	0.6463	0.2357	0.6463	0.2615	$\frac{\mathrm{ng}}{\mathrm{L\,min}} \frac{\mathrm{pmol}}{\mathrm{L}} / \frac{\mathrm{mg}}{\mathrm{dL}}$
k_δ	$\mathcal{U}$	3.5000	1.6962	0.4000	0.1888	0.4000	0.1706	$\frac{\mathrm{ng}}{\mathrm{L}} / \frac{\mathrm{mg}}{\mathrm{dL}}$
k_{h1}	$\mathcal{LN}$	0.0102	0.0054	0.0102	0.0059	0.0102	0.0057	$\mathrm{min^{-1}}$
k_{h2}	$\mathcal{LN}$	0.1192	0.0664	0.1192	0.0584	0.1192	0.0737	$\mathrm{min^{-1}}$
k_{h3}	$\mathcal{LN}$	0.0257	0.0146	0.0257	0.0142	0.0257	0.0129	$\mathrm{min^{-1}}$
V_H		38.5000	0.0000	38.5000	0.0000	38.5000	0.0000	$\mathrm{mL\,kg^{-1}}$

Table A.3: Distribution, mean, and standard deviation of basal values in TNDM, T2DM, and T1DM subjects.

Compartment	Sign	TNDM	T2DM	T1DM	Unit
Glucose kinetics	G^{b}	$\mathcal{LN}(89.47, 3.87)$	$\mathcal{LN}(119.91, 6.21)$	$\mathcal{LN}(120.88, 5.47)$	$\mathrm{mg\,dL^{-1}}$
Hepatic glucose production	$S_{\mathrm{G}}^{\mathrm{b}}$	$\mathcal{LN}(1.91, 0.23)$	$\mathcal{LN}(2.04, 0.28)$	$\mathcal{LN}(2.84, 0.39)$	$\mathrm{mg\,kg^{-1}\,min^{-1}}$
Insulin kinetics	I^{b}	$\mathcal{LN}(25.43, 5.10)$	$\mathcal{LN}(59.81, 11.43)$	$\mathcal{LN}(106.41, 18.22)$	$\mathrm{pmol\,L^{-1}}$
Glucagon kinetics	H^{b}	$\mathcal{LN}(126.79, 25.39)$	$\mathcal{LN}(210.47, 46.91)$	$\mathcal{LN}(56.01, 10.38)$	$\mathrm{ng\,L^{-1}}$

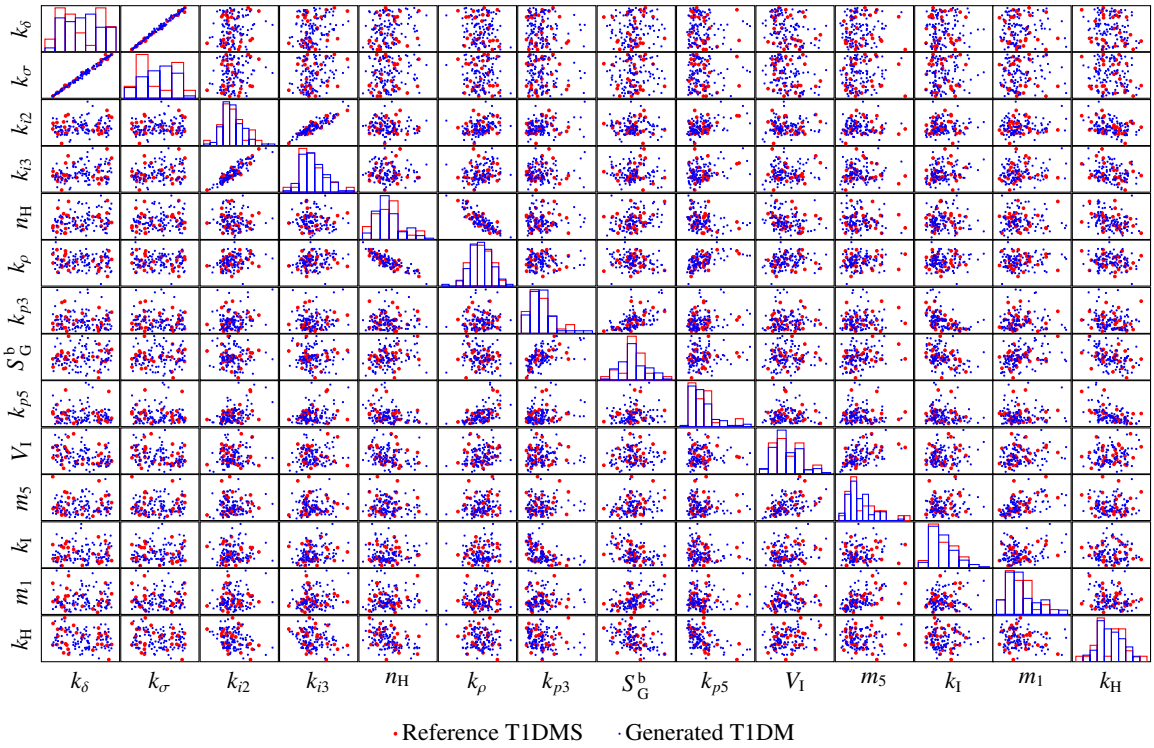

Figure A.1: Combined scatter and histogram plot of the 14 parameters with the highest pairwise correlation coefficients ($|\rho| \geq 0.5$). The main diagonal shows the histogram (normalized to the probability density function) of each parameter. All other axes are scatter plots between every parameter pair. Reference sets from T1DMS subjects ($n = 30$, red dots) are compared to generated T1DM virtual subjects ($n = 100$, blue dots). Note that tick labels have been omitted here for better readability.

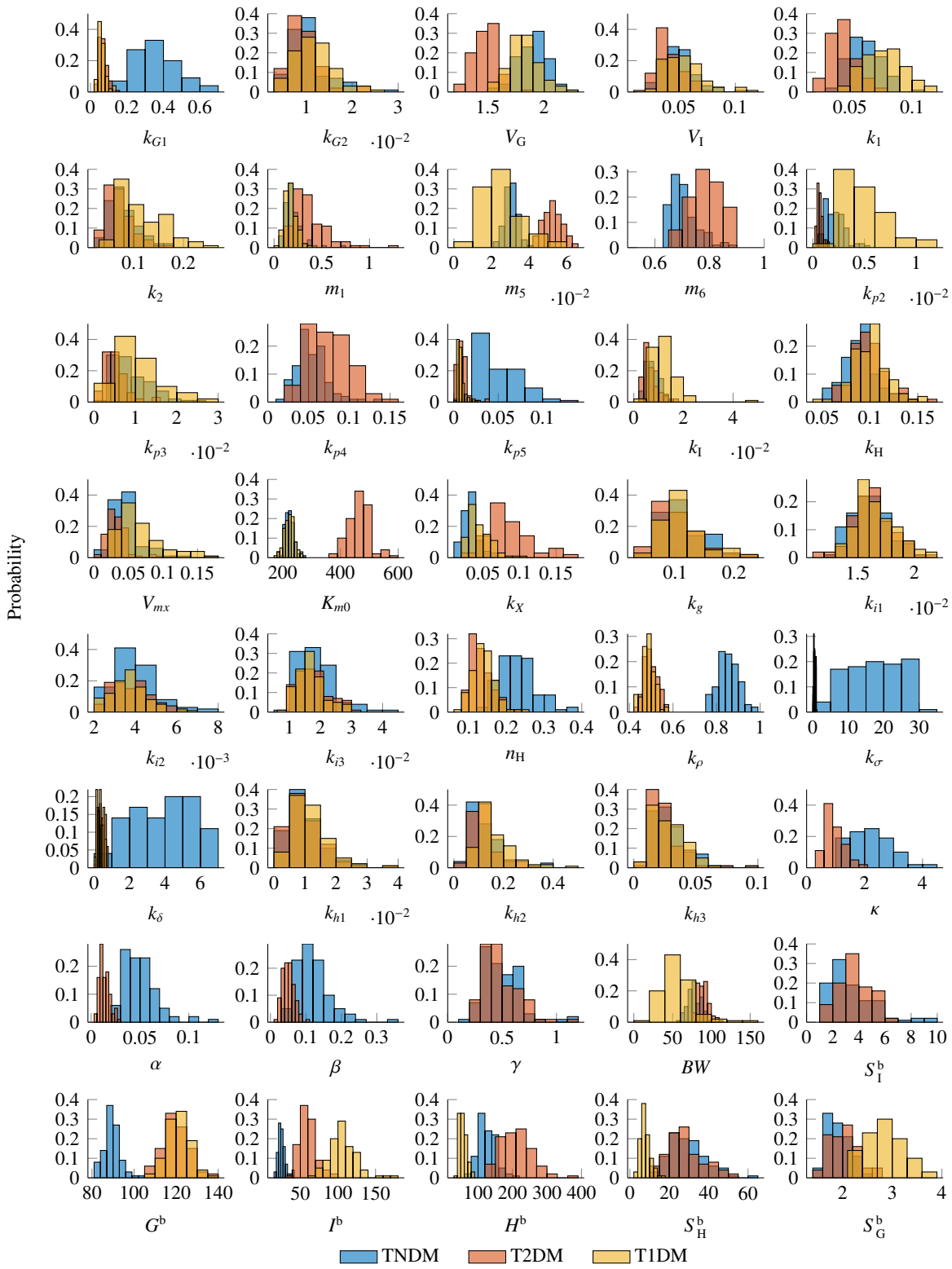

Figure A.2: Histogram (normalized to probability) of all model parameters grouped by TNDM (blue), T2DM (red), and T1DM (yellow) virtual subjects.

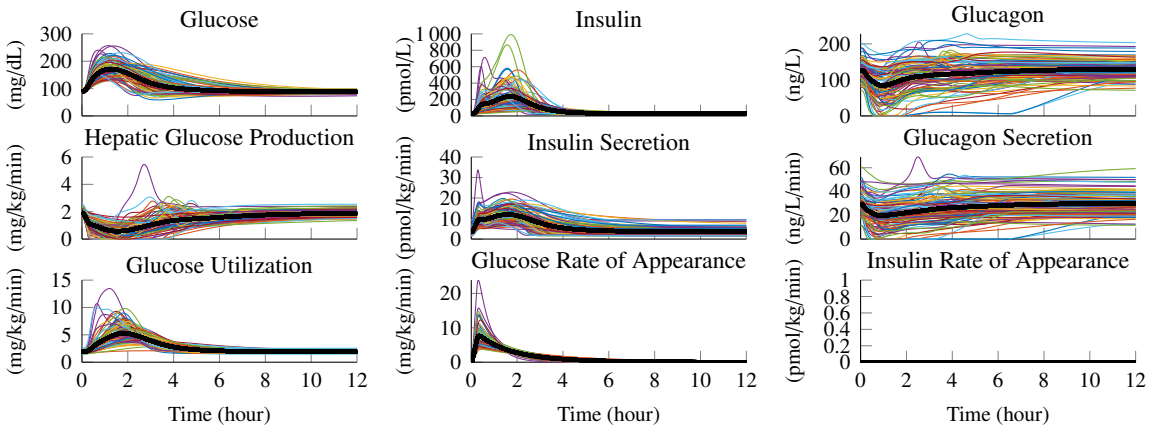

Figure A.3: MTT simulation outputs for 100 virtual TNDM subjects. Ensemble means drawn in black.

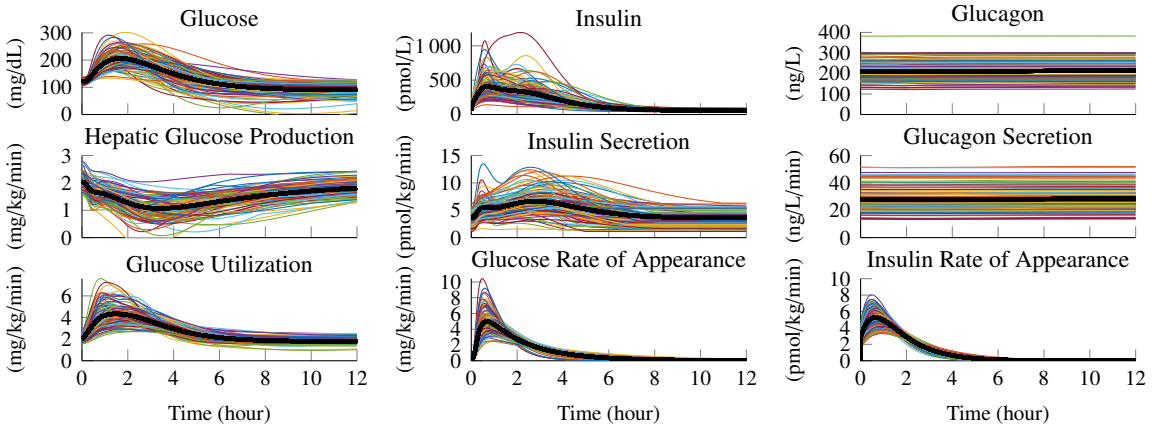

Figure A.4: MTT simulation outputs for 100 virtual T2DM subjects. Ensemble means drawn in black. Note the significant low glucose levels for several subjects which is not physiologic. However, as the patients are randomly picked, the default insulin bolus may be too high for these subjects. However, when the whole population is considered, individual time courses are not of importance.

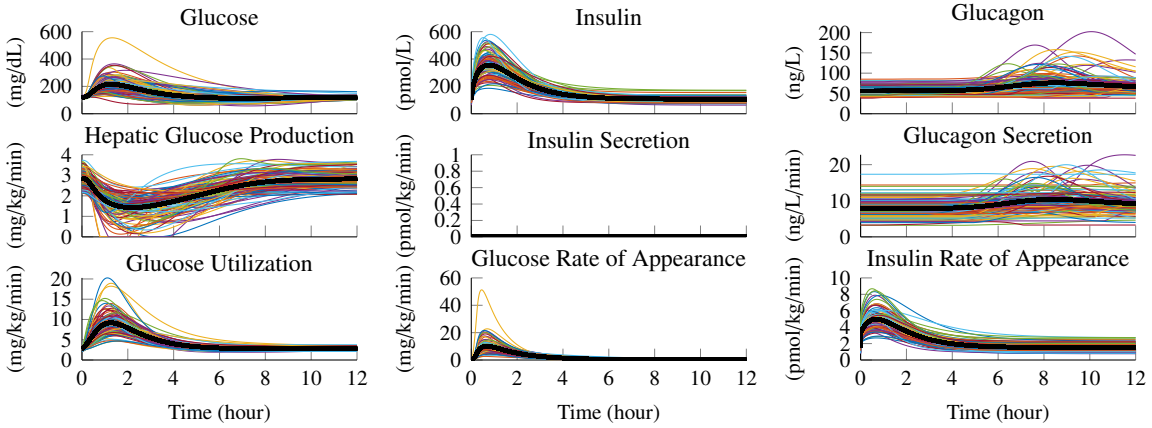

Figure A.5: MTT simulation outputs for 100 virtual T1DM subjects. Ensemble means drawn in black.

B Systems Analysis

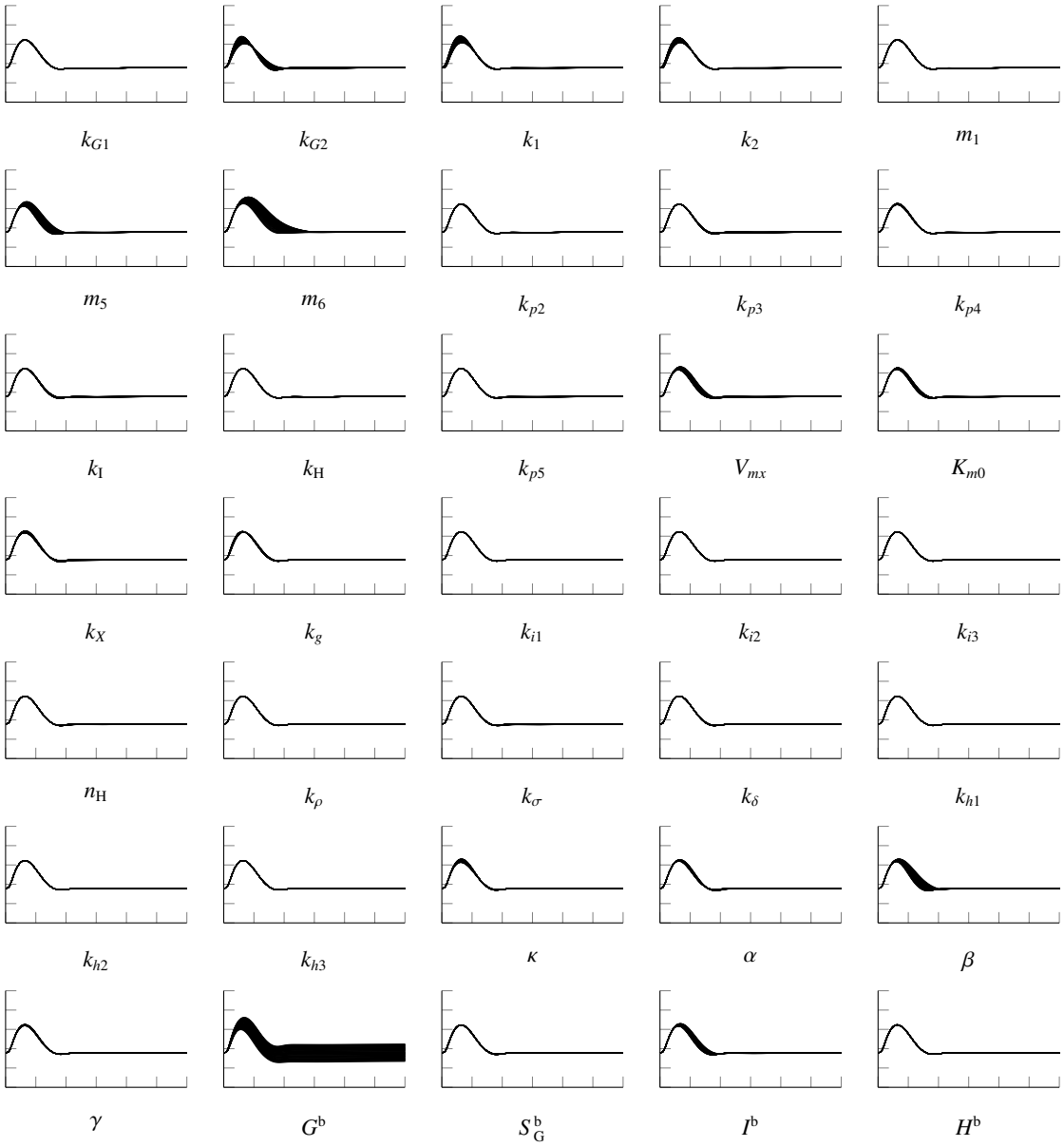

Figure B.1: Variability induced in glucose model output after deflection of each single parameter in TNDM.

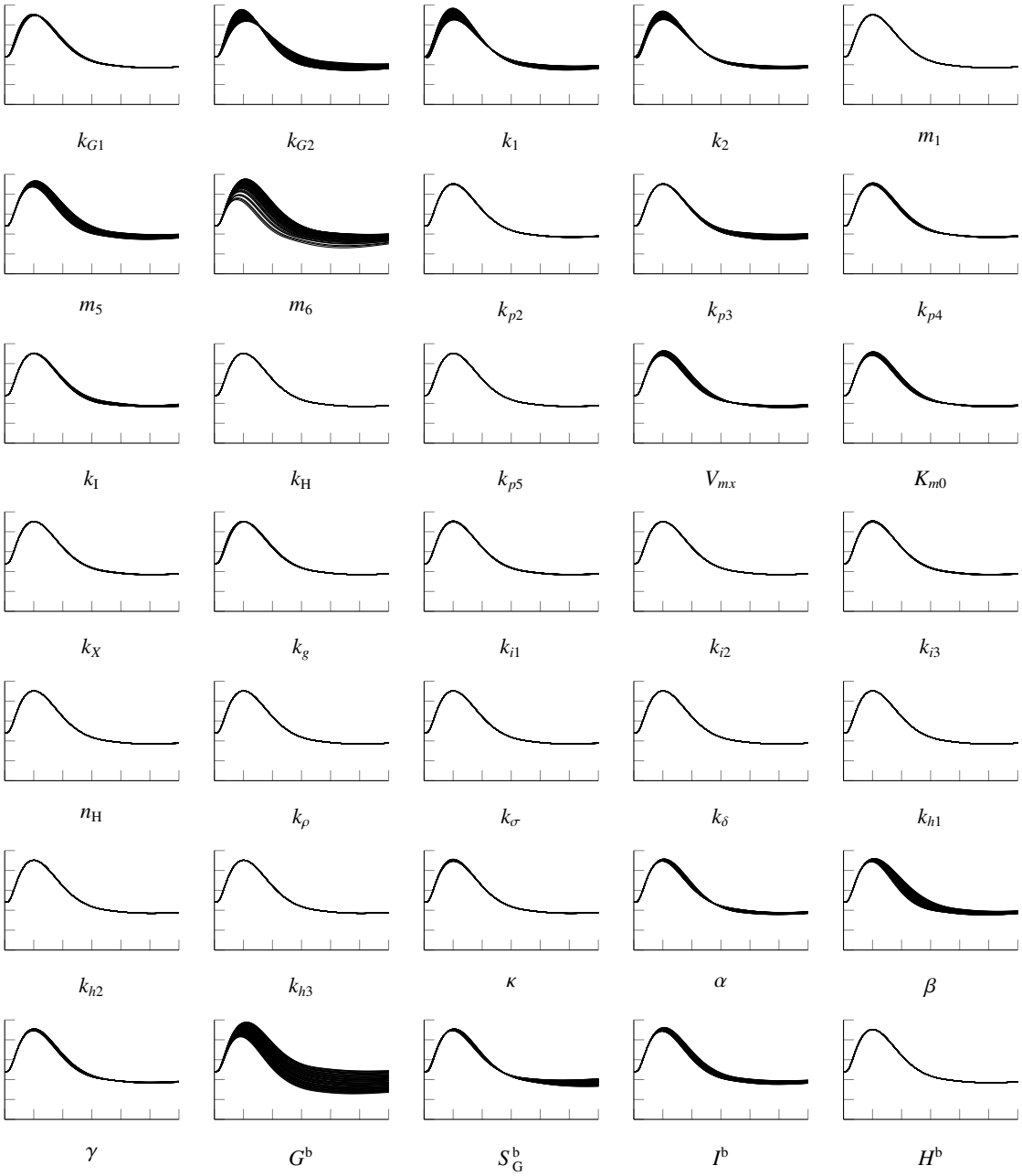

Figure B.2: Variability induced in glucose model output after deflection of each single parameter in T2DM.

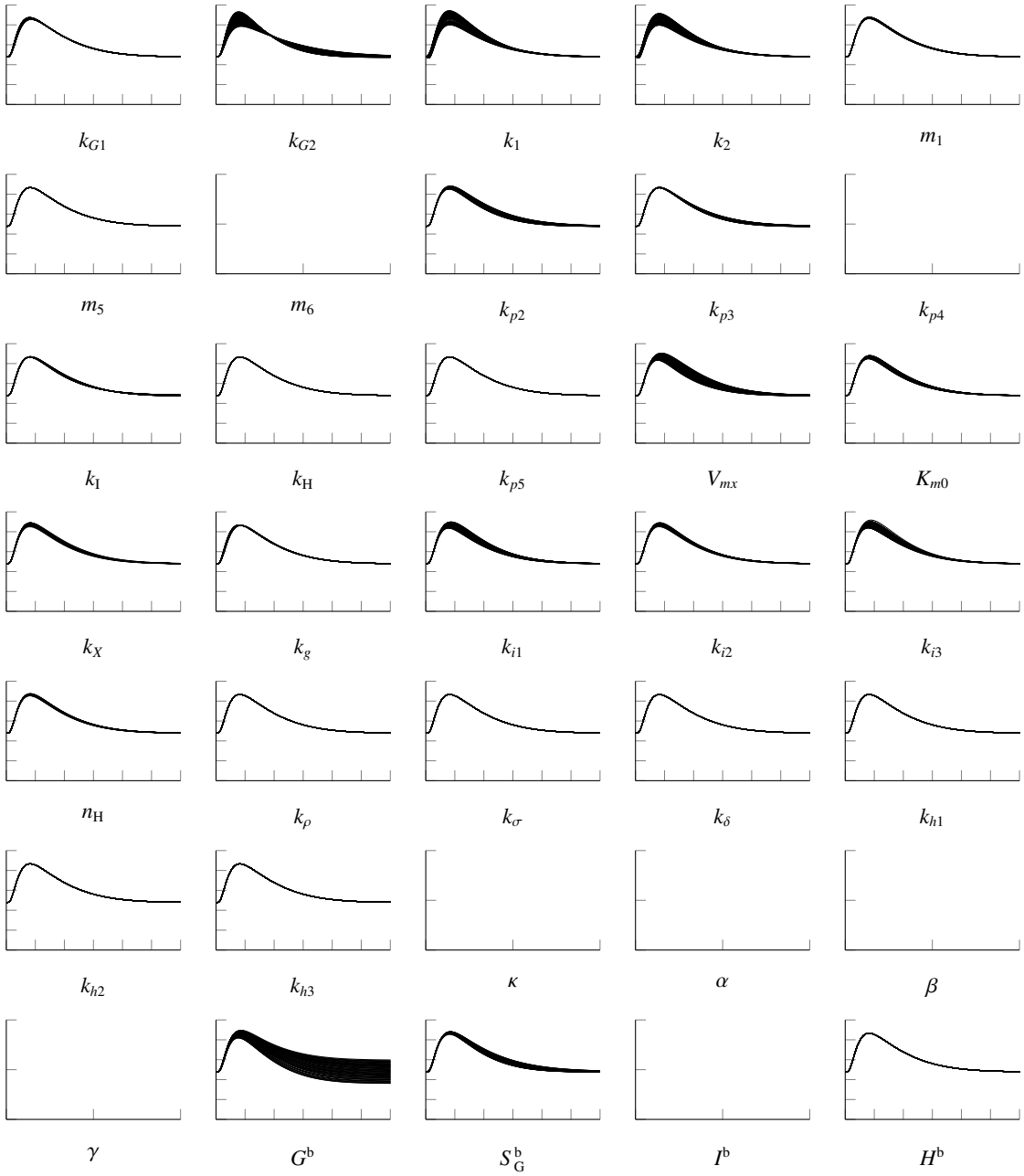

Figure B.3: Variability induced in glucose model output after deflection of each single parameter in T1DM.

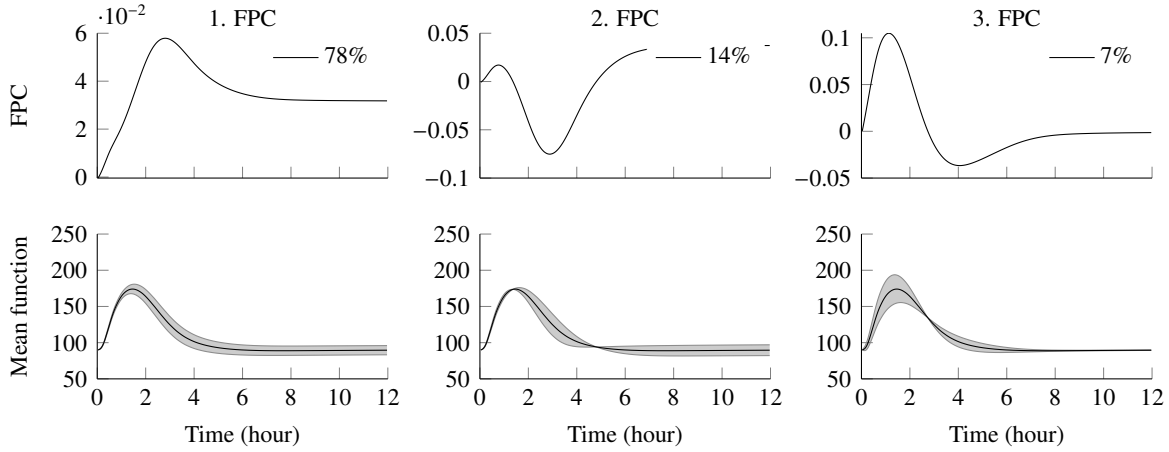

Figure B.4: First three functional principal components (FPC) for glucose model output (upper panel) and mean function plus and minus multiples of each FPC (lower panel) for TNDM.

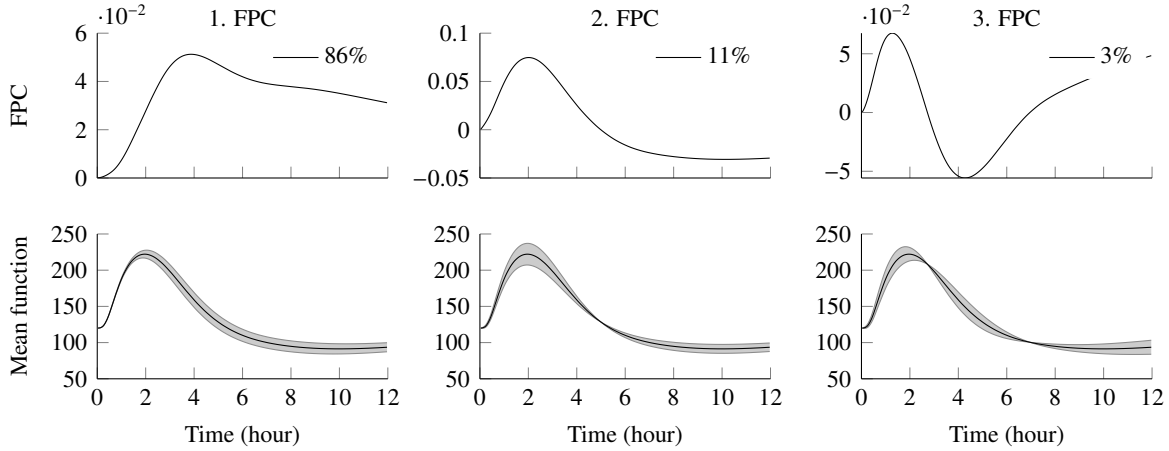

Figure B.5: First three functional principal components (FPC) for glucose model output (upper panel) and mean function plus and minus multiples of each FPC (lower panel) for T2DM.

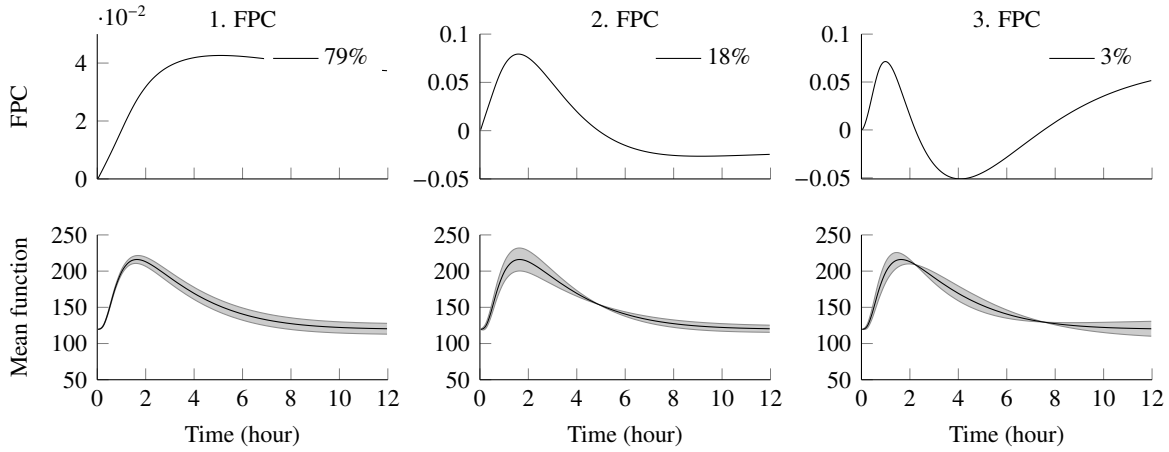

Figure B.6: First three functional principal components (FPC) for glucose model output (upper panel) and mean function plus and minus multiples of each FPC (lower panel) for T1DM.

Table B.1: First-order indices, S_i, and total-order indices, S_{T_i}, for TNDM.

	FPCs	Parameter									
		G^{b}	m_6	β	m_5	I^{b}	V_{mx}	k_{G2}	k_1	k_2	K_{m0}
S_i	1.	0.79	0.07	0.04	0.03	0.01	0.00	−0.01	−0.01	−0.01	−0.01
	2.	0.18	0.28	0.22	0.16	0.06	0.06	0.03	0.00	0.01	0.02
	3.	0.00	0.00	−0.01	−0.01	−0.01	−0.01	0.44	0.27	0.15	−0.01
S_{T_i}	1.	0.80	0.08	0.05	0.04	0.02	0.01	0.00	0.00	0.00	0.00
	2.	0.19	0.29	0.22	0.17	0.05	0.06	0.03	0.00	0.00	0.01
	3.	0.02	0.06	0.03	0.03	0.01	0.02	0.47	0.28	0.17	0.00

Table B.2: First-order indices, S_i, and total-order indices, S_{T_i}, for T2DM.

	FPCs	Parameter									
		G^{b}	m_6	m_5	k_{G2}	β	I^{b}	k_{p3}	k_1	$S_{\mathrm{G}}^{\mathrm{b}}$	V_{mx}
S_i	1.	0.52	0.28	0.05	0.02	0.04	0.02	0.01	−0.01	−0.01	0.00
	2.	0.03	0.17	0.02	0.30	0.01	0.01	0.03	0.30	0.08	0.07
	3.	0.07	0.01	0.01	0.29	0.12	−0.01	0.02	0.03	0.23	0.05
S_{T_i}	1.	0.54	0.30	0.06	0.03	0.05	0.03	0.02	0.00	0.01	0.00
	2.	0.03	0.18	0.02	0.30	0.01	0.01	0.03	0.30	0.09	0.08
	3.	0.09	0.06	0.03	0.30	0.15	0.02	0.04	0.05	0.25	0.08

Table B.3: First-order indices, S_i, and total-order indices, S_{T_i}, for T1DM.

	FPCs	Parameter									
		G^{b}	V_{mx}	k_{i3}	k_1	k_2	$S_{\mathrm{G}}^{\mathrm{b}}$	k_{G2}	k_{p2}	k_{i1}	m_1
S_i	1.	0.82	0.05	0.01	0.02	0.01	0.02	0.00	0.02	0.00	0.00
	2.	0.08	0.08	0.10	0.29	0.19	0.02	0.32	0.02	0.04	0.02
	3.	0.06	0.29	0.06	0.00	−0.01	0.10	0.30	0.07	0.04	−0.01
S_{T_i}	1.	0.84	0.06	0.02	0.03	0.02	0.03	0.00	0.02	0.01	0.00
	2.	0.06	0.06	0.09	0.28	0.18	0.01	0.31	0.01	0.03	0.00
	3.	0.08	0.30	0.07	0.03	0.02	0.13	0.32	0.08	0.05	0.00

$$\widehat{\boldsymbol{W}}_{C_{TNDM}} = \begin{bmatrix}
1.3 & * & * & * & * & * & * & * & * & * & * & * & 0 & 0 & * & 0 & 0 & * & * \\
* & 48 & * & * & * & * & * & * & * & * & * & * & 0 & 0 & * & 0 & 0 & * & * \\
* & * & 33 & * & * & * & * & * & * & * & * & * & * & * & * & * & * & * & * \\
* & * & * & 67 & * & * & * & * & * & * & * & * & * & * & * & * & * & * & * \\
* & * & * & * & 28 & * & * & * & * & * & * & * & * & * & * & * & * & * & * \\
* & * & * & * & * & 30 & * & * & * & * & * & * & * & * & * & * & * & * & * \\
* & * & * & * & * & * & 21 & * & * & * & * & * & * & * & * & * & * & * & * \\
* & * & * & * & * & * & * & 17 & * & * & * & * & * & * & * & * & * & * & * \\
* & * & * & * & * & * & * & * & 1.4 & * & * & * & 0 & 0 & * & * & * & * & * \\
* & * & * & * & * & * & * & * & * & 1000 & * & * & * & * & * & * & * & * & * \\
* & * & * & * & * & * & * & * & * & * & 270 & * & * & * & * & * & * & * & * \\
* & * & * & * & * & * & * & * & * & * & * & 140 & * & * & * & * & * & * & * \\
0 & 0 & * & * & * & * & * & * & 0 & * & * & * & 0.15 & * & * & 0 & 0 & * & * \\
0 & 0 & * & * & * & * & * & * & 0 & * & * & * & * & 0.058 & * & 0 & 0 & * & * \\
* & * & * & * & * & * & * & * & * & * & * & * & * & * & 76 & * & * & * & * \\
0 & 0 & * & * & * & * & * & * & * & * & * & * & 0 & 0 & * & 3.9 & * & * & * \\
0 & 0 & * & * & * & * & * & * & * & * & * & * & 0 & 0 & * & * & 0.1 & * & * \\
* & * & * & * & * & * & * & * & * & * & * & * & * & * & * & * & * & 69 & * \\
* & * & * & * & * & * & * & * & * & * & * & * & * & * & * & * & * & * & 3.4
\end{bmatrix} \tag{B.1}$$

$$\widehat{\boldsymbol{W}}_{C_{T2DM}} = \begin{bmatrix}
7 & * & * & * & * & * & * & * & * & * & * & * & 0 & 0 & * & 0 & 0 & * & * \\
* & 45 & * & * & * & * & * & * & * & * & * & * & 0 & 0 & * & 0 & 0 & * & * \\
* & * & 160 & * & * & * & * & * & * & * & * & * & * & * & * & * & * & * & * \\
* & * & * & 48 & * & * & * & * & * & * & * & * & * & * & * & * & * & * & * \\
* & * & * & * & 150 & * & * & * & * & * & * & * & * & * & * & * & * & * & * \\
* & * & * & * & * & 21 & * & * & * & * & * & * & * & * & * & * & * & * & * \\
* & * & * & * & * & * & 7.7 & * & * & * & * & * & * & * & * & * & * & * & * \\
* & * & * & * & * & * & * & 5.9 & * & * & * & * & * & * & * & * & * & * & * \\
* & * & * & * & * & * & * & * & 0.44 & * & * & * & 0 & 0 & * & * & * & * & * \\
* & * & * & * & * & * & * & * & * & 1800 & * & * & * & * & * & * & * & * & * \\
* & * & * & * & * & * & * & * & * & * & 170 & * & * & * & * & * & * & * & * \\
* & * & * & * & * & * & * & * & * & * & * & 90 & * & * & * & * & * & * & * \\
0 & 0 & * & * & * & * & * & * & 0 & * & * & * & 0.11 & * & * & 0 & 0 & * & * \\
0 & 0 & * & * & * & * & * & * & 0 & * & * & * & * & 0.044 & * & 0 & 0 & * & * \\
* & * & * & * & * & * & * & * & * & * & * & * & * & * & 2.7 & * & * & * & * \\
0 & 0 & * & * & * & * & * & * & * & * & * & * & 0 & 0 & * & 3.9 & * & * & * \\
0 & 0 & * & * & * & * & * & * & * & * & * & * & 0 & 0 & * & * & 0.1 & * & * \\
* & * & * & * & * & * & * & * & * & * & * & * & * & * & * & * & * & 2.5 & * \\
* & * & * & * & * & * & * & * & * & * & * & * & * & * & * & * & * & * & 0.007
\end{bmatrix} \tag{B.2}$$

$$\widehat{\boldsymbol{W}}_{C_{T1DM}} = \begin{bmatrix}
4.4 & * & * & * & * & 0 & * & 0 & 0 & 0 & * & * & 0 & 0 & * & 0 & 0 & * & 0 \\
* & 39 & * & * & * & 0 & * & 0 & 0 & 0 & * & * & 0 & 0 & * & 0 & 0 & * & 0 \\
* & * & 2300 & * & * & * & * & 0 & 0 & * & * & * & * & * & * & * & * & * & * \\
* & * & * & 1200 & * & * & * & 0 & 0 & * & * & * & * & * & * & * & * & * & * \\
* & * & * & * & 2300 & * & * & 0 & 0 & * & * & * & * & * & * & * & * & * & * \\
0 & 0 & * & * & * & 48 & * & 0 & 0 & * & * & * & * & * & * & 0 & 0 & * & * \\
* & * & * & * & * & * & 13 & 0 & 0 & * & * & * & * & * & * & * & * & * & * \\
0 & 0 & 0 & 0 & 0 & 0 & 0 & 0 & 0 & 0 & 0 & 0 & 0 & 0 & 0 & 0 & 0 & 0 & 0 \\
0 & 0 & 0 & 0 & 0 & 0 & 0 & 0 & 0 & 0 & 0 & 0 & 0 & 0 & 0 & 0 & 0 & 0 & 0 \\
0 & 0 & * & * & * & * & * & 0 & 0 & 2700 & * & * & * & * & * & 0 & 0 & * & * \\
* & * & * & * & * & * & * & 0 & 0 & * & 730 & * & * & * & * & * & * & * & * \\
* & * & * & * & * & * & * & 0 & 0 & * & * & 380 & * & * & * & * & * & * & * \\
0 & 0 & * & * & * & * & * & 0 & 0 & * & * & * & 0.18 & * & * & 0 & 0 & * & * \\
0 & 0 & * & * & * & * & * & 0 & 0 & * & * & * & * & 0.073 & * & 0 & 0 & * & * \\
* & * & * & * & * & * & * & 0 & 0 & * & * & * & * & * & 4.8 & * & * & * & * \\
0 & 0 & * & * & * & 0 & * & 0 & 0 & 0 & * & * & 0 & 0 & * & 3.9 & * & * & 0 \\
0 & 0 & * & * & * & 0 & * & 0 & 0 & 0 & * & * & 0 & 0 & * & * & 0.1 & * & 0 \\
* & * & * & * & * & * & * & 0 & 0 & * & * & * & * & * & * & * & * & 4.4 & * \\
0 & 0 & * & * & * & * & * & 0 & 0 & * & * & * & * & * & * & 0 & 0 & * & 0.024
\end{bmatrix} \tag{B.3}$$

$$\widehat{W}_{O_{TNDM}} = \begin{bmatrix}
0.001 & * & * & * & * & * & * & * & * & * & * & * & * & * & * & * & * & * & * \\
* & 0.001 & * & * & * & * & * & * & * & * & * & * & * & * & * & * & * & * & * \\
* & * & 28 & * & * & * & * & * & * & * & * & * & * & * & * & * & * & * & * \\
* & * & * & 15 & * & * & * & * & * & * & * & * & * & * & * & * & * & * & * \\
* & * & * & * & 1.5 & * & * & * & * & * & * & * & * & * & * & * & * & * & * \\
* & * & * & * & * & 20 & * & * & * & * & * & * & * & * & * & * & * & * & * \\
* & * & * & * & * & * & 1.1 & * & * & * & * & * & * & * & * & * & * & * & * \\
* & * & * & * & * & * & * & 450 & * & * & * & * & * & * & * & * & * & * & * \\
* & * & * & * & * & * & * & * & 1.7 & * & * & * & * & * & * & * & * & * & * \\
* & * & * & * & * & * & * & * & * & 0.97 & * & * & * & * & * & * & * & * & * \\
* & * & * & * & * & * & * & * & * & * & 1.1 & * & * & * & * & * & * & * & * \\
* & * & * & * & * & * & * & * & * & * & * & 2 & * & * & * & * & * & * & * \\
* & * & * & * & * & * & * & * & * & * & * & * & 1.5 & * & * & * & * & * & * \\
* & * & * & * & * & * & * & * & * & * & * & * & * & 1.9 & * & * & * & * & * \\
* & * & * & * & * & * & * & * & * & * & * & * & * & * & 3.8 & * & * & * & * \\
* & * & * & * & * & * & * & * & * & * & * & * & * & * & * & 0.53 & * & * & * \\
* & * & * & * & * & * & * & * & * & * & * & * & * & * & * & * & 110 & * & * \\
* & * & * & * & * & * & * & * & * & * & * & * & * & * & * & * & * & 9.1 & * \\
* & * & * & * & * & * & * & * & * & * & * & * & * & * & * & * & * & * & 3.8
\end{bmatrix} \tag{B.4}$$

$$\widehat{W}_{O_{T2DM}} = \begin{bmatrix}
0.001 & * & * & * & * & * & * & * & * & * & * & * & * & * & * & * & * & * & * \\
* & 0.001 & * & * & * & * & * & * & * & * & * & * & * & * & * & * & * & * & * \\
* & * & 31 & * & * & * & * & * & * & * & * & * & * & * & * & * & * & * & * \\
* & * & * & 18 & * & * & * & * & * & * & * & * & * & * & * & * & * & * & * \\
* & * & * & * & 2.4 & * & * & * & * & * & * & * & * & * & * & * & * & * & * \\
* & * & * & * & * & 27 & * & * & * & * & * & * & * & * & * & * & * & * & * \\
* & * & * & * & * & * & 1.3 & * & * & * & * & * & * & * & * & * & * & * & * \\
* & * & * & * & * & * & * & 18 000 & * & * & * & * & * & * & * & * & * & * & * \\
* & * & * & * & * & * & * & * & 7.8 & * & * & * & * & * & * & * & * & * & * \\
* & * & * & * & * & * & * & * & * & 0.15 & * & * & * & * & * & * & * & * & * \\
* & * & * & * & * & * & * & * & * & * & 13 & * & * & * & * & * & * & * & * \\
* & * & * & * & * & * & * & * & * & * & * & 17 & * & * & * & * & * & * & * \\
* & * & * & * & * & * & * & * & * & * & * & * & 2.9 & * & * & * & * & * & * \\
* & * & * & * & * & * & * & * & * & * & * & * & * & 3.4 & * & * & * & * & * \\
* & * & * & * & * & * & * & * & * & * & * & * & * & * & 4.3 & * & * & * & * \\
* & * & * & * & * & * & * & * & * & * & * & * & * & * & * & 2.6 & * & * & * \\
* & * & * & * & * & * & * & * & * & * & * & * & * & * & * & * & 450 & * & * \\
* & * & * & * & * & * & * & * & * & * & * & * & * & * & * & * & * & 0.18 & * \\
* & * & * & * & * & * & * & * & * & * & * & * & * & * & * & * & * & * & 12
\end{bmatrix} \tag{B.5}$$

$$\widehat{W}_{O_{T1DM}} = \begin{bmatrix}
0.002 & * & * & * & * & * & * & 0 & 0 & * & * & * & * & * & * & * & * & * & * \\
* & 0.002 & * & * & * & * & * & 0 & 0 & * & * & * & * & * & * & * & * & * & * \\
* & * & 18 & * & * & * & * & 0 & 0 & * & * & * & * & * & * & * & * & * & * \\
* & * & * & 15 & * & * & * & 0 & 0 & * & * & * & * & * & * & * & * & * & * \\
* & * & * & * & 1.5 & * & * & 0 & 0 & * & * & * & * & * & * & * & * & * & * \\
* & * & * & * & * & 76 & * & 0 & 0 & * & * & * & * & * & * & * & * & * & * \\
* & * & * & * & * & * & 10 & 0 & 0 & * & * & * & * & * & * & * & * & * & * \\
0 & 0 & 0 & 0 & 0 & 0 & 0 & 0 & 0 & 0 & 0 & 0 & 0 & 0 & 0 & 0 & 0 & 0 & 0 \\
0 & 0 & 0 & 0 & 0 & 0 & 0 & 0 & 0 & 0 & 0 & 0 & 0 & 0 & 0 & 0 & 0 & 0 & 0 \\
* & * & * & * & * & * & * & 0 & 0 & 3.3 & * & * & * & * & * & * & * & * & * \\
* & * & * & * & * & * & * & 0 & 0 & * & 7.9 & * & * & * & * & * & * & * & * \\
* & * & * & * & * & * & * & 0 & 0 & * & * & 9.7 & * & * & * & * & * & * & * \\
* & * & * & * & * & * & * & 0 & 0 & * & * & * & 19 & * & * & * & * & * & * \\
* & * & * & * & * & * & * & 0 & 0 & * & * & * & * & 33 & * & * & * & * & * \\
* & * & * & * & * & * & * & 0 & 0 & * & * & * & * & * & 4.3 & * & * & * & * \\
* & * & * & * & * & * & * & 0 & 0 & * & * & * & * & * & * & 2.5 & * & * & * \\
* & * & * & * & * & * & * & 0 & 0 & * & * & * & * & * & * & * & 440 & * & * \\
* & * & * & * & * & * & * & 0 & 0 & * & * & * & * & * & * & * & * & 0.13 & * \\
* & * & * & * & * & * & * & 0 & 0 & * & * & * & * & * & * & * & * & * & 12
\end{bmatrix} \tag{B.6}$$

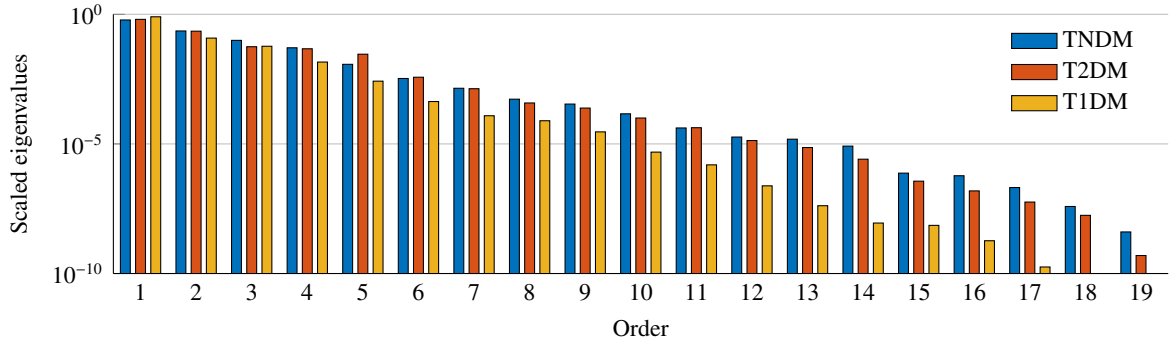

Figure B.7: Scaled eigenvalues of the observability Gramian $\boldsymbol{W}_{\mathrm{O}}$ in the MTT scenario for TNDM (blue), T2DM (red), and T1DM (yellow) subjects. In comparison to the steady-state scenario in Fig. 5.20 the eigenvalue progression is similar. In total, their magnitudes are higher in all groups and the values in T2DM are closer to those in TNDM.

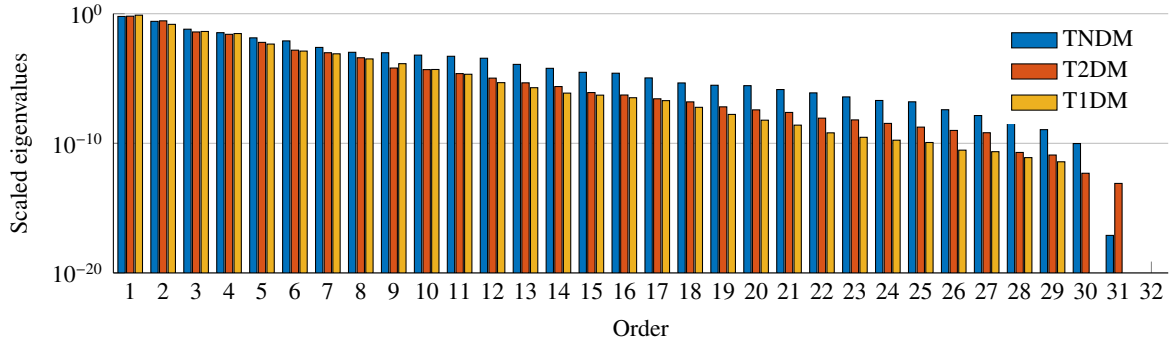

Figure B.8: Scaled eigenvalues of the observability Gramian $\boldsymbol{W}_{\mathrm{O}}^{\star}$ in the STS scenario for TNDM (blue), T2DM (red), and T1DM (yellow) subjects. Eigenvalues from order 32 until 53 are zero and not shown in the graphic.

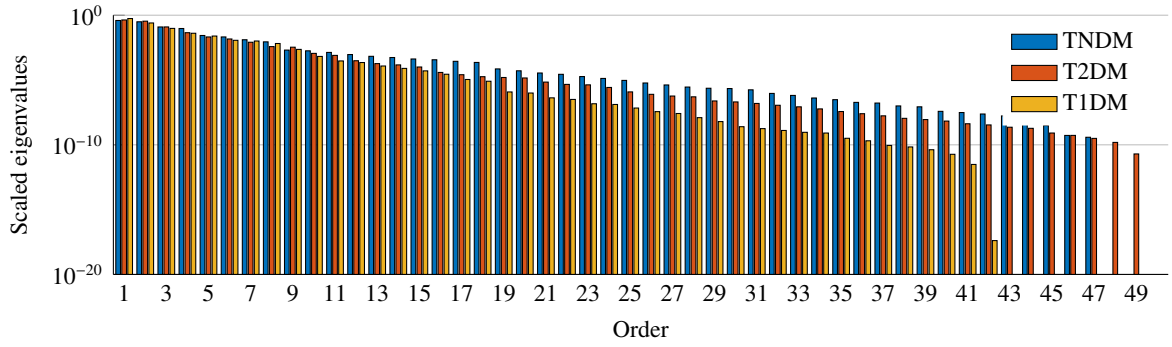

Figure B.9: Scaled eigenvalues of the observability Gramian $\boldsymbol{W}_{\mathrm{O}}^{\star}$ in the MTT scenario for TNDM (blue), T2DM (red), and T1DM (yellow) subjects. All eigenvalue are zero beginning from order 50 and therefore cropped from the graphic. In TNDM and T2DM eigenvalues are almost equal.

Table B.4: Overview on identifiable parameters depending on the group (TNDM, T2DM, T1DM) and the scenario (steady-state (STS), meal tolerance test (MTT)). Identifiable variables are labeled with a checkmark (✓), non-identifiable elements have no entry.

Parameter	STS			MTT		
	TNDM	**T2DM**	**T1DM**	**TNDM**	**T2DM**	**T1DM**
k_1	✓	✓	✓	✓	✓	✓
k_2	✓	✓	✓	✓	✓	✓
m_1	✓	✓	✓	✓	✓	✓
m_5	✓	✓		✓	✓	
m_6	✓	✓	✓	✓	✓	✓
k_{p2}	✓	✓	✓	✓	✓	✓
k_{p3}	✓	✓	✓	✓	✓	✓
k_{p4}	✓	✓		✓	✓	
k_{I}				✓	✓	✓
k_{p5}				✓	✓	✓
k_{H}				✓	✓	✓
V_{mx}				✓	✓	✓
K_{m0}	✓	✓	✓	✓	✓	✓
k_X				✓	✓	✓
κ				✓	✓	
α				✓	✓	
β				✓	✓	
γ	✓	✓		✓	✓	
k_{G1}				✓	✓	✓
k_{G2}				✓	✓	✓
k_g				✓	✓	✓
k_{i1}			✓		✓	✓
k_{i2}			✓		✓	✓
k_{i3}			✓		✓	✓
n_{H}				✓	✓	✓
k_ρ				✓	✓	✓
k_σ				✓	✓	✓
k_δ				✓	✓	✓
k_{h1}						
k_{h2}						
k_{h3}						
G^{b}	✓	✓	✓	✓	✓	✓
I^{b}	✓	✓	✓	✓	✓	✓
H^{b}				✓	✓	✓

C Model Identification

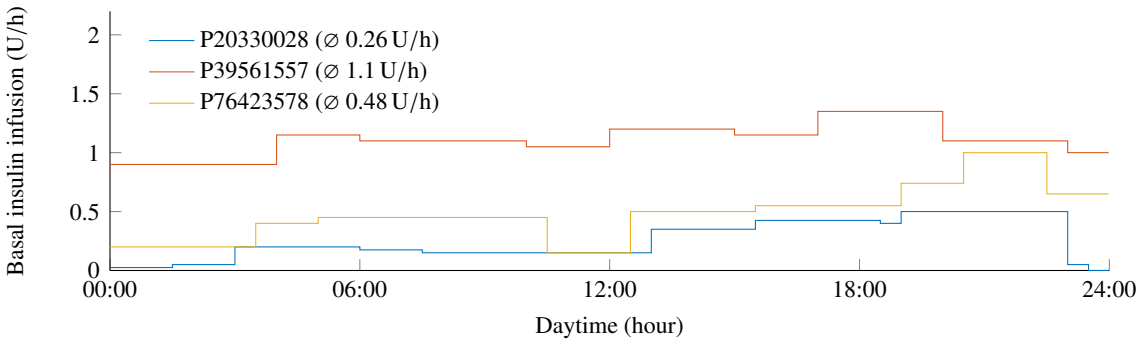

Figure C.1: Basal insulin infusion rates for T1DM subjects (daily mean given in parenthesis).

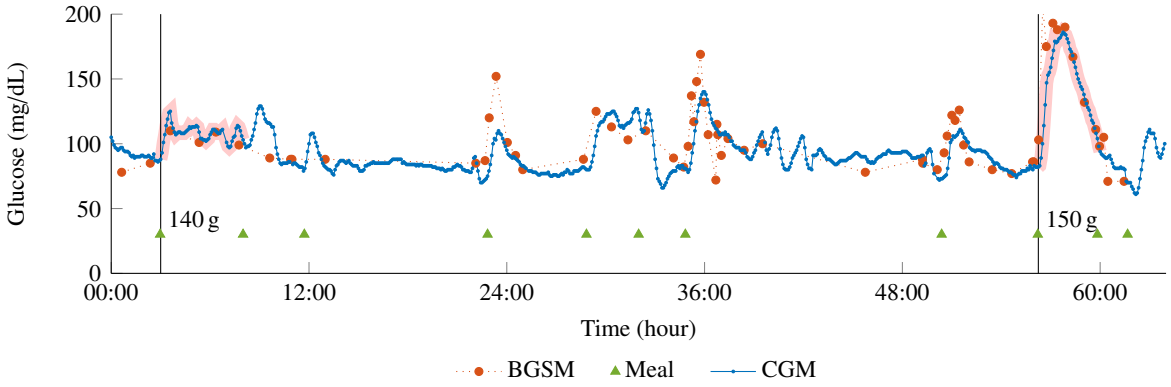

Figure C.2: Differences in the postprandial glucose course of one subject to two meals of a similar amount of CHO. Left (red highlight): glucose values in response to a pizza of 140 g CHO. Right (red highlight): glucose values in response to "Mother's Christmas Stollen" of 150 g CHO.

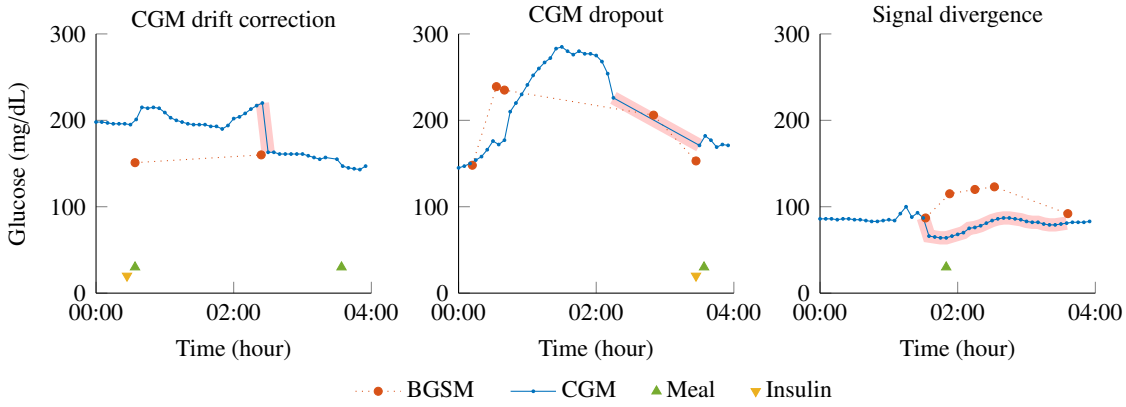

Figure C.3: Artifacts (red highlight) in BGSM and CGM records. Left panel: large difference between the signals and CGM correction after calibration with a BGSM measurement. Middle panel: CGM dropout for 1 h. Right panel: BGSM and CGM signals drifting apart.

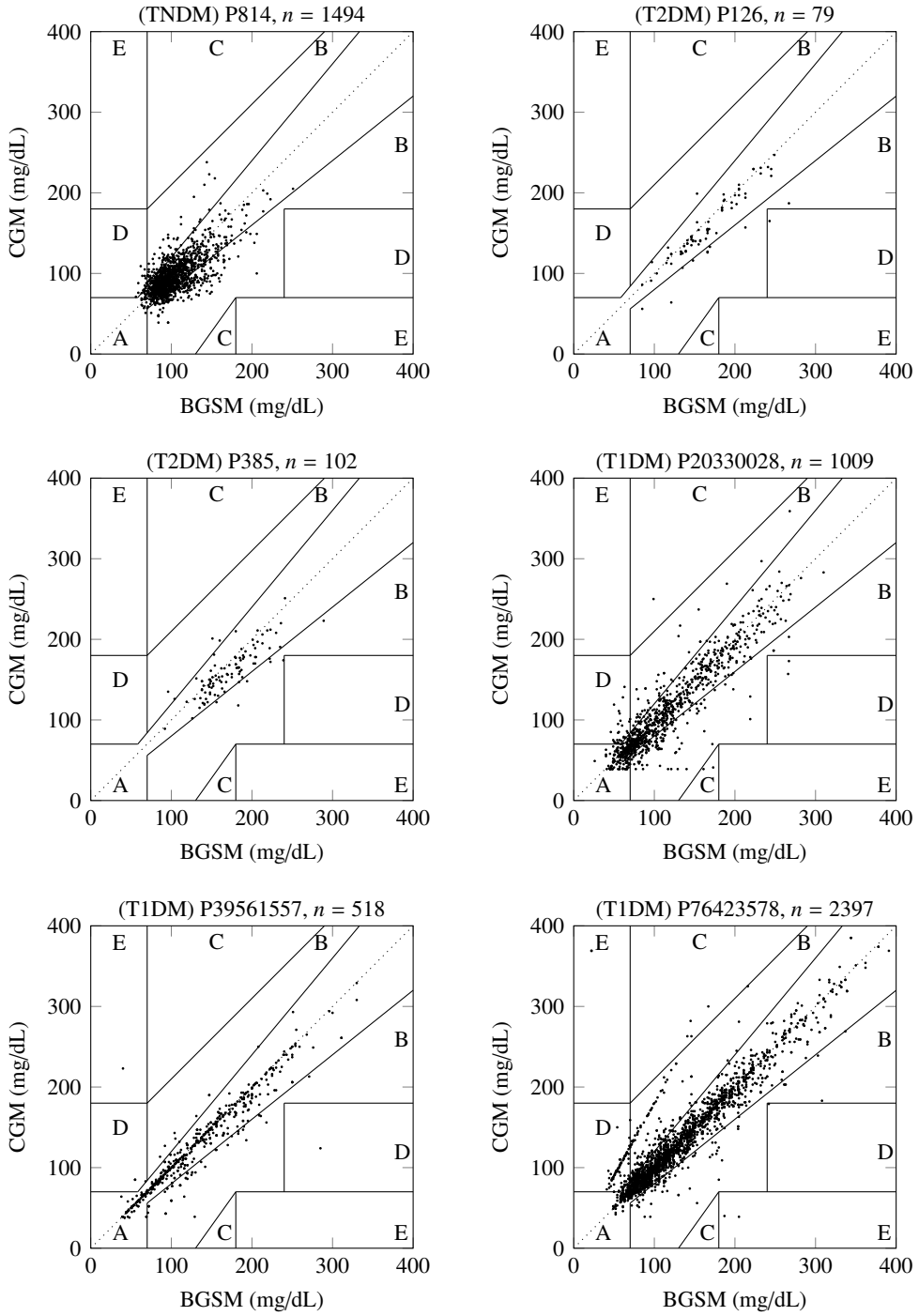

Figure C.4: EGA of n paired blood glucose (BGSM) and continuous glucose (CGM) measurements for one TNDM subject (upper left), 2 T2DM subjects (upper right and middle left), and 3 T1DM (middle right and bottom panel). The whole measurement interval is considered here as reported in Table 6.1. Note that the number of paired values is lower that the total number of BGSM samples as not every BGSM value can be assigned to a CGM value or vice versa.

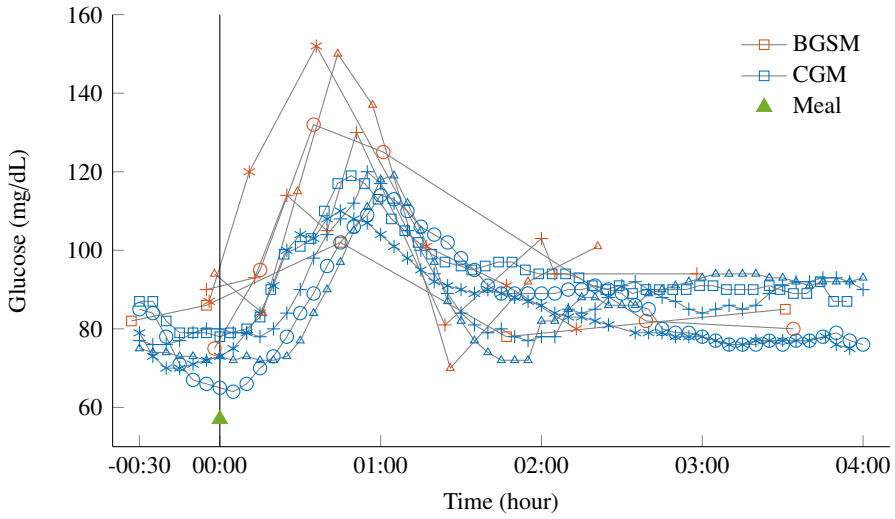

Figure C.5: Time courses of five exemplary selected BGSM (red marker) and CGM (blue marker) signals after a meal of 50 ± 2 g CHO in a TNDM subject, synchronized at 00:00.

Table C.1: Comparison of nominal and identified parameters for the TNDM case in Section 6.2.1. Mean and standard deviation for the nominal parameters derived from 100 virtual TNDM subjects, mean and standard deviation for the identified parameters derived from $r = 25$ repetitions of the optimization. RMSE is the root mean squared error between measured and simulated output.

Parameter	Nominal	Identified	95 % *t*-value[1]	95 % *F*-value[2]
G^{b}	89.4704 ± 3.8749	93 (fixed)	–	–
I^{b}	25.4260 ± 5.0998	37 (fixed)	–	–
k_1	0.0621 ± 0.0128	0.0488 ± 0.0000	10.4141	3×10^{9}
m_5	0.0305 ± 0.0034	0.2096 ± 0.0000	174.1118	2×10^{12}
V_{mx}	0.0469 ± 0.0232	0.0373 ± 0.0000	3.0154	3×10^{10}
β	0.1193 ± 0.0476	0.0135 ± 0.0000	55.1905	2×10^{13}
κ	2.2172 ± 0.7021	0.5886 ± 0.0000	39.5949	1×10^{10}
k_{p3}	0.0090 ± 0.0043	0.0021 ± 0.0000	29.6309	4×10^{9}
α	0.0501 ± 0.0168	0.0774 ± 0.0000	15.5296	2×10^{7}
k_X	0.0326 ± 0.0108	0.0823 ± 0.0000	29.4363	2×10^{7}
RMSE	19.2934	5.2176		

[1]Reference two-sided t-value (95 %): $t(0.975, 26 \ldots 100) = 2.056 \ldots 1.984$.
[2]Reference F-value (95 %): $F(99, 24) = 1.84$.

Table C.2: Comparison of nominal and identified parameters for the T2DM case in Section 6.2.1. Mean and standard deviation for the nominal parameters derived from 100 virtual T2DM subjects, mean and standard deviation for the identified parameters derived from $r = 25$ repetitions of the optimization. RMSE is the root mean squared error between measured and simulated output.

Parameter	Nominal	Identified	95 % *t*-value[1]	95 % *F*-value[2]
G^{b}	119.9087 ± 6.2109	163.8 (fixed)	–	–
I^{b}	59.8123±11.4268	59 (fixed)	–	–
k_1	0.0438 ± 0.0110	0.0272 ± 0.0050	9.7182	4.7623
V_{mx}	0.0331 ± 0.0173	0.0407 ± 0.0095	4.1496	3.2906
β	0.0499 ± 0.0167	0.0255 ± 0.0004	17.8246	1907.8683
κ	0.9632 ± 0.3419	0.7114 ± 0.0181	7.0457	357.1145
k_{p3}	0.0052 ± 0.0027	0.0002 ± 0.0159	11.6494	0.0290
k_{p2}	0.0007 ± 0.0003	0.0076 ± 0.0005	57.3438	0.3467
α	0.0137 ± 0.0052	0.0156 ± 0.0051	4.3889	1.0667
γ	0.4845 ± 0.1680	2.4414 ± 0.1187	48.5553	2.0045
m_5	0.0525 ± 0.0052	0.0999 ± 0.0042	46.5536	1.5679
RMSE	39.6662	7.9173		

[1]Reference two-sided t-value (95 %): $t(0.975, 26 \ldots 100) = 2.056 \ldots 1.984$.
[2]Reference F-value (95 %): $F(99, 24) = 1.84$.

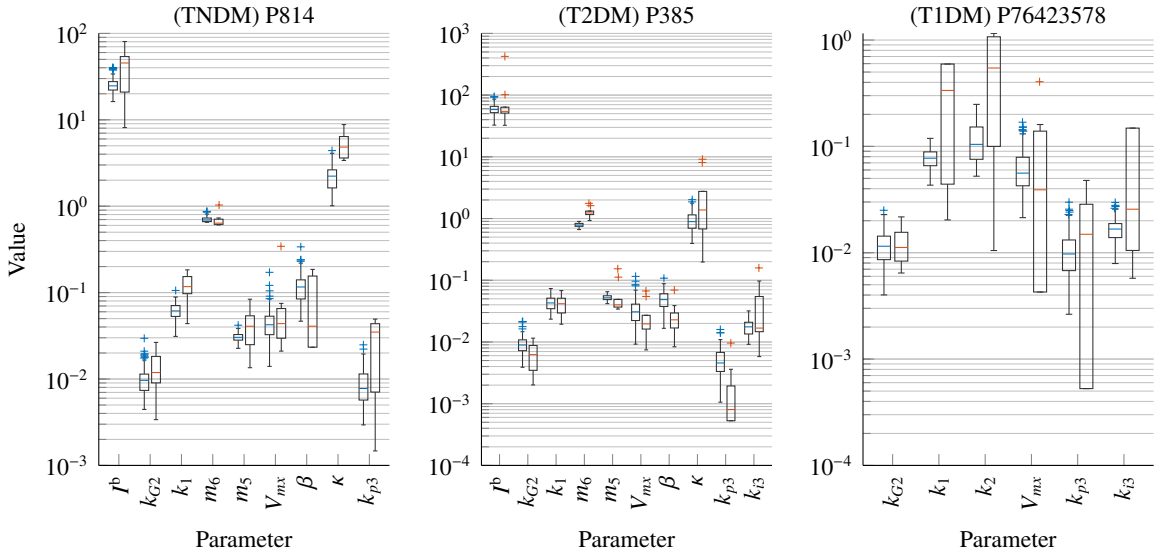

Figure C.6: Distribution of identified parameters from experimental CGM data in three subjects. Left hand side (blue) of each bar pair shows the distribution of the parameter obtained from the nominal 100 virtual subjects. Right hand side of each pair (red) represents the identified parameters.

Table C.3: Configuration parameters of the EKF: initial state covariance $\boldsymbol{P}_0^+$ and process noise covariance $\boldsymbol{Q}$.

State	TNDM		T2DM		T1DM	
	$\text{diag}\left(\sqrt{\boldsymbol{P}_0^+}\right)$	$\text{diag}\left(\sqrt{\boldsymbol{Q}}\right)$	$\text{diag}\left(\sqrt{\boldsymbol{P}_0^+}\right)$	$\text{diag}\left(\sqrt{\boldsymbol{Q}}\right)$	$\text{diag}\left(\sqrt{\boldsymbol{P}_0^+}\right)$	$\text{diag}\left(\sqrt{\boldsymbol{Q}}\right)$
x_1	10 000	10 000	10 000	10 000	10 000	10 000
x_2	10 000	10 000	10 000	10 000	10 000	10 000
x_3	163.56	100	217.54	10	224.72	100
x_4	231.53	100	116.84	10	135.21	100
x_5	163.56	100	217.54	10	224.72	100
x_6	2.27	0.23	3.73	0.37	2.21	0.22
x_7	2.62	0.26	17.60	1.76	1.50	0.15
x_8	7.5	1×10^{-5}	7.5	1×10^{-5}	0	1×10^{-5}
x_9	1.78	0.18	23.82	2.38	0	1×10^{-5}
x_{10}	250	1×10^{-5}	250	1×10^{-5}	0	1×10^{-5}
x_{11}	45.44	4.54	93.37	9.34	43.25	4.32
x_{12}	45.44	4.54	93.37	9.34	43.25	4.32
x_{13}	0	1×10^{-5}	700	1×10^{-5}	34.58	3.46
x_{14}	0	1×10^{-5}	250	1×10^{-5}	21.82	2.18
x_{15}	126	12.6	208	20.8	56.98	5.70
x_{16}	0	1×10^{-5}	0	1×10^{-5}	0	1×10^{-5}
x_{17}	0	1×10^{-5}	0	1×10^{-5}	0	1×10^{-5}
x_{18}	3	1×10^{-5}	3	1×10^{-5}	3	1×10^{-5}
x_{19}	27.72	2.77	27.96	2.80	7.66	0.77

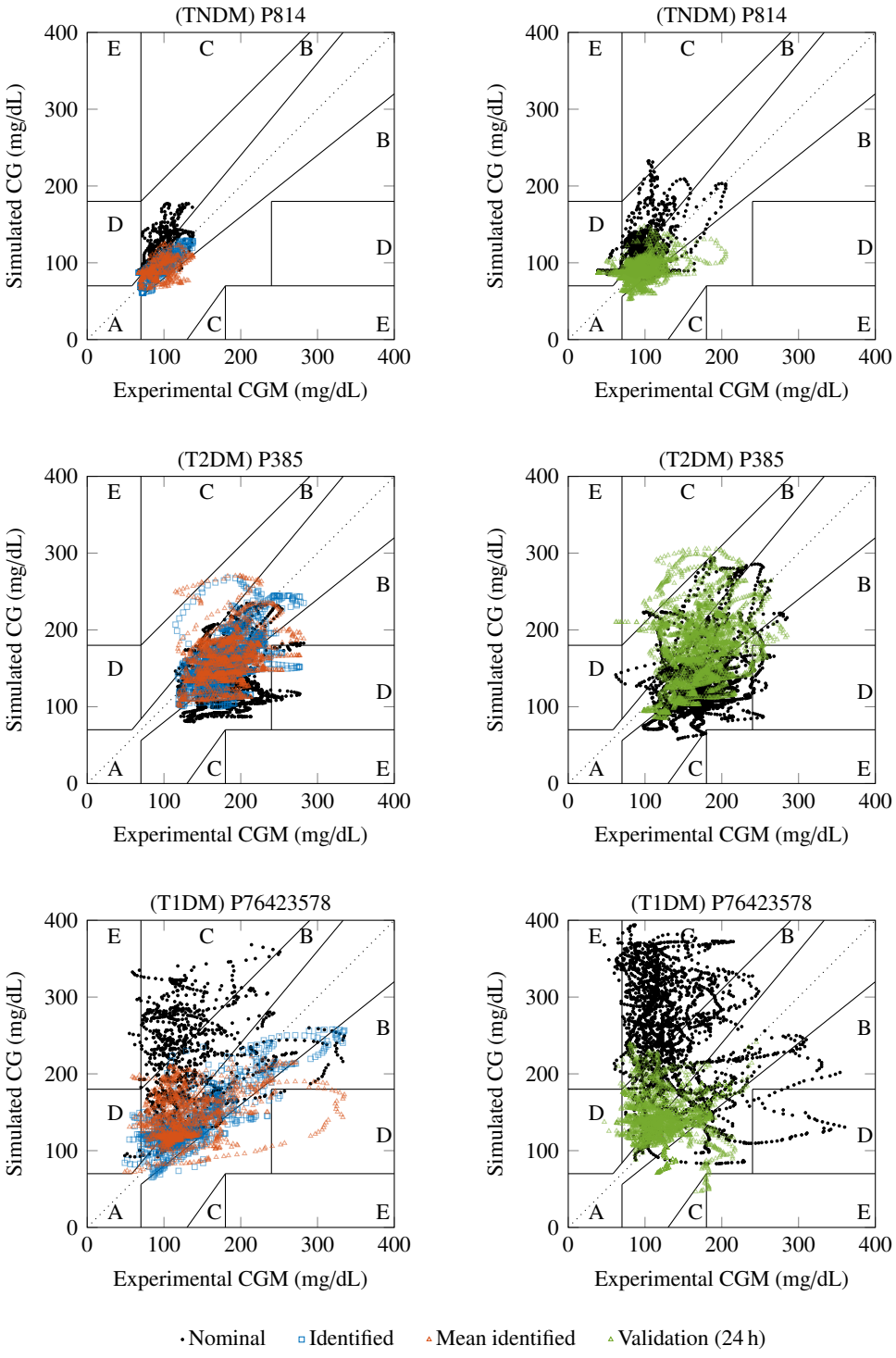

Figure C.7: EGA of paired experimental CGM data and simulated CG signals for three subjects: P814 (upper), P385 (middle), and P76423578 (lower panel). CGM records obtained from $r = 10$ measurement sequences, simulation data generated by the models: nominal (black), identified (blue), and mean identified (red) on the left side each, further validated on r additional full-day intervals (green) on the right side each.

List of Figures

List of Tables

List of Abbreviations and Symbols

Medical Terms

BG	Blood Glucose
BGSM	Blood Glucose Self-Management
CG	Continuous Glucose
CG-EGA	Continuous Glucose-Error Grid Analysis
CGM	Continuous Glucose Measurement
CGS	Continuous Glucose Sensor
CHO	Carbohydrates
CSII	Continuous Subcutaneous Insulin Infusion
CU	Carbohydrate Unit
ECG	Electrocardiogram
EEG	Electroencephalography
EGA	Error Grid Analysis
eHealth	Electronic Health
i.m.	intramuscular
i.p.	intraperitoneal
i.v.	intravenous
ICT	Intensified Conventional insulin Therapy
IFG	Impaired Fasting Glucose
IGT	Impaired Glucose Tolerance
IIR	Insulin Infusion Rate
IIT	Insulin Infusion Test
IMFSIGT	(Insulin-Modified) Frequently Sampled Intravenous Glucose Tolerance Test
ISF	Interstitial Fluid
ISR	Insulin Secretion Rate
IVGTT	Intravenous Glucose Tolerance Test
mHealth	Mobile Health
MPC	Model Predictive Control
MTT	Meal Tolerance Test
OGTT	Oral Glucose Tolerance Test
OMM	Oral Minimal Model
s.c.	subcutaneous

T1DM	Type 1 Diabetes Mellitus
T2DM	Type 2 Diabetes Mellitus
TNDM	Type Non-Diabetic Mellitus, note: this is not a common term, but here it is used for a consistent abbreviation scheme to distinguish between non-diabetic and diabetic subjects

Abbreviations

AAT-Sampling	All-[factors]-At-a-Time-Sampling
ACF	AutoCorrelation Function
ANOVA	ANalysis Of VAriance
API	Application Programming Interface
ARMA(X)	Autoregressive-Moving-Average (eXogenous inputs)
BAN	Body Area Network
CC	Correlation Coefficient
CDF	Cumulative Distribution Function
EE	Elementary Effect
EET	Elementary Effects Test
EKF	Extended Kalman Filter
FPC	Functional Principal Component
FPCA	Functional Principal Component Analysis
HDMR	High-Dimensional Model Representation
HSV	Hankel Singular Values
HTML	HyperText Markup Language
JSON	JavaScript Object Notation
KF	Kalman Filter
LHS	Latin Hypercube Sampling
MAE	Mean Absolute Error
MAPD	Mean Absolute Percentage Difference
MARD	Mean Absolute Relative Difference
MoDiM	Model-based Diabetes Monitoring
NFC	Near Field Communication
OAT-Sampling	One-[factor]-At-a-Time-Sampling
PACF	Partial AutoCorrelatation Function
PC	Principal Component
PCA	Principal Component Analysis
PCC	Partial Correlation Coefficient
PDF	Probability Density Function
PRCC	Partial Rank Correlation Coefficient
REST	Representational State Transfer
RMSE	Root Mean Squared Error

SA	Sensitivity Analysis
SRCC	Spearman Rank Correlation Coefficient
UA	Uncertainty Analysis
UKF	Unscented Kalman Filter
VBSA	Variance-Based Sensitivity Analysis

Mathematical Notations and Symbols

$\dot{\square}$	Time derivative
$\bar{\square}$	Sample mean value
$\hat{\square}$	Identified value
$\tilde{\square}$	Estimated value
$\square_i^{(j)}$	Indices i and j
$\square_k$	Discrete-time notation when used with a vector
$\square^-$	A priori Kalman estimate
$\square^+$	A posteriori Kalman estimate
λ	Eigenvalue
μ	Mean value
$\mu_i^\star$	Mean of elementary effect of input factor i
$\bar{\mu}_i^\star$	Overall mean of elementary effect of input factor i
ψ	Basis function
ρ	Correlation coefficient
Σ , $\widehat{\Sigma}$, $\widetilde{\Sigma}$	General nonlinear system, augmented, transformed system
σ	Standard deviation
σ^2	Variance
$\sigma_i^\star$	Standard deviation of elementary effect of input factor i
$\mathbf{0}$	Null matrix of appropriate dimension
$\boldsymbol{A}$	Linear state matrix in state-space notation
$\boldsymbol{B}$	Linear input matrix in state-space notation
$\mathrm{Cov}\{\square\}$	Covariance
$\boldsymbol{C}$	Linear output matrix in state-space notation
C_i	Substance concentration in compartment i
c_i	Scale factor
c_v	Coefficient of variation
d_i	Scale factor
$\mathcal{E}$	General set
$\mathcal{E}_u$, $\mathcal{E}_x$	Set of standard unit vectors
$\mathrm{E}\{\square\}$	Expectation value
E_C , E_O	Generalized energy transfer
$\boldsymbol{F}$	Linearized state matrix in state-space notation
F_{ij}	Substance flux from compartment i to compartment j

FVE	Fraction of Variance Explained
$\mathbf{f}(\blacksquare)$	General (non-)linear state function
$f(\blacksquare)$	General scalar, (non-)linear function
$\boldsymbol{G}$	Linearized output matrix in state-space notation
$\mathbf{g}(\blacksquare)$	General (non-)linear output function
$\boldsymbol{I}$	Unit matrix of appropriate dimension
$\boldsymbol{K}$	Kalman gain
K	Number of input factors
k	Discrete-time index
$\mathcal{LN}$	Log-normal distribution
M	Number of model inputs
$\mathcal{N}$	Normal distribution
N , $\hat{N}$	Number of model states, augmented states
n	Number of samples, measurements, or observations
O	Number of model outputs
$\boldsymbol{P}$	Estimation error covariance matrix
P	Number of model parameters
P_i	Endogenous production into compartment i
$\boldsymbol{p}$	Vector of system parameters
$\mathcal{Q}_u$, $\mathcal{Q}_x$	Set of scale factors
$\boldsymbol{Q}$	Process noise covariance matrix
Q	Objective function
Q_i	Substance mass in compartment i
q	Number of functional principal components
$\mathcal{R}_u$, $\mathcal{R}_x$	Set of orthogonal matrices
$\boldsymbol{R}$	Measurement noise covariance matrix
r	Number of repetitions, number of grid points
$\mathcal{S}$, $\hat{\mathcal{S}}$	Subject, identified subject
S_i	First-order sensitivity index of input factor i
$\bar{S}_i$	Overall first-order sensitivity index of input factor i
S_{T_i}	Total-order sensitivity index of input factor i
$\bar{S}_{T_i}$	Overall total-order sensitivity index of input factor i
t	Continuous-time
t_h	Filter prediction horizon
t_s	Filter shift window
t_w	Filter estimation window
$\mathcal{U}$	Uniform distribution
U_i	Exogenous input into compartment i
$\boldsymbol{u}$	Vector of system inputs

$\mathrm{Var}\{\blacksquare\}$	Variance
$\boldsymbol{V}$	General linear transformation matrix
V_i	Volume of compartment i
$\boldsymbol{v}$	Measurement noise
$\boldsymbol{W}_\mathrm{C}$, $\widehat{\boldsymbol{W}}_\mathrm{C}$, $\widetilde{\boldsymbol{W}}_\mathrm{C}$	Controllability Gramian, empirical Gramian, transformed matrix
$\boldsymbol{W}_\mathrm{I}$	Identifiability Gramian matrix
$\boldsymbol{W}_\mathrm{O}$, $\widehat{\boldsymbol{W}}_\mathrm{O}$, $\boldsymbol{W}_\mathrm{O}^\star$, $\widetilde{\boldsymbol{W}}_\mathrm{O}$	Observability Gramian, empirical Gramian, augmented, transformed matrix
$\boldsymbol{w}$	Process noise
X	Stochastic input factor
$\boldsymbol{x}$, $\hat{\boldsymbol{x}}$, $\tilde{\boldsymbol{x}}$	Vector of system states, augmented, transformed vector
$\boldsymbol{x}_0$, $\boldsymbol{x}_\mathrm{f}$	Vector of initial and final system states
Y	Stochastic output
$\boldsymbol{y}$	Vector of system outputs
$\boldsymbol{z}$	Vector of disturbances

List of Own Publications

Tolks, C.; Ament, C. (2015a). *Analyse und Ordnungsreduktion von Modellen der Glukose-Insulin-Homöostase auf Basis Empirischer Gramscher Matrizen*. Regelungstechnisches Kolloquium. Boppard, Germany.
URL: http://www.iosb.fraunhofer.de/servlet/is/52331/.

Tolks, C.; Ament, C. (2015b). *Empirische Gramsche Matrizen für die Zustands- und Parameterraumreduktion von Modellen der Glukose-Insulin-Homöostase*. GMA Fachausschuss 1.30. Anif/Salzburg, Austria.
URL: http://www.gma.tu-darmstadt.de/gma/index.de.jsp.

Tolks, C.; Ament, C. (2017a). Identification of parameters of the glucose-insulin homeostasis under everyday live conditions. In: *2017 IEEE EMBS International Conference on Biomedical & Health Informatics (BHI)*, pp. 81–84.
DOI: 10.1109/BHI.2017.7897210.

Tolks, C.; Ament, C. (2017b). Model Order Reduction of Glucose-Insulin Homeostasis Using Empirical Gramians and Balanced Truncation. In: *IFAC-PapersOnLine* 50 (1), pp. 14735–14740.
DOI: 10.1016/j.ifacol.2017.08.2576.

Tolks, C.; Ament, C.; Eberle, C. (2018a). A Mobile Platform for Model-based Monitoring of Glucose-Insulin Homeostasis for Diabetics. In: *CHASE '18: Proceedings of the 2018 IEEE/ACM International Conference on Connected Health*. Ed. by Association for Computing Machinery. New York, NY, USA, pp. 15–16.
DOI: 10.1145/3278576.3278583.

Tolks, C.; Ament, C.; Eberle, C. (2018b). Model-driven Classification of Different Diabetes Types within a Personalized Diabetes Management. In: *Annual International Conference of the IEEE Engineering in Medicine and Biology Society*, pp. 5818–5821.
DOI: 10.1109/EMBC.2018.8513641.

Tolks, C.; Ament, C.; Eberle, C. (2019). Model of the Glucose-Insulin Metabolism Incorporating Both Type 1 and Type 2 Diabetes (accepted). In: *2019 IEEE Austria International Biomedical Engineering Conference (AIBEC)*.

Tolks, C.; Ament, C.; Eberle, C. (2020). Multi-Step Approach for Sensitivity Analysis for a Unified Model of Glucose-Insulin Metabolism. In: *IFAC-PapersOnLine* 53 (2), pp. 16394–16399.
DOI: 10.1016/j.ifacol.2020.12.680.

List of References

Acciaroli, G.; Vettoretti, M.; Facchinetti, A.; Sparacino, G. (2018). Calibration of Minimally Invasive Continuous Glucose Monitoring Sensors: State-of-The-Art and Current Perspectives. In: *Biosensors* 8 (1).
DOI: 10.3390/bios8010024.

Ackerman, E.; Rosevear, J. W.; McGuckin, W. F. (1964). A Mathematical Model of the Glucose-tolerance test. In: *Physics in Medicine and Biology* 9 (2), pp. 203–213.
DOI: 10.1088/0031-9155/9/2/307.

Adeva-Andany, M. M. et al. (2019). Metabolic effects of glucagon in humans. In: *Journal of Clinical & Translational Endocrinology* 15, pp. 45–53.
DOI: 10.1016/j.jcte.2018.12.005.

Andreassen, S. et al. (1994). A probabilisic approach to glucose prediction and insulin dose adjustment: description of metabolic model and pilot evaluation study. In: *Computer Methods and Programs in Biomedicine* 41 (3-4), pp. 153–165.
DOI: 10.1016/0169-2607(94)90052-3.

Andres, R.; Cader, G.; Zierler, K. L. (1956). The quantitatively minor role of carbohydrate in oxidative metabolism by skeletal muscle in intact man in the basal state; measurements of oxygen and glucose uptake and carbon dioxide and lactate production in the forearm. In: *Journal of Clinical Investigation* 35 (6), pp. 671–682.
DOI: 10.1172/JCI103324.

Antoulas, A. C. (2005). *Approximation of large-scale dynamical systems*. Vol. 6. Advances in design and control. Philadelphia: Society for Industrial and Applied Mathematics.
ISBN: 0-89871-529-6.

Antoulas, A. C.; Sorensen, D. C. (2001). Approximation of large-scale dynamical systems: An overview. In: *International Journal of Applied Mathematics and Computer Science* 11 (5), pp. 1093–1121.
URL: http://eudml.org/doc/207547.

Aronoff, S. L.; Berkowitz, K.; Shreiner, B.; Want, L. (2004). Glucose Metabolism and Regulation: Beyond Insulin and Glucagon. In: *Diabetes Spectrum* 17 (3), pp. 183–190.
DOI: 10.2337/diaspect.17.3.183.

Asarani, N. A. M. et al. (2020). Efficacy, safety, and user experience of DIY or open-source artificial pancreas systems: a systematic review. In: *Acta Diabetologica*.
DOI: 10.1007/s00592-020-01623-4.

Ascensia Diabetes Care Deutschland GmbH (2016). *Contour® Next One*.
URL: https://www.diabetes.ascensia.de/produkte/contour-next-one (visited on 07/04/2020).

Balakrishnan, N. P.; Rangaiah, G. P.; Samavedham, L. (2011). Review and Analysis of Blood Glucose (BG) Models for Type 1 Diabetic Patients. In: *Industrial & Engineering Chemistry Research* 50 (21), pp. 12041–12066.
DOI: 10.1021/ie2004779.

Balakrishnan, N. P.; Samavedham, L.; Rangaiah, G. P. (2014). Personalized mechanistic models for exercise, meal and insulin interventions in children and adolescents with type 1 diabetes. In: *Journal of Theoretical Biology* 357, pp. 62–73.
DOI: 10.1016/j.jtbi.2014.04.038.

Basu, A.; Dalla Man, C.; Basu, R., et al. (2009). Effects of type 2 diabetes on insulin secretion, insulin action, glucose effectiveness, and postprandial glucose metabolism. In: *Diabetes Care* 32 (5), pp. 866–872.
DOI: 10.2337/dc08-1826.

Basu, A.; Dalla Man, C.; Mariatoffolo, G., et al. (2004). Effect of type 2 diabetes on meal glucose fluxes and insulin secretion. In: *Diabetes* 53, A579.
ISSN: 0012-1797.

Basu, R. et al. (2003). Use of a novel triple-tracer approach to assess postprandial glucose metabolism. In: *American Journal of Physiology - Endocrinology and Metabolism* 284 (1), E55–69.
DOI: 10.1152/ajpendo.00190.2001.

Baur, U.; Benner, P.; Feng, L. (2014). Model Order Reduction for Linear and Nonlinear Systems: A System-Theoretic Perspective. In: *Archives of Computational Methods in Engineering* 21 (4), pp. 331–358.
DOI: 10.1007/s11831-014-9111-2.

Beck, R. W. et al. (2017). Effect of Continuous Glucose Monitoring on Glycemic Control in Adults With Type 1 Diabetes Using Insulin Injections: The DIAMOND Randomized Clinical Trial. In: *JAMA* 317 (4), pp. 371–378.
DOI: 10.1001/jama.2016.19975.

Bequette, B. W. (2004). Optimal estimation applications to continuous glucose monitoring. In: *American Control Conference, 2004. Proceedings of the 2004*. Vol. 1, pp. 958–962.
DOI: 10.23919/ACC.2004.1383731.

Bequette, B. W. (2005). A Critical Assessment of Algorithms and Challenges in the Development of a Closed-Loop Artificial Pancreas. In: *Diabetes Technology & Therapeutics* 7 (1), pp. 28–47.
DOI: 10.1089/dia.2005.7.28.

Bequette, B. W. (2010). Continuous Glucose Monitoring - Real-Time Algorithms for Calibration, Filtering and Alarms. In: *Journal of Diabetes Science and Technology* 4 (2), pp. 404–419.
DOI: 10.1177/193229681000400222.

Bergenstal, R. M.; Gavin, J. R. (2005). The role of self-monitoring of blood glucose in the care of people with diabetes: report of a global consensus conference. In: *The American journal of medicine* 118 (Suppl 9A), pp. 1–6.
DOI: 10.1016/j.amjmed.2005.07.055.

Bergman, R. N. (1989). Lilly lecture 1989. Toward physiological understanding of glucose tolerance. Minimal-model approach. In: *Diabetes* 38 (12), pp. 1512–1527.
DOI: 10.2337/diab.38.12.1512.

Bergman, R. N.; Bucolo, R. J. (1974). Interaction of insulin and glucose in the control of hepatic glucose balance. In: *The American Journal of Physiology* 227 (6), pp. 1314–1322.
DOI: 10.1152/ajplegacy.1974.227.6.1314.

Bergman, R. N.; Cobelli, C. (1980). Minimal modeling, partition analysis, and the estimation of insulin sensitivity. In: *Federation Proceedings* 39 (1), pp. 110–115.
ISSN: 0014-9446.

Bergman, R. N.; Ider, Y. Z.; Bowden, C. R.; Cobelli, C. (1979). Quantitative estimation of insulin sensitivity. In: *The American Journal of Physiology* 236 (6), E667–E677.
DOI: 10.1152/ajpendo.1979.236.6.E667.

Bergman, R. N.; Phillips, L. S.; Cobelli, C. (1981). Physiologic evaluation of factors controlling glucose tolerance in man: Measurement of insulin sensitivity and beta-cell glucose sensitivity from the response to intravenous glucose. In: *Journal of Clinical Investigation* 68, pp. 1456–1467.
DOI: 10.1172/JCI110398.

Best, J. D.; Taborsky, G. J.; Halter, J. B.; Porte, D. (1981). Glucose disposal is not proportional to plasma glucose level in man. In: *Diabetes* 30 (10), pp. 847–850.
DOI: 10.2337/diab.30.10.847.

Binder, C. (1969). Absorption of injected insulin. A clinical-pharmacological study. In: *Acta pharmacologica et toxicologica* 27 Suppl 2, pp. 1–84.
DOI: 10.1111/j.1600-0773.1969.tb03069.x.

Binder, C.; Lauritzen, T.; Faber, O.; Pramming, S. (1984). Insulin pharmacokinetics. In: *Diabetes Care* 7 (2), pp. 188–199.
DOI: 10.2337/diacare.7.2.188.

Blauw, H. et al. (2016). Pharmacokinetics and pharmacodynamics of various glucagon dosages at different blood glucose levels. In: *Diabetes, Obesity & Metabolism* 18 (1), pp. 34–39.
DOI: 10.1111/dom.12571.

Boiroux, D. et al. (2016). Model Identification using Continuous Glucose Monitoring Data for Type 1 Diabetes. In: *IFAC-PapersOnLine* 49 (7), pp. 759–764.
DOI: 10.1016/j.ifacol.2016.07.279.

Bolie, V. W. (1961). Coefficients of normal blood glucose regulation. In: *Journal of Applied Physiology* 16 (5), pp. 783–788.
DOI: 10.1152/jappl.1961.16.5.783.

Borgonovo, E.; Plischke, E. (2016). Sensitivity analysis: A review of recent advances. In: *European Journal of Operational Research* 248 (3), pp. 869–887.
DOI: 10.1016/j.ejor.2015.06.032.

Boscari, F. et al. (2018). Head-to-head comparison of the accuracy of Abbott FreeStyle Libre and Dexcom G5 mobile. In: *Nutrition, Metabolism and Cardiovascular Diseases: NMCD* 28 (4), pp. 425–427.
DOI: 10.1016/j.numecd.2018.01.003.

Breda, E. et al. (2001). Oral glucose tolerance test minimal model indexes of beta-cell function and insulin sensitivity. In: *Diabetes* 50 (1), pp. 150–158.
DOI: 10.2337/diabetes.50.1.150.

Brehm, A. et al. (2006). The role of endocrine counterregulation for estimating insulin sensitivity from intravenous glucose tolerance tests. In: *Journal of Clinical Endocrinology & Metabolism* 91 (6), pp. 2272–2278.
DOI: 10.1210/jc.2006-0019.

Breton, M. D.; Kovatchev, B. P. (2008). Analysis, Modeling, and Simulation of the Accuracy of Continuous Glucose Sensors. In: *Journal of Diabetes Science and Technology* 2 (5), pp. 853–862.
DOI: 10.1177/193229680800200517.

Breton, M. D.; Kovatchev, B. P., et al. (2015). Simulation of endogenous and exogenous glucose/insulin/glucagon interplay in type 1 diabetic patients. WO/2015/003124.

Bryson, A.; Johansen, D. (1965). Linear filtering for time-varying systems using measurements containing colored noise. In: *IEEE Transactions on Automatic Control* 10 (1), pp. 4–10.
DOI: 10.1109/TAC.1965.1098063.

Buckingham, B. A. et al. (2009). Preventing Hypoglycemia Using Predictive Alarm Algorithms and Insulin Pump Suspension. In: *Diabetes Technology & Therapeutics* 11 (2), pp. 93–97.
DOI: 10.1089/dia.2008.0032.

Campbell, K.; McKay, M. D.; Williams, B. J. (2006). Sensitivity analysis when model outputs are functions. In: *Reliability Engineering & System Safety* 91 (10-11), pp. 1468–1472.
DOI: 10.1016/j.ress.2005.11.049.

Campbell, N. A.; Reece, J. B.; Urry, L. A. (2016). *Biologie*. 10., aktualisierte Auflage. Hallbergmoos: Pearson.
ISBN: 9783868942590.

Campolongo, F.; Cariboni, J.; Saltelli, A. (2007). An effective screening design for sensitivity analysis of large models. In: *Environmental Modelling & Software* 22 (10), pp. 1509–1518.
DOI: 10.1016/j.envsoft.2006.10.004.

Campolongo, F.; Saltelli, A. (1997). Sensitivity analysis of an environmental model: an application of different analysis methods. In: *Reliability Engineering & System Safety* 57 (1), pp. 49–69.
DOI: 10.1016/S0951-8320(97)00021-5.

Campolongo, F.; Saltelli, A.; Cariboni, J. (2011). From screening to quantitative sensitivity analysis. A unified approach. In: *Computer Physics Communications* 182 (4), pp. 978–988.
DOI: 10.1016/j.cpc.2010.12.039.

Cappon, G. et al. (2017). Wearable Continuous Glucose Monitoring Sensors: A Revolution in Diabetes Treatment. In: *Electronics* 6 (3), p. 65.
DOI: 10.3390/electronics6030065.

Carlson, D. (1986). What are Schur complements, anyway? In: *Linear Algebra and its Applications* 74, pp. 257–275.
DOI: 10.1016/0024-3795(86)90127-8.

Carson, E. R.; Cobelli, C. (2014). *Modelling methodology for physiology and medicine*. 2. ed. Elsevier insights. Amsterdam: Elsevier.
ISBN: 9780124115576.

Caumo, A.; Bergman, R. N.; Cobelli, C. (2000). Insulin sensitivity from meal tolerance tests in normal subjects: a minimal model index. In: *Journal of Clinical Endocrinology & Metabolism* 85 (11), pp. 4396–4402.
DOI: 10.1210/jcem.85.11.6982.

Caumo, A.; Cobelli, C. (1993). Hepatic glucose production during the labeled IVGTT: estimation by deconvolution with a new minimal model. In: *The American Journal of Physiology* 264 (5 Pt 1), E829–41.
DOI: 10.1152/ajpendo.1993.264.5.E829.

Celeste, R. et al. (1978). The role of glucagon in the regulation of blood glucose: Model studies. In: *Bulletin of Mathematical Biology* 40 (1), pp. 59–77.
DOI: 10.1007/BF02463130.

Chee, F.; Fernando, T.; van Heerden, P. (2003). Closed-loop glucose control in critically Ill patients using continuous glucose monitoring system (CGMS) in real time. In: *IEEE Transactions on Information Technology in Biomedicine* 7 (1), pp. 43–53.
DOI: 10.1109/TITB.2003.808509.

Chee, F.; Fernando, T. (2007). *Closed-Loop Control of Blood Glucose*. 1st ed. Lecture notes in control and information sciences. Berlin: Springer.
ISBN: 3-540-74030-9.

Cherrington, A. D. et al. (1976). The role of insulin and glucagon in the regulation of basal glucose production in the postabsorptive dog. In: *Journal of Clinical Investigation* 58 (6), pp. 1407–1418.
DOI: 10.1172/JCI108596.

Christiansen, M. P.; Bailey, T. S., et al. (2013). A New-Generation Continuous Glucose Monitoring System: Improved Accuracy and Reliability Compared with a Previous-Generation System. In: *Diabetes Technology & Therapeutics* 15 (10), pp. 881–888.
DOI: 10.1089/dia.2013.0077.

Christiansen, M. P.; Garg, S. K., et al. (2017). Accuracy of a Fourth-Generation Subcutaneous Continuous Glucose Sensor. In: *Diabetes Technology & Therapeutics* 19 (8), pp. 446–456. DOI: 10.1089/dia.2017.0087.

Clarke, S. F.; Foster, J. R. (2012). A history of blood glucose meters and their role in self-monitoring of diabetes mellitus. In: *British Journal of Biomedical Science* 69 (2), pp. 83–93. DOI: 10.1080/09674845.2012.12002443.

Clarke, W. L. (2005). The Original Clarke Error Grid Analysis (EGA): Diabetes Technology & Therapeutics. In: *Diabetes Technology & Therapeutics* 7 (5), pp. 776–779. DOI: 10.1089/dia.2005.7.776.

Clarke, W. L.; Anderson, S. M.; Breton, M. D., et al. (2009). Closed-loop Artificial Pancreas Using Subcutaneous Glucose Sesing and Insulin Delivery and a Model Predictive Control Algorithm: The Virginia Experience. In: *Journal of Diabetes Science and Technology* 3 (5), pp. 1031–1038. DOI: 10.1177/193229680900300506.

Clarke, W. L.; Anderson, S. M.; Farhy, L. S., et al. (2005). Evaluating the Clinical Accuracy of Two Continuous Glucose Sensors Using Continuous Glucose-Error Grid Analysis. In: *Diabetes Care* 28 (10), pp. 2412–2417. DOI: 10.2337/diacare.28.10.2412.

Clarke, W. L.; Cox, D. J., et al. (1987). Evaluating Clinical Accuracy of Systems for Self-Monitoring of Blood Glucose. In: *Diabetes Care* 10 (5), pp. 622–628. DOI: 10.2337/diacare.10.5.622.

Clarke, W. L.; Kovatchev, B. P. (2009). Statistical tools to analyze continuous glucose monitor data. In: *Diabetes Technology & Therapeutics* 11 Suppl 1, S45–54. DOI: 10.1089/dia.2008.0138.

Cobelli, C.; Carson, E. R. (2008). *Introduction to Modeling in Physiology and Medicine*. 1st ed. Biomedical Engineering. Academic Press Inc. ISBN: 0121602400.

Cobelli, C.; Dalla Man, C., et al. (2009). Diabetes: Models, Signals, and Control. In: *IEEE Reviews in Biomedical Engineering* 2, pp. 54–96. DOI: 10.1109/RBME.2009.2036073.

Cobelli, C.; Pacini, G.; Toffolo, G. M.; Sacca, L. (1986). Estimation of insulin sensitivity and glucose clearance from minimal model: new insights from labeled IVGTT. In: *American Journal of Physiology - Endocrinology and Metabolism* 250 (5), E591–E598. DOI: 10.1152/ajpendo.1986.250.5.E591.

Cobelli, C.; Romanin-Jacur, G. (1976). Controllability, Observability and Structural Identifiability of Multi Input and Multi Output Biological Compartmental Systems. In: *IEEE Transactions on Biomedical Engineering* BME-23 (2), pp. 93–100. DOI: 10.1109/TBME.1976.324568.

Cobelli, C.; Schiavon, M., et al. (2016). Interstitial Fluid Glucose Is Not Just a Shifted-in-Time but a Distorted Mirror of Blood Glucose: Insight from an In Silico Study. In: *Diabetes Technology &*

Therapeutics 18 (8), pp. 505–511.
DOI: 10.1089/dia.2016.0112.

Cobelli, C.; Toffolo, G. M.; Ferrannini, E. (1984). A Model of Glucose Kinetics and Their Control by Insulin, Compartmental and Noncompartmental Approaches. In: *Mathematical Biosciences* 72 (2), pp. 291–315.
DOI: 10.1016/0025-5564(84)90114-7.

Coleman, T. F.; Li, Y. (1996). An Interior Trust Region Approach for Nonlinear Minimization Subject to Bounds. In: *SIAM Journal on Optimization* 6 (2), pp. 418–445.
DOI: 10.1137/0806023.

Cretti, A. et al. (2001). Assessment of beta-cell function during the oral glucose tolerance test by a minimal model of insulin secretion. In: *European Journal of Clinical Investigation* 31 (5), pp. 405–416.
DOI: 10.1046/j.1365-2362.2001.00827.x.

Cukier, R. I. et al. (1973). Study of the sensitivity of coupled reaction systems to uncertainties in rate coefficients. I Theory. In: *SIAM review. Society for Industrial and Applied Mathematics* 59 (8), pp. 3873–3878.
DOI: 10.1063/1.1680571.

Dagogo-Jack, S.; Rattarasarn, C.; Cryer, P. (1994). Reversal of hypoglycemia unawareness, but not defective glucose counterregulation, in IDDM. In: *Diabetes* 43 (12), pp. 1426–1434.
DOI: 10.2337/diab.43.12.1426.

Dalla Man, C. (2005a). Insulin sensitivity by oral glucose minimal models: validation against clamp. In: *American Journal of Physiology - Endocrinology and Metabolism* 289 (6), E954–E959.
DOI: 10.1152/ajpendo.00076.2005.

Dalla Man, C. (2005b). Measurement of selective effect of insulin on glucose disposal from labeled glucose oral test minimal model. In: *American Journal of Physiology - Endocrinology and Metabolism* 289 (5), E909–E914.
DOI: 10.1152/ajpendo.00299.2004.

Dalla Man, C.; Breton, M. D.; Cobelli, C. (2009). Physical Activity into the Meal Glucose–Insulin Model of Type 1 Diabetes: In silico Studies. In: *Journal of Diabetes Science and Technology* 3 (1), pp. 56–67.
DOI: 10.1177/193229680900300107.

Dalla Man, C.; Camilleri, M.; Cobelli, C. (2006). A System Model of Oral Glucose Absorption: Validation on Gold Standard Data. In: *IEEE Transactions on Biomedical Engineering* 53 (12), pp. 2472–2478.
DOI: 10.1109/TBME.2006.883792.

Dalla Man, C.; Caumo, A.; Cobelli, C. (2002). The oral glucose minimal model: estimation of insulin sensitivity from a meal test. In: *IEEE Transactions on Biomedical Engineering* 49 (5), pp. 419–429.
DOI: 10.1109/10.995680.

Dalla Man, C.; Micheletto, F., et al. (2014). The UVA/PADOVA Type 1 Diabetes Simulator: New Features. In: *Journal of Diabetes Science and Technology* 8 (1), pp. 26–34.
DOI: 10.1177/1932296813514502.

Dalla Man, C.; Raimondo, D. M.; Rizza, R. A.; Cobelli, C. (2007). GIM, Simulation Software of Meal Glucose-Insulin Model. In: *Journal of Diabetes Science and Technology* 1 (3), pp. 323–330.
DOI: 10.1177/193229680700100303.

Dalla Man, C.; Rizza, R. A.; Cobelli, C. (2006). Mixed meal simulation model of glucose-insulin system. In: *Engineering in Medicine and Biology Society, 2006. EMBS '06. 28th Annual International Conference of the IEEE*, pp. 307–310.
DOI: 10.1109/IEMBS.2006.260810.

Dalla Man, C.; Rizza, R. A.; Cobelli, C. (2007). Meal Simulation Model of the Glucose-Insulin System. In: *IEEE Transactions on Biomedical Engineering* 54 (10), pp. 1740–1749.
DOI: 10.1109/TBME.2007.893506.

Dalla Man, C.; Toffolo, G. M., et al. (2006). A Model of Glucose Production During a Meal. In: *Engineering in Medicine and Biology Society, 2006. EMBS '06. 28th Annual International Conference of the IEEE*, pp. 5647–5650.
DOI: 10.1109/IEMBS.2006.260809.

Dalla Man, C.; Toffolo, G. M., et al. (2008). Use of labeled oral minimal model to measure hepatic insulin sensitivity. In: *American Journal of Physiology - Endocrinology and Metabolism* 295 (5), E1152–9.
DOI: 10.1152/ajpendo.00486.2007.

Damiano, E. R. et al. (2014). A comparative effectiveness analysis of three continuous glucose monitors: The Navigator, G4 Platinum, and Enlite. In: *Journal of Diabetes Science and Technology* 8 (4), pp. 699–708.
DOI: 10.1177/1932296814532203.

Dassau, E.; Bequette, B. W.; Buckingham, B. A.; Doyle, F. J. (2008). Detection of a Meal Using CGM: Implications for an artificial beta-cell. In: *Diabetes Care* 31, pp. 295–300.
DOI: 10.2337/dc07-1293.

De Gaetano, A.; Panunzi, S.; Eliopoulos, D., et al. (2014). Mathematical Modeling of Renal Tubular Glucose Absorption after Glucose Load. In: *Plos One* 9 (1).
DOI: 10.1371/journal.pone.0086963.

De Gaetano, A.; Panunzi, S.; Matone, A., et al. (2013). Routine OGTT: a robust model including incretin effect for precise identification of insulin sensitivity and secretion in a single individual. In: *Plos One* 8 (8), e70875.
DOI: 10.1371/journal.pone.0070875.

DeFronzo, R. A. (1992). Pathogenesis of type 2 (non-insulin dependent) diabetes mellitus: a balanced overview. In: *Diabetologia* 35 (4), pp. 389–397.
DOI: 10.1007/BF00401208.

DeFronzo, R. A.; Tobin, J. D.; Andres, R. (1979). Glucose clamp technique: a method for quantifying insulin secretion and resistance. In: *American Journal of Physiology - Endocrinology and Metabolism* 237 (3), E214–E223.
DOI: 10.1152/ajpendo.1979.237.3.E214.

Deiss, D. et al. (2006). Improved Glycemic Control in Poorly Controlled Patients with Type 1 Diabetes Using Real-Time Continuous Glucose Monitoring. In: *Diabetes Care* 29 (12), pp. 2730–2732.
DOI: 10.2337/dc06-1134.

Dexcom, Inc. (2017). *Dexcom G5® Mobile CGM System*.
URL: https://www.dexcom.com/g5-mobile-cgm (visited on 07/03/2020).

Dinneen, S. F.; Gerich, J. E.; Rizza, R. A. (1992). Carbohydrate metabolism in non-insulin-dependent diabetes mellitus. In: *The New England Journal of Medicine* 327 (10), pp. 707–713.
DOI: 10.1056/NEJM199209033271007.

Dobbins, R. L. et al. (1995). Compartmental modeling of glucagon kinetics in the conscious dog. In: *Metabolism: Clinical and Experimental* 44 (4), pp. 452–459.
DOI: 10.1016/0026-0495(95)90051-9.

Dt. Apotheker-Verl. (2014). *Europäisches Arzneibuch, 8. Ausgabe, 6. Ergänzungsband: Amtl. dt. Ausg.* Stuttgart and Eschborn: Dt. Apotheker-Verl.
ISBN: 9783769262537.

Eaton, R. P. et al. (1980). Prehepatic insulin production in man: kinetic analysis using peripheral connecting peptide behavior. In: *Journal of Clinical Endocrinology & Metabolism* 51 (3), pp. 520–528.
DOI: 10.1210/jcem-51-3-520.

Eberle, C.; Ament, C. (2011). The Unscented Kalman Filter estimates the plasma insulin from glucose measurement. In: *Biosystems : Journal of Biological and Information Processing Sciences* 103 (1), pp. 67–72.
DOI: 10.1016/j.biosystems.2010.09.012.

Eberle, C.; Ament, C. (2012a). Identifiability and online estimation of diagnostic parameters with in the glucose insulin homeostasis. In: *Biosystems : Journal of Biological and Information Processing Sciences* 107 (3), pp. 135–141.
DOI: 10.1016/j.biosystems.2011.11.003.

Eberle, C.; Ament, C. (2012b). Real-Time State Estimation and Long-Term Model Adaptation: A Two-Sided Approach toward Personalized Diagnosis of Glucose and Insulin Levels. In: *Journal of Diabetes Science and Technology* 6 (5), pp. 1148–1158.
DOI: 10.1177/193229681200600520.

Eberle, C.; Ament, C. (2019). Digitale Diabetologie – Eine quantitative Analyse diabetesspezifischer mHealth-Apps. In: *Diabetologie und Stoffwechsel*.
DOI: 10.1055/s-0039-1688129.

Eberle, C.; Ament, C. (2020). A combined in vivo and in silico model shows specific predictors of individual trans-generational diabetic programming. In: *Journal of Developmental Origins of*

Health and Disease, pp. 1–8.
DOI: 10.1017/S2040174420000471.

Efron, B.; Tibshirani, R. (1986). Bootstrap Methods for Standard Errors, Confidence Intervals, and Other Measures of Statistical Accuracy. In: *Statistical Science* 1 (1), pp. 54–75.
DOI: 10.1214/ss/1177013815.

Elleri, D. et al. (2011). Automated Overnight Closed-Loop Glucose Control in Young Children with Type 1 Diabetes. In: *Diabetes Technology & Therapeutics* 13 (4), pp. 419–424.
DOI: 10.1089/dia.2010.0176.

Emami, A. et al. (2017). Modeling Glucagon Action in Patients With Type 1 Diabetes. In: *IEEE Journal of Biomedical and Health Informatics* 21 (4), pp. 1163–1171.
DOI: 10.1109/JBHI.2016.2593630.

Facchinetti, A.; Sparacino, G.; Cobelli, C. (2007). Reconstruction of Glucose in Plasma from Interstitial Fluid Continuous Glucose Monitoring Data: Role of Sensor Calibration. In: *Journal of Diabetes Science and Technology* 1 (5), pp. 617–623.
DOI: 10.1177/193229680700100504.

Facchinetti, A.; Sparacino, G.; Cobelli, C. (2010). Modeling the Error of Continuous Glucose Monitoring Sensor Data: Critical Aspects Discussed through Simulation Studies. In: *Journal of Diabetes Science and Technology* 4 (1), pp. 4–14.
DOI: 10.1177/193229681000400102.

Fan, J. (2015). *PACE: Principal Analysis by Conditional Expectation*.
URL: http://www.stat.ucdavis.edu/PACE/ (visited on 11/08/2019).

Farhy, L. S.; McCall, A. L. (2010). Models of glucagon secretion, their application to the analysis of the defects in glucagon counterregulation and potential extension to approximate glucagon action. In: *Journal of Diabetes Science and Technology* 4 (6), pp. 1345–1356.
DOI: 10.1177/193229681000400608.

Ferrannini, E.; Bjorkman, O., et al. (1985). The disposal of an oral glucose load in healthy subjects. A quantitative study. In: *Diabetes* 34 (6), pp. 580–588.
DOI: 10.2337/diab.34.6.580.

Ferrannini, E.; Cobelli, C. (1987a). The kinetics of insulin in man. I. General aspects. In: *Diabetes/Metabolism Reviews* 3 (2), pp. 335–363.
DOI: 10.1002/dmr.5610030201.

Ferrannini, E.; Cobelli, C. (1987b). The kinetics of insulin in man. II. Role of the liver. In: *Diabetes/Metabolism Reviews* 3 (2), pp. 365–397.
DOI: 10.1002/dmr.5610030202.

Ferrannini, E.; Groop, L. C. (1989). Hepatic glucose production in insulin-resistant states. In: *Diabetes/Metabolism Reviews* 5 (8), pp. 711–726.
DOI: 10.1002/dmr.5610050806.

Ferrannini, E.; Simonson, D. C., et al. (1988). The disposal of an oral glucose load in patients with non-insulin-dependent diabetes. In: *Metabolism: Clinical and Experimental* 37 (1), pp. 79–85.
DOI: 10.1016/0026-0495(88)90033-9.

Ferri, S.; Kojima, K.; Sode, K. (2011). Review of glucose oxidases and glucose dehydrogenases: a bird's eye view of glucose sensing enzymes. In: *Journal of Diabetes Science and Technology* 5 (5), pp. 1068–1076.
DOI: 10.1177/193229681100500507.

Fisher, M. E. (1991). A semiclosed-loop algorithm for the control of blood glucose levels in diabetics. In: *IEEE Transactions on Biomedical Engineering* 38 (1), pp. 57–61.
DOI: 10.1109/10.68209.

Fonseca, V. A. (2006). *Clinical diabetes: Translating research into practice*. Philadelphia, PA: Saunders Elsevier.
ISBN: 9781416002734.

Fraunhofer IMS (2012-09-03). *Blutzucker messen ohne Pieks*. Duisburg.
URL: https://www.ims.fraunhofer.de/de/Presse/Presseinformationen/2012/Blutzucker_messen_ohne_Pieks.html (visited on 02/04/2020).

Freckmann, G.; Baumstark, A., et al. (2014). Evaluation of 12 blood glucose monitoring systems for self-testing: system accuracy and measurement reproducibility. In: *Diabetes Technology & Therapeutics* 16 (2), pp. 113–122.
DOI: 10.1089/dia.2013.0208.

Freckmann, G.; Hagenlocher, S., et al. (2007). Continuous glucose profiles in healthy subjects under everyday life conditions and after different meals. In: *Journal of Diabetes Science and Technology* 1 (5), pp. 695–703.
DOI: 10.1177/193229680700100513.

Freckmann, G.; Link, M., et al. (2018). Measurement Performance of Two Continuous Tissue Glucose Monitoring Systems Intended for Replacement of Blood Glucose Monitoring. In: *Diabetes Technology & Therapeutics* 20 (8), pp. 541–549.
DOI: 10.1089/dia.2018.0105.

Freckmann, G.; Pleus, S., et al. (2013). Performance evaluation of three continuous glucose monitoring systems: comparison of six sensors per subject in parallel. In: *Journal of Diabetes Science and Technology* 7 (4), pp. 842–853.
DOI: 10.1177/193229681300700406.

Freckmann, G.; Schmid, C., et al. (2012). System accuracy evaluation of 43 blood glucose monitoring systems for self-monitoring of blood glucose according to DIN EN ISO 15197. In: *Journal of Diabetes Science and Technology* 6 (5), pp. 1060–1075.
DOI: 10.1177/193229681200600510.

Fu, Z.; Gilbert, E. R.; Liu, D. (2013). Regulation of Insulin Synthesis and Secretion and Pancreatic Beta-Cell Dysfunction in Diabetes. In: *Current diabetes reviews* 9 (1), pp. 25–53.
DOI: 10.2174/157339913804143225.

Garg, S. et al. (2006). Improvement in glycemic excursions with a transcutaneous, real-time continuous glucose sensor: a randomized controlled trial. In: *Diabetes Care* 29 (1), pp. 44–50.
DOI: 10.2337/diacare.29.01.06.dc05-1686.

Geevan, C. P.; Rao, J. S.; Rao, G. S.; Bajaj, J. S. (1990). A mathematical model for insulin kinetics III. Sensitivity analysis of the model. In: *Journal of Theoretical Biology* 147 (2), pp. 255–263.
DOI: 10.1016/S0022-5193(05)80055-4.

Geffen, D. et al. (2008). Observability based parameter identifiability for biochemical reaction networks. In: *American Control Conference, 2008. Proceedings of the 2008*, pp. 2130–2135.
DOI: 10.1109/ACC.2008.4586807.

Georga, E. I.; Protopappas, V. C.; Bellos, C. V.; Fotiadis, D. I. (2014). Wearable systems and mobile applications for diabetes disease management. In: *Health and Technology* 4 (2), pp. 101–112.
DOI: 10.1007/s12553-014-0082-y.

Gerich, J. E.; Davis, J., et al. (1979). Hormonal mechanisms of recovery from insulin-induced hypoglycemia in man. In: *The American Journal of Physiology* 236 (4), E380–5.
DOI: 10.1152/ajpendo.1979.236.4.E380.

Gerich, J. E.; Lorenzi, M., et al. (1975). Abnormal Pancreatic Glucagon Secretion and Postprandial Hyperglycemia In Diabetes Mellitus. In: *JAMA* 234 (2), pp. 159–5.
DOI: 10.1001/jama.1975.03260150029015.

Gifford, R. (2013). Continuous glucose monitoring: 40 years, what we've learned and what's next. In: *ChemPhysChem : a European journal of chemical physics and physical chemistry* 14 (10), pp. 2032–2044.
DOI: 10.1002/cphc.201300172.

Girardin, C. M.; Huot, C.; Gonthier, M.; Delvin, E. (2009). Continuous glucose monitoring: a review of biochemical perspectives and clinical use in type 1 diabetes. In: *Clinical Biochemistry* 42 (3), pp. 136–142.
DOI: 10.1016/j.clinbiochem.2008.09.112.

Gradel, A. K. J. et al. (2018). Factors Affecting the Absorption of Subcutaneously Administered Insulin: Effect on Variability. In: *Journal of Diabetes Research* 2018.
DOI: 10.1155/2018/1205121.

Grewal, M. S.; Andrews, A. P. (2008). *Kalman filtering: Theory and practice using MATLAB*. 3. edition. Hoboken, NJ: Wiley.
ISBN: 978-0-470-17366-4.

Grodsky, G. M. (1972). A threshold distribution hypothesis for packet storage of insulin and its mathematical modeling. In: *Journal of Clinical Investigation* 51 (8), pp. 2047–2059.
DOI: 10.1172/JCI107011.

Gylfe, E.; Gilon, P. (2014). Glucose regulation of glucagon secretion. In: *Diabetes Research and Clinical Practice* 103 (1), pp. 1–10.
DOI: 10.1016/j.diabres.2013.11.019.

Hahn, J.; Edgar, T. F. (2002). An improved method for nonlinear model reduction using balancing of empirical gramians. In: *Computers & Chemical Engineering* 26 (10), pp. 1379–1397. DOI: 10.1016/S0098-1354(02)00120-5.

Hajizadeh, I.; Turksoy, K.; Cengiz, E.; Cinar, A. (2017). Real-time estimation of plasma insulin concentration using continuous subcutaneous glucose measurements in people with type 1 diabetes. In: *2017 American Control Conference (ACC)*, pp. 5193–5198. DOI: 10.23919/ACC.2017.7963761.

Heinemann, L.; Benesch, C.; DeVries, J. H. (2016). AP@home: The Artificial Pancreas Is Now at Home. In: *Journal of Diabetes Science and Technology* 10 (4), pp. 950–958. DOI: 10.1177/1932296816632002.

Helton, J. C.; Johnson, J. D.; Sallaberry, C. J.; Storlie, C. B. (2006). Survey of sampling-based methods for uncertainty and sensitivity analysis. In: *Reliability Engineering & System Safety* 91 (10-11), pp. 1175–1209. DOI: 10.1016/j.ress.2005.11.017.

Hernando, M. E. et al. (2008). Definition of information technology architectures for continuous data management and medical device integration in diabetes. In: *Journal of Diabetes Science and Technology* 2 (5), pp. 899–905. DOI: 10.1177/193229680800200523.

Himpe, C. (2018). emgr—The Empirical Gramian Framework. In: *Algorithms* 11 (7), p. 91. DOI: 10.3390/a11070091.

Himpe, C. (2020a). *Comparing (Empirical-Gramian-Based) Model Order Reduction Algorithms*. URL: http://arxiv.org/pdf/2002.12226v1.

Himpe, C. (2020b). *emgr - EMpirical GRamian Framework (5.8)*. DOI: 10.5281/zenodo.3779889.

Himpe, C.; Ohlberger, M. (2013). A Unified Software Framework for Empirical Gramians. In: *Journal of Mathematics* 2013 (9), pp. 1–6. DOI: 10.1155/2013/365909.

Himpe, C.; Ohlberger, M. (2014). Cross-Gramian-Based Combined State and Parameter Reduction for Large-Scale Control Systems. In: *Mathematical Problems in Engineering* 2014 (2), pp. 1–13. DOI: 10.1155/2014/843869.

Himpe, C.; Ohlberger, M. (2016). A note on the cross Gramian for non-symmetric systems. In: *Systems Science & Control Engineering* 4 (1), pp. 199–208. DOI: 10.1080/21642583.2016.1215273.

Hinshaw, L. et al. (2015). Glucagon sensitivity and clearance in type 1 diabetes: Insights from in vivo and in silico experiments. In: *American Journal of Physiology - Endocrinology and Metabolism* 309 (5), E474–86. DOI: 10.1152/ajpendo.00236.2015.

Holt, R. I. G.; Cockram, C.; Fyvberg, A.; Goldstein Barry J. (2010). *Textbook of Diabetes*. 4. Wiley-Blackwell.
ISBN: 9781405191814.

Homma, T.; Saltelli, A. (1996). Importance measures in global sensitivity analysis of nonlinear models. In: *Reliability Engineering & System Safety* 52 (1), pp. 1–17.
DOI: 10.1016/0951-8320(96)00002-6.

Hora, S. C.; Iman, R. L. (1986). *Comparison of Maximus/Bounding and Bayes/Monte Carlo for fault tree uncertainty analysis*.
URL: https://www.osti.gov/biblio/5824798-comparison-maximus-bounding-bayes-monte-carlo-fault-tree-uncertainty-analysis (visited on 02/04/2020).

Hovorka, R. (2006). Continuous glucose monitoring and closed-loop systems. In: *Diabetic Medicine* 23 (1), pp. 1–12.
DOI: 10.1111/j.1464-5491.2005.01672.x.

Hovorka, R.; Canonico, V., et al. (2004). Nonlinear model predictive control of glucose concentration in subjects with type 1 diabetes. In: *Physiological Measurement* 25 (4), pp. 905–920.
DOI: 10.1088/0967-3334/25/4/010.

Hovorka, R.; Chassin, L. J.; Ellmerer, M., et al. (2008). A simulation model of glucose regulation in the critically ill. In: *Physiological Measurement* 29 (8), pp. 959–978.
DOI: 10.1088/0967-3334/29/8/008.

Hovorka, R.; Chassin, L. J.; Wilinska, M. E., et al. (2004). Closing the Loop: The Adicol Experience. In: *Diabetes Technology & Therapeutics* 6 (3), pp. 307–322.
DOI: 10.1089/152091504774197990.

Iman, R. L.; Helton, J. C. (1988). An Investigation of Uncertainty and Sensitivity Analysis Techniques for Computer Models. In: *Risk Analysis* 8 (1), pp. 71–90.
DOI: 10.1111/j.1539-6924.1988.tb01155.x.

Ingalls, B. P.; Sauro, H. M. (2003). Sensitivity analysis of stoichiometric networks: an extension of metabolic control analysis to non-steady state trajectories. In: *Journal of Theoretical Biology* 222 (1), pp. 23–36.
DOI: 10.1016/S0022-5193(03)00011-0.

Insel, P. A. et al. (1975). Insulin Control of Glucose Metabolism in Man: A New Kinetic Analysis. In: *Journal of Clinical Investigation* 55, pp. 1057–1066.
DOI: 10.1172/JCI108006.

International Diabetes Federation (2019). *IDF Diabetes Atlas*. International Diabetes Federation.
ISBN: 978-2-930229-87-4.

International Organization for Standardization (2013). *In vitro diagnostic test systems - Requirements for blood-glucose monitoring systems for self-testing in managing diabetes mellitus*. Berlin.
URL: https://www.beuth.de/de/norm/din-en-iso-15197/240790833 (visited on 02/19/2019).

Iooss, B.; Lemaître, P. (2015). A Review on Global Sensitivity Analysis Methods. In: *Uncertainty management in simulation-optimization of complex systems*. Ed. by G. Dellino; C. Meloni. Vol. 59. Operations Research/Computer Science Interfaces Series. New York et al., pp. 101–122.
DOI: 10.1007/978-1-4899-7547-8_5.

Isermann, R.; Münchhof, M. (2011). *Identification of dynamic systems: An introduction with applications*. Berlin: Springer.
ISBN: 978-3-540-78878-2.

Islam, S. M. R. et al. (2015). The Internet of Things for Health Care: A Comprehensive Survey. In: *IEEE Access* 3, pp. 678–708.
DOI: 10.1109/ACCESS.2015.2437951.

Jansen, M. J. W. (1999). Analysis of variance designs for model output. In: *Computer Physics Communications* 117 (1-2), pp. 35–43.
DOI: 10.1016/S0010-4655(98)00154-4.

Jansen, M. J. W.; Rossing, W. A. H.; Daamen, R. A. (1994). Monte Carlo Estimation of Uncertainty Contributions from Several Independent Multivariate Sources. In: *Predictability and Nonlinear Modelling in Natural Sciences and Economics*. Ed. by J. Grasman; G. van Straten. Dordrecht and Boston, pp. 334–343.
DOI: 10.1007/978-94-011-0962-8_28.

Julier, S. J.; Uhlmann, J. K. (1997). New extension of the Kalman filter to nonlinear systems. In: *Signal Processing, Sensor Fusion, and Target Recognition VI*. Ed. by I. Kadar. SPIE Proceedings, p. 182.
DOI: 10.1117/12.280797.

Kalman, R. E. (1960). A New Approach to Linear Filtering and Prediction Problems. In: *Journal of Basic Engineering* 82 (1), pp. 35–45.
DOI: 10.1115/1.3662552.

Kapitza, C. et al. (2010). CGM during excercise in Patients with Type 1 Diabetes on Continuous Subcutaneous Insulin Infusion. In: *Journal of Diabetes Science and Technology* 4 (1), pp. 123–131.
DOI: 10.1177/193229681000400116.

Keenan, D. B.; Mastrototaro, J. J.; Voskanyan, G.; Steil, G. M. (2009). Delays in Minimally Invasive Continuous Glucose Monitoring Devices: A Review of Current Technology. In: *Journal of Diabetes Science and Technology* 3 (5), pp. 1207–1214.
DOI: 10.1177/193229680900300528.

Keith-Hynes, P.; Mize, B.; Robert, A.; Place, J. (2014). The Diabetes Assistant: A Smartphone-Based System for Real-Time Control of Blood Glucose. In: *Electronics* 3 (4), pp. 609–623.
DOI: 10.3390/electronics3040609.

Kesavadev, J. et al. (2020). The Do-It-Yourself Artificial Pancreas: A Comprehensive Review. In: *Diabetes therapy : research, treatment and education of diabetes and related disorders* 11 (6), pp. 1217–1235.
DOI: 10.1007/s13300-020-00823-z.

El-Khatib, F. H.; Jiang, J.; Damiano, E. R. (2007). Adaptive Closed-Loop Control Provides Blood-Glucose Regulation using dual Subcutaneous Insulin and Glucagon Infusion in Diabetic Swine. In: *Journal of Diabetes Science and Technology* 1 (2), pp. 181–192.
DOI: 10.1177/193229680700100208.

El-Khatib, F. H.; Jiang, J.; Damiano, E. R. (2009). A Feasibility Study of Bihormonal Closed-Loop Blood Glucose Control using dual subcutaneous infusion of Insulin and Glucagon in Ambulatory Diabetic Swine. In: *Journal of Diabetes Science and Technology* 3 (4), pp. 789–803.
DOI: 10.1177/193229680900300428.

El-Khatib, F. H.; Jiang, J.; Gerrity, R. G.; Damiano, E. R. (2007). Pharmacodynamics And Stability of Subcutaneously Infused Glucagon in A Type 1 Diabetic Swine Model In Vivo. In: *Diabetes Technology & Therapeutics* 9 (2), pp. 135–144.
DOI: 10.1089/dia.2006.0006.

El-Khatib, F. H.; Russell, S. J., et al. (2010). A Bihormonal Closed-Loop Artificial Pancreas for Type 1 Diabetes. In: *Science Translational Medicine* 2 (27), 27ra27.
DOI: 10.1126/scitranslmed.3000619.

Knobbe, E. J.; Buckingham, B. A. (2005). The Extended Kalman Filter for Continuous Glucose Monitoring. In: *Diabetes Technology & Therapeutics* 7 (1), pp. 15–27.
DOI: 10.1089/dia.2005.7.15.

Knop, F. K. et al. (2007). Inappropriate suppression of glucagon during OGTT but not during isoglycaemic i.v. glucose infusion contributes to the reduced incretin effect in type 2 diabetes mellitus. In: *Diabetologia* 50 (4), pp. 797–805.
DOI: 10.1007/s00125-006-0566-z.

Kobayashi, T. et al. (1983). The pharmacokinetics of insulin after continuous subcutaneous infusion or bolus subcutaneous injection in diabetic patients. In: *Diabetes* 32 (4), pp. 331–336.
DOI: 10.2337/diab.32.4.331.

Kovatchev, B. P.; Anderson, S. M.; Heinemann, L.; Clarke, W. L. (2008). Comparison of the numerical and clinical accuracy of four continuous glucose monitors. In: *Diabetes Care* 31 (6), pp. 1160–1164.
DOI: 10.2337/dc07-2401.

Kovatchev, B. P.; Breton, M. D.; Dalla Man, C.; Cobelli, C. (2009). In Silico Preclinical Trials: A Proof of Concept in Closed-Loop Control of Type 1 Diabetes. In: *Journal of Diabetes Science and Technology* 3 (1), pp. 44–55.
DOI: 10.1177/193229680900300106.

Kovatchev, B. P.; Clarke, W. L., et al. (2005). Quantifying temporal glucose variability in diabetes via continuous glucose monitoring: Mathematical methods and clinical application. In: *Diabetes Technology & Therapeutics* 7 (6), pp. 849–862.
DOI: 10.1089/dia.2005.7.849.

Kovatchev, B. P.; Gonder-Frederick, L. A.; Cox, D. J.; Clarke, W. L. (2004). Evaluating the Accuracy of Continuous Glucose-Monitoring Sensors: Continuous glucose-error grid analysis illustrated by

TheraSense Freestyle Navigator data. In: *Diabetes Care* 27 (8), pp. 1922–1928.
DOI: 10.2337/diacare.27.8.1922.

Kovatchev, B. P.; King, C., et al. (2006). Clinical Assessment and Mathematical Modeling of the Accuracy of Continuous Glucose Sensors (CGS). In: *Engineering in Medicine and Biology Society, 2006. EMBS '06. 28th Annual International Conference of the IEEE*, pp. 71–74.
DOI: 10.1109/IEMBS.2006.260114.

Kovatchev, B. P.; Patek, S. D.; Ortiz, E. A.; Breton, M. D. (2015). Assessing sensor accuracy for non-adjunct use of continuous glucose monitoring. In: *Diabetes Technology & Therapeutics* 17 (3), pp. 177–186.
DOI: 10.1089/dia.2014.0272.

Kovatchev, B. P.; Raimondo, D. M., et al. (2008). In Silico Testing and in Vivo Experiments with Closed-Loop Control of Blood Glucose in Diabetes. In: *IFAC Proceedings Volumes* 41 (2), pp. 4234–4239.
DOI: 10.3182/20080706-5-KR-1001.00712.

Kraegen, E. W.; Chisholm, D. J. (1984). Insulin responses to varying profiles of subcutaneous insulin infusion: kinetic modelling studies. In: *Diabetologia* 26 (3), pp. 208–213.
DOI: 10.1007/bf00252409.

Kramer, C. K. et al. (2014). Glucagon response to oral glucose challenge in type 1 diabetes: lack of impact of euglycemia. In: *Diabetes Care* 37 (4), pp. 1076–1082.
DOI: 10.2337/dc13-2339.

Kuure-Kinsey, M.; Palerm, C. C.; Bequette, B. W. (2006). A Dual-Rate Kalman Filter for Continuous Glucose Monitoring. In: *Engineering in Medicine and Biology Society, 2006. EMBS '06. 28th Annual International Conference of the IEEE*. Vol. 2006, pp. 63–66.
DOI: 10.1109/IEMBS.2006.260057.

Laffel, L. (2016). Improved Accuracy of Continuous Glucose Monitoring Systems in Pediatric Patients with Diabetes Mellitus: Results from Two Studies. In: *Diabetes Technology & Therapeutics* 18 Suppl 2, S223–33.
DOI: 10.1089/dia.2015.0380.

Lall, S.; Marsden, J. E.; Glavaški, S. (1999). Empirical Model Reduction of Controlled Nonlinear Systems. In: *IFAC Proceedings Volumes* 32 (2), pp. 473–478.
DOI: 10.1016/S1474-6670(17)56442-3.

Lanzola, G. et al. (2016). Remote Blood Glucose Monitoring in mHealth Scenarios: A Review. In: *Sensors* 16 (12).
DOI: 10.3390/s16121983.

Leal, Y. et al. (2010). Real-Time Glucose Estimation Algorithm for Continuous Glucose Monitoring Using Autoregressive Models. In: *Journal of Diabetes Science and Technology* 4 (2), pp. 391–403.
DOI: 10.1177/193229681000400221.

Lehmann, E. D.; Deutsch, T. (1992). A physiological model of glucose-insulin interaction in type 1 diabetes mellitus. In: *J. Biomedical Engineering* 14 (3), pp. 235–242.
DOI: 10.1016/0141-5425(92)90058-S.

Lepore, M. et al. (2000). Pharmacokinetics and pharmacodynamics of subcutaneous injection of long-acting human insulin analog glargine, NPH insulin, and ultralente human insulin and continuous subcutaneous infusion of insulin lispro. In: *Diabetes* 49 (12), pp. 2142–2148.
DOI: 10.2337/diabetes.49.12.2142.

Lindgren, O. et al. (2011). Incretin hormone and insulin responses to oral versus intravenous lipid administration in humans. In: *The Journal of clinical endocrinology and metabolism* 96 (8), pp. 2519–2524.
DOI: 10.1210/jc.2011-0266.

Ljung, L.; Glad, T. (1994). On global identifiability for arbitrary model parametrizations. In: *Automatica* 30 (2), pp. 265–276.
DOI: 10.1016/0005-1098(94)90029-9.

Luenberger, D. G. (1964). Observing the State of a Linear System. In: *IEEE Transactions on Military Electronics* 8 (2), pp. 74–80.
DOI: 10.1109/TME.1964.4323124.

Lunze, J. (2014). *Regelungstechnik 2: Mehrgrößensysteme, Digitale Regelung*. Berlin, Heidelberg.
DOI: 10.1007/978-3-642-53944-2.

Lunze, K. (2014). *Blood glucose control in diabetic Göttingen Minipigs: Zugl.: Aachen, Techn. Hochsch., Diss., 2014*. Berichte aus der Medizintechnik. Aachen: Shaker.
ISBN: 9783844032321.

Lunze, K. et al. (2013). Blood glucose control algorithms for type 1 diabetic patients: A methodological review. In: *Biomedical Signal Processing and Control* 8 (2), pp. 107–119.
DOI: 10.1016/j.bspc.2012.09.003.

Lv, D.; Breton, M. D.; Farhy, L. S. (2013). Pharmacokinetics modeling of exogenous glucagon in type 1 diabetes mellitus patients. In: *Diabetes Technology & Therapeutics* 15 (11), pp. 935–941.
DOI: 10.1089/dia.2013.0150.

Lynch, S. M.; Bequette, B. W. (2002). Model predictive control of blood glucose in type I diabetics using subcutaneous glucose measurements. In: *American Control Conference, 2002. Proceedings of the 2002*, pp. 4039–4043.
DOI: 10.1109/ACC.2002.1024561.

Magni, L. et al. (2007). Model Predictive Control of Type 1 Diabetes: An in Silico Trial. In: *Journal of Diabetes Science and Technology* 1 (6), pp. 804–812.
DOI: 10.1177/193229680700100603.

Magni, P.; Sparacino, G.; Bellazzi, R.; Cobelli, C. (2006). Reduced sampling schedule for the glucose minimal model: importance of Bayesian estimation. In: *American Journal of Physiology - Endocrinology and Metabolism* 290 (1), E177–E184.
DOI: 10.1152/ajpendo.00241.2003.

Marchetti, G. et al. (2008). An Improved PID Switching Control Strategy for Type 1 Diabetes. In: *IEEE Transactions on Biomedical Engineering* 55 (3), pp. 857–865.
DOI: 10.1109/TBME.2008.915665.

Marino, S.; Hogue, I. B.; Ray, C. J.; Kirschner, D. E. (2008). A methodology for performing global uncertainty and sensitivity analysis in systems biology. In: *Journal of Theoretical Biology* 254 (1), pp. 178–196.
DOI: 10.1016/j.jtbi.2008.04.011.

Marmarelis, V. Z. (2014). *Data-driven modeling for diabetes: Diagnosis and treatment*. Lecture notes in bioengineering. Springer Berlin Heidelberg.
ISBN: 9783642544637.

McKay, M. D.; Beckman, R. J.; Conover, W. J. (1979). A Comparison of Three Methods for Selecting Values of Input Variables in the Analysis of Output from a Computer Code. In: *Technometrics* 21 (2), p. 239.
DOI: 10.2307/1268522.

McVittie, G. (2020). *Generate JavaScript Using MATLAB Coder*.
URL: https://de.mathworks.com/matlabcentral/fileexchange/69973-generate-javascript-using-matlab-coder (visited on 07/04/2020).

Meier, J. J.; Kjems, L. L., et al. (2006). Postprandial suppression of glucagon secretion depends on intact pulsatile insulin secretion: further evidence for the intraislet insulin hypothesis. In: *Diabetes* 55 (4), pp. 1051–1056.
DOI: 10.2337/diabetes.55.04.06.db05-1449.

Meier, J. J.; Veldhuis, J. D.; Butler, P. C. (2005). Pulsatile insulin secretion dictates systemic insulin delivery by regulating hepatic insulin extraction in humans. In: *Diabetes* 54 (6), pp. 1649–1656.
DOI: 10.2337/diabetes.54.6.1649.

Messori, M.; Incremona, G. P.; Cobelli, C.; Magni, L. (2018). Individualized model predictive control for the artificial pancreas: In silico evaluation of closed-loop glucose control: IEEE Control Systems, 38(1), 86-104. In: *IEEE Control Systems* 38 (1), pp. 86–104.
DOI: 10.1109/MCS.2017.2766314.

Micheletto, F.; Dalla Man, C.; Vella, A.; Cobelli, C. (2010). A Model of Glucagon Secretion and Action in Healthy Subjects. In: *Proceedings of 10th Diabetes Technology Meeeting (DTM)*, A105.

Misgeld, B. J.; Tenbrock, P. G.; Leonhardt, S. (2017). Reduced-order filtering for insulin sensitivity estimation under external disturbances. In: *2017 American Control Conference (ACC)*, pp. 1444–1449.
DOI: 10.23919/ACC.2017.7963156.

Moore, B. C. (1981). Principal component analysis in linear systems: Controllability, observability, and model reduction. In: *IEEE Transactions on Automatic Control* 26 (1), pp. 17–32.
DOI: 10.1109/TAC.1981.1102568.

Morris, M. D. (1991). Factorial Sampling Plans for Preliminary Computational Experiments. In: *Technometrics* 33 (2), p. 161.
DOI: 10.2307/1269043.

Mosekilde, E. et al. (1989). Modeling absorption kinetics of subcutaneous injected soluble insulin. In: *Journal of Pharmacokinetics and Biopharmaceutics* 17 (1), pp. 67–87.
DOI: 10.1007/BF01059088.

Müller, H.-G. (2008). Functional modeling of longitudinal data. In: *Longitudinal Data Analysis*. Ed. by G. Fitzmaurice; M. Davidian; G. Verbeke; G. Molenberghs. Chapman and Hall/CRC, pp. 223–251.
ISBN: 9780429142673.

Natalucci, S. et al. (2003). Glucose Absorption and Insulin Sensitivity from Oral Glucose Tolerance Test. In: *Engineering in Medicine and Biology Society, 2003. Proceedings of the 25th Annual International Conference of the IEEE*. Vol. 3, pp. 2758–2760.
DOI: 10.1109/IEMBS.2003.1280488.

Nelder, J. A.; Mead, R. (1965). A Simplex Method for Function Minimization. In: *The Computer Journal* 7 (4), pp. 308–313.
DOI: 10.1093/comjnl/7.4.308.

Nielsen, M. F. et al. (1998). Normal glucose-induced suppression of glucose production but impaired stimulation of glucose disposal in type 2 diabetes: evidence for a concentration-dependent defect in uptake. In: *Diabetes* 47 (11), pp. 1735–1747.
DOI: 10.2337/diabetes.47.11.1735.

Nucci, G.; Cobelli, C. (2000). Models of subcutaneous insulin kinetics. A critical review. In: *Computer Methods and Programs in Biomedicine* 62 (3), pp. 249–257.
DOI: 10.1016/s0169-2607(00)00071-7.

Open Humans (2018). *Open Humans*.
URL: https://www.openhumans.org/ (visited on 10/31/2020).

Oviedo, S.; Vehí, J.; Calm, R.; Armengol, J. (2017). A review of personalized blood glucose prediction strategies for T1DM patients. In: *International Journal for Numerical Methods in Biomedical Engineering* 33 (6), pp. 1–21.
DOI: 10.1002/cnm.2833.

Pacini, G.; Bergman, R. N. (1986). MINMOD: a computer program to calculate insulin sensitivity and pancreatic responsicity from the frequently sampled intracenous glucose tolerance test. In: *Computer Methods and Programs in Biomedicine* 23 (2), pp. 113–122.
DOI: 10.1016/0169-2607(86)90106-9.

Pacini, G.; Tonolo, G., et al. (1998). Insulin sensitivity and glucose effectiveness: minimal model analysis of regular and insulin-modified FSIGT. In: *The American Journal of Physiology* 274 (4), E592–9.
DOI: 10.1152/ajpendo.1998.274.4.E592.

Palerm, C. C.; Bequette, B. W. (2007). Hypoglycemia Detection and Prediction Using Continuous Glucose Monitoring - A Study on Hypoglycemic Clamp Data. In: *Journal of Diabetes Science and Technology* 1 (5), pp. 624–629.
DOI: 10.1177/193229680700100505.

Papula, L. (2016). *Vektoranalysis, Wahrscheinlichkeitsrechnung, Mathematische Statistik, Fehler- und Ausgleichsrechnung: Mit 550 Abbildungen, zahlreichen Beispielen aus Naturwissenschaft und Technik sowie 295 Übungsaufgaben mit ausführlichen Lösungen*. 7., überarbeitete und erweiterte Auflage. Vol. / Lothar Papula ; Band 3. Lehrbuch. Wiesbaden: Springer Vieweg.
ISBN: 978-3-658-11924-9.

Parker, R. S.; Doyle, F. J.; Peppas, N. A. (1999). A Model-Based Algorithm for Blood Glucose Control in Type I Diabetic Patients. In: *IEEE Transactions on Biomedical Engineering* 46 (2), pp. 148–157.
DOI: 10.1109/10.740877.

Parkes, J. L.; Slatin, S. L.; Pardo, S.; Ginsberg, B. H. (2000). A new consensus error grid to evaluate the clinical significance of inaccuracies in the measurement of blood glucose. In: *Diabetes Care* 23 (8), pp. 1143–1148.
DOI: 10.2337/diacare.23.8.1143.

Pianosi, F. et al. (2016). Sensitivity analysis of environmental models: A systematic review with practical workflow. In: *Environmental Modelling & Software* 79, pp. 214–232.
DOI: 10.1016/j.envsoft.2016.02.008.

Piccinini, F.; Dalla Man, C.; Vella, A.; Cobelli, C. (2016). A Model for the Estimation of Hepatic Insulin Extraction After a Meal. In: *IEEE Transactions on Biomedical Engineering* 63 (9), pp. 1925–1932.
DOI: 10.1109/TBME.2015.2505507.

Pickup, J.; Mattock, M.; Kerry, S. (2002). Glycaemic control with continuous subcutaneous insulin infusion compared with intensive insulin injections in patients with type 1 diabetes: meta-analysis of randomised controlled trials. In: *BMJ (Clinical research ed.)* 324 (7339), p. 705.
DOI: 10.1136/bmj.324.7339.705.

Pistikopoulos, E. N.; Velliou, E. G.; Naşcu, I., eds. (2018). *Modelling optimization and control of biomedical systems*. First. Hoboken, NJ: John Wiley & Sons.
ISBN: 978-1-118-96559-7.

Polonsky, K. S.; Given, B. D.; Hirsch, L. J., et al. (1988). Abnormal patterns of insulin secretion in non-insulin-dependent diabetes mellitus. In: *The New England Journal of Medicine* 318 (19), pp. 1231–1239.
DOI: 10.1056/NEJM198805123181903.

Polonsky, K. S.; Given, B. D.; van Cauter, E. (1988). Twenty-four-hour profiles and pulsatile patterns of insulin secretion in normal and obese subjects. In: *Journal of Clinical Investigation* 81 (2), pp. 442–448.
DOI: 10.1172/JCI113339.

Prager, R.; Wallace, P.; Olefsky, J. M. (1986). In vivo kinetics of insulin action on peripheral glucose disposal and hepatic glucose output in normal and obese subjects. In: *Journal of Clinical Investigation* 78 (2), pp. 472–481.
DOI: 10.1172/JCI112599.

Radomski, D.; Glowacka, J. (2019). Sensitivity Analysis of the Insulin-Glucose Mathematical Model. In: *Information Technology in Biomedicine*. Advances in Intelligent Systems and Computing. Cham, pp. 455–468.
DOI: 10.1007/978-3-319-91211-0_40.

Ramsay, J.; Hooker, G.; Graves, S. (2009). *Functional Data Analysis with R and MATLAB*. 1. Use R! Springer.
ISBN: 9780387981840.

Rebrin, K.; Steil, G. M. (2000). Can interstitial glucose assessment replace blood glucose measurements? In: *Diabetes Technology & Therapeutics* 2 (3), pp. 461–472.
DOI: 10.1089/15209150050194332.

Rebrin, K.; Steil, G. M.; van Antwerp, W. P.; Mastrototaro, J. J. (1999). Subcutaneous glucose predicts plasma glucose independent of insulin: implications for continuous monitoring. In: *American Journal of Physiology - Endocrinology and Metabolism* 277 (3), E561–E571.
DOI: 10.1152/ajpendo.1999.277.3.E561.

Rizza, R. A.; Mandarino, L. J.; Gerich, J. E. (1981). Dose-response characteristics for effects of insulin on production and utilization of glucose in man. In: *The American Journal of Physiology* 240 (6), E630–9.
DOI: 10.1152/ajpendo.1981.240.6.E630.

Russell, S. J. (2008). Continuous Glucose Monitoring Awaits Its "Killer App". In: *Journal of Diabetes Science and Technology* 2 (3), pp. 490–494.
DOI: 10.1177/193229680800200321.

Russell, S. J. et al. (2016). Day and night glycaemic control with a bionic pancreas versus conventional insulin pump therapy in preadolescent children with type 1 diabetes: A randomised crossover trial. In: *The Lancet Diabetes & Endocrinology* 4 (3), pp. 233–243.
DOI: 10.1016/S2213-8587(15)00489-1.

Saad, A. et al. (2012). Diurnal pattern to insulin secretion and insulin action in healthy individuals. In: *Diabetes* 61 (11), pp. 2691–2700.
DOI: 10.2337/db11-1478.

Saccà, L.; Sherwin, R. S.; Hendler, R.; Felig, P. (1979). Influence of continuous physiologic hyperinsulinemia on glucose kinetics and counterregulatory hormones in normal and diabetic humans. In: *Journal of Clinical Investigation* 63 (5), pp. 849–857.
DOI: 10.1172/JCI109384.

Saltelli, A. (2002). Making best use of model evaluations to compute sensitivity indices. In: *Computer Physics Communications* 145 (2), pp. 280–297.
DOI: 10.1016/S0010-4655(02)00280-1.

Saltelli, A. (2008). *Global sensitivity analysis: The primer*. Chichester, England, and Hoboken, NJ: John Wiley.
ISBN: 978-0-470-05997-5.

Saltelli, A.; Andres, T. H.; Homma, T. (1993). Sensitivity analysis of model output: An investigation of new techniques. In: *Computational Statistics & Data Analysis* 15 (2), pp. 211–238.
DOI: 10.1016/0167-9473(93)90193-W.

Saltelli, A.; Annoni, P., et al. (2010). Variance based sensitivity analysis of model output. Design and estimator for the total sensitivity index. In: *Computer Physics Communications* 181 (2), pp. 259–270.
DOI: 10.1016/j.cpc.2009.09.018.

Saltelli, A.; Chan, K.; Scott, E. M., eds. (2000). *Sensitivity analysis*. Wiley series in probability and statistics. Chichester: Wiley.
ISBN: 0471998923.

Saltelli, A.; Marivoet, J. (1990). Non-parametric statistics in sensitivity analysis for model output: A comparison of selected techniques. In: *Reliability Engineering & System Safety* 28 (2), pp. 229–253.
DOI: 10.1016/0951-8320(90)90065-U.

Saltelli, A.; Ratto, M.; Tarantola, S.; Campolongo, F. (2005). Sensitivity analysis for chemical models. In: *Chemical Reviews* 105 (7), pp. 2811–2828.
DOI: 10.1021/cr040659d.

Saltelli, A.; Tarantola, S. (2002). On the Relative Importance of Input Factors in Mathematical Models. In: *Journal of the American Statistical Association* 97 (459), pp. 702–709.
DOI: 10.1198/016214502388618447.

Saltelli, A.; Tarantola, S.; Campolongo, F. (2000). Sensitivity Analysis as an Ingredient of Modeling. In: *Statistical Science* 15 (4), pp. 377–395.
DOI: 10.1214/ss/1009213004.

Saltelli, A.; Tarantola, S.; Chan, K. P.-S. (1999). A Quantitative Model-Independent Method for Global Sensitivity Analysis of Model Output. In: *Technometrics* 41 (1), p. 39.
DOI: 10.2307/1270993.

Schatz, H. (2006). *Diabetologie kompakt: Grundlagen und Praxis*. 4. Stuttgart: Thieme.
ISBN: 3-13-137724-0.

Schmidt, K. D. (2011). *Maß und Wahrscheinlichkeit*. 2., durchges. Aufl. Springer-Lehrbuch. Berlin, Heidelberg.
DOI: 10.1007/978-3-642-21026-6.

Schwartz, N. S.; Clutter, W. E.; Shah, S. D.; Cryer, P. (1987). Glycemic thresholds for activation of glucose counterregulatory systems are higher than the threshold for symptoms. In: *Journal of Clinical Investigation* 79 (3), pp. 777–781.
DOI: 10.1172/JCI112884.

Seaquist, E. R. et al. (2013). Hypoglycemia and diabetes: a report of a workgroup of the American Diabetes Association and the Endocrine Society. In: *Diabetes Care* 36 (5), pp. 1384–1395. DOI: 10.2337/dc12-2480.

Segre, G.; Turco, G. L.; Vercellone, G. (1973). Modeling blood glucose and insulin kinetics in normal, diabetic and obese subjects. In: *Diabetes* 22 (2), pp. 94–103. DOI: 10.2337/diab.22.2.94.

Seino, Y. et al. (1978). Failure of suppress plasma glucagon concentrations by orally administered glucose in diabetic patients after treatment. In: *Diabetes* 27 (12), pp. 1145–1150. DOI: 10.2337/diab.27.12.1145.

Shah, P. et al. (2000). Lack of suppression of glucagon contributes to postprandial hyperglycemia in subjects with type 2 diabetes mellitus. In: *Journal of Clinical Endocrinology & Metabolism* 85 (11), pp. 4053–4059. DOI: 10.1210/jcem.85.11.6993.

Sherwin, R. S. et al. (1974). A model of the kinetics of insulin in man. In: *Journal of Clinical Investigation* 53 (5), pp. 1481–1492. DOI: 10.1172/JCI107697.

Shichiri, M.; Asakawa, N., et al. (1986). Telemetry glucose monitoring device with needle-type glucose sensor: a useful tool for blood glucose monitoring in diabetic individuals. In: *Diabetes Care* 9 (3), pp. 298–301. DOI: 10.2337/diacare.9.3.298.

Shichiri, M.; Yamasaki, Y., et al. (1982). Wearable Artificial Endocrine Pancreas with Needle-Type Glucose Sensor. In: *The Lancet* 320 (8308), pp. 1129–1131. DOI: 10.1016/S0140-6736(82)92788-X.

Simon, D. (2006). *Optimal state estimation: Kalman, H [infinity], and nonlinear approaches*. Hoboken, NJ: Wiley-Interscience. ISBN: 978-0-471-70858-2.

Sin, G.; Gernaey, K. V. (2009). Improving the Morris method for sensitivity analysis by scaling the elementary effects. In: *19th European Symposium on Computer Aided Process Engineering*. Ed. by J. Jeżowski; J. Thullie. Vol. 26. Computer-aided chemical engineering. Amsterdam, pp. 925–930. DOI: 10.1016/S1570-7946(09)70154-3.

Sobol', I. (1993). Sensitivity Estimates for Nonlinear Mathematical Models. In: *Math. Model. Comp. Exp* 1 (4), pp. 407–414.

Sorensen, J. T. (1985). A physiologic model of glucose metabolism in man and its use to design and assess improved insulin therapies for diabetes. PhD Thesis. Cambridge, MA, USA: Massachusetts Institute of Technology.

Sparacino, G. et al. (2007). Glucose Concentration can be Predicted Ahead in Time From Continuous Glucose Monitoring Sensor Time-Series. In: *IEEE Transactions on Biomedical Engineering* 54 (5), pp. 931–937. DOI: 10.1109/TBME.2006.889774.

Steil, G. M.; Rebrin, K.; Darwin, C., et al. (2006). Feasibility of automating insulin delivery for the treatment of type 1 diabetes. In: *Diabetes* 55 (12), pp. 3344–3350.
DOI: 10.2337/db06-0419.

Steil, G. M.; Rebrin, K.; Mastrototaro, J., et al. (2003). Determination of plasma glucose during rapid glucose excursions with a subcutaneous glucose sensor. In: *Diabetes Technology & Therapeutics* 5 (1), pp. 27–31.
DOI: 10.1089/152091503763816436.

Steil, G. M.; Rebrin, K.; Mastrototaro, J. J. (2006). Metabolic modelling and the closed-loop insulin delivery problem. In: *Diabetes Research and Clinical Practice* 74, S183–S186.
DOI: 10.1016/S0168-8227(06)70028-6.

Streif, S.; Findeisen, R.; Bullinger, E. (2006). Relating Cross Gramians and Sensitivity Analysis in Systems Biology. In: *Proceedings of the 17th International Symposium on Mathematical Theory of Networks and Systems (MTNS 2006)*, pp. 437–442.
URL: https://www.researchgate.net/publication/258108613_Relating_cross_Gramians_and_sensitivity_analysis_in_systems_biology (visited on 10/21/2014).

Sumner, T. (2010). Sensitivity Analysis in Systems Biology Modelling and its Application to a Multi-Scale Model of Blood Glucose Homeostasis. PhD Thesis. London: University College London.
URL: http://discovery.ucl.ac.uk/19896/1/19896.pdf (visited on 03/08/2019).

Sumner, T.; Shephard, E.; Bogle, I. D. L. (2012). A methodology for global-sensitivity analysis of time-dependent outputs in systems biology modelling. In: *Journal of the Royal Society, Interface* 9 (74), pp. 2156–2166.
DOI: 10.1098/rsif.2011.0891.

Sun, C.; Hahn, J. (2006). Parameter reduction for stable dynamical systems based on Hankel singular values and sensitivity analysis. In: *Chemical Engineering Science* 61 (16), pp. 5393–5403.
DOI: 10.1016/j.ces.2006.04.027.

The Epsilon Group (2013). *UVA/Padova Type 1 Diabetes Metabolic Simulator*.
URL: https://tegvirginia.com/software/t1dms-2014/ (visited on 05/06/2020).

The MathWorks, Inc. (2019). *Matlab®*. Natick, MA, USA.
URL: https://www.mathworks.com (visited on 07/03/2020).

The Nightscout Data Commons Committee (2018). *Nightscout Data Commons*.
URL: https://www.openhumans.org/activity/nightscout-data-commons/ (visited on 10/31/2020).

The Nightscout Foundation (2018). *xDrip+*.
URL: https://github.com/NightscoutFoundation/xDrip (visited on 07/10/2020).

Thomas, A.; Heinemann, L. (2006). Unblutiges Glukosemonitoring: Enttäuschungen und Hoffnungen. In: *Diabetes, Stoffwechsel und Herz* 4, pp. 3–15.

Thomé-Duret, V. et al. (1996). Use of a subcutaneous glucose sensor to detect decreases in glucose concentration prior to observation in blood. In: *Analytical Chemistry* 68 (21), pp. 3822–3826.
DOI: 10.1021/ac960069i.

Toffolo, G. M.; Bergman, R. N., et al. (1980). Quantitative estimation of beta cell sensitivity to glucose in the intact organism: a minimal model of insulin kinetics in the dog. In: *Diabetes* 29 (12), pp. 979–990.
DOI: 10.2337/diab.29.12.979.

Toffolo, G. M.; Breda, E., et al. (2001). Quantitative indexes of beta-cell function during graded up&down glucose infusion from C-peptide minimal models. In: *American Journal of Physiology - Endocrinology and Metabolism* 280 (1), E2–10.
DOI: 10.1152/ajpendo.2001.280.1.E2.

Toffolo, G. M.; Cobelli, C. (2003). The hot IVGTT two-compartment minimal model: an improved version. In: *American Journal of Physiology - Endocrinology and Metabolism* 284 (2), E317–E321.
DOI: 10.1152/ajpendo.00499.2001.

Toffolo, G. M.; Grandi, F. de; Cobelli, C. (1995). Estimation of beta-cell sensitivity from intravenous glucose tolerance test C-peptide data. Knowledge of the kinetics avoids errors in modeling the secretion. In: *Diabetes* 44 (7), pp. 845–854.
DOI: 10.2337/diab.44.7.845.

Ullah, S.; Finch, C. F. (2013). Applications of functional data analysis: A systematic review. In: *BMC Medical Research Methodology* 13, p. 43.
DOI: 10.1186/1471-2288-13-43.

Unger, R. H. (1971). Glucagon physiology and pathophysiology. In: *The New England Journal of Medicine* 285 (8), pp. 443–449.
DOI: 10.1056/NEJM197108192850806.

Unger, R. H.; Orci, L. (1976). Physiology and pathophysiology of glucagon. In: *Physiological Reviews* 56 (4), pp. 778–826.
DOI: 10.1152/physrev.1976.56.4.778.

van Riel, N. A. W. (2006). Dynamic modelling and analysis of biochemical networks: mechanism-based models and model-based experiments. In: *Briefings in Bioinformatics* 7 (4), pp. 364–374.
DOI: 10.1093/bib/bbl040.

Verily Life Sciences LLC (2018-11-16). *Update on our Smart Lens program with Alcon*.
URL: https://blog.verily.com/2018/11/update-on-our-smart-lens-program-with.html (visited on 02/05/2020).

Vettoretti, M.; Cappon, G., et al. (2018). Continuous Glucose Monitoring: Current Use in Diabetes Management and Possible Future Applications. In: *Journal of Diabetes Science and Technology* 12 (5), pp. 1064–1071.
DOI: 10.1177/1932296818774078.

Vettoretti, M.; Facchinetti, A.; Sparacino, G.; Cobelli, C. (2017). A Model of Self-Monitoring Blood Glucose Measurement Error. In: *Journal of Diabetes Science and Technology* 11 (4), pp. 724–735.
DOI: 10.1177/1932296817698498.

Vigersky, R. A. et al. (2012). Short- and long-term effects of real-time continuous glucose monitoring in patients with type 2 diabetes. In: *Diabetes Care* 35 (1), pp. 32–38.
DOI: 10.2337/dc11-1438.

Villena Gonzales, W.; Mobashsher, A. T.; Abbosh, A. (2019). The Progress of Glucose Monitoring—A Review of Invasive to Minimally and Non-Invasive Techniques, Devices and Sensors. In: *Sensors* 19 (4).
DOI: 10.3390/s19040800.

Visentin, R. et al. (2018). The UVA/Padova Type 1 Diabetes Simulator Goes From Single Meal to Single Day. In: *Journal of Diabetes Science and Technology* 12 (2), pp. 273–281.
DOI: 10.1177/1932296818757747.

Wentholt, I. M. E.; Hart, A. A. M.; Hoekstra, J. B. L.; DeVries, J. H. (2007). Relationship between interstitial and blood glucose in type 1 diabetes patients: delay and the push-pull phenomenon revisited. In: *Diabetes Technology & Therapeutics* 9 (2), pp. 169–175.
DOI: 10.1089/dia.2006.0007.

Wilinska, M. E. et al. (2010). Simulation environment to evaluate closed-loop insulin delivery systems in type 1 diabetes. In: *Journal of Diabetes Science and Technology* 4 (1), pp. 132–144.
DOI: 10.1177/193229681000400117.

Wong, J. et al. (2008). A Subcutaneous Insulin Pharmacokinetic Model for Computer Simulation in a Diabtes Decision Support Role : Model Structure and Parameter Identification. In: *Journal of Diabetes Science and Technology* 2 (4), pp. 658–671.
DOI: 10.1177/193229680800200417.

World Health Organization (1999). *Definition, diagnosis and classification of diabetes mellitus and its complications: report of a WHO consultation. Part 1, Diagnosis and classification of diabetes mellitus: WHO/NCD/NCS/99.2*. Ed. by World Health Organization. Geneve.
URL: https://apps.who.int/iris/handle/10665/66040 (visited on 02/02/2020).

World Health Organization (2006). *Definition and diagnosis of diabetes mellitus and Intermediate Hyperglycemia: Report of a WHO/IDF Consultation*. Geneve: WHO Document Production Services.
ISBN: 9241594934.

Worthington, D. R. L. (1997). Minimal model of food absorption in the gut. In: *Informatics for Health and Social Care* 22 (1), pp. 35–45.
DOI: 10.3109/14639239709089833.

Yalow, R. S.; Berson, S. A. (1960). Immunoassay of endogenous plasma insulin in man. In: *Journal of Clinical Investigation* 39, pp. 1157–1175.
DOI: 10.1172/JCI104130.

Yamanishi, Y.; Tanaka, Y. (2005). Sensitivity analysis in functional principal component analysis. In: *Computational Statistics* 20 (2), pp. 311–326.
DOI: 10.1007/BF02789706.

Yang, J. (2011). Convergence and uncertainty analyses in Monte-Carlo based sensitivity analysis. In: *Environmental Modelling & Software* 26 (4), pp. 444–457.
DOI: 10.1016/j.envsoft.2010.10.007.

Yao, F.; Müller, H.-G.; Wang, J.-L. (2005). Functional Data Analysis for Sparse Longitudinal Data. In: *Journal of the American Statistical Association* 100 (470), pp. 577–590.
DOI: 10.1198/016214504000001745.

Yki-Järvinen, H.; Koivisto, V. A. (1986). Natural course of insulin resistance in type I diabetes. In: *The New England Journal of Medicine* 315 (4), pp. 224–230.
DOI: 10.1056/NEJM198607243150404.

Yki-Järvinen, H.; Young, A. A.; Lamkin, C.; Foley, J. E. (1987). Kinetics of glucose disposal in whole body and across the forearm in man. In: *Journal of Clinical Investigation* 79 (6), pp. 1713–1719.
DOI: 10.1172/JCI113011.

Yuce, M. R. (2010). Implementation of wireless body area networks for healthcare systems. In: *Sensors and Actuators A: Physical* 162 (1), pp. 116–129.
DOI: 10.1016/j.sna.2010.06.004.

Zakai, A. (2011). Emscripten: an LLVM-to-JavaScript compiler. In: *Proceedings of the ACM international conference companion on Object oriented programming systems languages and applications companion*. New York, NY, pp. 301–312.
DOI: 10.1145/2048147.2048224.

Zavitsanou, S. (2014). Modelling, Optimisation and Model Predictive Control of Insulin Delivery Systems in Type 1 Diabetes Mellitus. PhD Thesis. London: Imperial College London.

Zecchin, C. et al. (2013). Physical activity measured by physical activity monitoring system correlates with glucose trends reconstructed from continuous glucose monitoring. In: *Diabetes Technology & Therapeutics* 15 (10), pp. 836–844.
DOI: 10.1089/dia.2013.0105.

Zheng, Y.; Rundell, A. (2006). Comparative study of parameter sensitivity analyses of the TCR-activated Erk-MAPK signalling pathway. In: *Systems Biology* 153 (4), pp. 201–211.
DOI: 10.1049/ip-syb:20050088.